THE MECHANICAL PROPERTIES OF COMPACTED CLAY FROM THE LAMBETH GROUP USING FIBRE REINFORCEMENT

by

Abdullah Ekinci

Supervised by:

Dr Pedro Ferreira

A dissertation submitted in partial fulfillment of the requirements for the degree of Doctor of Philosophy Ph.D.

in the

Faculty of Engineering Science

Civil, Environmental and Geomatic Engineering

July 2016

Declaration

I hereby declare that the work presented in this thesis is solely my own work and that to the best of my knowledge the work is original except where otherwise indicated by reference to other authors. No part of this work has been submitted for any other degree or diploma.

Abdullah Ekinci

July 2016

Abstract

Slope failures related to pore-water dissipation, stress relaxation and desiccation cracks are major problems occurring in the UK ageing road network. The remediation works are known to cause congestion and delays that, in turn, cause financial loss and discomfort to users. Our industry partner, Mouchel, believe that it is possible to reduce the number of slope failures, maintenance costs and bring large social benefits by using soil reinforcement to reinstate failed slopes.

The use of fibre reinforced soils has been a topic of research for many years, however not many applications have been seen so far. Fibres have the potential to reduce environmental impact by improving soil properties and allowing the use of local available soils. In order to increase its use, it is important to understand how the inclusion of fibres can improve soil properties, particularly in heavily overconsolidated soils, where the compacted composite has “peds” carrying properties of the intact soil.

To study the soil improvement, a new compaction methodology was developed, mimicking the behaviour of the site compacted composite. Series of drained and undrained triaxial tests were performed in reinforced and unreinforced laboratory compacted samples, as well site compacted samples. In order to better understand the effect of structure, reconstituted samples were also tested.

The results show that the reinforced samples, tested below a critical confining pressure, have higher strength than the unreinforced samples, whilst above this pressure the strength reduces. The data revealed that the reinforced samples appear to have a unique critical state line, whilst the unreinforced soil seems to have a transitional behaviour with a set of parallel critical state lines. The normalisation, by the intrinsic normal compression line, shows that it is possible to identify part of the state boundary surface of the compacted samples and these plot above the intrinsic state boundary surface.

From the “Karls”, that I admire the most…

“The philosophers have only interpreted the world, in various ways. The point, however, is to change it.”

Karl Marx

“To acquire competence in the field of earthwork engineering one must live with the soil. One must love it and observe its performance not only in the laboratory but also in the field, to become familiar with those of its manifold properties that are not disclosed by boring records…”

Karl Terzaghi

Acknowledgements

Firstly, I would like to acknowledge the support of my supervisor, Dr. Pedro Ferreira, who has been more than a supervisor through this period, a lifelong friend. This thesis would not be possible without his enormous encouragement, support, guidance and contributions. I will always recall his tremendous knowledge in soil mechanics and also the variety of intellectual conversations we had in this several years. He thought me how to be patient, wise and a good person.

Special thanks goes to Prof. Matthew Coop who has been always available for discussions. His endless vision on soil mechanics has enlighten a number of shades which enabled a clear path.

I am very thankful to the contributions of Mr. Paul Mennell who has always been patient when I needed modifications in my equipment and fixing the never ending equipment failures. I would also like to express my gratitude to Mr. Steven Ackerley, from Imperial College, for his guidance and help with the triaxial testing at the start of this research.

I cannot forget the ones who, I believe, have contributed in many ways on this thesis; friends – Omid, Zohreh, Elena, Ramtin, Hussam, Stella, Anna Maria, Ali, Adel, Giannis, Raul, Amin, Eleni, Xenia, Artemis, Randolph. Omid, it was not as easy as you think!!Thanks for convincing me.

I would like to acknowledge the support of my family Ayse, Aydan, Cezar, Kemal who were always supportive in many ways throughout these hard times.

Last but not least, it would not be possible to finalise this thesis without my lovely fiancé. Nursan`s encouragement, patience and positive attitude in life where truly inspiring to me.

List of publications from this work:

Ekinci, A. 2010. Improvement of the mechanical properties of compacted clay from the Lamberth group using Fibre Reinforcement. *Proceedings of the 11th BGA Young Geotechnical Engineers Symposium*, Bristol, United Kingdom, 33-35.

Ekinci, A. & Ferreira, P. M. V. 2012, The undrained mechanical behaviour of a fibre-reinforced heavily over-consolidated clay, *Proceedings of the ISSMGE - TC 211 International Symposium on Ground Improvement*, Brussels, Belgium.

Ekinci, A. & Ferreira, P. M. V. 2012, Effects of fibre inclusion on stress strain behaviour of a compacted over-consolidated clay from Lambeth Group, *Proceedings of the International Conference on Ground Improvement and Ground Control*, Wollongong, Australia.

Ekinci, A. & Ferreira, P. M. V. 2012, Effects of fibre reinforcement in the shrinkage behaviour of compacted clay, *Proceedings of the 3rd International Conference on New Developments in Soil Mechanics and Geotechnical Engineering*, Nicosia, Cyprus.

Table of Contents

List of Figures

List of Tables

List of Symbols

Symbol

Δl	axial length
l_0	initial sample length
A_0	initial area
A	cross sectional area
A_{cr}	current sample cross sectional area
V_v	volume of voids
V_0	initial volume
ΔV	change in volume measured by volume gauge
V, V_T	total volume of sample
V_w	volume of water
V_s	volume of solids
w_0	initial water content
w_f	final water content
w	water content of sample
γ_i	bulk unit weight
γ_{di}	dry unit weight
γ_s	solid unit weight
γ_w	water unit weight
ρ_w	density of water
ρ	density of soil
e	voids ratio
e_0	initial voids ratio
e_f	final voids ratio
e_c	void ratio at specific time
e^*	Voids ratio on the intrinsic curve

e_{100}	Voids ratio on the NICL for 100kPa vertical pressure
e_{1000}	Voids ratio on the NICL for 1000kPa vertical pressure
v	specific volume
I_v	void index
R	the lever arm ratio
B	coefficient of saturation
I_p	plasticity index
G_s	specific gravity of solids
σ'_a	axial effective stress
σ_a	axial total stress
σ'_r	radial effective stress
σ_r	radial total stress
σ_{mb}	membrane correction for barrelling
σ_{dr}	drain correction
σ_e^*	equivalent pressure
$\sigma_{\grave{v}}$	vertical effective stress
σ_v	total vertical stress
q, q'	deviatoric stress
F_{dwh}	dead weight on the hanger
u	pore water pressure
Δu	change in pore water pressure
ε_v	volumetric strain rate
ε_a	axial strain
ε_r	radial strain
ε_s	shear strain
ε_e	end of test strain
ε_f	strain at the shear plane formation

p'	mean effective stress
p'_e	equivalent pressure on the NCL at current void ratio of soil
p^*_e	equivalent pressure on the INCL at current void ratio of soil
$p\grave{}_{cs}$	equivalent pressure on the group CSL at current void ratio of soil
$p\grave{}_{cs(in)}$	equivalent pressure on the individual CSL at current void ratio of soil
λ	gradient of the NCL in the v-lnp` space
λ*	gradient of the INCL in the v-lnp` space
Γ	specific volume on the CSL for p`=1kPa
M	critical state stress ratio
N*	specific volume on the INCL for p`=1kPa
N	specific volume on the NCL for p`=1kPa
κ	gradient of the swelling line in the v-lnp` space (1D)
Cs	swelling index
Cc	compression Index
$G_0\grave{}$	monotonic shear modulus
G_{eq}	equivalent elastic shear modulus
E'	drained young`s modulus
E_u	undrained young`s modulus
T	travel time (in s)
L	tip-to-tip travel distance
t_a	first point of deflection
t_b	first point reversal
t_c	first point of inflection
v_s	velocity of shear wave

ABBREVIATIONS

NCL	Normal Compression Line
CSL	Critical State Line
WF	Wykeham Farrance
1D	One-dimensional
CRSP	Constant Rate Strain Pump
CS	Critical State
SBS	State Boundary Surface
SBS*	Intrinsic State Boundary Surface
LBS	Local Boundary Surface
INCL	Intrinsic Normal Compression Line
PWP	Pore Water Pressure
LL	Liquid Limit
PL	Plastic Limit

INTRODUCTION

In this thesis, entitled 'The mechanical properties of compacted clay from the Lambeth group using fibre reinforcement', the outcome of a research project, carried out by the author, at the Department of Civil, Environmental and Geomatics Engineering, University College London (UCL), UK is presented, in partial fulfilment of the University of London degree of Doctorate in Philosophy in the area of Soil Mechanics. The research project was carried out in collaboration between UCL and the engineering consulting company Mouchel (MRBL Limited) with financial support from a research grant from EPSRC.

1.1 Background

Slope failure, due to pore-water increase, stress relaxation and desiccation cracks, is one of the major problems commonly observed on the UK road network. The remediation works on the UK road network cause congestion and delays that, in turn, cause financial loss. In order to decrease the recurrent time of maintenance during slope stability work, Mouchel (the project's industrial partner), in a departure from standards, approved by the Highways Agency, carried out a pilot field study, using artificial fibres, mixed and compacted with a natural soil, to remediate slope failures. This research project was commissioned to study the behaviour of such composite by testing samples prepared in the laboratory and collected from site.

The use of tensile elements in soil structures is not new. Some 3,000 or more years ago, the Babylonians were the first ancient nation to use palm branches to manufacture clay bricks. The Agar-Quf Ziggurat, an Iraqi temple, was made of clay bricks reinforced with woven reed mats, laid horizontally on a layer of sand and gravel, at vertical centre spaces between 0.5m and 2.0m (Kerisel 1975). The Babylonians were followed by the Romans who used earth-reinforcing techniques, as evidenced by the reed, to reinforce earth levees constructed along the Tiber River (the third biggest river in Italy) and the

wharf of the Port of Londinium (London) in the 1st Century BC. Later, the Chinese, more than 2,000 years ago, used tree branches to reinforce clay and gravel to build the Great Wall of China.

In the 1930s, the modern concept of soil reinforcing was proposed by Casagrande, during his lectures at Harvard University, who idealized the problem in the form of a weak soil reinforced by high-strength membranes laid horizontally in layers. However, it was Vidal in the 1960s who investigated this field in detail. Vidal's concept was to lie flat reinforcing strips horizontally in a frictional soil, as this enabled the interaction between the soil and the reinforcement, to create a friction force, to hold the soil in place (Jones 1996). Reinforcing soil with a tensile element is still a common practice in many developing countries, where soil and straw are mixed to be used as a construction material.

The standard fibre-reinforced soil is generally defined as a soil mass containing randomly distributed discrete elements (fibres), that provide an improvement in the mechanical behaviour of the soil composite (Li 2005). Numerous experiments have been conducted to determine the effects of discrete fibres on the behaviour of granular soils, the vast majority focusing only on the short-term characteristics and total shearing strength of the fibre-soil mixture. Therefore, there is a lack of data relating to the long-term effects of the fibre reinforcement within the clay structure and very little is known about their behaviour in situ.

Most of the previous research on fibre reinforced soil revealed that the addition of fibres to a soil strata caused an increase in peak shear strength and a decrease in the post-peak strength. Researchers quantified the increase in shear strength to the increase in friction angle and cohesion, which can be determined by testing fibre-reinforced specimens. In present geotechnical practice, the design of fibre reinforcement requires specific testing of fibre reinforced specimens, which may be expensive and inefficient.

Also, there is limited knowledge about the effects that the field techniques currently have on the mix, compaction of the soil fibre and their performance. The author adapted the compaction method used in-situ for laboratory conditions, where the soil structure is, to some extend, preserved, as O`Connor (1994) and analysed both, in-situ compacted reinforced and laboratory compacted reinforced samples.

1.2 Aims and Objectives

This research project aims to study five major objectives, with an over-arching aim of analysing proposed composite in the light of critical state soil mechanics, to be able to predict the behaviour of fibres as a micro reinforcement in compacted clays. The five objectives are:

- **Effect of fibre reinforcement in the shrinkage behaviour of the compacted clay.** The stability of clay slopes and liners is intimately connected to desiccation cracking. To mitigate this problem, research has been performed on mixtures of soil with additives such as lime, cement and/or fibres. Chemical additives tend to generate stiff materials and may leach and create environmental problems; therefore, fibre reinforcement became an interesting alternative as it reduces the cracking formation and cracking propagation in soils subjected to cycles of wetting and drying, as well as accommodating certain displacements. In this study, results of a pilot study on reinforced and unreinforced compacted samples of clay from the Lambeth Group, subjected to desiccation, are presented. Sample height, diameter and weight were measured. Digital imaging was also performed in order to verify the occurrence of desiccation cracking. A discussion on the issue of crack dessication is presented in Chapter 8.
- **Mapping the alignment of fibres generated by the compaction of heavily over-consolidated clay**. Previous researches proposed that fibres are randomly distributed. However, the spreading of fibre in-situ depends on specific equipment and mixing procedures. It is expected that fibres placed during field applications will show a horizontal orientation due to their self-weight, presence of soil peds and compaction method used. Alignment studies of fibre-reinforced soil is quantified in Chapter 7, by comparing samples of the in-situ compacted material, obtained by block sampling, and samples prepared in the laboratory, to map the fibre distribution throughout the samples and to assess the difference caused by the in-situ and laboratory compaction.

- **Large strain behaviour.** Chapter 10 is dedicated to present, discuss and assess the behaviour of in-situ compacted reinforced, laboratory compacted reinforced, laboratory compacted unreinforced and reconstituted unreinforced Lambeth group clay samples at large strains (up to 30% strain) based on all the triaxial

test data that is available for analysis. By means of a series of cross-comparisons, the factors influencing the materials behaviour have been discussed and identified. The main investigations performed were:

  - One-Dimensional compression behaviour
  - Isotropic compression behaviour
  - Increase in shear strength caused by the addition of fibres
  - Application of critical state soil mechanics normalisation methods
  - Determination of state boundary surfaces

- **Small strain behaviour**. To study the effect of the fibres on the small strain elastic shear modulus of the composite. Several tests have been performed on a Bender elements modified oedometer cell to measure vertical dynamic shear moduli of laboratory compacted fibre reinforced and unreinforced clay samples. Additionally, the monotonic shear moduli, based on internal axial strain measurements, on triaxial apparatus have been studied on all triaxial tests throughout the project.

- **Effect of peds in compaction.** Analysis of large and small strain behaviour of the studied materials enabled the characterisation and understanding of the behaviour of compacted clay peds (clay lumps), generated by the rotavator (soil/fibre mixing equipment), in a variety of sizes, that still retain the characteristics of the intact soil, with and without reinforcement. The differences between the fibre reinforced and unreinforced ped compacted, as well as the destructured (reconstituted) samples are studied.

The test results have provided data which was used to analyse the behaviour of the new material and its use in the maintenance of existing slopes, embankment cuts and construction of new ones, along the highway network in the UK and, ultimately, worldwide.

The findings have provided a better understanding of the effects of discrete fibre reinforcement on heavily over-consolidated clays and the effects of in-situ mixing and compaction techniques in the response of the composite soil. This will provide effective guidance in the construction and remediation of slope failures and the widespread use of

this type of reinforcement as an effective way to reduce maintenance works and costs on road embankments and cuttings. Improvements in soil characteristics using micro-reinforcement will also lead to a more sustainable way of using poor construction soils. Because of the high cost of material disposal and the associated environmental problems, increasing pressure is applied on the engineering community to find alternative solutions to dispose of unsuitable soils, by adequate their mechanical characteristics to specific project requirements. One of the alternatives is the use of micro-reinforcement, especially since there is a potential to use fibres from recycled materials, reducing even further the associated environmental cost.

1.3 Methodology

Further in this study, besides the evaluation of a single test, a group evaluation and cross group evaluation of certain aspects was made. Therefore, Table 1 presents a definition of what is intended by a “group of specimens”, as this term is employed throughout the thesis.

In order to achieve the five main objectives of this project, this research was concentrated on a state-of-the-art literature review and practical studies with a wide range of laboratory testing. In the theoretical studies, a comprehensive review of the available literature on related fields was performed. The literature review began with basic mechanical behaviour of fibre reinforcement throughout human history to observe the development of soil reinforcement. In addition, established techniques of soil improvement to date were studied in separate areas within the literature review. While the shear behaviours of cohesive and granular soils are fundamentally different, much of the knowledge acquired on the behaviour of granular soils reinforced with fibres is significant to fibre reinforced clay. Therefore, the literature review includes categorized behaviour characteristics of a variety of soil and fibre types, such as swelling, compaction, desiccation cracking, hydraulic conductivity, shrinkage behaviour and alignment of fibres. Furthermore, for simplification and an idealization of fibre reinforced soil behaviour, fundamentals of Critical State Soil Mechanics were studied. Finally, the final three sections of literature review chapter covered compression behaviour, large strain and small strain behaviour.

In chapter 3, the characteristics of the soil tested in the current study and its engineering properties were highlighted with reference to the lithological characterization of the natural clay. The available literature were evaluated, together with the data obtained from this study on the Lambeth group. This was used as a background to the analysis of the obtained tests results.

Table 1. Description of used specimens throughout this study

Name:	**Description:**
RECONSTITUTED	• Soil used was excavated from site as 300 mm peds. • Sealed in plastic bag until the further preparation for testing. • Reconstituted upto 1.5 times liquid limit Burland (1990) • Further details of preparation technique can be seen in Section 5.9.2.1
UNREINFORCED	• Soil used was excavated from site as 300 mm peds. • Sealed in plastic bag until the further preparation for testing. • Peds are further braked down to 15 – 20 mm • Prepared for testing by standard compaction without fibres. • Further details of preparation technique can be seen in Section 5.9.2.3
REINFORCED	• Soil used was excavated from site as 300 mm peds. • Sealed in plastic bag until the further preparation for testing. • Peds are further braked down to 15 – 20 mm • Prepared for testing by standard compaction with fibres. • Further details of preparation technique can be seen in Section 5.9.2.2
IN-SITU	• Undisturbed samples were block sampled from fibre treated slope at same site that above specimens obtained. • Block samples are stored in wooden cases until testing. • Samples are trimmed from block samples. • Further details of preparation technique can be seen in Section 5.9.2.4

The goal of this practical study is to achieve the five main objectives. To understand the mechanical behaviour of the reconstituted, reinforced, unreinforced and in-situ soils, consolidated drained (CD) and consolidated undrained (CU) tests were performed. The

testing program for this study contains 27 triaxial tests. This series of triaxial tests were performed to assess the strength and stiffness of the samples at isotropic stresses varying from 50 to 500kPa, consistent with the stresses applied in the majority of the engineering problems. In agreement with the industrial partner, only one type of fibre and quantity was investigated.

The details of the Laboratory apparatus, test procedures and calculations/corrections were presented in detail chapters 4, 5, 6 .

In Chapter 7, the methodology and the results of the fibre alignment of compacted samples were presented, in order to understand the effect of the alignment in the shearing. In order to assess the fibre alignment of in-situ and laboratory-compacted samples, a few in-situ and laboratory-compacted samples were dissected.

Chapter 8, presented the results of a pilot study on reinforced and unreinforced compacted samples of clay from the Lambeth Group, subjected to desiccation. The samples were compacted using the standard energy in different initial moisture contents and later allowed to air dry. Height, diameter and weight were monitored.

Beside of the advanced soil testing, conventional equipment such as oedometers were used to understand the one-dimensional compression behaviour of the specimens. Since reconstituted specimens will form the reference point to evaluate the structure of the new composites, the intrinsic compression characteristics are vastly important to highlight. Additionally, a modified oedometer cell with bender elements was used. The monotonic shear moduli for the group of materials will be evaluated with high resolution local instrumentation. With the use of a series of cross-comparisons, the influence of fibres in the material behaviour was distinguished and identified.

2. LITERATURE REVIEW

This chapter will begin discussing the basic mechanical behaviour of fibre reinforced soils, followed by general Critical State framework that this study will use to assess the behaviour of all specimens. Findings from previous researchers are cross-compared and examined in an attempt to present a general background to the mechanical behaviour of fibre reinforced, natural and reconstituted clays against which the behaviour of reconstituted, reinforced, unreinforced and in-situ Lambeth group clay will be examined.

2.1 Established Techniques of Soil Improvement

In this section, a general overview of ground improvement techniques will be made, in order to acknowledge the available literature in the field.

Ground improvement methods can be divided into eight main categories where in this section, a brief description of each will be done, including the main application areas.

Densification

Munfakh (1997) summarised that granular materials are normally stabilized by densification. This will result in lower settlements, increased bearing capacity and liquefaction resistance. At the ground level, densification is achieved by surface compaction using conventional rollers. Where at depth, the densification is more difficult, special techniques and equipments are employed; among them are vibrocompaction, dynamic compaction, blasting and compaction grouting.

Consolidation

The most difficult problem encountered during excavation works is ground water level. The presence of water reduces the effective stress and consequently the shear strength. Certain techniques are available to control the ground water and to ensure an economical and safe construction system. Common consolidation methods are preloading, wick drains, electro-osmosis and vacuum consolidation (Steinberg 1998).

Weight Reduction

Munfakh (1997) reported that the weight reduction is another method of ground improvement control that involves the use of lightweight material in embankment construction to reduce the load on compressible soils. Such a method is commonly used on highways to provide a weight credit that reduces the settlement of the highway embankment, improving its stability against sliding and global failure. Common methods are wood chips, shell, slag, tyre chips, flowable fill and geofoam.

Reinforcement

Soil as a material does not have tensile strength unless it is bonded (residual soils). In order to improve strength in tension, reinforcing materials can be placed in the soil mass for improvement. Traditional techniques of soil reinforcement accommodate the use of continuous planar inclusions (e.g. geotextiles, geogrids and metallic strips) within earth structures. Such additions provide tensile resistance to the soil in a preferential orientation.

Chemical Treatment

Lime, Cement, fly-ash, silicate, asphalt and many other chemicals are used to stabilize weak soils. Such stabilisation chemicals offer increased strength and decreased compressibility, achieved via binding the soil particles together. In lime stabilization, Munfakh (1997) stated that an ion exchange reduces the soil's plasticity and improves its workability. The ion exchange is then followed by a chemical reaction that increases the shear strength. In surface stabilization, the chemicals are mixed with the soil with an appropriate amount of water, the mix is then compacted using conventional compaction equipment and procedures. When at depth, the chemicals are applied by injection, or by

deep mixing methods. Permeation, jet or fracture grouting, soil mixing and lime columns are a few of the well-known chemical treatment methods in use nowadays.

Thermal Stabilization

Carl (1999) stated that ground freezing and vitrification are two major thermal stabilization methods. Both heating and freezing can be used for ground improvement. Heating fine-grain soil to high temperatures can produce significant and irreversible property improvements, including a decrease in swelling and compressibility and an increase in strength. Frozen wet soil is much stronger and less permeable than the unfrozen soil, artificial ground freezing can be used for temporary ground strengthening, particularly for excavation support. Occasionally permanent ground-freezing applications are also used in permafrost areas where such application is costly exercise and used in specific projects only.

Electrotreatment

Electrokinetic soil remediation is an emerging technology that has attracted increased interest among scientists and governmental officials in the past decade. This method aims to remove heavy metal contaminants from low permeability contaminated soils under the influence of an applied direct current. Duncan et al. (2014) reported that the electrokinetic remediation or fencing, electro heating, and bioelectrokinetic remediation are well-known methods in this field of soil stabilization.

Biotechnical Stabilization

Biotechnical stabilization and soil bioengineering can be used to stabilize slopes against erosion and shallow slope failures. The biotechnical stabilization method consists of using live vegetation combined with inert structural or mechanical components, such as retaining structures, revetments and ground cover systems. For example, plants can be established in the front opening of gabion walls and cellular grids or on the benches of tied retaining walls. The vegetation and mechanical elements work together as an integrated system to provide erosion protection or slope stabilization (Carl 1999).

2.2 Basic Mechanical Behaviour of Fibre reinforced soils

Fibre content, length and aspect ratio are the factors causes improvement in the mechanical behaviour of soil. However, contribution of fibre has seen up to a limit in such factors mentioned above, where over such limit adverse effect have been observed in the mechanical behaviour of soil.

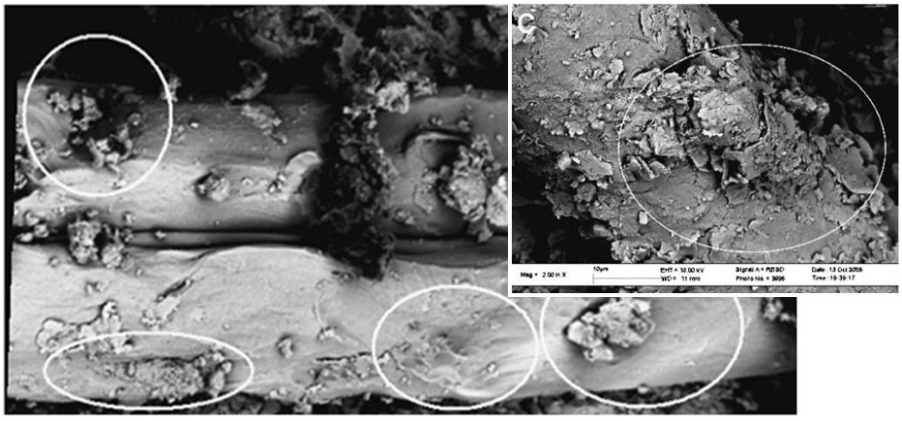

Figure 2-1. Pits and grooves formed on the fibre surface. (Tang et al. 2007)

Tang et al. (2007) stated that the improvement was due to development of tension in the fibres. In Figure 2-1 it can be seen that the fibre has many clay minerals adhered to its surface, exerting influence in the bond strength and friction between the fibre and the soil matrix. Authors claimed that the dispersed discrete fibres act as a spatial three-dimensional network (Figure 2-2) to interlock soil grains, help grains to form a unitary coherent matrix and restrict the displacement. The authors also reported that due to the interfacial force, the fibres in the matrix are difficult to slide and they are able to bear tensile stress, as the sketch in Figure 2-3.

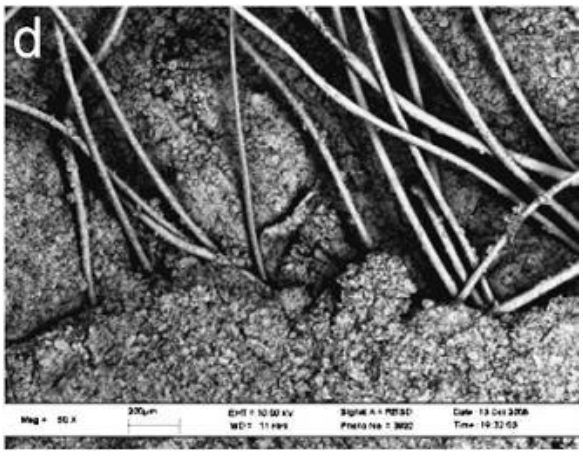

Figure 2-2. Fibre distribution in soil matrix (Tang et al. 2007)

However, the increase is nonlinear due to the variations in fibre orientation. After the upper limit is reached, shear strength decreases due the increase in the length, and aspect ratio of fibre. This decrease is due to lack of interlock of the soil particles where thereafter large displacement occurs and soil particles do not act as a single coherent matrix (Tang et al. 2007). Similarly, authors reported that beyond certain fibre content shear strength starts to reduce due the reduction in density, caused by the low specific gravity of the fibres.

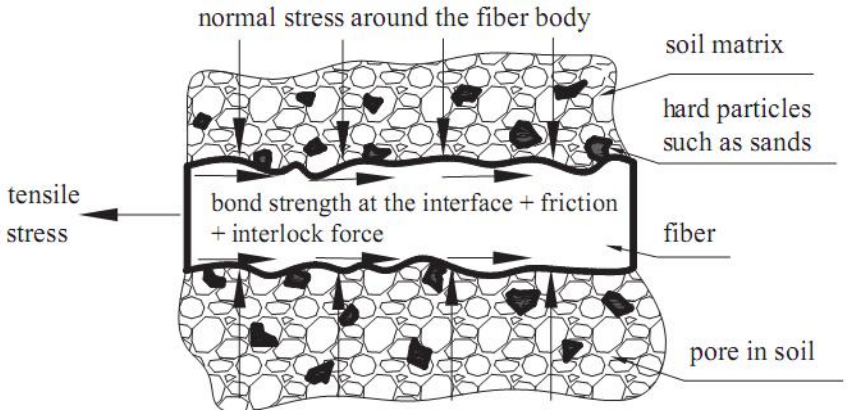

Figure 2-3. Sketch of mechanical behaviour at the interface between fibre surface and soil matrix.(Tang et al. 2007)

2.2.1 Compaction

Studies conducted by Miller & Rifai (2004) and Al-Tabbaa & Aravinthan (1998) on polypropylene-fibre-reinforced soils have shown that the addition of up to 1.0% of the weight of dry soil in fibres had a minor effect on the magnitude of the dry density or the optimum moisture content of the composite. (Figure 2-4)

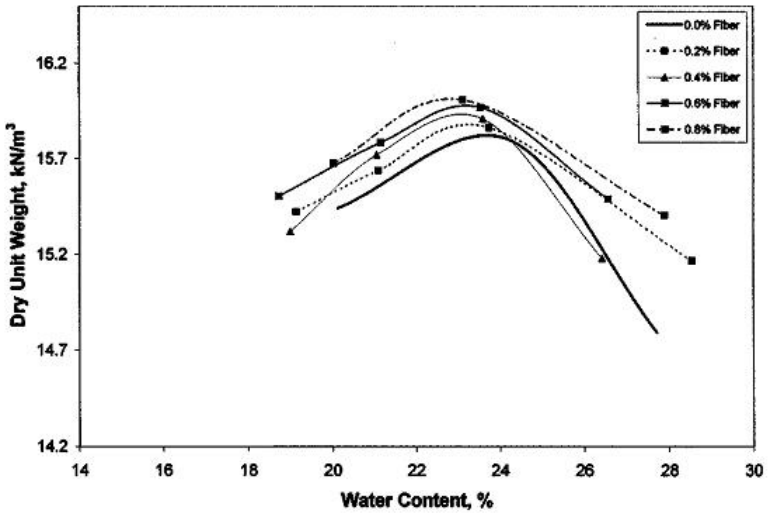

Figure 2-4. Compaction curves for various fibre contents Miller & Rifai (2004)

Furthermore Cetin et al. (2006) and Prabakar & Sridhar (2002) have reported that the inclusion of higher percentage of polypropylene fibres found to impede the compaction process. The authors prove that the inclusion of fibres reduced the maximum dry density and increased the optimum moisture content. This phenomenon can be seen in Figure 2-5.

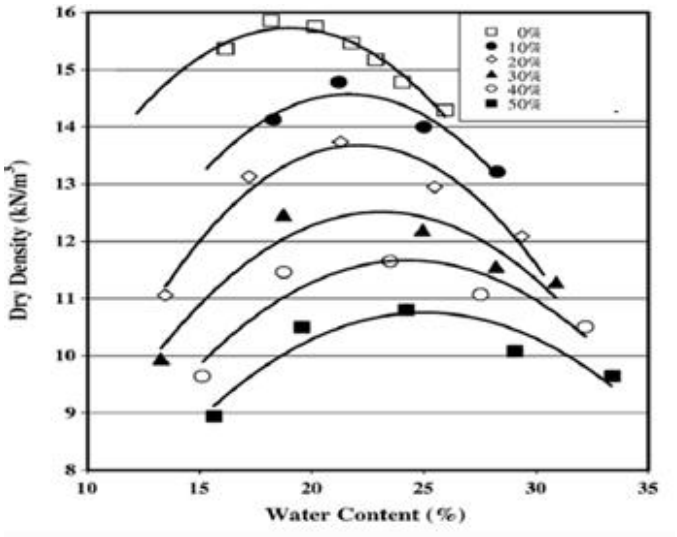

Figure 2-5. Standard proctor test curve for the clayey soil alone and tire-chips mixtures. (Cetin et al. 2006)

Investigators attributed the change in maximum dry density to the following factors:

- Fibres have a specific gravity at about 1 g/cm^3 whereas the soil particles have a value of about 2.7 g/cm^3. As the fibre content is increased, the low density fibres replace the high-density soil grains, resulting in a lower composite density.
- The presence of the fibres decreases the effectiveness of the compaction process at a given energy level, resulting in a lower dry density at a given moisture content.

Additionally, Wang et al. (2003) identified that, with the addition of fibres, more water is required to lubricate the soil grains during compaction, resulting in higher optimal moisture contents. Investigators Abdi et al. (2008) have also reported that an increase in moisture content reduces the contribution of fibres to the strength and ductility of the composite. This was attributed to the lubricating effects of water in reducing the load transfer between the clay particles and the fibres.

The results of a study by Wang et al. (2003) have shown that the reinforcing fibres impeded the compaction process and thus the increased the fibre content, had the same

effect as reducing the compaction effort. Furthermore, Kumar & Everett (2003) believed that the degree of compaction is one of the factors affecting the undrained strength of soils reinforced with fibres. Results of study presented in Figure 2-6 proves that, when the compaction degree is increased, the strength of soils reinforced with fibre is increased. Consequently, the tensile stress, acting against the mobilised tensile strength, is found to be primarily the fibres response to shear deformation. The authors concluded that the failure is a composite of slippage and yielding of fibres. In the researches of fibre-reinforced composites, they show only limited stretching and breakage so there is a possibly of slipping occurring between the fibres. Thus Kumar et al. (2006) believe that the chance of fibre slipping is more limited and is further controlled by the degree of compaction.

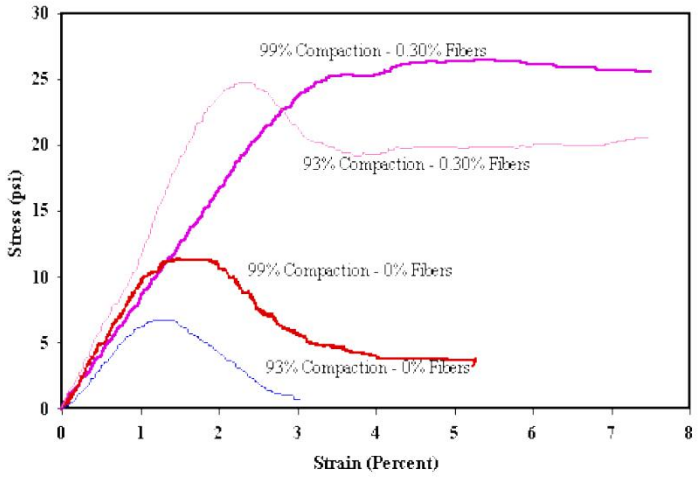

Figure 2-6. Comparison of increase in strength of selected samples (Kumar & Everett 2003)

2.2.2 Swelling

Punthutaecha et al. (2007) reported that expansive soils are relatively stiff and have high plasticity characteristics. Additionally, such soils experience contraction and expansion movements due to environmental and seasonal moisture changes. Furthermore, the authors reported that due to the very low confining stresses and higher moisture content changes, the expansive nature of the soil is most obvious near the ground surface. As a result, Steinberg (1998) reported that the soils tend to lift the infrastructure built on them, which can cause damage to structures, particularly light buildings and pavements. In some cases, much more damage is caused by swelling than other natural disasters, including earthquakes and floods.

Many researchers Mirzababaei et al. (2009); Abdi et al. (2008); Viswanadham et al. (2009); Cai et al. (2006); Loehr et al. (2000); Al-Akhras et al. (2008) and Punthutaecha et al. (2007) have investigated the effect of natural and synthetic fibres (the majority of them polypropylene) on the swelling properties of clayey soils. They concluded that the inclusion of fibres up to a certain percentage reduced the swelling pressure and the swelling potential of the clayey soils significantly (Figure 2-7). The authors also pointed out that, when soil swelling occurs, the flexible polymeric fibres in the soil are stretched and tension in the fibres resists the further swelling. The resistance offered by the fibres against swelling depends upon the soil-fibre contact area. Additionally Viswanadham et al. (2009) and Al-Akhras et al. (2008) conducted study on the swelling pressure of fibre reinforced clays where reported that addition of fibre reduces the swelling pressure compared to unreinforced specimen.

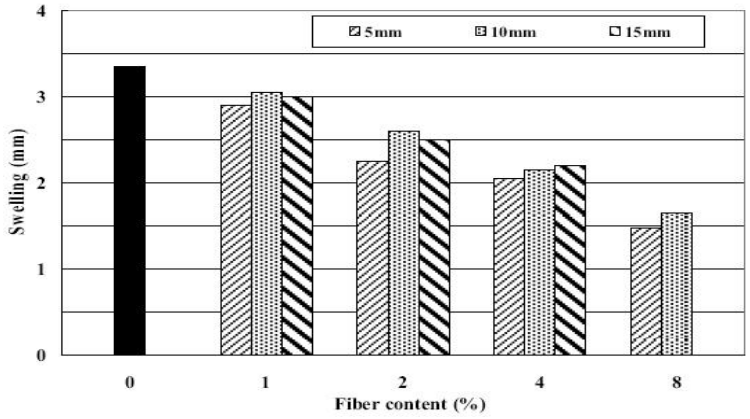

Figure 2-7. Variation of swelling with fibre content and length. (Abdi et al. 2008)

The major factors affecting the swelling properties are reported to be the moisture content of the composite, the fibre content and the aspect ratio of the fibres. Loehr et al. (2000) found that the magnitude of the swelling potential is much greater for specimens prepared on the dry side of the optimum moisture content than for specimens prepared on the wet side of the optimum moisture content (Figure 2-8). Whereas, studies conducted by Al-Akhras et al. (2008); Loehr et al. (2000); Punthutaecha et al. (2007) and Cai et al. (2006) suggest that a reduction of the swelling potential and pressure is more dependent on fibre content than moisture content. It has been proven by the above-named authors that swelling potential and pressure are reduced by the addition of up to 2% (dry weight of soil) of fibres; after such fibre percentage the swelling properties reach a plateau condition. Punthutaecha et al. (2007) explained that the

polypropylene fibres at higher dosage levels are difficult to compact and hence may have resulted in a larger void distribution in the fibre-treated soils. Such void distribution resulted in increased swelling properties comparable to those of untreated soils.

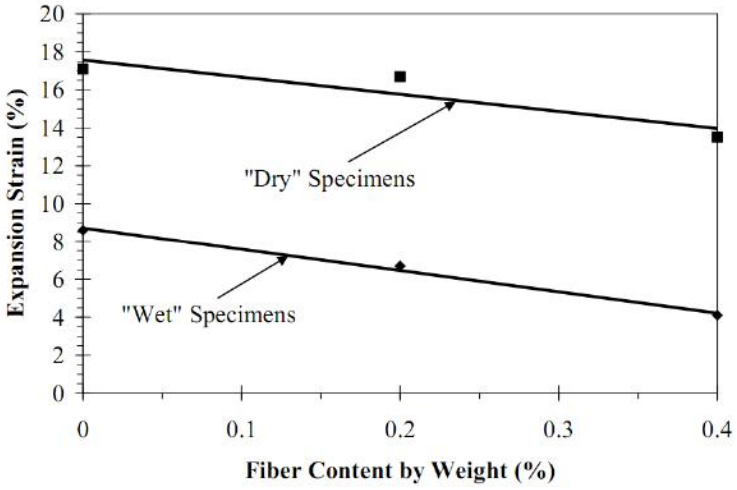

Figure 2-8. Maximum strain versus various fibre dosages for samples compacted both 2% dry and 2% wet of optimum (J.Bowders et al. 2000)

Similarly, Al-Akhras et al. (2008) expressed that the aspect ratio (l/b) is a factor which reduces the amount of swelling up to a certain ratio which, if exceeded, results in lower resistance to swelling (Figure 2-9). Authors added that, at higher aspect ratios of fibre, the fibre would be subjected to bending and folding, which reduces the contact area between the clay and the fibre, leading to lower resistance to swelling. Furthermore, similarly to high fibre content, compaction efficiency would decrease which will lead to higher swelling pressure and swelling potential.

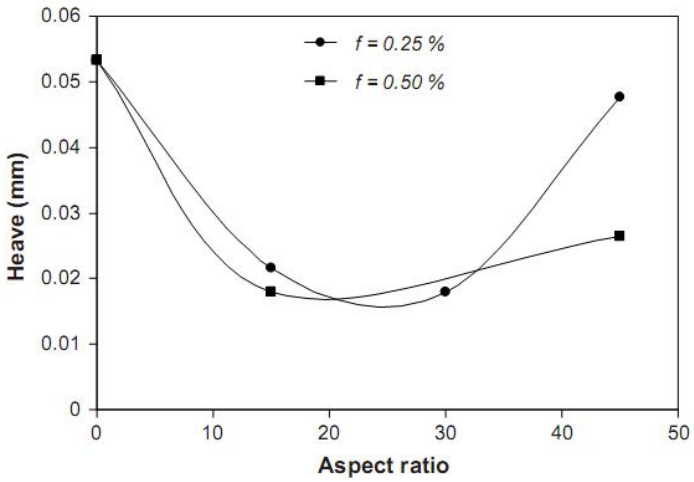

Figure 2-9. Variation of heave with aspect ratio (Al-Akhras et al. 2008).

In the same study, the authors claims that, when the reduction of swelling potential due to fibre addition is compared with other kinds of stabilizers such as ash, cement, lime etc; fibre addition has been found to swell significantly more than above named chemical stabilisers. Ikizler et al. (2009) believe that the low reduction in swelling pressures due to fibre treatment can be attributed to the presence of fibres which create drainage paths for the dissipation of pore pressure in loaded soil specimens.

2.2.3 Shrinkage Behaviour

Many earth structures, such as slopes and highway embankments, are constructed from clay soils. During the seasonal effects of drying and wetting, desiccation cracks are formed near the surface. As these cycles continue, water fills these cracks, increasing the depth of the cracked clay zone which may eventually reach 3m or more. A variety of research was done in order to eliminate or mitigate the desiccation cracking in soils. Albright et al. (2004) have considered the use of surface moisture barriers, placed above the soil layer to be protected. Moreover Omidi et al. (1996) and Vipulanandan & Leung (1991) have considered soil additives (lime, sand and cement) in order to increase the soil strength and resistance to cracking. However, based on the previous studies, the additives are not capable of suppressing the desiccation cracking of clayey soils with high water contents and other issues must be considered, such as the environmental impact of such additives.

In order to assess the effect of inclusion of fibres into clay, Abdi et al. (2008) and Miller & Rifai (2004) used a variety of testing programmes. Prior to shearing, some samples were compacted in a specific mould and the cracks were assessed after the samples were allowed to dry over a certain period of time (24 hours, 3 days or 30 days) while another set of samples were submitted to wetting/drying cycles. Observations of the cracks were done using two distinct methods. In the first method, Harianto et al. (2008) monitor the cracks with the naked eye and collect two types of data: volume change (height and diameter measurements) and surface cracking measurements. The data is recorded at the end of drying or at the end of the wetting period, depending on the testing programme. In the second method, Miller & Rifai (2004) recorded sample geometrical features by using digital imaging software where the crack dimensions are measured using the pixel information of the digital images. Harianto et al. (2008) and

Miller & Rifai (2004) used the data obtained via this method to develop a mathematical model to evaluate the magnitude of the desiccation cracks.

As illustrated in Figure 2-10 by Abdi et al. (2008) for specimens without fibres, a few wide cracks developed along the surface. For specimens of the same soil reinforced with fibres, the pattern changes and numerous cracks with smaller dimensions developed. The same authors have also revealed that the inclusion of fibre content, up to a certain percentage, significantly reduces the crack formation. Miller & Rifai (2004) and Tang et al. (2007) concluded that the inclusion of fibres in soil improve the tensile strength, reducing the crack formation. Moreover, the authors concluded that when local cracks appear in a reinforced specimen, the fibres going across these cracks go into tension, transferring these loads to the soil by friction. This effectively impedes further development of cracks and improves the toughness of the stabilized soil, by changing the failure mode of the soil. Fibre reinforcement can also mitigate potential cracking induced by differential settlements because fibre reinforcement increases the ductility of the soil.

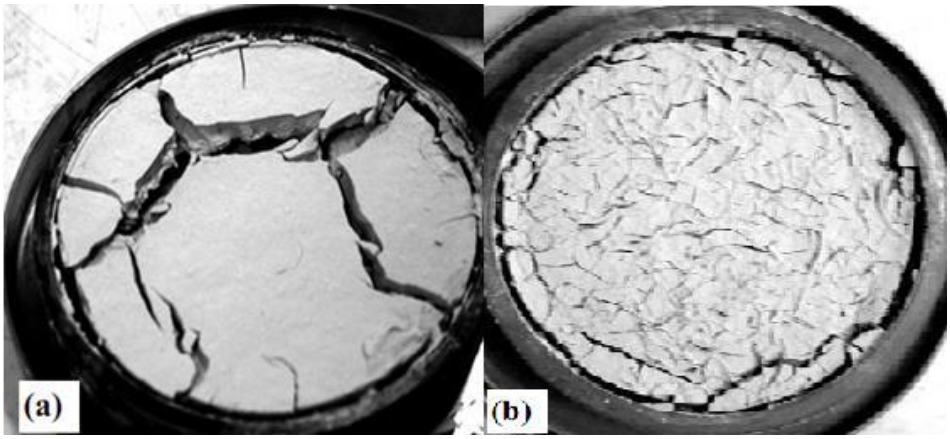

Figure 2-10. Desiccation cracking (a) Unreinforced sample (b) Reinforced sample (Abdi et al. 2008)

Shulley et al. (1997) and Ziegler et al. (1998) concluded that exceeding a certain percentage of fibre content was not practical due to the difficulty in mixing the materials to obtain a uniform distribution of fibres within the soil. They found that the inclusion of fibres over certain limits caused the development of voids during the compaction and encouraged crack development.

Miller & Rifai (2004) used the surface area of cracks occurred on reinforced and unreinforced specimens after dry-wet cycles to determine the crack intensity factor (CIF). Authors defined CIF as the percentage of the cracked area to the total surface area of the specimens. Additionally, authors introduced a factor called crack reduction(CR) factor to be able to compare soil-fibre mixtures. Crack reduction was calculated using the following equation:

$$CR = \frac{(CIF_n - CIF_F).100}{CIF_n} \quad 1$$

Where;

CIF_n = crack intensity factor for natural soil specimen in percentage

CIF_F = crack intensity factor for reinforced soil specimen in percentage

As can be seen in Figure 2-11 Miller & Rifai (2004) presented that fibre contents above 0.6% of the dry weight significantly reduced the crack reduction parameter of fibres. Additionally, the authors mentioned that when the reinforced soil was subjected to wetting/drying cycles, the effectiveness of the fibres was not as evident.

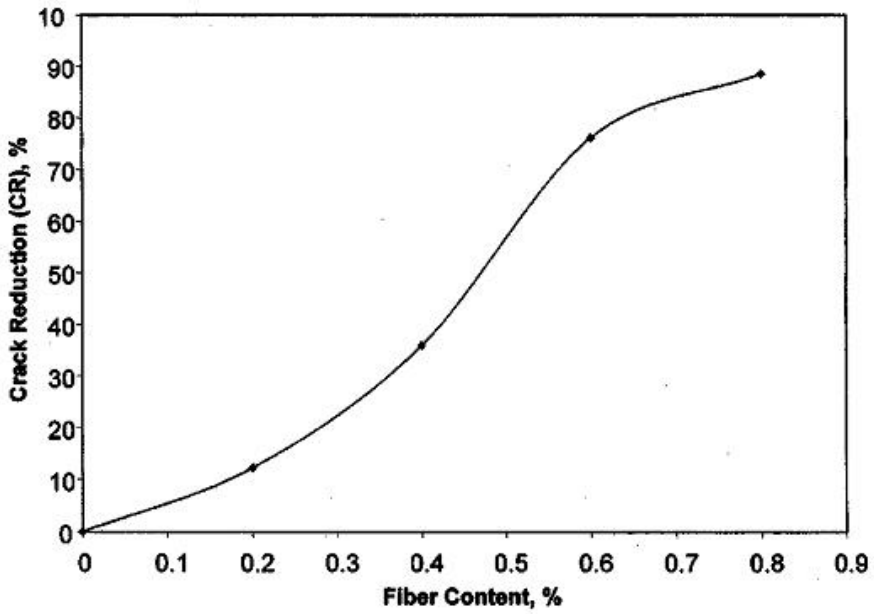

Figure 2-11. Crack reduction for various fibre contents (Miller & Rifai 2004)

2.2.4 Hydraulic Conductivity

Cedergren (1977) reported that the behaviour of stabilized soil under saturated conditions is greatly influenced by the drainage characteristics of the fill material used. Moreover Ahmed (1993) reported that a well-drained material will prevent the development of excess pore pressures during loading and also accelerates consolidation of underlying low-permeability strata, by providing a drainage path, thereby enhancing the stability of structures. Another function of compacted clay soil is in waste contamination. In such application, low hydraulic conductivity is important to reduce or eliminate the movement of contaminants or dangerous leachate; therefore, hydraulic conductivity is an essential information for many applications where fibres might be used for soil reinforcement.

In order to assess the effect of random fibre inclusion on hydraulic conductivity, investigators Miller & Rifai (2004); Maher & Ho (1994); Abdi et al. (2008); Özkul & Baykal (2007) and Cetin et al. (2006) conducted a variety of experimental programmes such as an ASTM hydraulic conductivity test on an odeometer, a flexible wall permeameter, a permeability test on triaxial equipment and a falling head method permeability test.

Although different types of reinforcement assessed in their study, the above-named authors all reported that hydraulic conductivity appears to be dependent on both the fibres' content and length, and permeability increases when these parameters increase. Such phenomena were explained by the authors, that fibres provide a drainage path for water to be drained out of the soil and as the fibre length and content increase, the drainage path increases and the water drains quicker. As can be seen in Figure 2-12, a study that supports the above theory, Abdi et al. (2008) conducted a hydraulic conductivity test on a kaolin rich clay soil, reinforced with polypropylene fibre, whom reported that such property is seen in low fibre content inclusions where at higher fibre contents length did not produce a significant effect on the hydraulic conductivity of the soil in respect to fibre length.

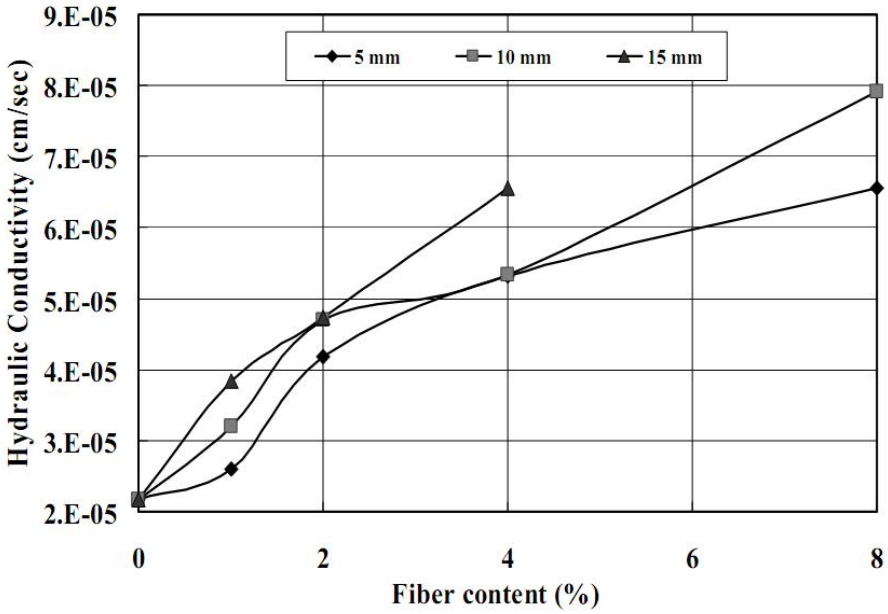

Figure 2-12. Effect of fibre content and length on hydraulic conductivity of samples (Abdi et al. 2008)

The results of various researches Miller & Rifai (2004); Maher & Ho (1994); Abdi et al. (2008) and Özkul & Baykal (2007) indicate that the fibre reinforcement can be used where low permeability and density are needed in exchange of weak foundation material. However, Cetin et al. (2006) disagree with the above statement and conclude that fibre-reinforced composite should not be used where drainage is necessary to prevent the development of positive pore pressures during the loading of fills under saturated conditions. They may, however, be used when mixed with high-permeability materials such as sands and gravels.

2.2.5 Alignment of Fibres

Özkul & Baykal (2006) studied the effect of compaction on composite materials and they showed that the ASTM Standard dynamic compaction process causes a preferential alignment of the fibres in a parallel direction to the compaction plane. Similarly, a study by Özkul & Baykal (2007) confirmed that the compaction process induces a preferential alignment of the fibres in the horizontal direction. This preferential alignment (±45 of horizontal) was found to be favourable for the improvement of shear strength because it does not coincide with the plane of maximum shear strain expected in a triaxial test. Correspondingly, Diambra et al. (2007) investigated the alignment of polypropylene fibres in sand. The samples were prepared using the moist tamping technique, which produces a soil-fibre fabric that resembles that of a compacted reinforced soil in the

field. The distribution was found to be far from isotropic: typically, 97% of fibres have an orientation that lies within ±45º of the horizontal plane.

Figure 2-13 presents the fibre length evaluation after isotropic compression tests conducted by Consoli et al. (2005). Authors determined the length of the fibres after an isotropic compression reaching 50 MPa, the results indicated that only about 20 % of the fibres retained their original length. The remaining of the fibres were reported to have broken into smaller length (~50%), or to have elongated (~30%).

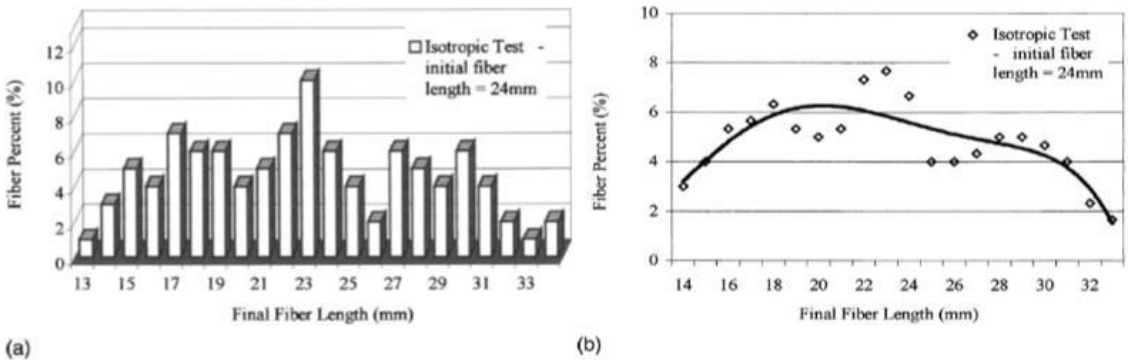

Figure 2-13. (a) Final fibre length after isotropic compression test; and (b)final fibre length after isotropic test-smoothed points (Consoli et al. 2005)

As can be seen on Figure 2-14, Silva Dos Santos et al. (2010) studied the behaviour of laboratory triaxial tests on quartzitic sand reinforced with polypropylene fibre and concluded that, at low confining pressures, the elongation shows that the fibres are still working in tension up to the end of shearing, so that their strength is still being mobilised at larger strains. Whereas shearing at high confining pressures caused breakage of the fibres to shorter lengths.

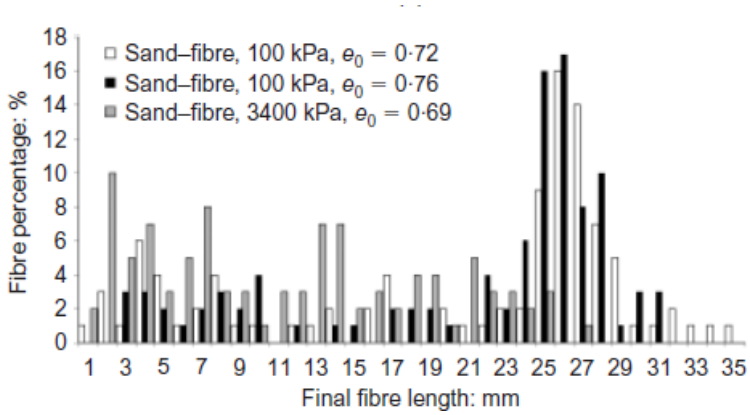

Figure 2-14. Evolution of fibre length under shearing low and high pressure tests (Dos Santos et al. 2010)

2.3 Critical State Soil Mechanics

As mentioned in the methodology (section 1.3), the main objective of this study is to understand "the mechanical behaviour of the fibre-reinforced soil in laboratory and in situ." Therefore, detailed fibre-clay interaction with a careful consideration of effects on clay peds will be studied to describe, interpret, and anticipate soil responses to various loadings. The framework used is essentially a theoretical model based on critical state soil mechanics – it is a critical state model developed by Roscoe et al. (1958). During this study, reconstituted, reinforced, unreinforced and in-situ Lambeth group clay tested on triaxial equipment will be analysed in the light of critical state framework.

Critical State Soil Mechanics (CSSM) is an idealization of soil behaviour. The CSSM captures the behaviour of soils that are of greatest importance to geotechnical engineers. The central idea in the CSSM is that all soils will fail on a unique failure surface in (q, p′, e) space. Thus, the CSSM incorporates volume changes in its failure criteria.

The CSSM is a tool used to make when predictions of soils response have to be done from changes in loading during and after construction. Although there is a debate on the application of CSSM to real soils, the ideas behind it are simple.

2.3.1 Basic Concepts

Most of the formulations in critical state models have been carried out in the conventional triaxial stress space (Figure 2-15) in order to confine attention to the conventional laboratory consolidation and triaxial test conditions. Khong (2004) stated that this would also enable a preliminary verification of the models. After the verification and validation processes, the models are generalized to the three-dimensional stress spaces.

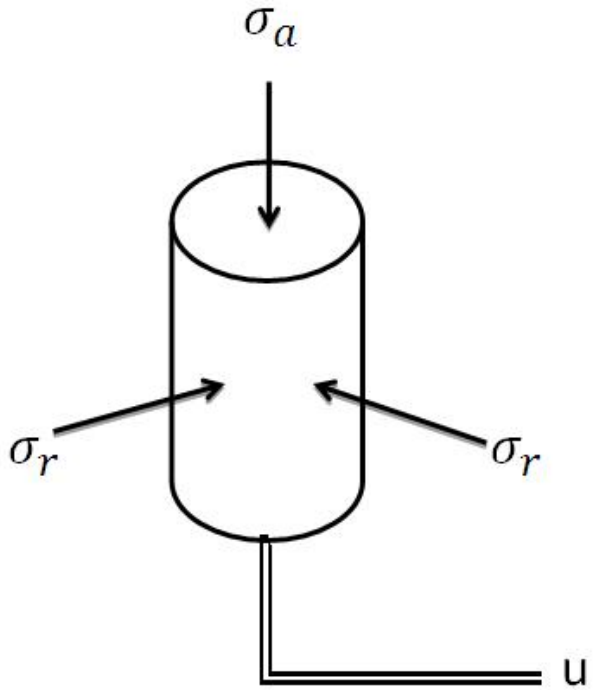

Figure 2-15. Conventional triaxial stress space

Three parameters are used to describe the (changing) state of soil samples in a triaxial test

These are:

- Mean effective stress

$$p' = \frac{1}{3}(\sigma'_a + 2\sigma'_r) = \frac{1}{3}(\sigma_a + 2\sigma_r) - u = p - u \qquad 2$$

- Deviatoric stress

$$q = (\sigma_a - \sigma_r) = q' \qquad 3$$

- Specific volume

Now $e = \frac{V_w}{V_s}$ and $w = \frac{V_w \gamma_w}{V_s G_s \gamma_w} = \frac{e}{G_s}$

Therefore $e = G_s w$ and $V = 1 + e = 1 + G_s w$

These three parameters (p', q and v) will vary during a triaxial test (v is constant for undrained test). The progress of a soil sample during a test can be represented by a

series of points describing a path in a three-dimensional space with axes p′, q and v. Different types of test (drained, undrained, compression or extension) will lead to different test paths in this (p′, q, v) space.

2.3.2 Soil Constants in Isotropic Compression (NCL)

In there extensive study of critical state framework Schofield & Wroth (1968) stated that in order to construct the critical state framework there are parameters which are soil constants. These fundamental parameters – N, Γ, M, λ, κ – can be measured in the standard triaxial test and/or can be obtained from other (conventional) geotechnical parameters. Typical values for particular soils are as follows (Table 2):

Table 2. Typical soil parameter values for particular soils (Diambra et al. 2007)

Soil Type	λ	κ	Γ	M
London Clay	0.161	0.062	2.759	0.888
Weald Clay	0.093	0.035	2.060	0.950
Kaolin	0.260	0.050	3.767	1.020
Glacial till	0.090	0.014	1.810	1.180
River sand	0.160	0.014	2.990	1.280
Decomp. Granite	0.090	0.005	2.040	1.590
Carbonate sand	0.340	0.003	4.350	1.650

In order to obtain soil constants N, Γ and κ, v or e against p’ or lnp’, graphs should be plotted with the data obtained either from the isotropic consolidation stage of a triaxial test or a one-dimensional consolidation test using an oedometer equipment (Figure 2-16).

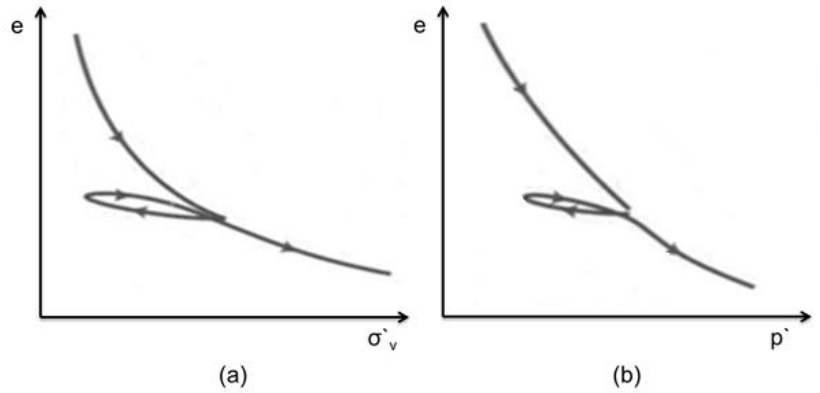

Figure 2-16. a) One-dimensional consolidation b) Isotropic consolidation tests

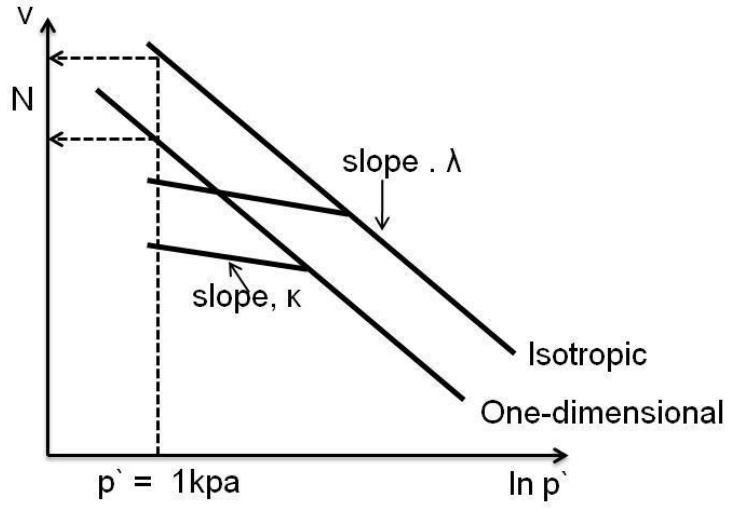

Figure 2-17. Schematic obtaining of soil parameters graphically

The normal compression line (NCL) obtained by compression of clay specimen from an initial state is plotted as linear in a semi-logarithmic scale of v against lnp'. The NCL line represents the following equation:

$$v = N - \lambda lnp' \qquad 4$$

The NCL forms the boundary to all possible states achievable by the soil. Any stress state to the left of the NCL has been reached by loading the specimen to a given stress (point on the NCL), then unloading (swelling) to the current state. Swelling lines are represented as straight lines in the semi-log plot v-lnp', and have the equation:

$$v = v_{\kappa} - \kappa lnp' \qquad 5$$

Deformations are assumed to be elastic on the swelling lines, also called unload-reload lines, while they are predominantly plastic on the NCL.

As can be seen in Figure 2-17, λ can be measured in the isotropic compression stage of a standard triaxial test by plotting data in v vs. lnp' and calculating the gradient which will give the λ. It is also related to the more conventional Compression Index Cc (measured by the oedometer) through a change of logarithm base:

$$\lambda = \frac{Cc}{2.303} \qquad 6$$

The soil constant N can also be measured in the isotropic compression stage by extending the line back to the specific volume axis, at p'=1 kPa on the v vs. lnp' graph.

Another soil constant, κ, can be measured in the unloading (swelling) stage of isotropic compression or one-dimensional compression. κ is the gradient of the swelling lines. It is also related to the Swelling Index Cs through a change of logarithm base:

$$\mathrm{K} = C_s/2.303 \qquad 7$$

2.3.3 The Critical State Line (CSL)

Soil will eventually reach a critical state by continuous shearing where further increase in shear strain will occur with no change in effective stress or volume. For example, in Figure 2-18, four specimens with different specific volumes, were sheared from the same stress, and they have monitored to reached the same critical state at large strains. The locus of all the critical state points for a given soil states a line in three-dimensional space, often referred to as Critical State Line. The projection of the Critical State Line in the q' vs. p' plane is a straight line equation:

$$q` = Mp` \qquad 8$$

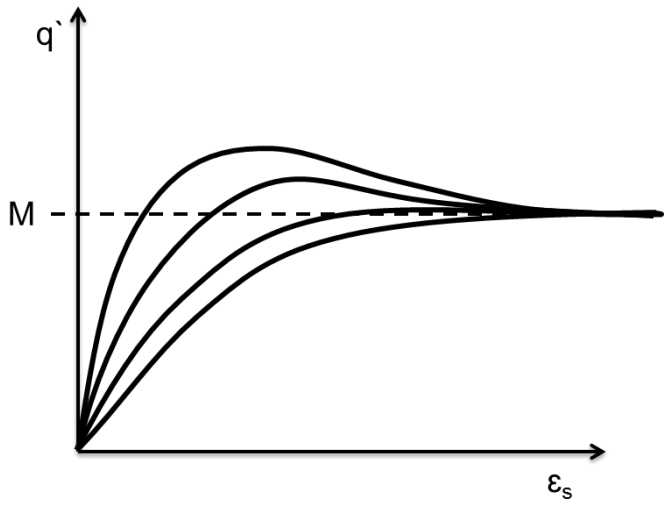

Figure 2-18. Schematic diagram of undrained triaxial tests stress-strain response

The projection of the Critical State Line in the v vs. lnp' plane is a straight line parallel to the Normal Compression Line, but lying beneath it; it is represented by the following equation (Schofield & Wroth 1968):

$$v = \Gamma - \lambda lnp` \qquad 9$$

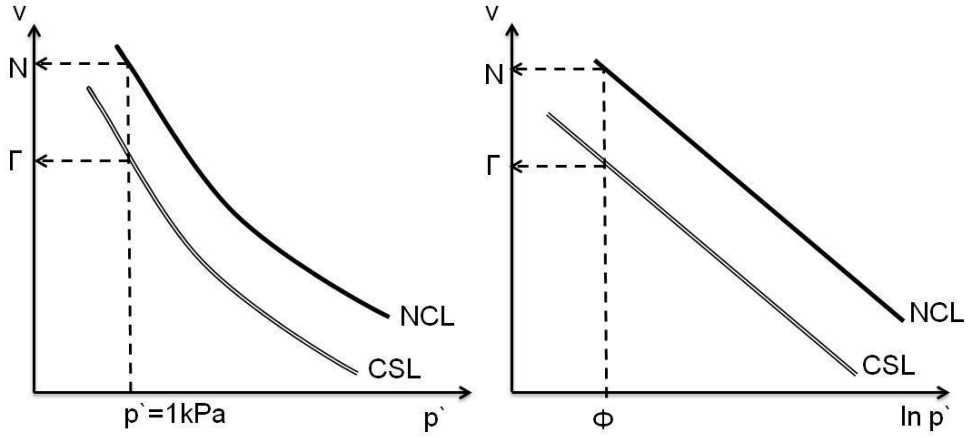

Figure 2-19. Obtaining critical state soil parameters

Soil constants N and Γ can be measured in the compression and shearing stages respectively, where the samples are taken to ultimate (critical state) conditions, and the data are plotted to v vs. p′ or lnp′ axes. Similarly, to NCL, the gradient of CSL is a soil constant, λ, and extrapolation to the specific volume axis at p′=1kPa gives the value of Γ (Figure 2-19).

2.3.4 Test Paths

The objective of drawing test paths is to find a way of combining the observed shearing behaviour of the clay into a coherent way. It is useful, at first, to discuss normally consolidated specimens, but the same ideas will be discussed for over-consolidated specimens in the following section.

Atkinson & Bransby (1978) discussed the basic principles of critical state soil mechanics where much of the evaluation about test paths in different testing conditions is a review of the authors' text. Therefore, individual contributions of authors which have led to the development of the critical state concept will not be referenced numerous times.

2.3.5 Undrained Shearing

For a better understanding of the test paths in undrained and normally consolidated clays, consider a symbolic set of undrained triaxial tests on isotopically compressed specimens, with each specimen being compressed to a different initial value of p′ and the samples which have been compressed to higher stresses exhibiting higher values of q′ at failure. The stress path followed by a family of such tests may be represented in the q′ vs. p′ graph illustrated in Figure 2-20a. At shearing stage the stress path started with the effective stress value (p′) which was obtained at the end of the isotropic consolidation stages (A_1,A_2,A_3) and followed a path which is specific for undrained tests on normally over-consolidated samples. The stress path continued its journey until it reached a critical state in which further shear strains can occur with no change in the effective stress or volume. These points are indicated as B_1, B_2, B_3 on Figure 2-20b. A best fit line on these final points will produce the critical state line on the q′ vs. p′ graph where the gradient of such line will give the critical state stress ratio, M

Translation of the path in the v vs. p′ graph can be seen in *Figure 2-20*b. Samples start out from the isotropic normal consolidation line (A_1, A_2, A_3) and travel to the left until points B_1, B_2, B_3 are reached and failure is considered to be reaching the critical state line. Test paths A1-B1, A2-B2 and A3-B3 follow a straight line, parallel to the horizontal axis, which indicates no specific volume change, which is due to the undrained condition of the testing. Therefore, the critical state criteria might be modified to constant pore water pressure for the undrained testing.

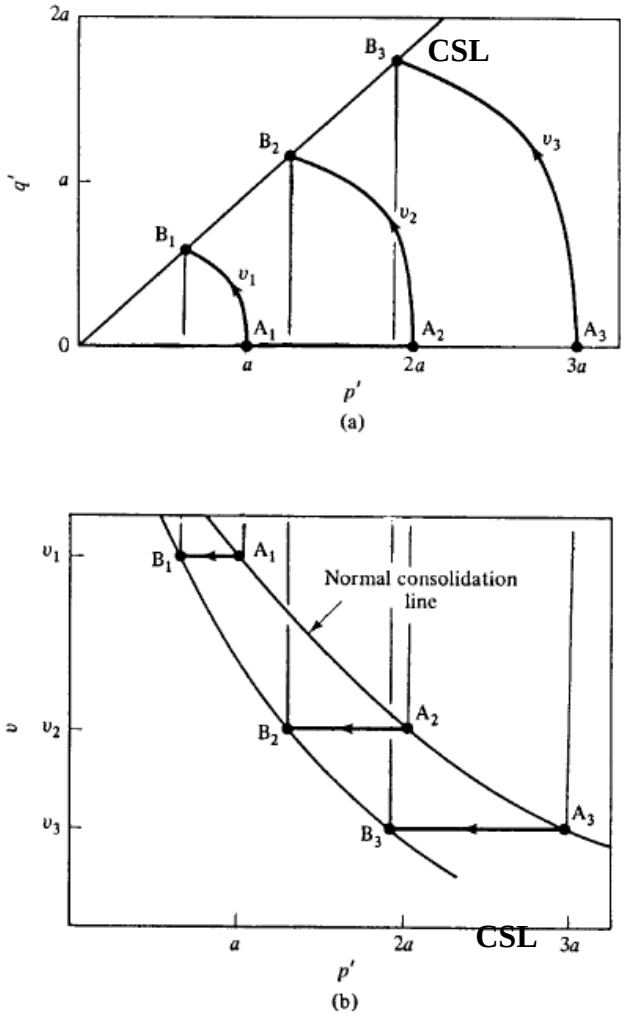

Figure 2-20. Stress paths in a) q′ vs. p' and b) v vs. p' graphs for undrained tests on normally consolidated samples (Atkinson & Bransby 1978)

2.3.6 Drained Shearing

The same concepts of constructing q′ vs. p′ and v vs. p′ graphs are followed on drained testing, where the stress paths show differences due to drained conditions. As expected, due to the dissipation of pore water pressure (no excess pore pressure build up), all the test paths are straight in q′ vs. p′ graphs (Figure 2-21a) and rise at a slope of 1 in 3, from the initial value p'_o of the mean normal effective stress, for each sample. The sample fails (i.e., there is no further change in stress, or volume, as large shear distortions occur) at values of q′ and p′ which define a straight line in q′ vs. p′ graph. The test paths are curved in the v vs. p′ graph, with each sample compressing as p′ increases. The failure points B1-B3 define a smooth curve which appears to be of a similar shape to the normal consolidation line (Atkinson & Bransby 1978).

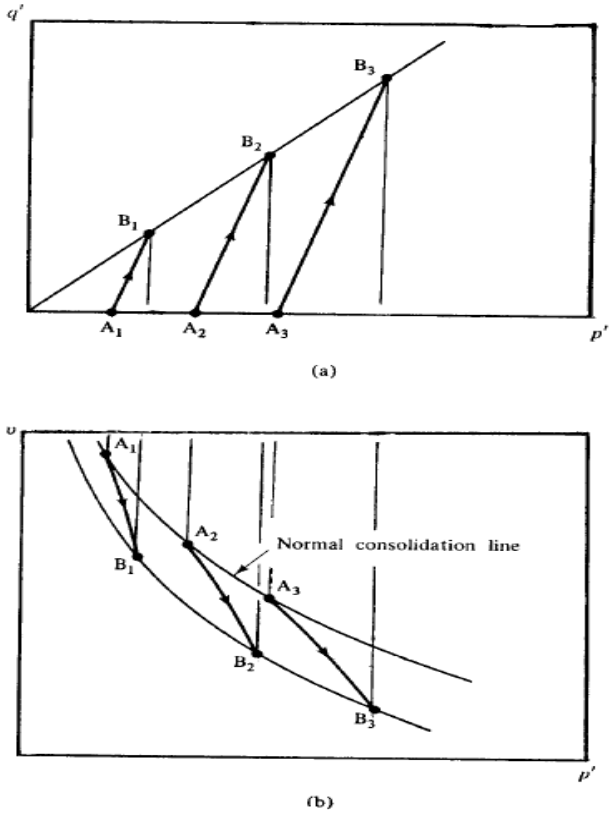

Figure 2-21. Stress paths in a) q′ vs. p′ and b) v vs. p′ graphs for drained triaxial tests on normally consolidated samples (Atkinson & Bransby 1978)

2.3.7 Drained and Undrained Shearing of Over-Consolidated Clay

Although over consolidated clay behaviour is more complicated than the normally consolidated clays, they can be analysed within the critical state concept. The characteristic of stress path for a heavily over-consolidated clay in a q′ vs. p′ space during a drained triaxial test is shown in Figure 2-22. Since σ'_r remains constant for a typically drained triaxial test,

$$\Delta q' = \Delta \sigma'_a \qquad 10$$

$$\Delta p' = \frac{\Delta \sigma'_a}{3} \qquad 11$$

And

$$\frac{\Delta q'}{\Delta p'} = 3 \qquad 12$$

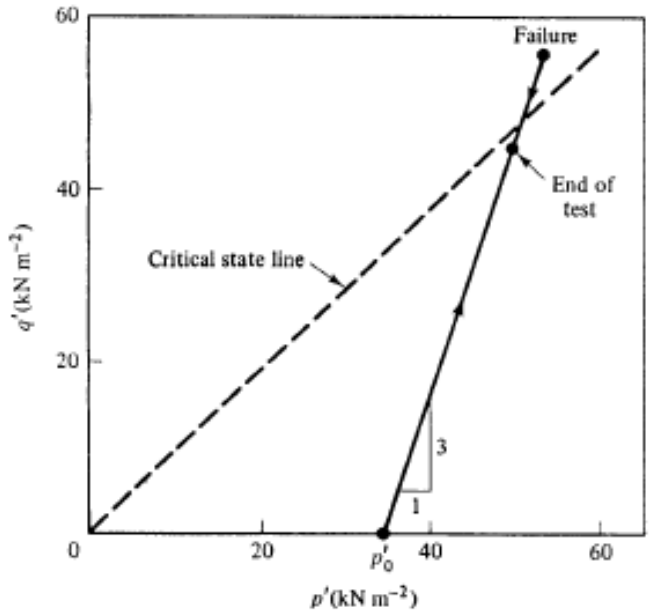

Figure 2-22. Stress path followed in a drained triaxial compression test on an over-consolidated clay (Atkinson & Bransby 1978)

The stress path for heavily over consolidated clays is identified by an increase in p′ and q′ until the peak strength is mobilized at stresses beyond those of the critical state line. After peak, a reduction of p′ and q′ towards the critical state line is followed. Consequently, for overconsolidated clays, the critical state line symbolises the "ultimate" strength.

2.3.8 Normalized Behaviour

Leroueil & Vaughan (1990) adapted an approach that has been widely used to compare the response of the natural soil to that of the corresponding reconstituted soil. In order to distinguish features of behaviour arising from structures from those related to change in state.

Previous sections of this chapter studied how two specimens sheared undrained from the NCL have the same response in terms of stress path and pore water pressure development, all differences between them being due to different stresses and specific volumes. In Figure 2-23b, three undrained tests are illustrated, starting from the NCL and travelling left towards the CSL. The stress paths are identical in the q′ vs. p′ and v vs. lnp′ plots, but of different sizes, because of the initial isotropic stress $p'_{e,}$ and, hence,

initial specific volume, are different for each test. However, by choosing axis that reflect the different stresses and specific volumes, a unique response could be obtained. This can be done by normalizing by a specific volume, by scaling the stresses or by dividing both p′ and q′ by p′e. A normalized plot in an undrained test can be seen in the full lines in Figure 2-23c (Baudet 2009). By doing so, normalized plots will allow different tests to be compared more readily and this provides the means of comparing drained and undrained tests.

The factor p'_e used, is simply the isotropic stress at the start of the shearing stage. In an undrained test, p'_e is constant throughout the test. However, p'_e changes during a drained tests, due to the volume changes in the sample. Nevertheless, it can be seen from Figure 2-23b (dashed lines) that the shape of each path will be the same for different values of v; each section could, therefore, be scaled down to the same form as that of the undrained tests in Figure 2-23c (dashed lines), by dividing the stresses q' and p' by the value of p'_e on the normal consolidation line at that specific volume. The parameter p'_e , the equivalent pressure, at any specific volume is, thus, obtained from Equation 4, on the NCL, as seen on figure Figure 2-24.

By using the current value of v at a particular time, p'e can be calculated as:

$$p`_e = exp[(N - v)/\lambda] \qquad 13$$

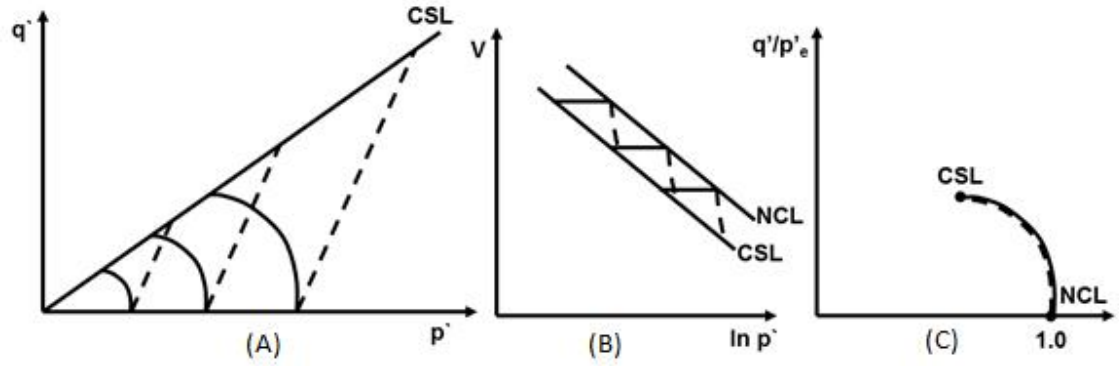

Figure 2-23. Schematic diagrams of drained and undrained triaxial tests (a) stress paths (b) volumetric response (c) normalized stress paths with respect to p_e' (Atkinson & Bransby 1978)

The procedure for obtaining p'_e value in a drained test can be seen in *Figure 2-24*. The current state of a sample is stated to be v_a , p'_a. The relevant value of p'_e for a sample in any state can be obtained by tracing a line at constant v from the current state (v_a, p'_a) to

the NCL and then reading the corresponding value of the mean normal stress to obtain p'_e.

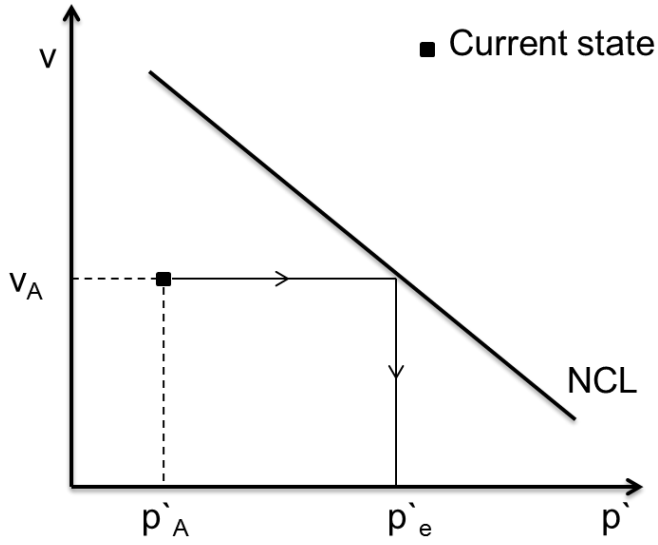

Figure 2-24. Method of obtaining the equivalent pressure p'e (After Atkinson & Bransby (1978)

Apart from the above traditional method of normalisation, researchers have adapted different normalisation methods due to the limitations such as requirement for higher stress testing or variation in initial specific volume on the critical state framework which are discussed in section 2.3.11 of this study.

In order to eliminate the influence of void ratio effect, Burland (1990) normalised the strength and the normal effective pressure by dividing them by the equivalent intrinsic pressure, σ_{ve}*. It can be seen from Figure 2-25 that the normalised failure surface for the intact clay lies slightly above the intrinsic Hvorslev surface. Such greater strength from a natural clay is attributed to microstructural effects by the author. Additionally, the author reported that the natural clay can exist in states well to the right of the intrinsic critical state line and Rendulic surface. Where this is a logical consequence of natural Sedimentation Compression Line (SCL) lying well to the right of the Intrinsic Compression Line (ICL).

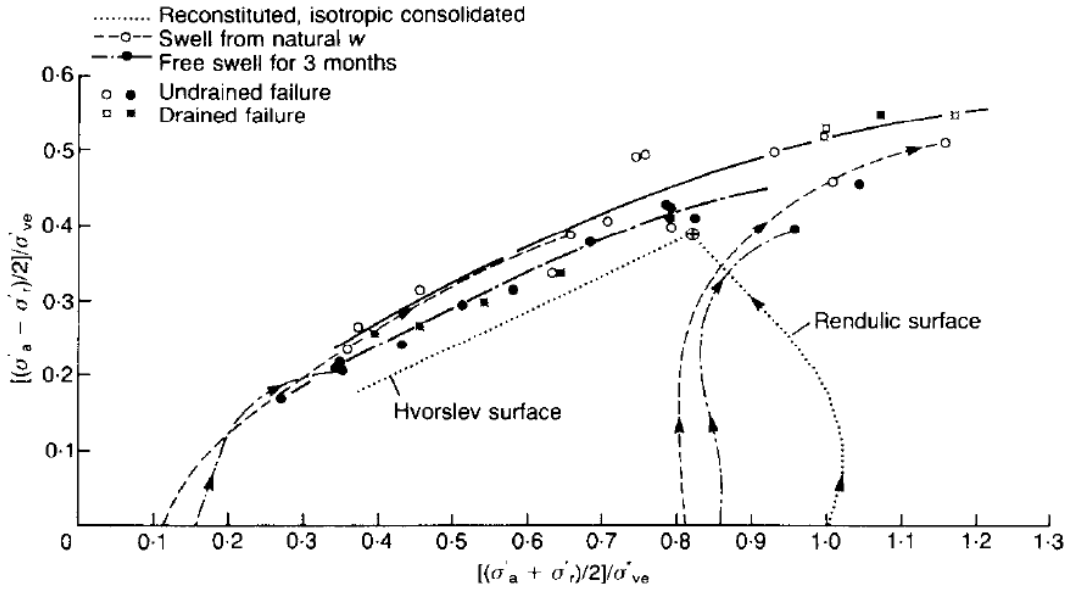

Figure 2-25. Todi Clay: results of triaxial compression test normalised by the equivalent pressure σve at failure (Burland 1990)*

In a study of cemented clays, Coop (2005) adopted a normalisation of triaxial shearing data with respect to an equivalent pressure on the CSL rather than the NCL (Figure 2-26) as in the case of an NCL, it could not be reached within the pressure capacity of the apparatus. It was reported by the author that the CSL of the cemented soil had a volumetric offset in the v:lnp` plane, lying higher than that of the uncemented soil and so the shearing behaviour of each soil has been normalised with respect to its respective (individual) CSL.

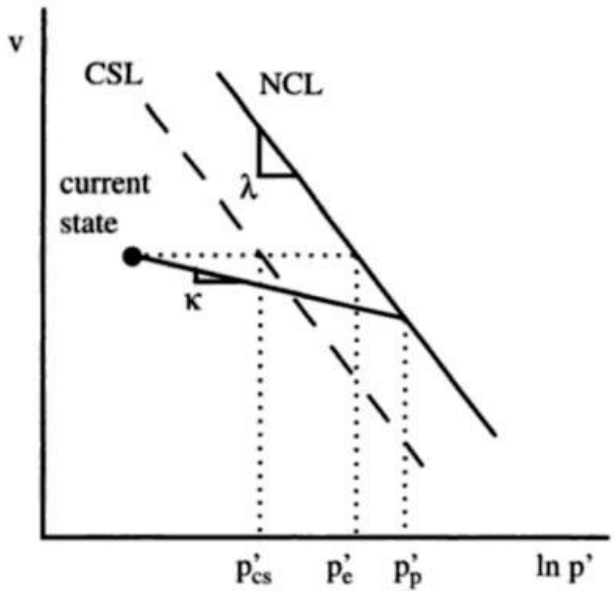

Figure 2-26. Definition of the normalising parameters (Coop 2005)

Ferreira & Bica (2006) used a group normalization method for a transitional soil from Botucatu sandstone. Tested soils were sampled from different areas located in the same quarry, each having a different void ratio, calculated from the sample dimensions, weight and moisture content. The mean values of the calculated void ratio for each block were 0.6, 0.66 and 0.7. Even though the soil was very similar, the authors assumed a family of parallel CSLs, depending on the above mentioned void ratio groups. Authors concluded that in order to apply the critical state framework to the transitional soils, the non-uniqueness of the CSL and the NCL must be taken into account.

Additionally Cuccovillo & Coop (1999) reported that normalizing triaxial data for shearing of structured soils with respect to the NCL and/or the CSL of the reconstituted soils have been very useful in highlighting, qualitatively, many features deriving from the soil structure. Nevertheless, such methods failed to provide a unified framework that could identify and fully describe mechanical features such as yielding, strength and a state boundary surface for structured soils.

2.3.9 Wet and Dry Side

It is convenient to distinguish between samples which lie below and above the critical state line. Schofield & Wroth (1968) reported that the samples above the critical state are referred to as being on the wet side of the critical state, and any sample falling into this category has a moisture content higher than a sample on the critical state line with the same value of p’. The second group of samples, below the CSL, are referred to as being on the dry side of the critical state (Figure 2-27). This classification is for grouping the samples together with similar pore pressure response and volume change behaviour.

The samples on the wet side of the CSL tend to contract while shearing. Therefore, during a drained test, the specific volume decreases while in an undrained test, positive excess pore water pressure is generated. At this side of the CSL, the ultimate strength is the critical state shear strength; in other words, the sample will fail at the CSL. Samples on the dry side of the CSL tend to dilate and will exhibit an initial reduction in specific volume, followed by a large increase after failure. The ultimate strength of a sample on the dry side of the CSL is the peak shear strength that is higher than the critical state

shear strength. However, after peak failure, the stresses will reduce until they are compatible with the CSL.

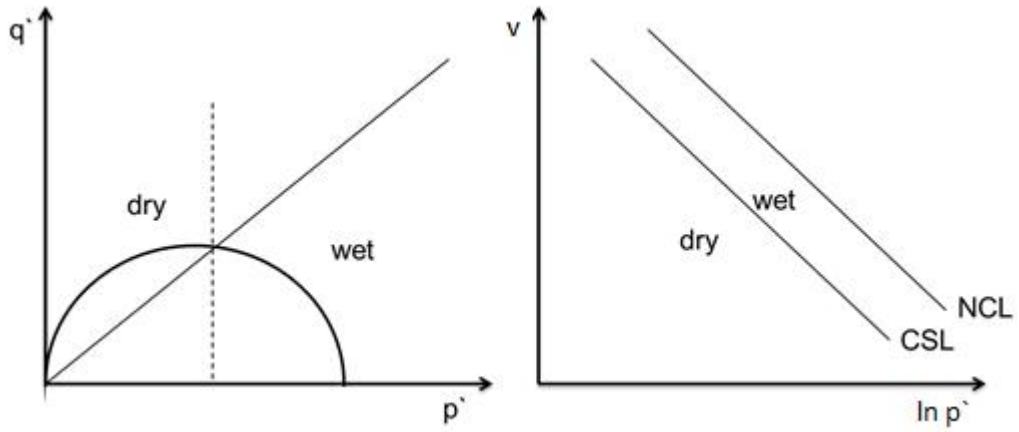

Figure 2-27. Schematic diagram of the dry and wet side of CSL

In order to determine the wet side of the state boundary surface(SBS), a normaly consolidated triaxial test is required, however this may be difficult for the case of stiff clays. Researchers Cotecchia & Chandler (2000) adapted high-pressure triaxial testing and identified the wet side of the SBS of stiff clays. However in their study, Gasparre et al. (2007) emphasized that Cotecchia & Chandler (2000) tested clay samples which had better-defined gross yield points in compression than London Clay. Additionally Gasparre et al. (2007) highlighted that only a limited number of high-pressure tests were conducted on the London clay due to the trend seen in the K_0 and isotropic compression tests indicating a very high pressure would be required to define the wet side of the intact SBS. Likewise a study by Hosseini Kamal et al. (2014) on UK stiff clays suggests that construction of the wet side of the boundary surface would require testing with confining stresses in tens of MPa and added that a unique boundary surface could only be interpreted if the compression path become either parallel to the intrinsic normal compression line or converge to it. More importantly, authors added that even reaching high pressures for such clays, identification of wet side of boundary surface would largely depend on the degree of curvature of the ICLs at extremely high pressures. Where, at such high pressures, the type of the normalisation of the shearing data that has been used may become invalid as the CSL, as well as the one-dimensional and isotropic ICLs, converge at zero void ratio.

2.3.10 State Boundary Surface

The state boundary space is constructed from all the effective stress paths for normally consolidated clay, lightly consolidated clay, over-consolidated clay and heavily over-consolidated clay at different initial stress states and different test conditions (drained and undrained).

Figure 2-28 illustrates the completed space of the state boundary. The wet side of the CSL is constructed with normally consolidated and/or lightly over-consolidated clays that exhibit an increase in stresses until reaching the Critical state. The surface defined when shearing all normally consolidated samples is known as the Roscoe surface. Roscoe surface is identified by the stress paths of normally consolidated and/or lightly over-consolidated clays.

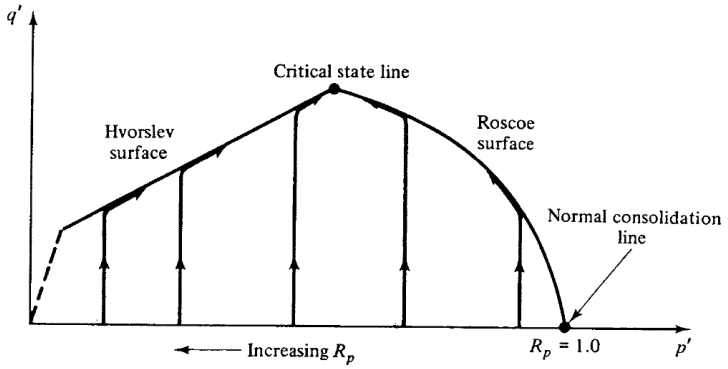

Figure 2-28. Representation of anticipated undrained tests paths for samples at different consolidation ratios (Atkinson & Bransby 1978)

In contrast, the dry side of the CSL is a straight line that is defined by the peak failure surface, called the Hvorslev surface, for heavily over-consolidated clays. After reaching this surface, the stresses tend toward the critical state line as shown in Figure 2-28 for undrained triaxial tests. It can be seen that the Hvorslev and Roscoe state boundary surfaces intersect at the critical state line. These surfaces can be better visualized in a 3D plot of q′ vs. p′ vs. v space, as in Figure 2-29.

The possible stress condition for a given soil are restricted by the tensile failure, Roscoe and Hvorslev surfaces. Likewise, the CSL defines the state of stress at which further changes of p′, q′, or v cannot occur (Boots M 1986).

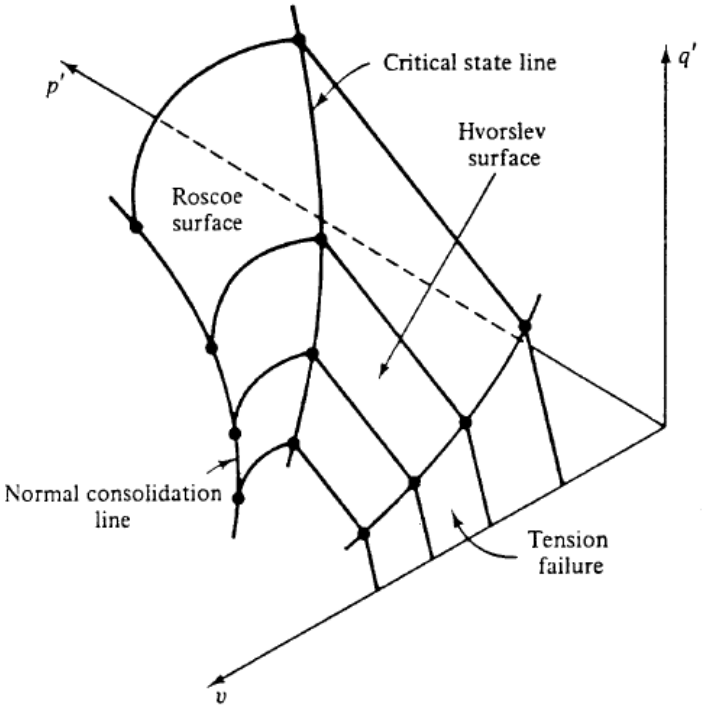

Figure 2-29. The complete state boundary surface in three dimensions q′ vs. p′ vs. v graph (Atkinson and Bransby 1978) (Atkinson & Bransby 1978)

Gens (1982) reported that the undrained effective stress paths followed by reconstituted sandy clay (Lower Cromer Till) samples, consolidated at different $\sigma`_1/\ \sigma`_3$ or t/p` ratios, did not collapse onto a unique SBS, when normalised by the Hvorslev equivalent pressure p`e (Figure 2-30). Instead, the normalised stress paths generate a series of Local Bounding Surfaces (LBS).

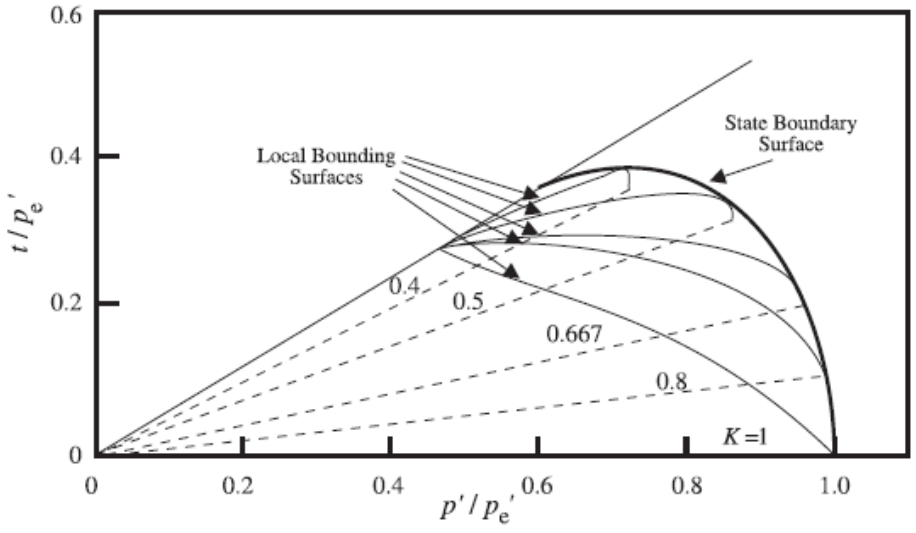

*Figure 2-30. Normalised undrained stress path for triaxial compression tests of samples consolidated at different values of K (*Jardine et al. 2004)

In the original text, Gens (1982) used the term Normalised Stress Path (NSP) rather than the Local Bounding Surfaces. This term was later introduced by Jardine et al. (2004). These authors summarised LBS as a boundary surface that exists within the more extensive State Boundary Surface (SBS), which provides the outermost boundary between permissible and non-permissible normalised effective stress states.

Jardine et al. (2004) stated that the $\sigma`_1/\ \sigma`_3$ or t/p` ratio experienced during consolidation defines each LBS seen in Figure 2-30. Furthermore, the LBS forms a surface that undrained static or cyclic tests (on samples that had experienced the same consolidation history) could not cross. The authors also stated that drained tests could cross the LBS and progress towards the SBS. Furthermore, authors observed that under such conditions, the specimens responded with a clear yielding and developed relatively larger shear and volumetric strains.

2.3.11 Limitations of the Critical State framework

The critical state framework can be satisfactorily applied to normally consolidated and lightly over-consolidated soils, where strains harden to a critical state. However, in heavily over-consolidated soils, which usually dilate, strains tend to localise (due to heterogeneities in the specimen), typically forming a shear band where high strains are concentrated (Figure 2-31).

When a shear band forms, even though the overall volume of the specimen does not change, water can be drawn from the rest of the specimen towards the shear band causing the soil within the shear band to dilate and soften (Figure 2-31).

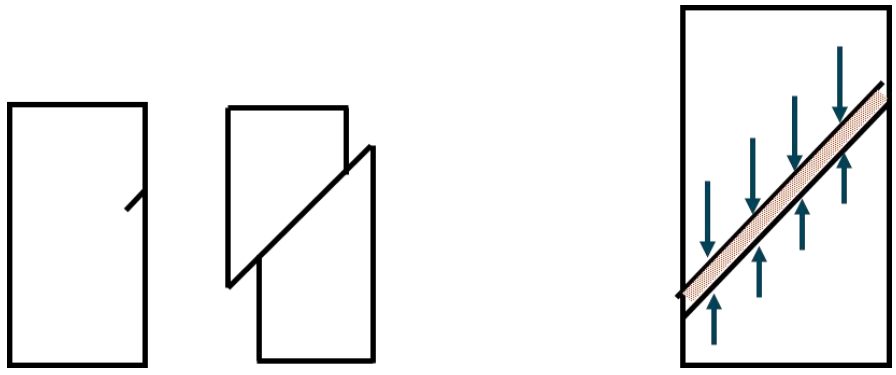

Figure 2-31. Schematic diagram of the effect of localization on an undrained stress path (Baudet 2009).

Similarly, Desrues et al. (1996) investigated shear band formation and concluded that when a samples fails by localisation, the void ratio achieved within the shear band is different than the global void ratio. Where the global void ratio is calculated based on global measurements; this gives rise to a significant doubt about the location of the critical state line in the v:lnp` plane, in the lower stress range.

Another limitation of critical state framework is highlighted by Coop (1999). Where the author attributes the curvature of the CSL, at low pressures, to incomplete experiments (Figure 2-32). According to the author, the overall shear strain required for a true critical state to be reached can be higher than the values reached by triaxial cells (around 25%). This means that soil would not reach its Critical State, leading to an incorrect identification of the CSL location.

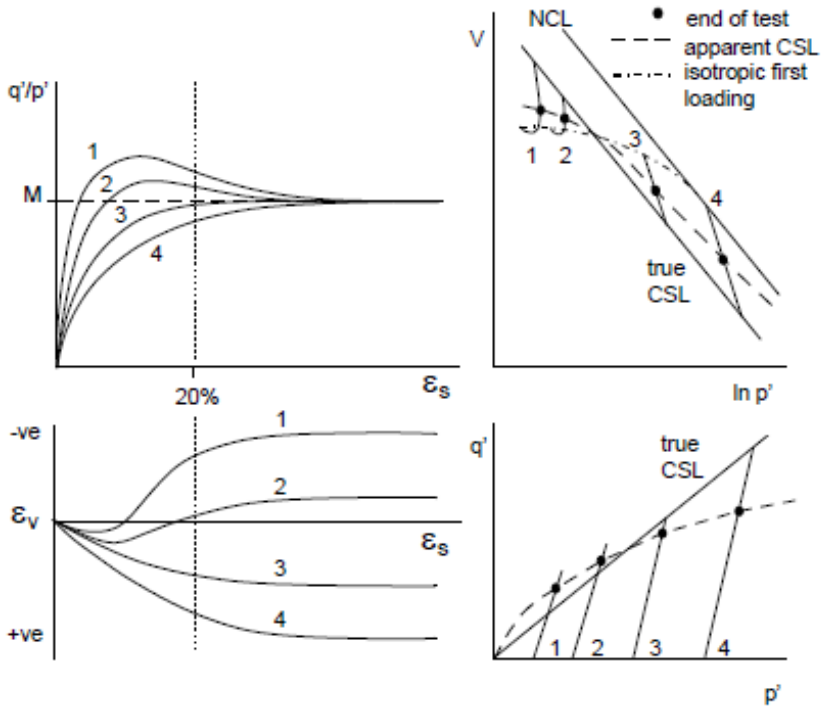

Figure 2-32. Effects of incomplete testing on the identification of the CSL (Coop 1999)

Coop (2015) presented the limitations of the Critical State Framework applied to the behaviour of natural and transitional soils. The author concluded that, at constant volume and stress, different specific volumes can only be maintained by different fabrics. Therefore robust fabrics (natural or reconstituted) will cause a dependency of

the final state on the initial specific volume, the main characteristic of transitional behaviour. The author also stated that, if the requirement to have a unique fabric can be disregarded, each initial state will give a unique normal compression line, critical state line and state boundary surfaces, where conventional soil mechanics can be applied accordingly.

2.4 Compression Behaviour

2.4.1 One-Dimensional compression

The common practice in order to define the effect of structure on the behaviour of a soil is to compare the mechanically altered soil with the same soil in a reconstituted state.

Terzaghi (1944) defined sensitivity, S_t, as the ratio between the undrained strength of the undisturbed clay and the undrained strength of the remoulded clay at the same void ratio. The sensitivity is generally considered as the parameter symbolizing the differences of the microstructures of the natural and the reconstituted clays. Since Terzaghi (1936), it has been noticed that fissured clay soil possesses reduced strength properties when compared with unfissured ones, and are consequently more prone to instability. (e.g. Fearon & Coop (2002); Cotecchia et al. (2006); Vitone & Cotecchia (2011))

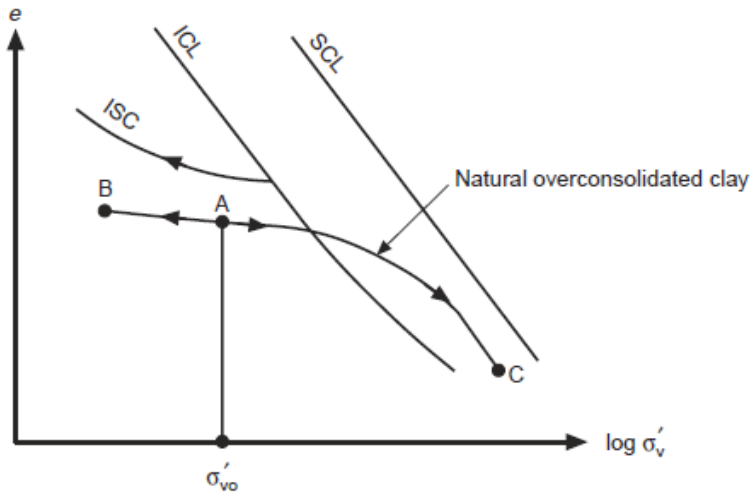

Figure 2-33 Compression and swelling of a natural over-consolidated clay (Burland et al. 1996)

It was noted by Burland et al. (1996) that, when an undisturbed sample of heavily over consolidated clay is compressed in an oedometer, the compression curve usually crosses the ICL (Intrinsic compression line) and then curves downwards, towards the ICL, as the soil structure breakdown begins to take place. This is shown by the line AC in Figure 2-33. Hight et al. (2007) plotted intact and natural sample data on Figure 2-34 and concluded that the yield of the natural London Clay is poorly defined, with compression paths that continue to diverge from the ICL even at higher stresses. Authors reported that the seen phenomena of the intact and reconstituted samples at high stresses may be a reflection of the clay aggregates in the natural clay, which are more easily broken down by the reconstitution process than by one-dimensional compression to high stresses.

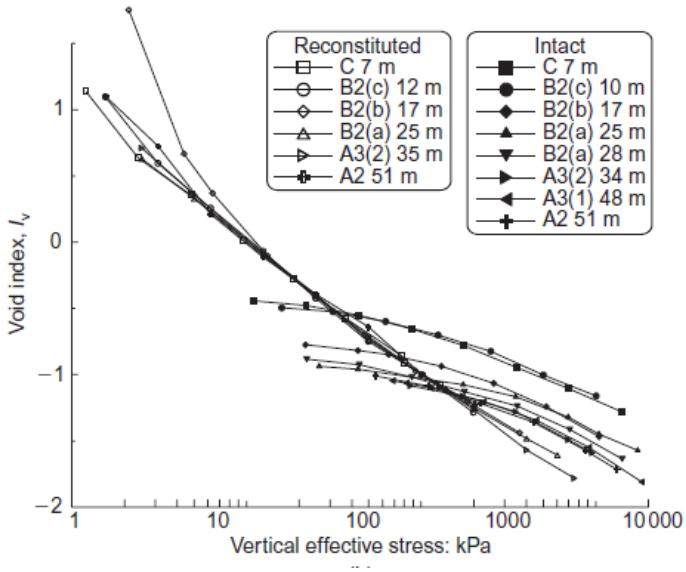

Figure 2-34. One-dimensional compression of reconstituted and intact London clay void index (Hight et al. 2007)

Additionally, as can be seen on Figure 2-35, in their extension of the sensitivity framework for fissured clays, Vitone & Cotecchia (2011) proposed that specimens with a high to very high fissuring intensity would yield before reaching the ICL, while un-fissured clays would yield outside of the ICL. In a similar research in London clay Hight et al. (2007) reported that the location of the intrinsic compression, in the e-σv` space, vary with the unit of the sample being tested; the more plastic units lying above those from slightly less plastic constitution. Additionally, the authors concluded that the slope of the intrinsic compression is scattering around the similar means for all units.

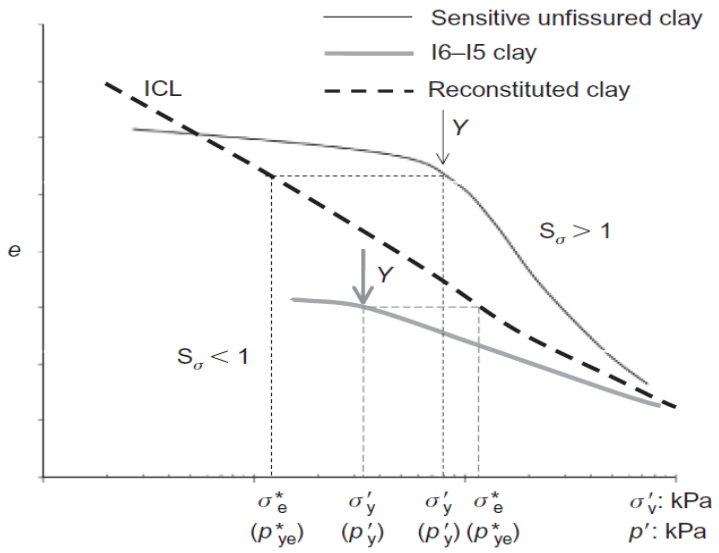

Figure 2-35. Compression behaviour of clays of different structure: either un-fissured, sensitive or reconstituted, or of fissuring intensity I5-I6 (Vitone & Cotecchia 2011)

Cotecchia & Chandler (2000) introduced the parameter $S_\sigma=\sigma`_y/\sigma^*_e$ (where $\sigma^*_e$ is the equivalent pressure on the ICL and $\sigma`_y$ is equivalent pressure, taken on the ICL for the void ratio of the natural clay at gross yield), defined as the stress sensitivity ratio, to quantify the influence of microstructure on the size of the gross yield pressures. Additionally, authors presented in Figure 2-35 the one-dimensional compression behaviour of clays with very high fissuring intensity to undisturbed clays, either sensitive or reconstituted. Authors reported that S_σ values higher than 1 were found in natural un-fissured clays and attributed to the natural microstructure of the soil. Whereas as can be seen in Figure 2-35 S_σ values found to be lower than 1 for very high fissuring intensity clays. Therefore, authors concluded that the combination of fissuring with the clay microstructure is found to weaken the clay by comparison with the reconstituted soil, irrespective of the microstructural features.

2.4.2 Isotropic compression behaviour

As can be seen at Figure 2-36 Consoli et al. (2005) studied the behaviour of polypropylene fibre-reinforced sand under isotropic compression and observed that the inclusion of fibres into sand can change isotropic compression behaviour. Authors also identified two distinct and parallel compression lines for the fibre-reinforced and non-reinforced sand.

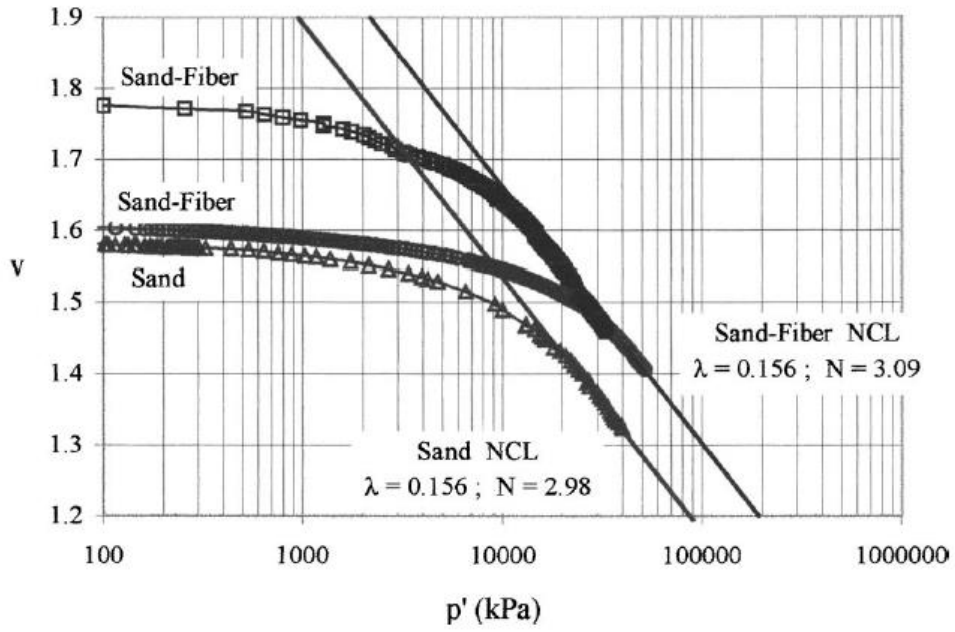

Figure 2-36. Isotropic compression data for sand and fibre-reinforced sand (Consoli et al. 2005)

Similarly, Silva Dos Santos et al. (2010) assessed the behaviour of the Osorio sand and a fibre-reinforced soil, concluding that, in the volumetric space, the NCL of the sand-fibre material is parallel and lies above that of the Osorio sand (Figure 2-37).

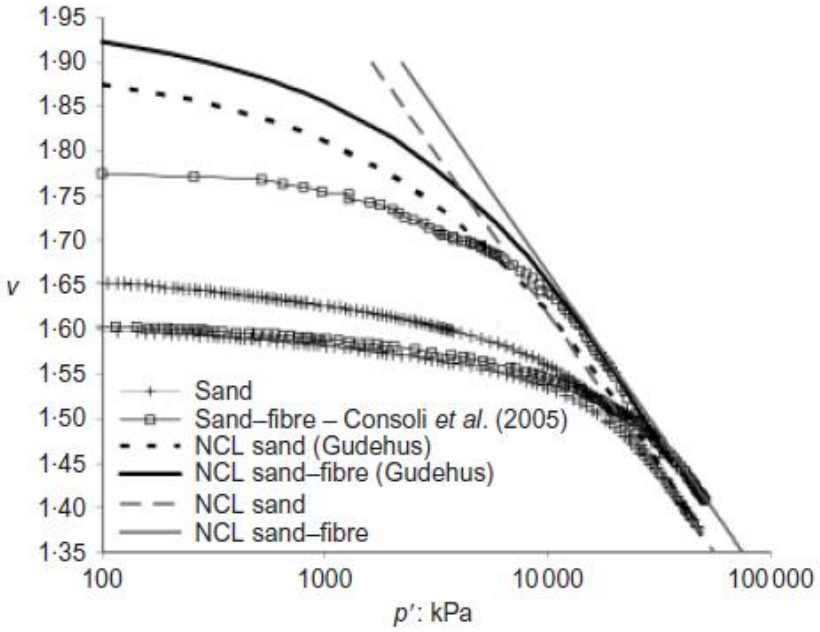

Figure 2-37. Isotropic compression data and NCLs for sand and fibre-reinforced sand (Dos Santos et al. 2010)

Beside one-dimensional compression behaviour of two scaly clays, Senerchia (SE) and Santa Croce di Magliona (SCM), Vitone & Cotecchia (2011) also studied the isotropic compression of these soils. These authors reported that the state that define the isotropic compression line of the natural scaly clay (INCL) plot on the left of the intrinsic normal compression line (INCL*). Additionally, as can be seen in Figure 2-38, the mild curvature of the isotropic compression curves of the scaly clays makes the gross yielding unclear. The authors also observed, during undrained shearing, the generation of positive excess pore water pressure; this can be seen on samples P8/11-2 and P5/3-2 on Figure 2-38; and SC8-70 on Figure 2-39. Where such phenomena confirms the contractive nature of the response to shear of the scaly clay. Moreover, such behaviour confirms the contractive nature of the scaly clay during shearing, and also confirm that isotropic gross yielding(Y) of the scaly clay occurring at the left of the NCL*, where Y, in Figure 2-38, has $p`_y$ =1200-1500kPa for the SE clay and 1000kPa for the SCM clay. It can be observed on Figure 2-38 and Figure 2-39 that the gradient of the isotropic compression line of the natural samples, λ, are smaller than the intrinsic compression line, λ*. Cotecchia & Chandler (2000) presented that values of S_σ > 1 depends on the sensitivity of the natural clay (the sensitivity framework). Also, for these clays S_σ decreases with compression post-gross yield (λ> λ*) as a result of microstructure weakening (destructuring).

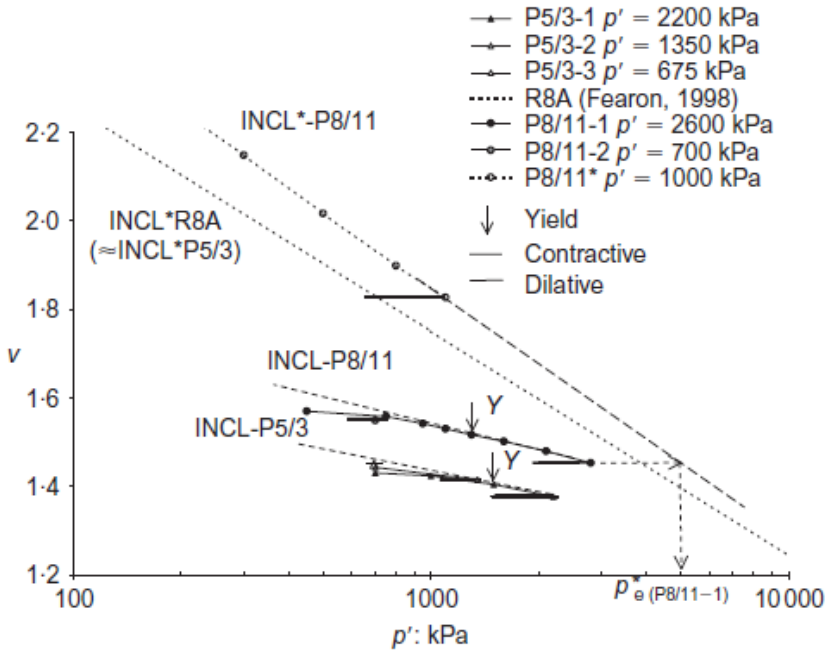

Figure 2-38. SE scaly clay: isotropic compression and undrained shear state paths followed by natural and reconstituted specimens (Vitone & Cotecchia 2011)

In summary, the results of the isotropic compression behaviour obtained by Vitone & Cotecchia (2011), combined with the general literature for unfissured clays, lead to the general compression behaviour frame work for clays shown in Figure 2-35, for one-dimensional compression. Therefore, the same framework can be applied to different constant stress ratio compressions ($q/p` \geq 0$) of clays whose fissuring structure vary from micro to meso scale.

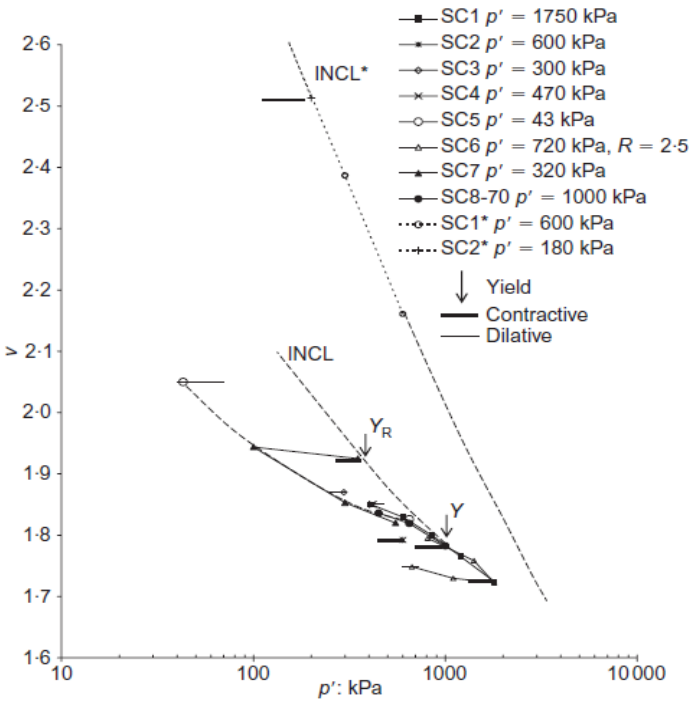

Figure 2-39. SCM scaly clay: isotropic compression and undrained shear state paths followed by natural and reconstituted specimens (Vitone & Cotecchia 2011)

2.5 Large Strain Behaviour

2.5.1 Shear strength increase of fibre-reinforced clay

Chen & Loehr (2008) conducted triaxial tests on reinforced and unreinforced specimens of Ottawa sand. The results show that reinforced specimens have higher excess pore pressures than unreinforced specimens. The authors also stated that during the undrained shearing, medium and dense reinforced specimens show a strain-hardening behaviour up to 20% strain; while unreinforced loose specimens showed peak strengths around 2%, followed by a noticeable strain softening. In another study, Li & Zornberg (2003) found that the addition of fibres has significantly increased the peak shear

strength and limited the post peak loss of strength on both cohesive and granular soils. These authors reported an increase in strain at failure, due to the addition of fibres and, consequently, a more ductile behaviour. Furthermore, Freilich et al. (2010) studied Eagle Ford (EF) clay, with a plasticity index (PI) of 49, and Silty Brown (SB) clay with a PI of 54, prepared by compacting layers of soil in splitting mould on vibrating table and applying vertical surcharge of 15kPa (controlled frequency and duration of vibration for consistency). They concluded that pore water pressure generated within the soil specimens, under undrained shearing, were consistently higher for the reinforced specimens. In all three articles mentioned above, the increase of pore water pressure is related to the effect of the fibres distributing stresses within the soil mass and therefore increasing the contractive deformation within the fibre soil mixture.

In a similar study, Li (2005) assessed the mechanical response of fibre-reinforced clay by carrying out Consolidated Undrained (CD) tests and concluded that fibre-reinforcement restrains the volume dilation that leads to an increase of the excess pore water pressure in undrained conditions. The author also concluded that an increase in the deviator stress due to fibres is not as obvious as in the case of sand.

On a study of fibre inclusion in the failure mechanism, Freilich et al. (2010) used triaxial specimens statically compacted, with a moisture content 2% lower than the optimum. These authors concluded that unreinforced specimens developed a failure plane while reinforced specimens tended to bulge. In a similar study, Tang et al. (2007) investigated the undrained shear strength behaviour of an expansive soil reinforced with synthetic fibres. The authors' observations of the failure mode of the specimens also revealed that unreinforced samples frequently fail with the formation of a shear plane without giving a clear warning in advance. For the reinforced samples, however, the formation of a shear failure plane is not obvious. Similar findings were shown by Özkul & Baykal (2007) on samples of a kaolin rich clay reinforced with rubber fibres. The authors have shown that unreinforced specimens tested in both undrained and drained conditions develop distinct slip planes whereas reinforced specimens, tested in a drained condition showed a barrelling type failure whilst those tested undrained showed the partial development of a shear plane.

2.5.2 Critical confining pressure of fibre-reinforced clay

Özkul & Baykal (2007) examined the influence of rubber fibre inclusion on the strength and shear behaviour of clay under various loading conditions; the contribution of fibres to the strength of clay was found to decrease with increasing level of confinement. Maher & Gray (1990) also studied the effect of confining pressure on the response of fibre reinforced sand samples under static loads. The findings revealed that there is a critical confining pressure beyond which the stress-strain behaviour of the sample changes from a curved profile to a linear envelope (or bilinear curve). It was found by the authors that the maximum increase in strength for reinforced sand occurred at confining pressures less than this critical value of pressure. They also reported that a limiting, confining pressure exists beyond which the presence of fibres tends to degrade the strength of the clay. Similar behaviour was also reported by Li & Zornberg (2005).

Silva Dos Santos et al. (2010) developed a framework for the fibre reinforced sand, concluding that the effect of the fibres on the shear strength seems to depend on the testing confining pressure. These effects reduce with the increase in confining pressure: in a test carried out at low (100 kPa) confining pressures, the shear strength of the reinforced sand is observed to be three to four times that of the pure sand as can be seen on Figure 2-40a, while at higher confining pressures, the gain found to be reduced to about 70% at 800kPa Figure 2-40b and 15 % at 3400kPa confining pressure Figure 2-40c.

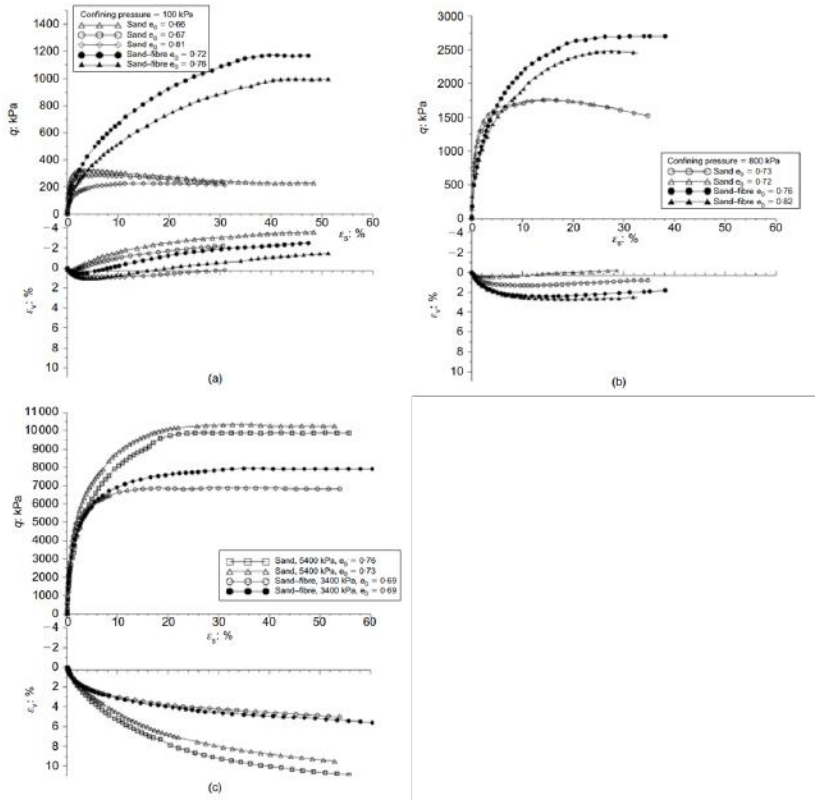

Figure 2-40. Stress–strain–volumetric response of natural sand and reinforced sand for confining pressures of (a) 100 kPa; (b) 800 kPa; (b) 3400 kPa to 5400 kPa (Dos Santos et al. 2010)

2.5.3 Sample size effect

Tang et al. (2007) have concluded that stress-strain curves of 38mm and 100mm samples are coincident for clay materials; however, Bishop & Little (1967) have shown that for a natural material, such as London Clay, planes of weakness are more evident in the preferred failure direction. The authors have shown that the strength of 38mm samples can reach values of the order of 1.5 times the strength of 100mm samples.

Lo (1970) reported that the effect of the size of the specimen on the measured strength of various materials has been highlighted in the study of Griffith`s theory of rupture. Where Griffith`s theory developed on the presence of microscopic flaws, often called Griffith cracks, in actual materials. Following the Griffith`s theory, Weibull (1939) reported that decrease in volume of specimens lead to increase in the mean strength and the standard deviation. It has been reported by Lo (1970) that Weibull`s theory has been applied to various materials, including rocks. The author indicated that a parallel and comparable condition exists in clays that are fissured or jointed. Additionally, the author stated that these discontinuities, in contrast to the Griffith cracks, are found in

macroscopic scale and may easily be detected by visual examination. Skempton & Petley (1967) presented a preliminary classification of different types of discontinuities which constitute planes of weaknesses. Additionally, Bishop & Little (1967) demonstrated the importance of sample size effect on the undrained strength of stiff fissured clays. The authors showed that the strength of London Clay, derived from in-situ shear box (600 x 600 mm) testing is 55% of that determined in an unconsolidated-undrained triaxial tests on a 38mm diameter, specimen obtained from borehole.

Lo (1970) concluded that the strength of fissured clays are bounded in the upper limit by the strength of the intact material and in the lower limit by the strength along the fissures. Authors also added that the if the size of the specimen is increased, the measured strength decreases continuously from the intact strength to the operational strength; in certain soils, the operational strength can be significantly higher than the fissured strength (Figure 2-41).

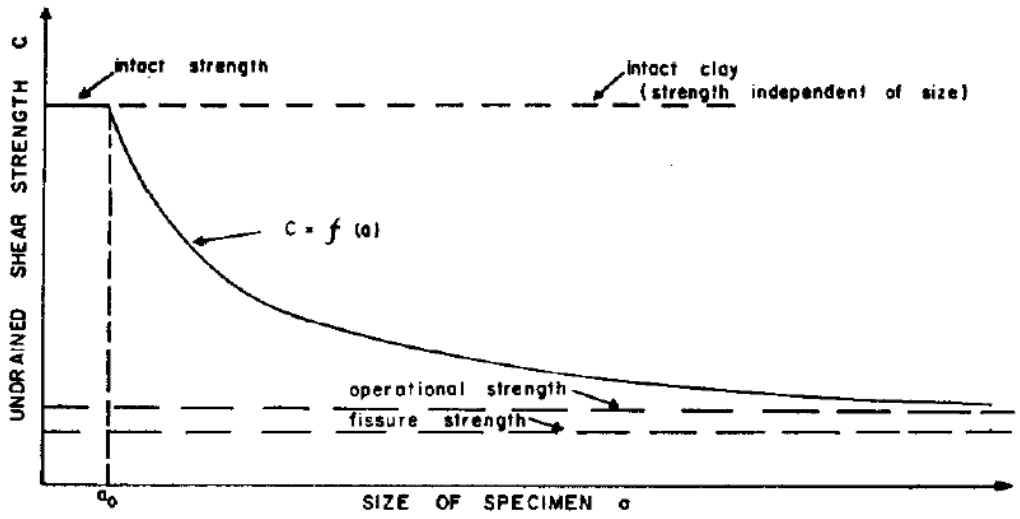

Figure 2-41. Diagram of strength-size relation (Lo 1970)

Hill (1963) defined the representative element volume (REV) as a specimen of a heterogeneous material that is entirely typical of the whole mixture on average, and contains a sufficient number of inclusions for the apparent properties to be independent of the surface values of traction and displacement, so long as these values are macroscopically uniform.

Marsland (1971) reported a continuous drop in mean strength with increasing sample size, although the difference between the mean specimen strength for a given sample size and that at the (REV) reduced to about 30% once the ratio of specimen diameter to discontinuity spacing exceeded unity.

Gasparre et al. (2007) indicates a problem in the testing of London clay in laboratory conditions: in order to obtain samples that yield a repeatable behaviour, the fissure spacing lead to dimensions for a representative element volume (REV) that are impractically large. Even using samples with 100 mm in diameter, there is a bipolar dataset, with either a fissure present that has an orientation that influences the strength, or not. A true REV would typically give strengths that are intermediate between the boundaries formed by the intact peak strength and the single fissure behaviour as Vitone & Cotecchia (2011) found in their extensive research in highly fissured clays rather than the lower bound that is often used for London clay.

In their extensive study of Lambeth group clays Hight et al. (2004) reported that fissures introduce a natural variability through differences in fissure spacing, orientation and form. Superimposed on this natural variability are the effects of sampling and testing, particularly specimen size. Higher-plasticity clays of the Upper and Lower mottled beds are described as extremely or very closely fissured. Therefore, 100mm diameter specimens were found to be more representative. In low plasticity materials of the Upper and Lower mottled beds, fissures were found to be more widely spaced, therefore may not be represented in the test specimens.

2.5.4 Structure

Holtz & Kovacs (1981) evaluated the clay soils using a scanning electron microscope (SEM) and reported that the discrete clay particles always seem to aggregate or flocculate together in sub microscopic fabric units called domains. Furthermore, domains group together to form clusters, which are large enough to, together, form peds and even groups of peds. These peds can be seen without a microscope; other macrostructural features such as joints and fissures constitute the macro fabric system. A schematic sketch of the mentioned system, proposed by Yong & Warkentin (1975), can be seen in Figure 2-42.

Yong & Warkentin (1975) identified “peds” as fabric units that can be identified visually with the naked eye and consist of an aggregation of clay particles where each ped consists of an aggregation of particles. Authors reported that an undisturbed clay soil has natural planes of weakness, which, as a result of shrinkage, are often enlarged into voids between soil units. These natural soil units are called peds; inter-particle bonding holds the particles together in the peds. Authors believes that when such a soil is remoulded, the inter-ped voids and the inter-particle bonds are destroyed. Additionally, the authors reported that, beside pores between peds, pores are also present within each ped, which may be stable but have irregular and narrow connections with the inter-ped pores.

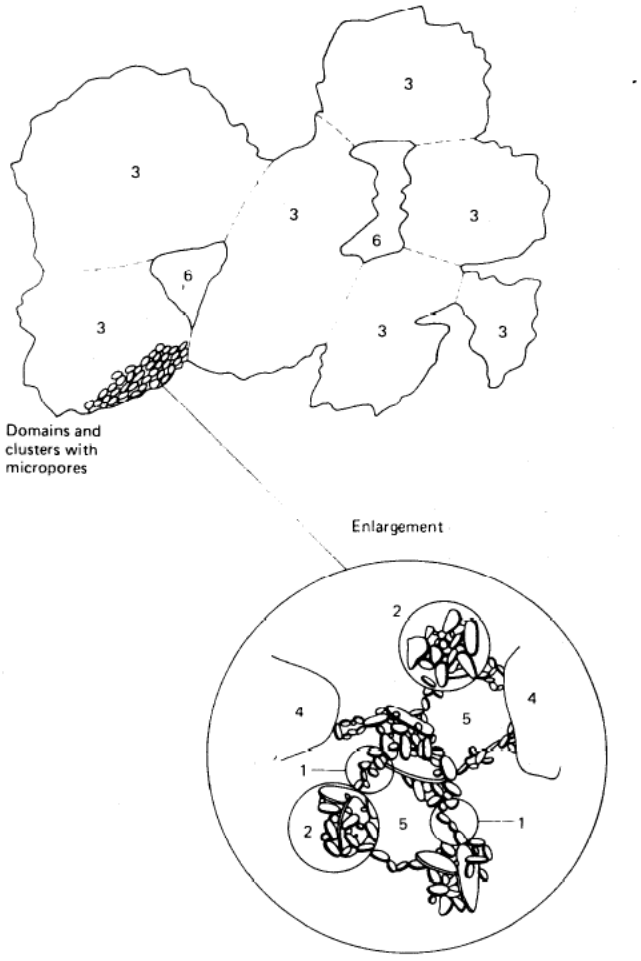

Figure 2-42. Schematic diagram of the soil microfabric and macrofabric system;(1)domain;(2)cluster;(3)ped;(4)silt grain;(5)micropore and (6) macropore (Yong & Warkentin (1975)

In Figure 2-43, Vitone & Cotecchia (2011) illustrate a framework for fissure intensity on structured clay behaviour, normalised by the equivalent intrinsic mean effective

stress, p^*_e, (q/ p^*_e vs $p`/ p^*_e$ space). Here, the state boundary surface of the unfissured clay is larger than that of the corresponding reconstituted clay, due to the effect of the stronger microstructure of the unfissured clay. On the other hand, the SBS of clays with high fissuring intensities are smaller than those of the reconstituted clay. The authors suggested that the intensive fissuring cause a decay in the mechanical properties of the clay, not only with respect to the original unfissured material, but also to the same soil when reconstituted.

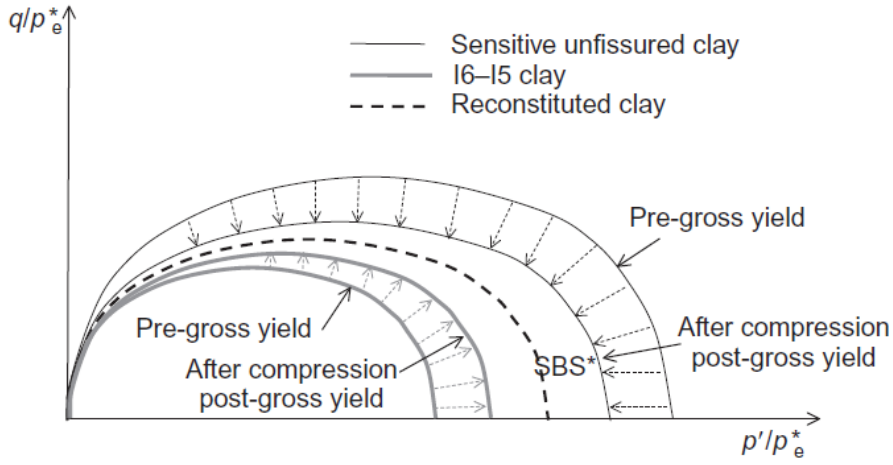

Figure 2-43. State boundary surface of natural and reconstituted clays (Vitone & Cotecchia 2011)

In their studies, Fearon & Coop (2002) on highly fissured clays and Vitone & Cotecchia (2011) on scaly clays found that due to the heavily sheared and slickensided nature of the scale surfaces, the peak strengths of the natural soil are lower than the critical state of the reconstituded soil. Whereas if the fissured material has matt surfaced fissures, the reduction is less pronounced and the peak strength generally remains above the critical state angle of shearing resistance.

In a similar study, Hight et al. (2007) found that there are two boundaries to the effective stress parameters of London clay that was not subjected to previous shearing. The upper bound is defined by the peak failure envelope of the intact clay without the presence of fissures. The lower bound is given by the parameters defining the strength of a fissure. Additionally, the authors reported that the effective stress parameters that apply to a particular volume of clay will lie between these two boundaries and will be determined by the spacing, extent and orientation of the fissures, by the direction of shearing, and by the kinematic constants – that is, whether potential shear surfaces can

pass through the lower-strength fissures. Meanwhile, the authors reported that there is a boundary, below the fissure strength for the clays, that have been previously sheared, that is determined by the amount of displacement on the shear surface and by whether that movement was on a pre-existing fissure or not. Authors believe that an assessment of strength requires knowledge of the fissure spacing, extend and orientations in relation to the direction of shearing, as well as the parameters defining the fissure strength. In the case of previously sheared clay, the location of the existing shear surface and the amount of shear strain on the fissure is required knowledge.

Chiu et al. (2010) constructed the state boundary surfaces for a compacted aged clay, shown on Figure 2-44. This figure presents the corresponding stress path of p^*_e normalised site compacted undisturbed specimens. As both reconstituted and undisturbed specimens were normalised by the same p^*_e, the influence of the soil structure can be isolated and assessed. Additionally, as can be seen in Figure 2-44b, it is found that all normalised effective stress paths of undisturbed samples reach states outside the intrinsic state boundary surfaces. It seems that the structure of the undisturbed samples confers to the soil an enlarged state boundary surface.

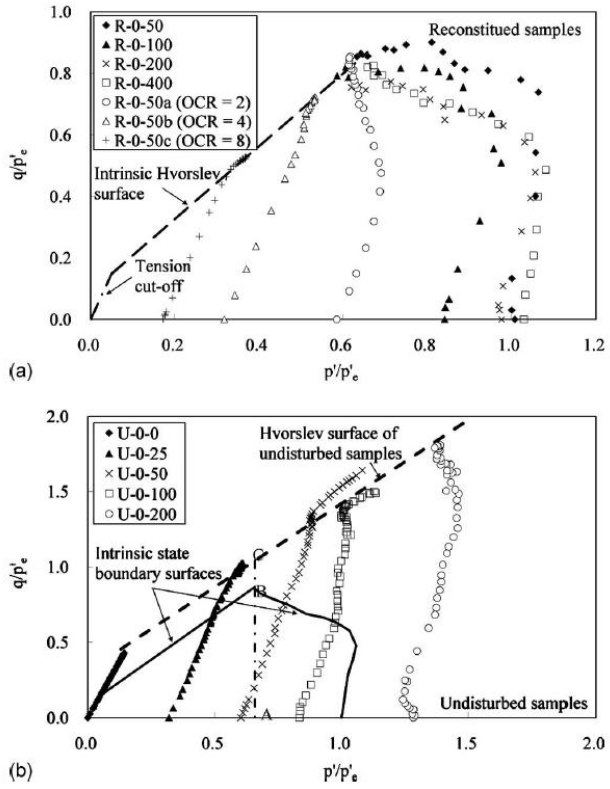

Figure 2-44. Normalized effect stress paths of saturated soil: (a) reconstituted samples; (b) undisturbed samples (Chiu et al. 2010)

Burland et al. (1996) suggested that the ratio of the undisturbed state to the critical state strength of the reconstituted state, normalised by the same e and p`, can be used as a measure of the influence of the structure on the strength at working stress. Consequently, Chiu et al. (2010) found that the ratio of normalised strength at the intrinsic critical state is 1.2 for the aged compacted clay.

Correspondingly, Gasparre et al. (2007) studied the influence of the structure on the behaviour of London clay. As can be seen on Figure 2-45, the authors, via normalising the effective stress paths of the clays from different units, presented that in compression, the peak states of the clay from different units plot significantly above the intrinsic SBS* for the isotopically consolidated samples, indicating a feature of the clays natural structure. Additionally, the ratio of the normalised strength, taken at the intrinsic critical state is about 1.2 for reconstituted specimens from the unit B2 and 1.35 for the ones from unit A3, which were sampled from a deeper location, showing that the effect of structure increasing with the depth of the unit.

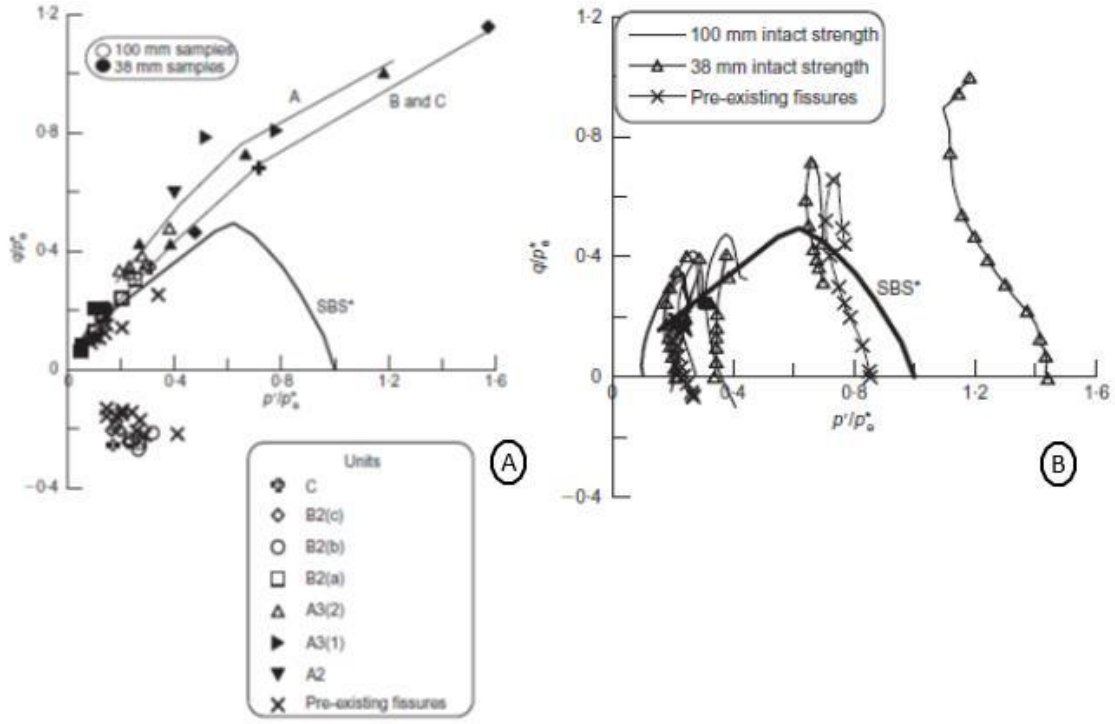

Figure 2-45. Normalised stresses: (a) peak states for samples from different units (open symbols 38mm samples and closed 100mm; units A3(1) and A2 38mm samples only); (b) normalised stress paths for unit A3(2) (Gasparre et. al.2007)

2.5.5 Fissuring

The data from Dzulynski (1977) and Mitchell (1993), was used by Vitone & Cotecchia (2011) to produce a new classification of structure scales (Table 3). They reported that a fissure pattern, present on clay mass, represents a structural feature at a scale that depends on the fissure spacing. The table has five divisions, from the megastructure to the microstructure. At both divisions 1 and 2, fissures consist of joints, sliding surfaces and faults through elements of side dimension 10–100 m and 1–10 m respectively (Dzulynski 1977). The mesostructure refers to the sample size and to fissure spacing of centimetres. In contrast to Mitchell (1993), the ministructure is here considered to be limited, on the lower side, to elements of 0.2 mm, whilst the microstructure holds everything below 0.2 mm in size (i.e. not visible to the naked eye). For clays, fissures represent discontinuities at divisions 1 to 4 (Table 3), where instead they may be considered part of the whole interparticle spacing at the micro scale.

Table 3. Scales of structure (Vitone & Cotecchia 2010)

	Scale	Name	Identification	Element
1	100 m to 10 m	Megastructure	Naked eye	Outctop
2	10 m to 1 m	Macrostructure	Naked eye	Outcrop-block
3	m to cm	Mesostructure	Naked eye	Specimen
4	cm to 0.2 mm	Ministructure	Naked eye and optical micrpscope	Clay ped - major cluster
5	< 0.2 mm	Microstructure	Optical microscope, SEM, TEM	Cluster - domain - particle

Thorne (1984) reported that the shear strength of a fissure is lower than that of the intact soil substance by an amount which depends on the degree of relative movement that has occurred along them. Figure 2-46, presented by Thorne (1984), widely concludes the studies of Skempton & Petley (1967) and Marsland (1971) on intact specimens and naturally fissured clays. The effective strength on dull or shiny surface fissures gave zero effective cohesion intercept on fissured surfaces and an effective angle of internal friction on the fissure surfaces equal to the global soil substance for the intact material. While slickensided surfaces showed an effective strength essentially similar to the laboratory residual values.

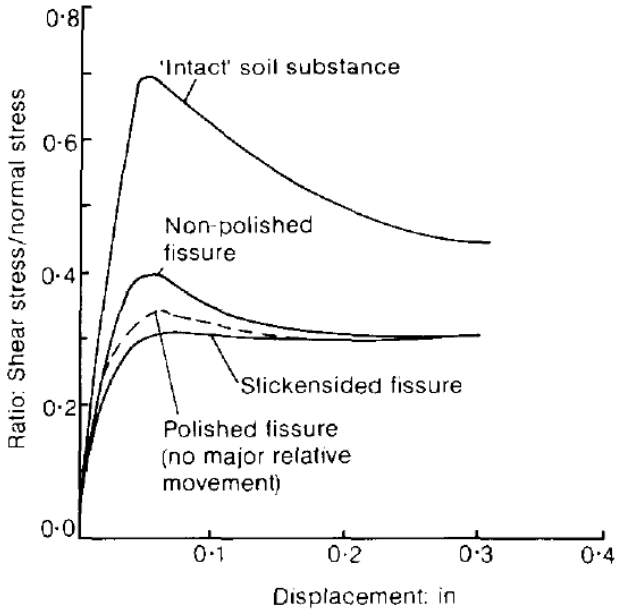

Figure 2-46. Diagrammatic representation of shear tests on soil substance and on various types of fissure surface (Thorne 1984)

Hight (1998) reported that fissures present in London clay are not polished but appears to represent surfaces of separation between compressed and aligned clay aggregates. Hight et al. (2007) observed that, from block sampling and sample preparation of London clay, the fissures tend to have a variable spacing from a few centimetres to few tens of centimetres, tend to be discontinuous and extend up to approximately 150 mm with orientations that are horizontal to sub-horizontal, and vertical to sub-vertical. Moreover, the authors illustrated that fissures have an important effect on shallow slope stability, where the clay separates on the fissures and joints into gravel and cobble-size blocks, causing superficial failures (Figure 2-47).

Figure 2-47. Shallow slope failures in Heathrow Terminal 5.(Hight et al. 2007)

2.6 Small Strain Behaviour

There are a variety in-situ and laboratory tests that can be carried out to obtain the stiffness of soil. A selection of moduli from oedometer tests, drained and undrained triaxial tests, resonant column tests, torsional shear tests, bender element tests, plate loading tests and cone penetration tests are a few of these tests.

Most of the research on the stiffness of fibre-reinforced soils is carried out on sandy soils. Chen & Loehr (2008); Yetimoglu et al. (2005); Michalowski & Čermák (2003); Esna-ashari & Asadi (2008); Heineck et al. (2005) used polypropylene fibres to reinforce sandy soil. Most of the above-named tests were carried out on fibre-reinforced and non-reinforced soils and showed that inclusion of fibres up to a certain content did not noticeably affect the initial stiffness of the soil. However by evaluation of Figure 2-48, Consoli et al. (1998) claims that an inclusion of 3% fibre will produced a substantial drop in the initial stiffness.

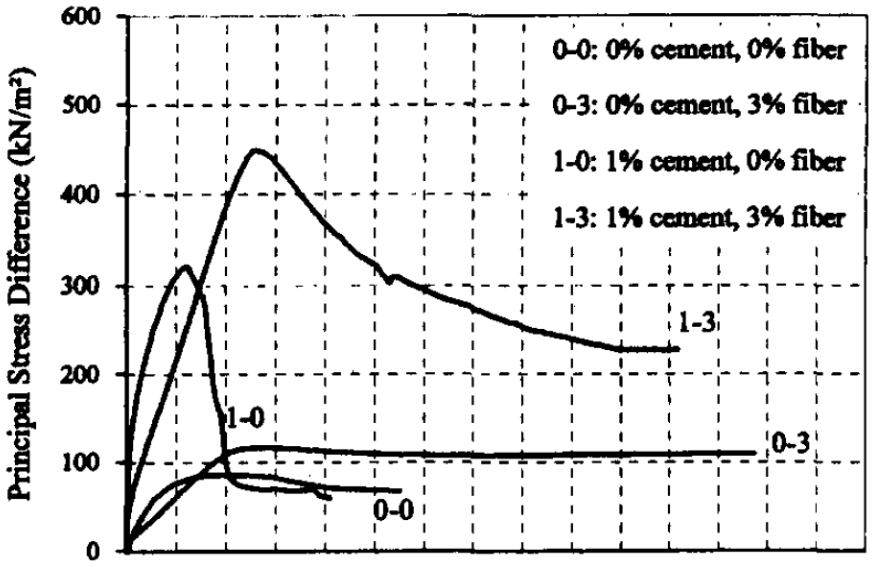

Figure 2-48. Stress-Strain-Volumetric response for unreinforced soil and fibre reinforced soil (Consoli et al. 1998)

Michalowski & Čermák (2003) also observed the similar behaviour and attributed the loss of initial stiffness to the change in the fabric of the sand produced by the fibres. Authors reported that the fibres are likely to cause non-homogenous porosity distribution since the long inclusions prevent grains from dense packing. Consequently, authors believe that the pockets of the matrix away from the fibres have porosity considerably lower than the sand in the immediate vicinity of the fibres. Furthermore,

authors stated that, during hydrostatic loading, the fibres are subjected to compression and bending, but, once shearing starts, the fibres under compression kink. Consequently, the stiffness in the initial stage of loading is lower than that for sand of comparably average porosity without fibres. Authors concluded that this effect was very distinct when large concentrations of fibres were used.

However, the above phenomena was not monitored in fine grained soils (fine sand, silt or clay) and no evidential decrease in stiffness was detected in the researches of Maher & Gray (1990) and Heineck et al. (2005) on fine-grained sand. Authors carried out bender element and resonant column tests, on reinforced and unreinforced sand specimens, and have shown that the introduction of fibres was not affecting the initial stiffness. Figure 2-49 presents measurements of small strain stiffness of Botucatu residual soil unreinforced and reinforced with polypropylene fibres with bender elements. It can be observed that the fibre reinforcement does not change the small strain stiffness of the BRS soil measured during the isotropic compression, which confirms that fibre reinforcement does not affect the behaviour at small strains. Nevertheless, authors reported that at moderate to larger strains the influence of fibres in the shear module is triggered through the mobilization of the tensile resistance of the fibres. This, in turn, result in an enhanced contribution of the fibres to the rigidity of the composite.

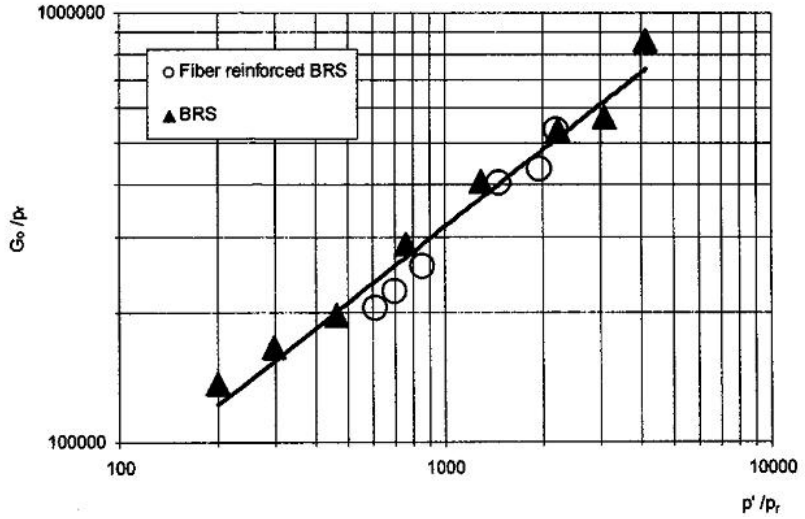

Figure 2-49. Effect of fibre inclusion on initial shear modulus (Go) of Botucatu residual soil unreinforced and reinforced with polypropylene fibres (Heineck et al. 2005)

Heineck et al. (2005) examined the small strain behaviour of fibre reinforced sand in triaxial equipment equipped with bender elements and concluded that the elastic shear

moduli of the studied soils, measured during isotropic compression, were the same for the soils in their un-reinforced and reinforced states.

As can be seen in section 2.2.5 of this chapter, the contribution of the fibres to the composite was found to be largest when they were in the direction of the largest extension of the composite (horizontal). Michalowski & Čermák (2003) supported this idea by concluding, in their research, that the vertical fibres in triaxial testing are subjected to compression. Where such response has adverse effect on the initial stiffness of the composite and no contribution on strength increase.

2.6.1 Monotonic Shear Moduli

Jardine (1992) reported that there are numerous factors affecting the magnitude of the soil shear stiffness including the elastic shear stiffness. Those factors can be listed as apparatus configuration; load cell to sample connections; accuracy of the pressure control; temperature stability; stress and strain history, including sampling and reconsolidation; creep strain rate prior to shearing and strain rate during shearing; resolution of the instrumentation and data interpretation, including normalisation.

Jardine (1995) proposed a kinematic strain hardening plasticity framework in order to interpret the soil behaviour who identified three kinematic surfaces Y_1, Y_2 and Y_3 (previously defined as Zone 1, 2, 3 by (Jardine 1992) in Figure 2-50). Y_1 and Y_2 existing within the conventional main yield surface. An outline of the framework developed by Jardine (1995) can be seen on Figure 2-51. As can be seen on the figure, within the zone limited by the Y_1 surface, the soil behaves in a linear elastic manner, where the strains are fully recoverable. The Y_2 surface corresponds to the zone beyond which the rate of plastic strain development accelerates by the change in direction of the strain increment vector. The authors claimed that this surface corresponds to the limit beyond which particle contacts fail and particle movement occurs.

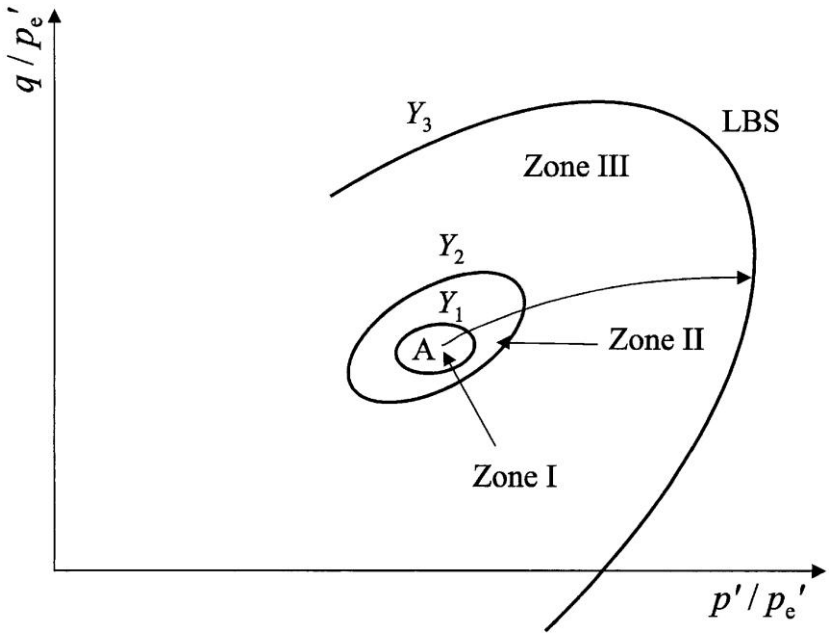

Figure 2-50. Identification of zone I, II, and III in triaxial space(Jardine 1992)

Y_3 surface reported to be the conventional geotechnical yield point associated with commencement of noticeable loss of stiffness, contraction, dilation and sudden failure. The Y_3 surface is recognised as a point where the effective stress path direction changes abruptly in undrained tests or where the strain increment direction changes direction in drained tests. Moreover, Jardine et al. (2004) reported that the Y_3 corresponds, in the normalised stress space, to the local boundary surface (LBS) which cannot be crossed by undrained stress paths.

Furthermore, Ishihara et al. (1975) observed that granular materials tested under extremely loose or very dense states enlighten an important feature of post yield behaviour of such materials. Shearing behaviour of such specimens show contractive behaviour at moderate strains which changes sharply at a certain stage to show a dilatant response. Authors characterised this "yield point" as Phase Transformation Point (PTP). Traditional response of granular material should continue to dilate post PTP until they develop stable critical states. Nevertheless, most practical experiments develop shear bifurcations and form shear bands that shorten this process before uniform critical states are reached. Jardine et al. (2001) reported that such behaviour relates to the micro-mechanical response of granular material after the buckling of the strong force network. Furthermore, Kuwano & Jardine (2007) in their study of kinematic yielding in Ham

River sand (HRS) proposed that the PTP points could be considered as a Y_4 yield point within their kinematic multi-yield framework.

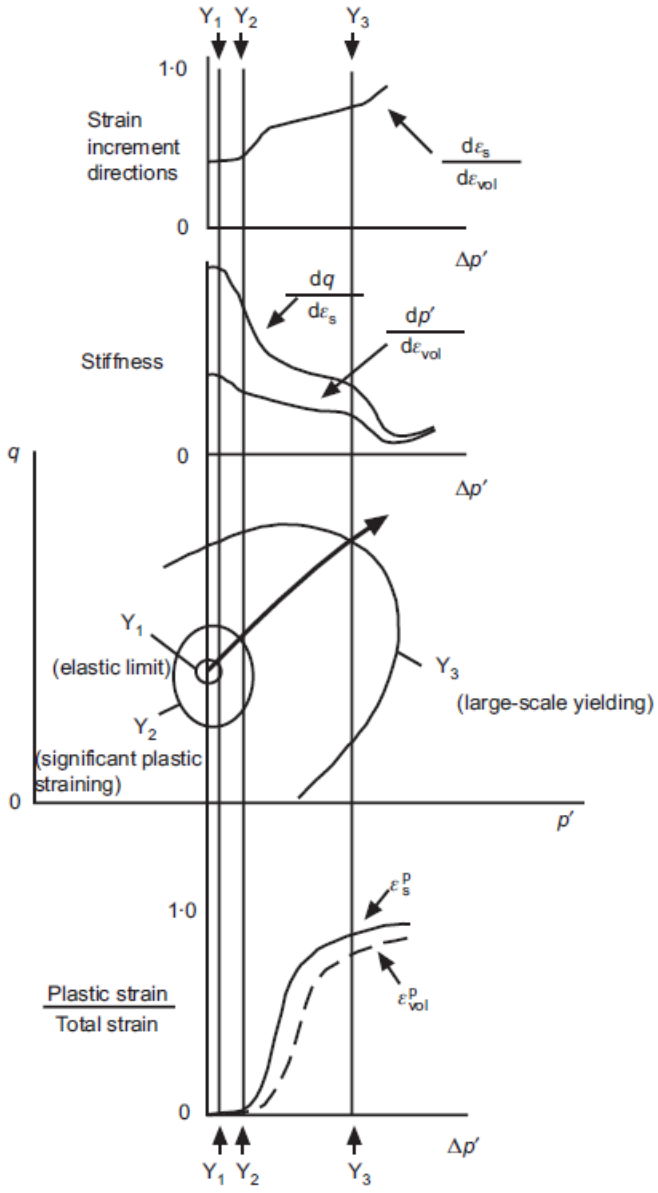

Figure 2-51. Scheme of multiple yield surfaces (Jardine 1995)

Figure 2-52 shows the location of the Y_1, Y_2,Y_3 and Y_4 yield surfaces for lightly over consolidated loose HRS sand samples

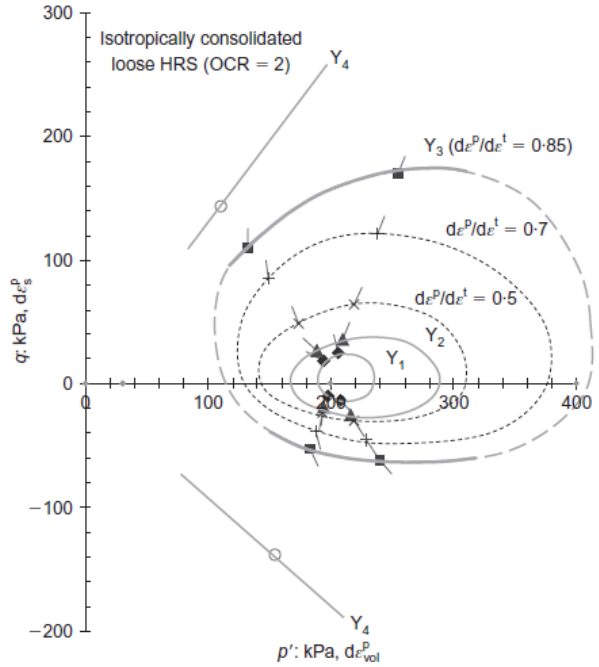

*Figure 2-52. Location of yield surfaces in loose HRS specimens (*Kuwano & Jardine 2007)

As can be seen in Figure 2-53 Gasparre et al. (2007b) identified the yield point at the end of the elastic region Y_1 of London clay where the stress strain curve deviates from linearity. As mentioned by Jardine (1995) the Y_2 kinematic surface was identified from drained tests as the points where the strain increment vectors rotate, by plotting volumetric against shear strain (Figure 2-54). Additionally, the Y_2 point can be identified in undrained tests from changes in the effective stress path direction or change of pore water pressure against strain.

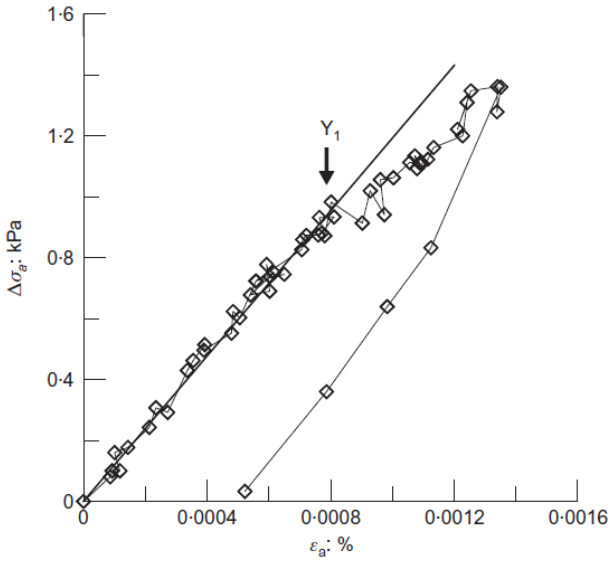

Figure 2-53. Drained axial probe test for identifying Y1 yielding. (Gasparre et al. 2007b)

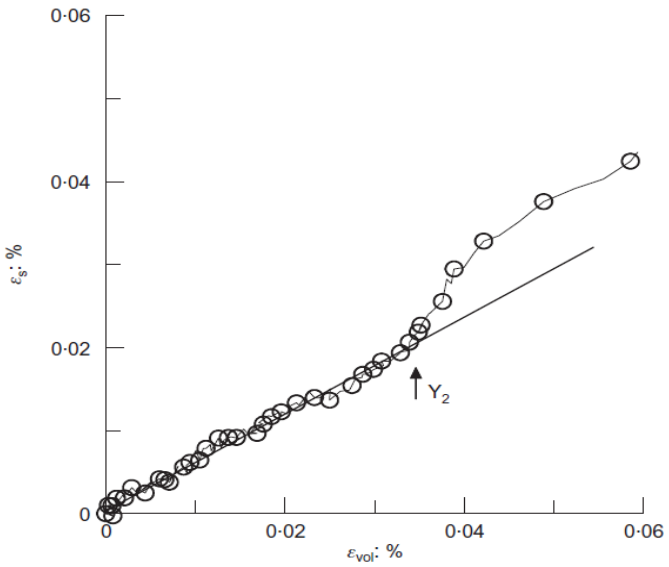

Figure 2-54. Y2 yield points in a drained test on a sample(Gasparre et al. 2007b)

Gasparre et al. (2007b) concluded that for any given depth, the behaviour was approximately cross-anisotropic linear elastic within a relatively small Y_1 yield surface, that surrounded the current effective stress point. The stiffness decayed with strain once a limit was reached, and data have been shown, from a wide variety of test types that typify the anisotropic and steeply non-linear trends exhibited by tests continued to failure. Authors additionally concluded that the Y_2, in many cases, appeared to correspond to a faster elastic-plastic stiffness decay with strain, and it was also found that there was a greater dependency on the behaviour on recent stress history for stress path approaches that exceeded Y_2.

Normalising the shear modulus with the effective stress (p`), at the start of the shearing is used by numerous researchers (e.g. Pantelidou & Impson (2007), Hight et al. (2007) and Grammatikopoulou et al. (2008)). Pantelidou & Impson (2007) used several methods of normalising secant stiffness at 0.01% shear strain. Normalisation with respect to the initial mean effective stress from laboratory tests was found to be successful in eliminating the effect of the effective stress on the data.

Ventouras (2005) investigated a variation of the stiffness of Thanet sand with different silt contents as well as in the reconstituted state, at different confinements. The author plotted the equivalent monotonic stiffness's against the mean effective stress, *p'*, at two specific strain levels of 0.01% and 0.1% in both drained and undrained conditions. It

was reported by the author that the amount of silt contained within tested intact specimens had a small impact on the monotonic stiffness behaviour of the Thanet sand; the low silt content soil showed slightly higher stiffness than the high silt content soil for both strain levels. The author also added that there is no measurable effect on the dynamic shear modulus. Furthermore, regarding the effect of structure, the intact samples appeared to show a slightly higher stiffness than the reconstituted samples.

Gasparre et al. (2014) conducted a study on stiffness measurements via LVDTs and reported that different methods of load cell to platen connection can lead to tilting and specimen bending, with both tensile and compressive strains developing at small strains. In their study authors evaluated five different connection methods shown on Figure 2-55. The connection method where a half ball connection is incorporated with a suction cap was found to give the best combined response of the internal transducers (Figure 2-56). The half ball permits a degree of rotation while the suction cap promotes uniform straining by offering a strong but flexible connection.

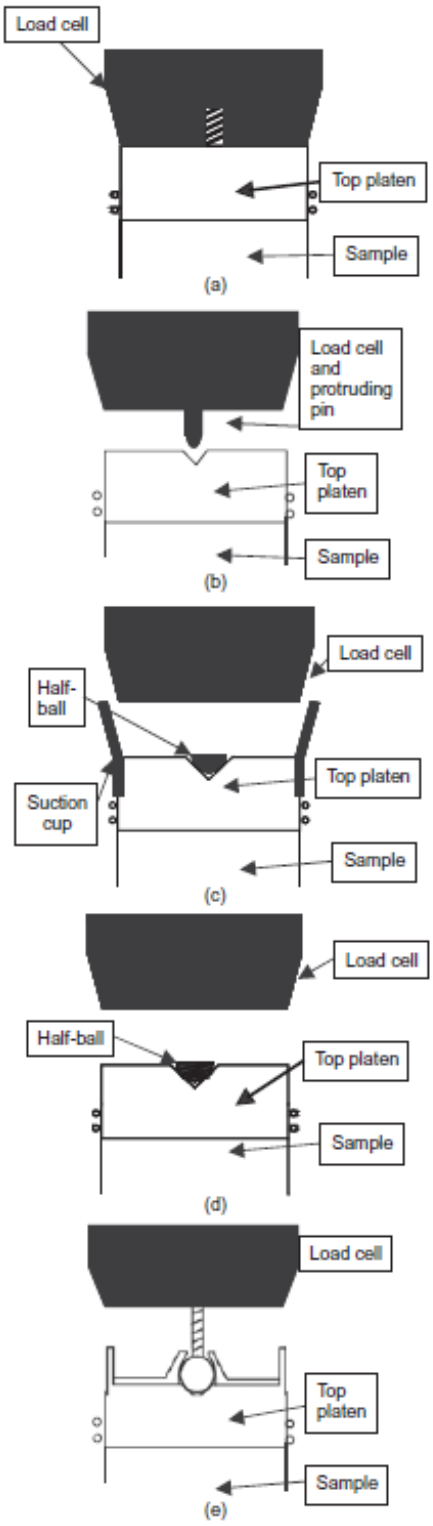

Figure 2-55. Load cell connection (a) rigid; (b) pin; (c) suction cap for 100 mm diameter samples with half-ball; (d) half-ball only; (e) fixed ball (Gasparre et al. 2014)

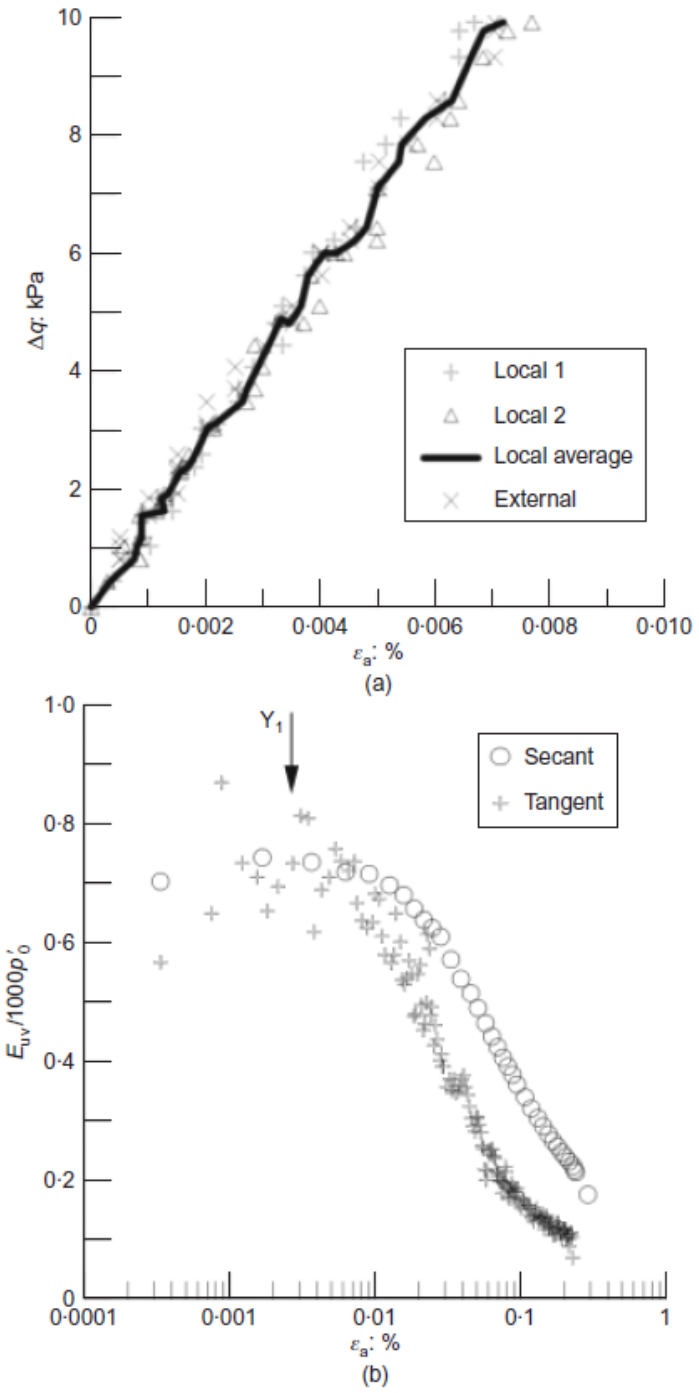

Figure 2-56. Undrained triaxial compression test on samples 8m below top of London Clay: (a) stress-strain data; (B) decay curves of normalised secant and tangent vertical stiffness. (Gasparre et al. 2014)

Hight et al. (2007) presented results from Gasparre (2005), Nishimura (2005) and commercially conducted tests, in Figure 2-57. The results were plotted in terms of the undrained secant modulus, E_u, normalised by the value of the mean effective stress prior to the start of the undrained shear. As can be seen from the graph, commercially

conducted results have higher values than the ones obtained by Gasparre (2005) and Nishimura (2005). Hight et al. (2007) reasoned such difference as followed;

(a) The rates of stress change on the approach path to the in situ stresses are lower in the IC Study.
(b) The pause periods between the end of reconsolidation and the start of undrained shear were of the order of 7 days, considerably longer than in commercial study.
(c) The rate of undrained shearing (0.02%/h) was 10 times slower than in the commercial study.
(d) The samples were stored for longer periods.
(e) The methods of local strain measurement differed.

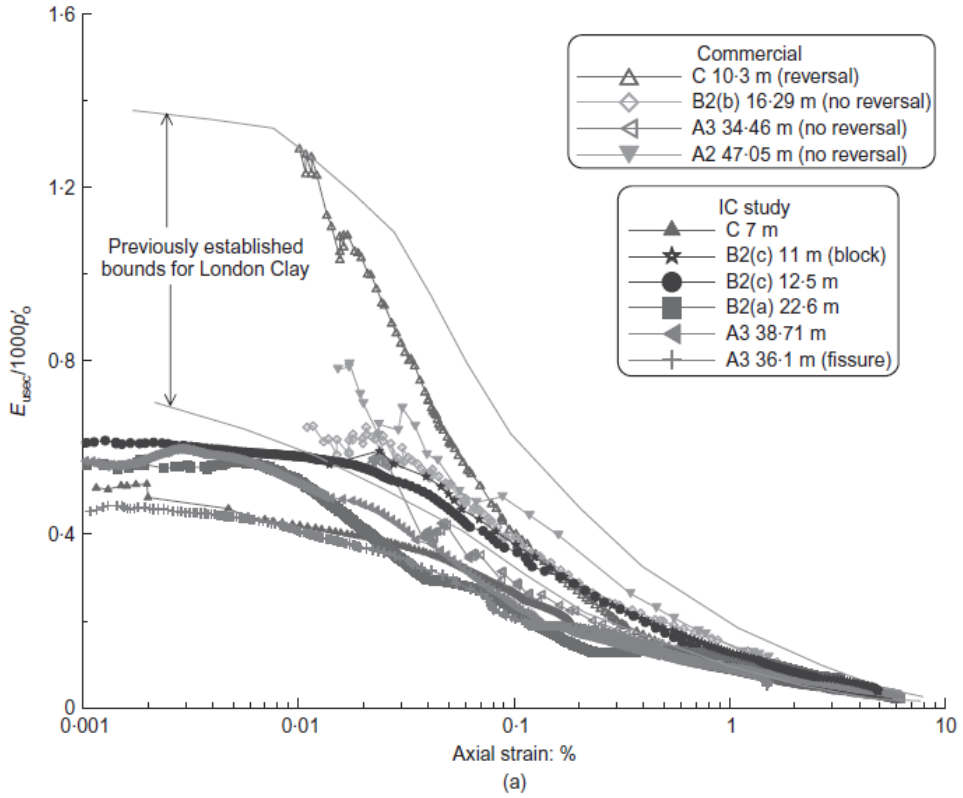

Figure 2-57. Normalised modulus decay curve for undrained triaxial compression (Hight et al. 2007)

Consoli et al. (2002) conducted a series of triaxial tests on reinforced and unreinforced specimens of fine sand with polyethylene fibres of different lengths. The results suggest that there is a small increase in the secant modulus calculated at 0.1% strain, caused by the inclusion of fibres. Unfortunately, authors reported that more data is required in order to reach a final conclusion.

Discrete element method (DEM) simulations by Dobry & Ng (1992) revealed that in a monotonic test, the secant stiffness G reduces progressively with shear strain. Authors reported that this is because of the separation or slippage of intergranular contacts as shear strain increases, thereby removing their associated contributions from the elastic stiffness of the assembly. Moreover Vardanega et al. (2013) stated that the above mentioned reduction is generally taken to be reversible when the strain direction is reversed because of the re-engagement of the previously slipping contact. Authors added that in the case of further reverse straining, the elastic content will once again be lost, and the stiffness will reduce as before. The rate of stiffness reduction on the reversed loading path can be taken to be half that of the original loading curve, because previously slipping elements must first recoil elastically until they are unloaded and then distort in the opposite direction, by the same amount, before they slip again.

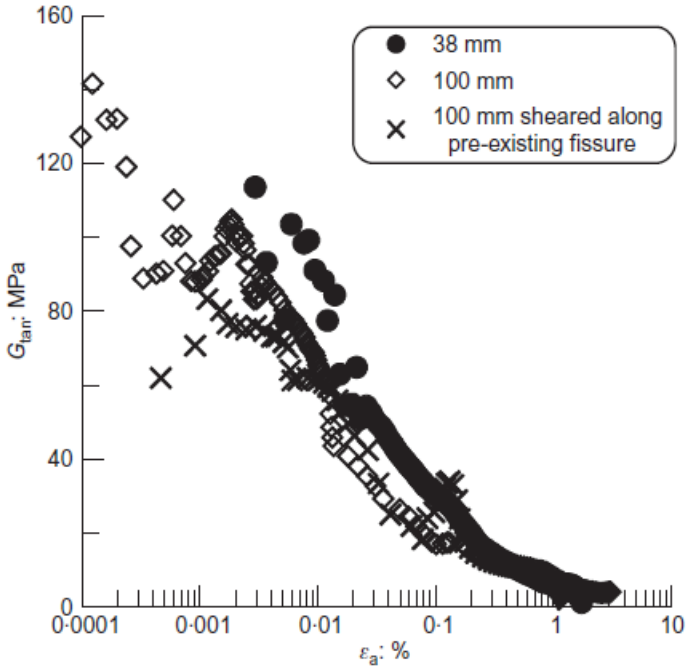

Figure 2-58. Comparison of tangent stiffness backbone curves for a sample that failed on a pre-existing fissure with samples that failed on new surfaces. (Gasparre et al. 2007)

The study conducted by Gasparre et al. (2007) considered the shear stiffness of the intact London clay from the fissuring point of view. Figure 2-58 presents undrained tangent shear stiffness degradation curves from the 100mm specimens from in-situ core samples that were subjected to similar testing. One of the samples ultimately failed on a

pre-existing fissure, without the development of a significant peak, whereas the others failed through the intact soil with a marked peak strength. Authors reported that the shear stiffness at small to intermediate strains is very similar, indicating that local compression or slipping along the fissure eventually contributes to the failure surface not to commence until large strains are reached. Additionally, authors mentioned that it might be argued that other (sub-horizontal or vertical) fissures existed equally in both samples and that affected stiffness more evidently, but that only in one sample did fissures affect shear strength. Moreover, a comparison made by the authors between 38 mm and 100 mm samples indicated that, unlike the average shear strength, there was no effect of sample size on stiffness. Authors also added that if the fissures affected the stiffness, the generally less fissured 38mm samples should have had significantly higher stiffness values.

Hight et al. (2007) explored the London clays stiffness anisotropy at small strain levels. The authors established that a strong elastic anisotropy within kinematic Y1 yield surfaces have been established over the depth profile, together with a second set of Y2 kinematic yield surfaces. Furthermore, the authors reported that stiffness anisotropy, which is related to preferred orientation of the clay aggregates, determined the generation of pore pressures during undrained shear and contributed, with the preferred orientation of the fissures, to the substantial undrained anisotropy of the clay. Correspondingly Vardanega et al. (2013) mentioned that a mechanism of reduction of stiffness can arise, at moderate strains, in undrained tests, as the result of the build-up of positive excess pore pressure with a consequential reduction of effective stresses. Authors attribute such behaviour to the tendency of the soil to densify as a result of moderate granular re-arrangement which is beyond 2% strain for clays.

3. MATERIALS

In this chapter, a description of the materials used in this research was made. The geological aspects of the Lambeth group clay has been examined through the site investigation carried out on the site obtained samples and available literature. Additionally, brief information has been given about the mechanical properties of the polypropylene fibres used in this study.

3.1 Geology of the Lambeth Group Clay

In Mouchel's field project, which was mainly focused on the maintenance of embankment slopes along the M25 (motorway around London, England) on a soil type formally designated as the Lambeth Group clay, a formation of the Tertiary period. Tertiary clays occur mainly in two areas of UK, one starts from the south-east of UK and continue to central southern areas of London where the second one occurs, south of Hampshire and northern parts of the Isle of Wight (Figure 3-1). The oldest of these are the clays of the Lambeth Group, where this name (derived from the London borough of Lambeth) has recently been introduced to incorporate what were previously designated the Woolwich and Reading Beds (Ellison et al. 1994). All of the Tertiary clay formations are over consolidated due to the erosion of later overlaying deposits. Cripps & Taylor (1987) reported that between 150m and 400m of overburden have been removed with an apparent westward increase in the degree of over-consolidation of London Clay, in the London area, i.e. more material has been eroded at the western limit.

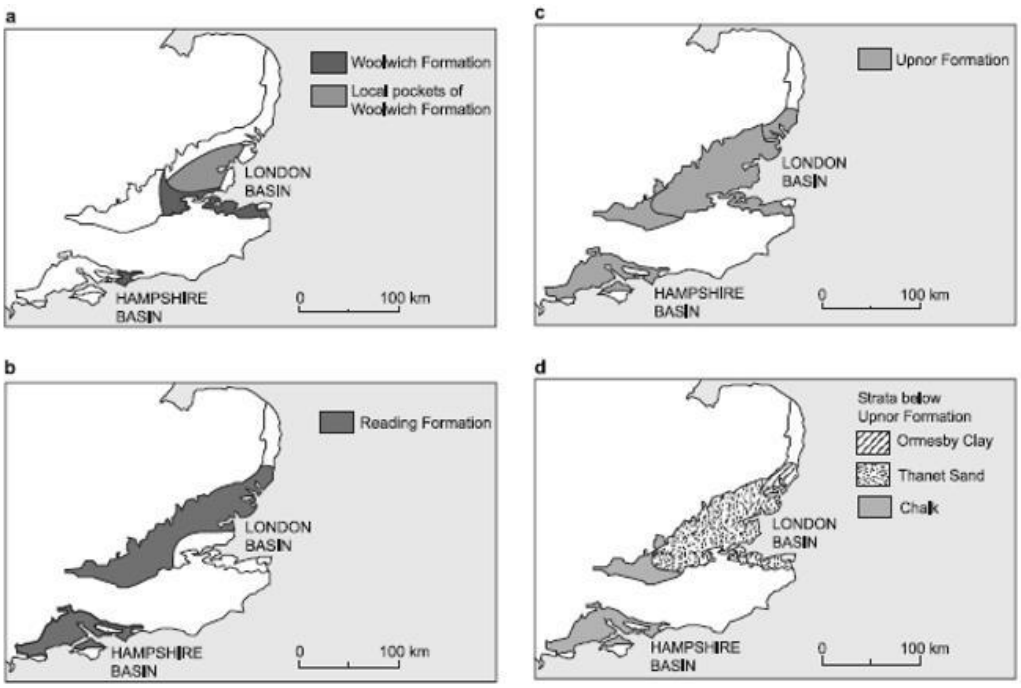

Figure 3-1. Distribution of the Lambeth Group: (a) Woolwich Formation, (b) Reading Formation, (c) Upnor Formation, (d) underlying strata (Hight et al. 2004)

The Industrial partner of this project commissioned a site investigation report at the site where samples were obtained for laboratory testing. Figure 3-2 indicates the instrumentation location plan, also indicating the location of inspection trenches. Bore hole and the trench logs can be seen in Figure 3-3 to Figure 3-5. Depending on the location where samples were obtained for the laboratory testing, the geologist who prepared the site investigation reports, classified the soil as Undivided Reading Formation from the Lambeth Group Clays. The obtained clay was defined by the geologist as soft to firm fissured greenish grey mottled yellowish brown and red clay. The fissured structure of the clay can be seen from Figure 3-6 to Figure 3-8. Additionally, the exact location of the trench made for this study can be seen in Figure 3-9 and Figure 3-10. The instrumentation commissioned for the site investigation report can be seen at the far end of the trench.

The test program for the site investigation consist of the determination of water contents, compaction, atterberg limits, particle size distribution and particle density. The results obtained by the following tests are included in the appendix of this study and they are in good agreement with results obtained in section 5.5.

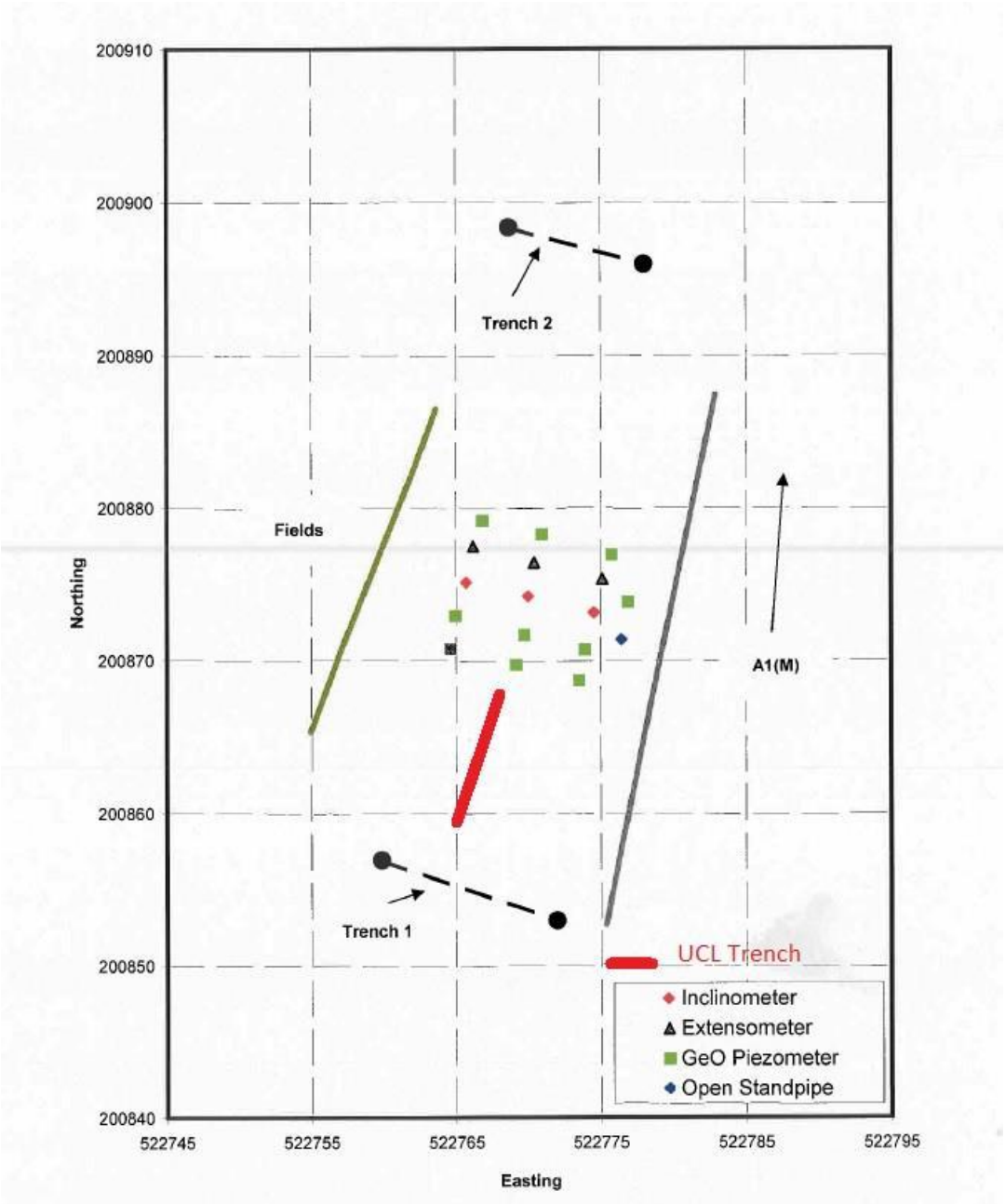

Figure 3-2. Instrumentation location plan indicating location of inspection trenches

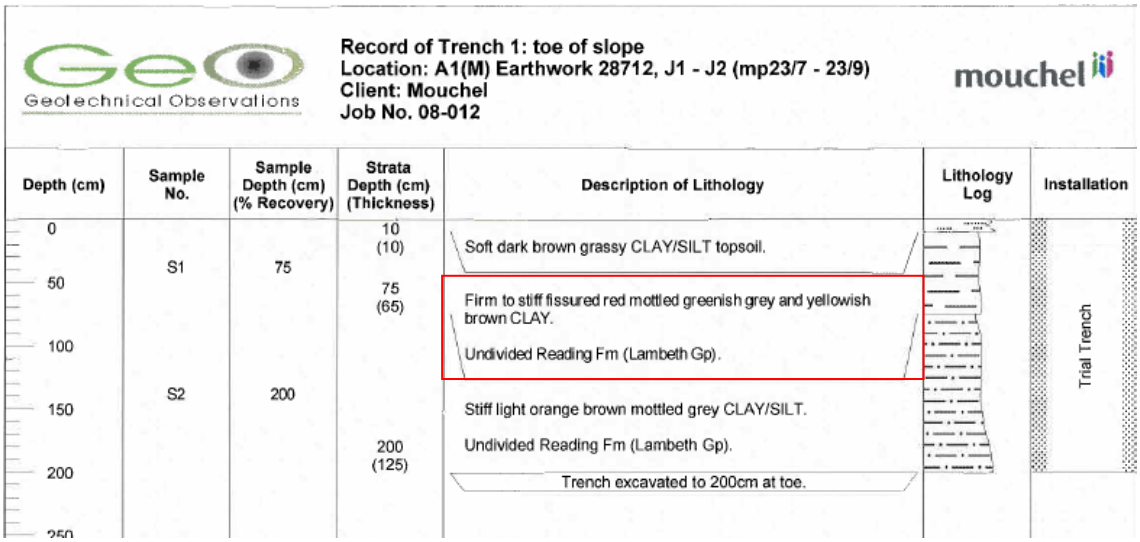

Figure 3-3. Record of trench 1at toe of slope.

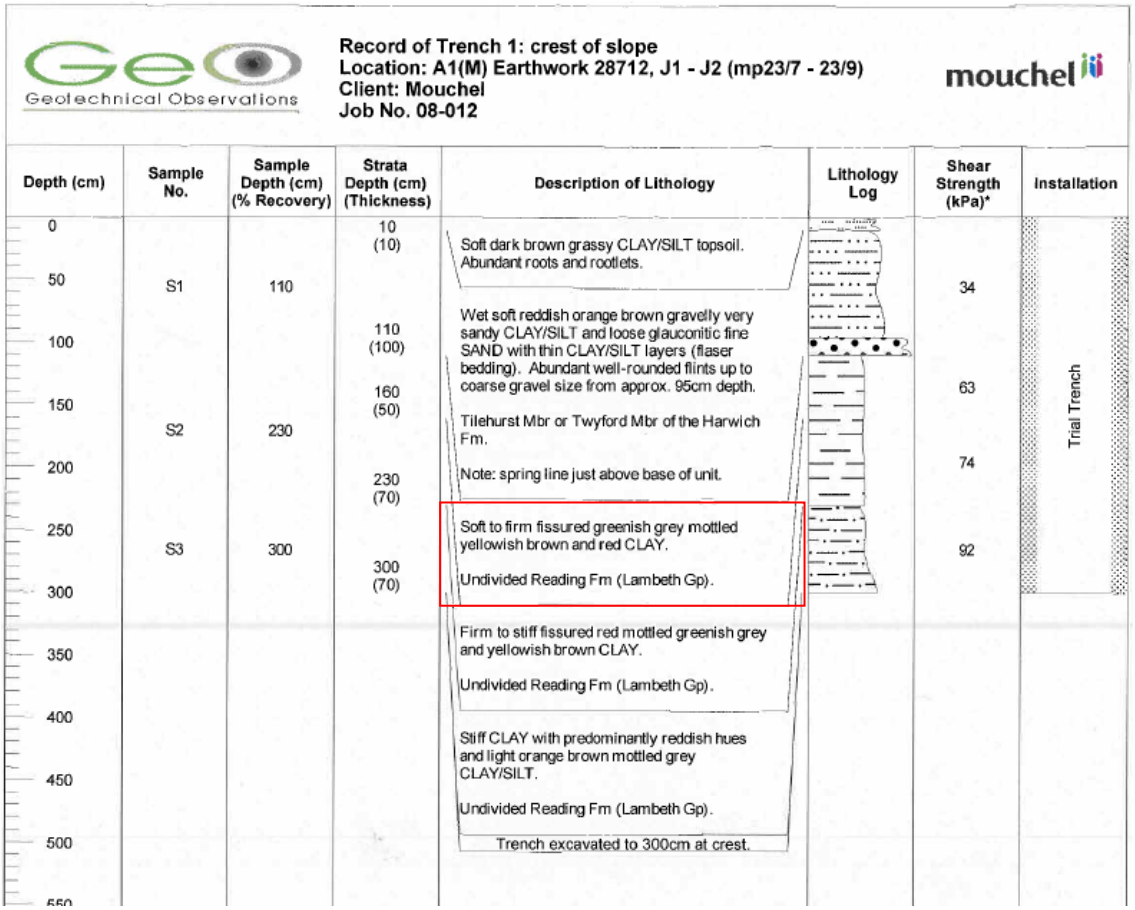

Figure 3-4. Record of trench 1 at crest of slope.

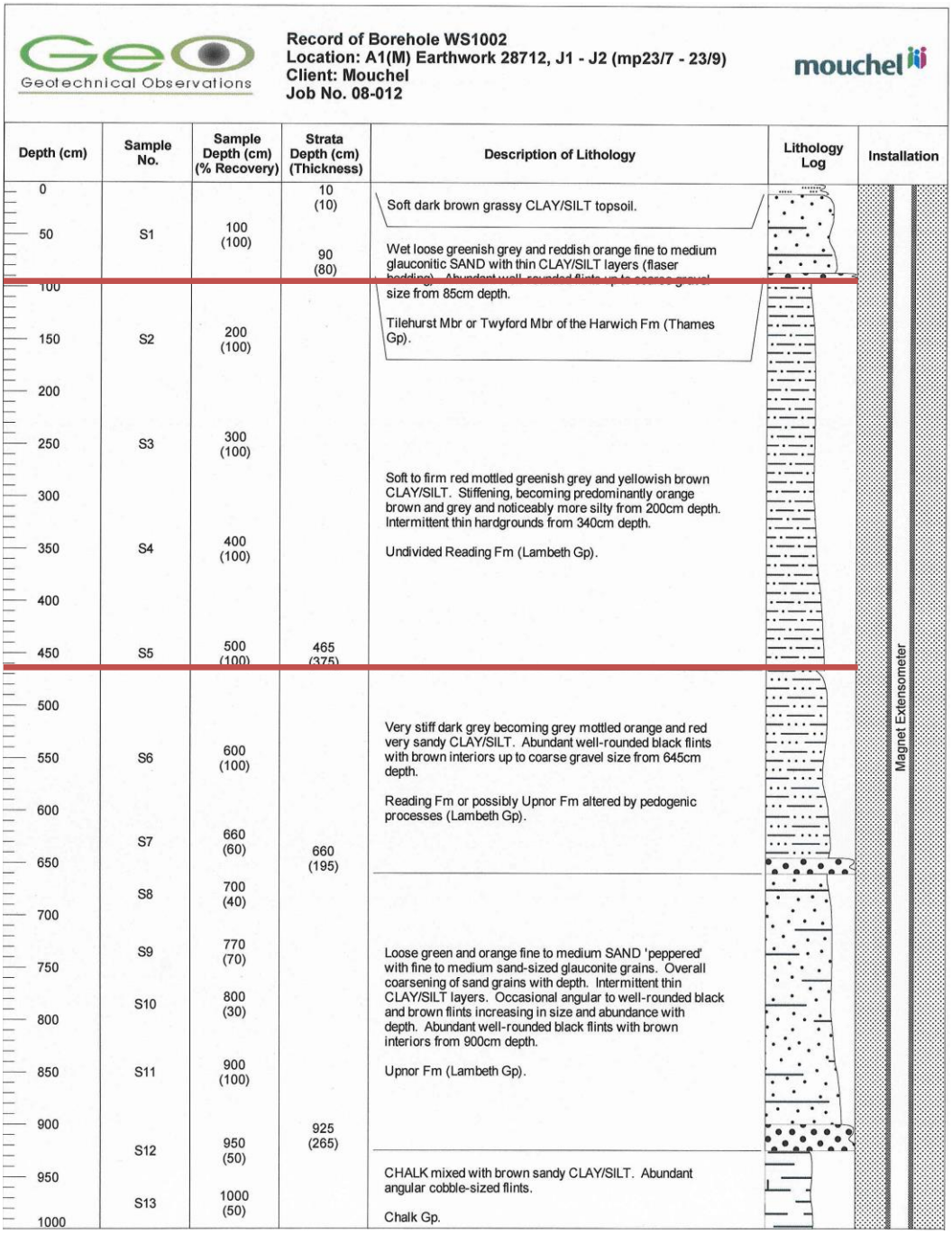

Figure 3-5. Record of borehole WS1002

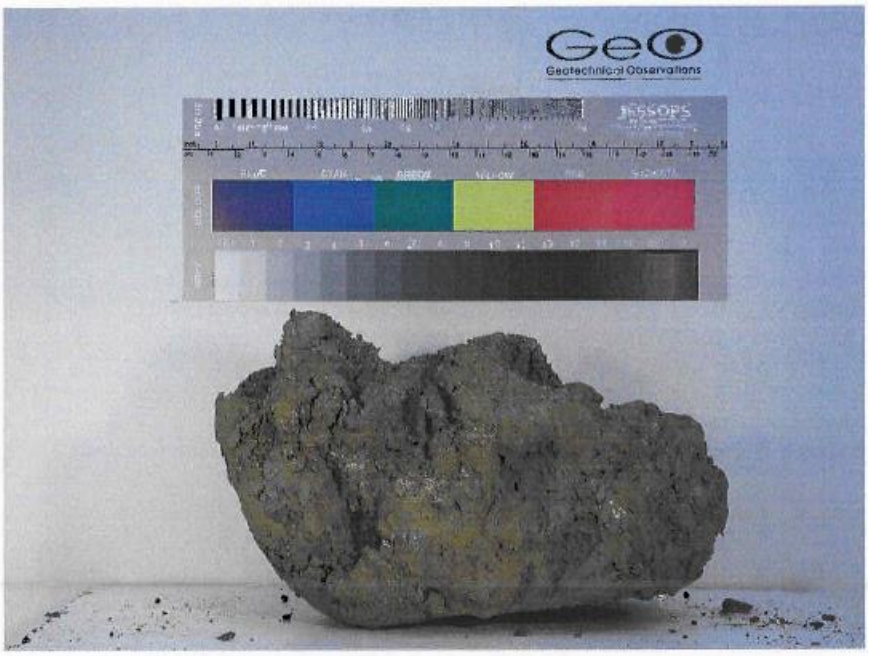

Figure 3-6 Trench 1, 1-2.2m soft to firm fissured Undivided Reading Formation (Lambeth Group)

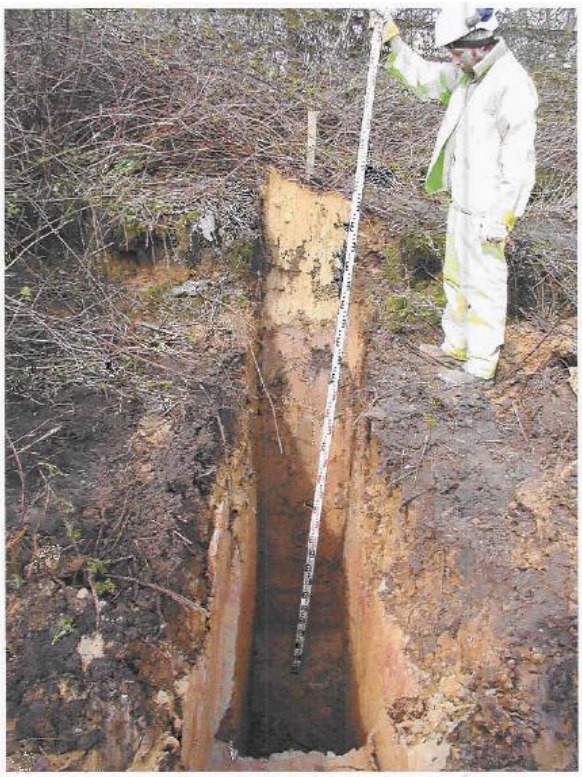

Figure 3-7. Trench 1 at the crest of the slope (view west): Harwich Formation (Thames Group) overlying Reading Formation (Lambeth Group)

Figure 3-8. Trench 1 mid-slope (view south): Reading Formation (`lower`mottled)(Lambeth Group)

Figure 3-9. UCL Trench for obtaining undisturbed samples

Figure 3-10. UCL UCL Trench- sampling of the the in-situ fibre compacted soil.

Deposition

The deposition of chalk across Europe followed by the increase in volcanic and tectonic activities which were related to the opening of the Atlantic Ocean in late Cretaceous and early Teriary time. These events accompanied by a global fall in sea level, resulted in an increase in land area. These were followed by folding associated with the rise of the Alps in southern Europe, leading to tilting and the erosion of the youngest part of the Chalk in southern England.

The deposition of Tertiary sediments took place around 58 million years ago, by the increase in the shallow sea, extending from the deeper waters of the North Sea Basin to cover the whole of south-east England. The Lambeth Group was formed in a relatively short interval about 56 to 55 million years ago, whilst the folding of the Lambeth Group took place in the Miocene epoch.

The significant variation in the sea level during the formation of the Lambeth group resulted in a periodic migration of the depositional environment and this was a major contributory factor in the complex lithological changes observed in the Lambeth Group.

The distinct and well known lithologies identified in the Lambeth group are the Upnor Formation, the Reading Formation and the Woolwich Formation. As defined by author of this study and the geologist that performed the site investigation report, the soil obtained for laboratory testing was classified as the Reading formation.

Reading Formation

As can be seen in Figure 3-11. The Reading formation is divided into two branches, separated by the Woolwich Formation. These branches are termed Upper Mottled Clay and Lower Mottled Clay.

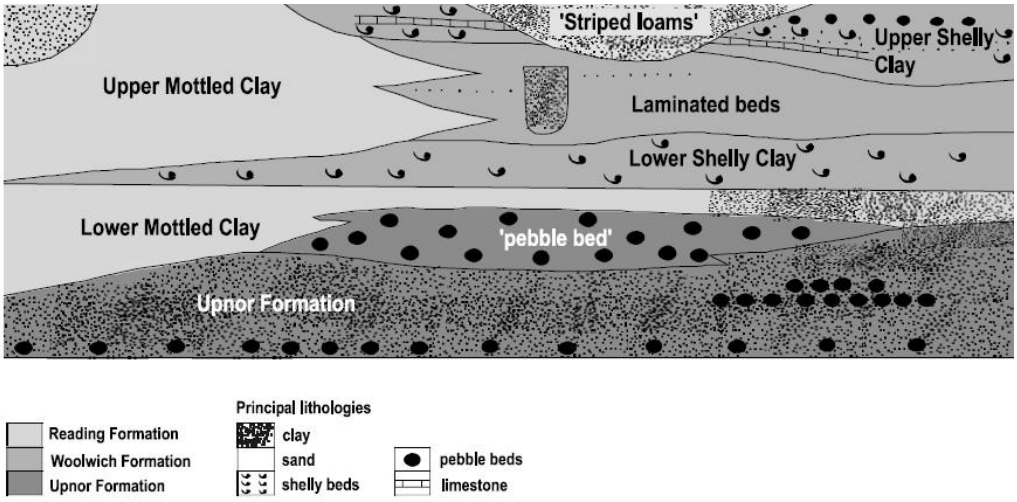

Figure 3-11. Generalised Lambeth Group succession in central London (Hight et al. 2004)

In areas where the Woolwich Formation intervene with the Mottled Clay, it has not been possible to identify the two branches by using Lithological criteria. Therefore, as can be seen in Figure 3-12 below those areas are named as undivided Reading Formation.

Hight et al. (2004) reported that the main lithology of the Reading formation is clay. An important amount of the formation comprises of largely unbedded, colour mottled silty clay and clay alone. Such lithology is named as the principal characteristics of the Reading Beds or plastic clays. Colours include pale green, pale grey-blue, pale brown, red-brown, dark brown and crimson reliant on the oxidation state of the sediments. Additionally, it has been reported that the clays contain numerous blocky texture fissures, many of them spoon-shaped (listric) and polished.

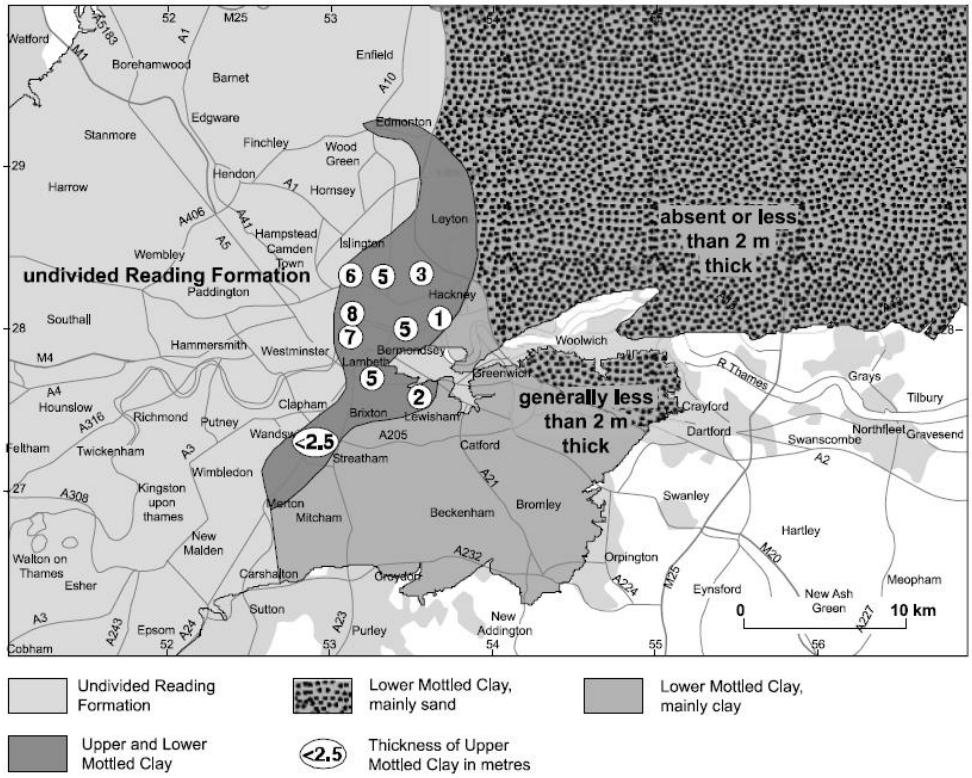

Figure 3-12. Distribution of Lambeth Group units in London: thicknesses of Reading Formation undivided and the Upper Mottled Clay and Lower Mottled Clay (Hight et al. 2004)

During the deposition of the Lambeth group, fissures with polished and slickensided surfaces have developed as a result of syndepositional desiccation throughout seasonal changes in ground moisture.

Ellison & Lake (1986) reported that the lower part of the undivided Reading Formation in Essex and the Lower Mottled Clay in London has a smectite-dominated clay mineral assemblage, similar to the Upnor Formation. In contrast, the Upper Mottled Clay and the top part of the undivided Reading Formation is dominated by illite with less smectite and some kaolinite that appears to replace smectite in places.

Hight et al. (2004) reported that the Lambeth group has been folded on reginal scale and the beds, in the majority of the London, dip generally at less than 1°. In those areas the Reading formation may contain shear planes and minor faults.

Due to periglacial slope processes, the Reading Formation is dominated by slope forms. These forms are likely to be mantled by 1- 3m of Head deposits containing shear surfaces, aligned roughly parallel to the ground surface. It has been reported by Spink (1991) that, immediately beneath the Head, periglacially weathered clay is generally

brecciated and appears softer than the clay beneath. Periglacial shearing of the Reading Formation is likely to be exacerbated by the presence of pre-existing shears (fissures) in the mottled clays.

Hight et al. (2004) also reported that the Lambeth group clays shows two distinct patterns of behaviour, depending whether they are low plasticity (I_p lower than approximately 25%) or of high plasticity (I_p higher than 35 %). Additionally, authors reported that Low-plasticity clays are non-brittle and have a residual angle of shear resistance, $\varphi`_r$, close to that at peak $\varphi`_p$. Moreover, as can be seen from Figure 3-13, the authors concluded that Lambeth group clays with low plasticity are able to dilate during shear without bifurcation, large strengths can be mobilised in undrained shear and the response is ductile.

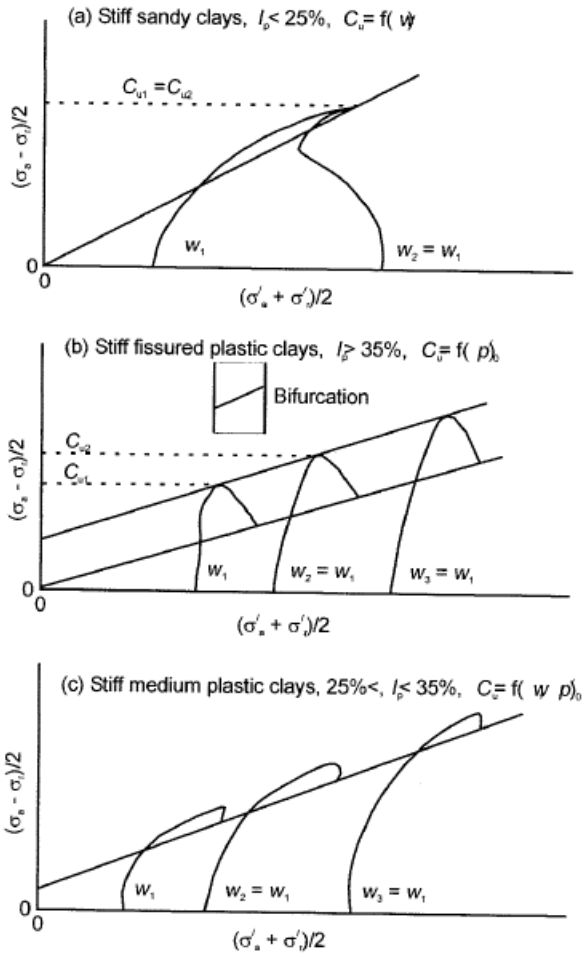

Figure 3-13. Classification of stiff clay behaviour in undrained shear on basis of the soil plasticity (Hight et al. 2004)

In contrast Hight et al. (2004) mentioned that more plastic clays experience a significant drop in friction angle, from peak to residual, and a brittle behaviour. As can be seen from Figure 3-13 these clays tend to bifurcate during shear so that undrained strength is a function of initial effective stress. Authors concluded that in absence of factors such as fissuring and cementing, clays having similar stress history but of low plasticity are expected to exhibit higher undrained strengths than clays of high plasticity.

The preparation method of the specimens used in this study has a direct influence on the initial moisture content of the samples at the beginning of 1-D consolidation or triaxial testing. Therefore it is worth to mention that Hight et al. (2004) emphasised that the undrained strength in low-plasticity clays is modified by changing the moisture content, where these changes cause a large change in undrained strength, increasing the range in measured strengths.

Hight et al. (2004) also mentioned that the effect of fissuring is highly dependent on the plasticity of the clays. Higher-plasticity clays are stated to have low-strength fissures where these fissures have a major effect on both undrained and drained strength. Additionally, authors mentioned that unfavourably oriented fissures give rise to a failure envelope corresponding to $c` = 0$, $\varphi`=14.5°$. On the other hand, fissures in low-plasticity clays are reported to be less likely to be polished unless they have been infilled by plastic clay. The authors observed that high strength was measured in fissured low-plasticity clays, suggesting that either the fissures were not represented or they have little impact on strength.

3.2 Polypropylene Fibre

Most of the research carried out on fibre reinforcement of soils have been carried out by using polypropylene fibres. Polypropylene fibres are the most commonly used synthetic material, mainly because of its environmental acceptability and low cost (Figure 3-14). Miller & Rifai (2004) identified the polypropylene as a hydrophobic and chemically inert material which does not absorb or react with the soil moisture or leachate where these are a few of the benefits of using such material.

Figure 3-14. Polypropylene fibres used in the study

The polypropylene fibres used in this investigation was provided by Mouchel Consulting Company. It has a width of 4mm, length of 63mm and thickness of about 0.021mm. Such dimensions were chosen for several reasons:

- These dimensions have been used in earlier studies by many of the researchers mentioned in this report on soil reinforcement. It is found to be the most suitable fibre length which contributes the most in terms of unconfined compressive strength, desiccation cracking, hydraulic conductivity and swelling
- Most importantly, the chosen dimensions were used by our industrial partner Mouchel in slope stability projects. Therefore, this has enabled testing of the in-situ prepared samples for comparison with laboratory prepared samples.

Some of the physical, chemical and mechanical properties of the fibres used in this study are presented in Table 4. These properties were provided by the manufacturer.

Table 4. Properties of fibres

Properties	Values
Specific gravity	0.91 g/cm^3
Denier	2610 (g/9000m)
Breaking tensile strength	350MPa
Modulus of elasticity	3500MPa
Melting point	165 °C
Burning point	590 °C
Acid and alkali resistance	Very good
Dispensability	Excellent
Moisture absorption	0%
Breaking elongation	18%
Thermal conductivity	Low
Electrical conductivity	Low
Colour	Brown

Silva Dos Santos et al. (2010) studied the behaviour of laboratory triaxial tests on quartzitic sand reinforced with polypropylene fibre. Authors performed tests on 38mm diameter and 76mm long specimens reinforced with 24mm long fibres. Such dimensions are giving a specimen size to fibre length ratio of (38/24) 1.58 which is aligned with the ratio used in this study (63/100). Authors reported that for the fibre length selected and these sizes of specimens, accumulated experience of working with fibre-reinforced sand has indeed show that boundary effects can be neglected.

3.3 Sample Size Effect

The size of the samples does not seem to affect the correlation between the compression, strength and stiffness response of the specimens. Vitone & Cotecchia (2011) mentioned that the existence of a micro to mini-structure of fissuring, will not affect the isotropic compression behaviour of the specimen with respect to the specimen size. Consequently, in this study a comparison between 38mm and 100mm un-reinforced specimens, in isotropic compression, can be seen in Figure 3-15. The compression line of both specimens seams to yield towards the same compression line, indicating no sample size effect.

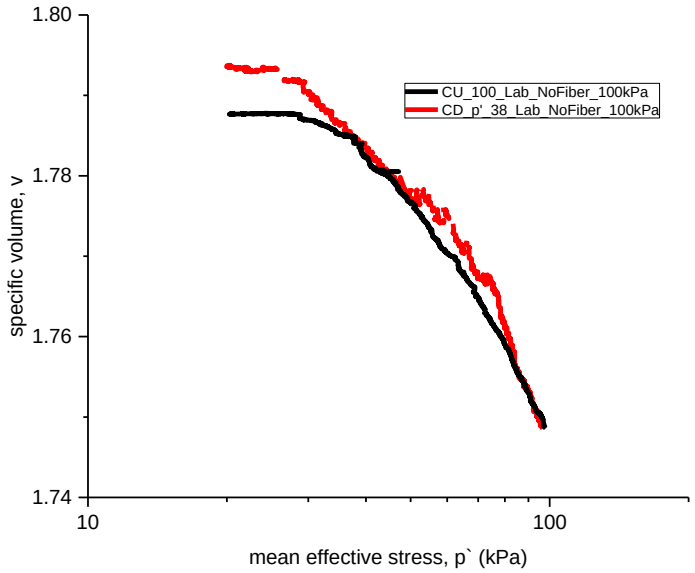

Figure 3-15. Isotropic Compression comparison of 38mm and 100m un-reinforced specimens for size effect

Furthermore, Gasparre (2005) reported that, regarding strength, no differences could be noticed between the 38mm and the 100mm diameter samples when the failure is through the intact soil. They plot together on a unique strength line, which is consistent with the study conducted by Costa-Filho (1984) on samples size effects. The differences in strength between 38mm and 100mm diameter samples only occur because there is a greater possibility for the larger samples to shear along large pre-existing fissures. In contrast, Yilmaz et al. (2015) studied the specimen size effect on the strength properties of cemented paste backfill through unconfined compressive strength tests. It was revealed that the diameter of the specimen greatly affects the overall mechanical strength for a constant height-to-diameter ratio. The most suitable specimen size with regards to the rate of strength development and the ultimate strengths was found to be D × H=5 × 10 cm, which constantly provided higher strength, regardless of the placement conditions, compared to the other specimen sizes 7.5 × 10 cm and 10 × 20 cm.

According to Figure 3-16, comparison of 38mm and 100mm unreinforced specimens' stress-strain relationship reveal that, due to the applied preparation technique, consistent strength results have been monitored independent of the specimen sizes.

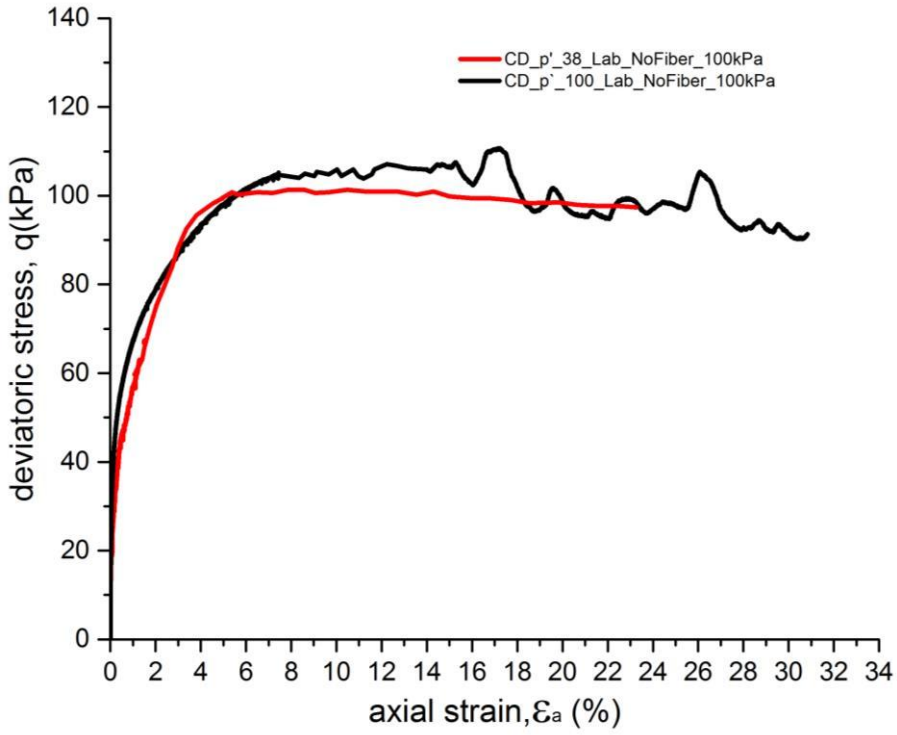

Figure 3-16 Stress-Strain comparison of 38mm and 100m un-reinforced specimens for size effect

Additionally, evaluation of the shear modulus degradation curves of 38mm and 100mm in Figure 4-17 shows that there was no effect of sample size on stiffness, similar to the compression and strength behaviour.

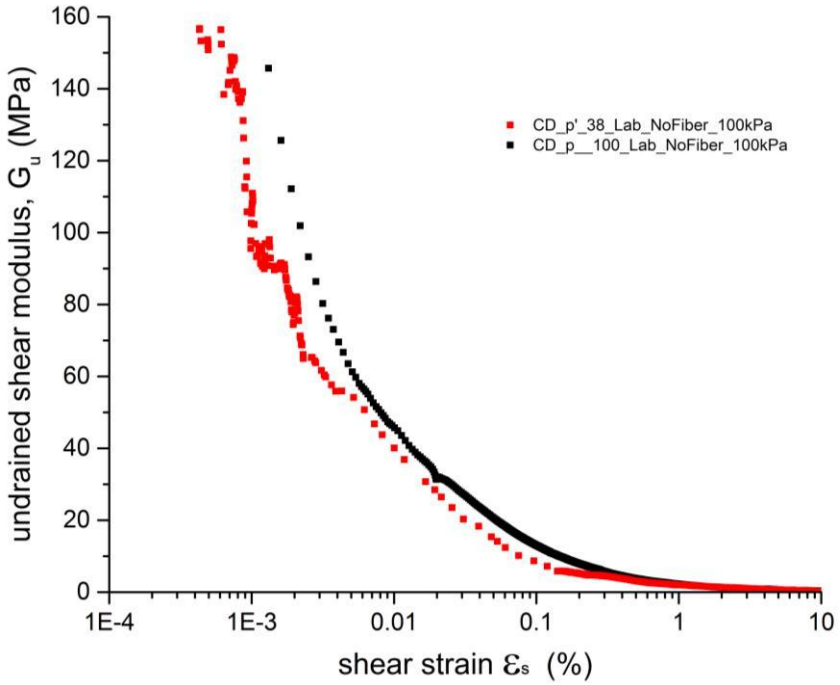

Figure 3-17 Shear modulus degradation curves of 38mm and 100m un-reinforced specimens

4. LABORATORY APPARATUS

The present study employed a one 100mm Bishop-Wesley triaxial testing system, two 38mm Bishop-Wesley triaxial testing system, two conventional oedometers and one bender element adapted oedometer. These are described and detailed in this chapter.

4.1 Compression Testing System

A conventional Oedometer apparatus was used to simulate one-dimensional consolidation in a laboratory environment. This is achieved by laterally restraining the sample and applying a sequence of loads where water flows out of the sample, while strains are permitted in the vertical direction. A schematic drawing of the oedometer cell used can be seen in Figure 4-1.

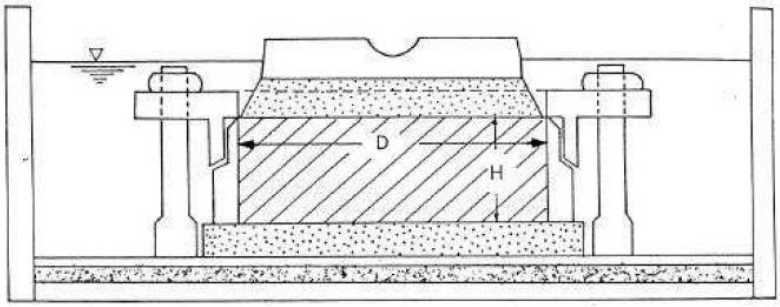

Figure 4-1. Representation of the oedometer cell (Sorensen 2006)

It can be seen from Figure 4-2 that a conventional oedometer cell have a rigid ring that contains the specimen. The ring sits on a porous stone where a second porous stone sits above the sample in order to permit double drainage. The rough dimensions of the ring are 76 mm diameter and 20mm in height. These dimensions are chosen to give a ratio of diameter to height greater than two, in order to reduce the effect of friction (Bishop and Henkel 1957), and to allow the use of enough peds to create a representative sample.

The oedometer cell sits on an aluminium base where the load is applied, through a lever arm, to the top cap of the cell. In order to avoid drying of the sample, during the consolidation test and to permit absorption of water during swelling, the specimen with the rigid ring are submerged in a water bath. The apparatuses used in this study can be seen in Figure 4-2. The stress and strain conditions are assumed to be axisymmetric and the friction where the soil makes contact with the ring is assumed to be zero. To measure the vertical displacement, a “Baty” brand dial gauge, with an accuracy of 0.002 mm, located on top of the platen, was used.

When testing reconstituted materials, starting from a slurry state, the initial vertical deformation was found to be very significant and hence the dial gauge had to be adjusted once or twice, to cope with the full range of vertical deformation of the sample.

Figure 4-2. Conventional oedometer apparatus

4.1.1 Bender Elements

Shear wave velocity measurement have been done in an apparatus designed by a previous PhD student from UCL CEGE, Sorensen (2006). Slight updates have been performed on the equipment, in order to adapt the required testing scheme. The Equipment comprises a multipurpose loading-frame and a modified Wykeham Farrance oedometer cell, fitted with bender elements for shear wave transmission. For this study instead of a loading cell, the lever arm and the dead weight hanger (ratio 1:11) have

been used in order to apply the required pressures to the sample. The setup of the oedometer testing system is shown in Figure 4-3 and the layout of the oedometer cell is shown in Figure 4-4.

Figure 4-3. a) Oedometer testing system setup for shear wave modulus measurement and b) bender element potted on a brass cartridge.

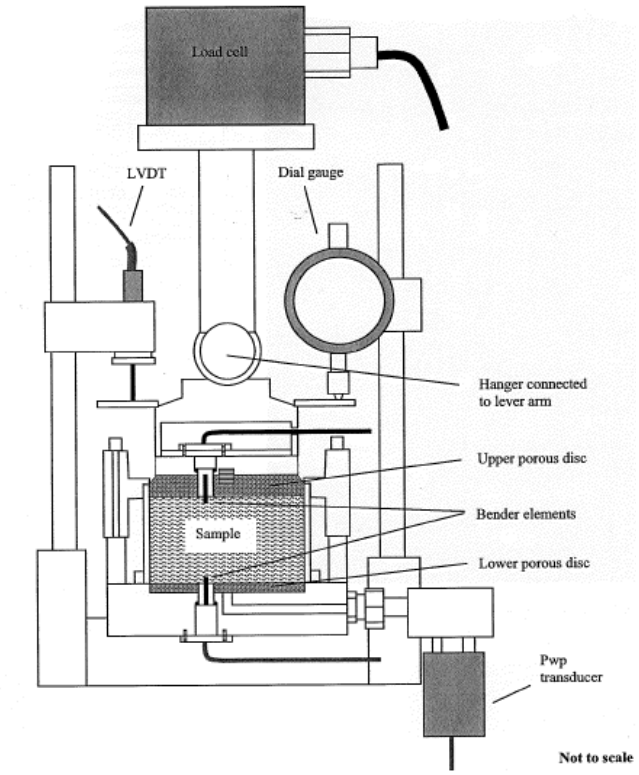

Figure 4-4 Schematic layout of the oedometer cellwith Bender elemetns (Sorensen 2006).

A standard 75mm diameter size oedometer cell, used to laterally confine the specimen, has been modified to allow for initial sample heights up to 40mm due to the bender elements. Features that have been retained from the original Wykeham Farrance cell, are a fixed rigid confining ring and a one-way top drainage with a base water pressure measurement through porous stones. The vertical displacement of the top cap was recorded by means of a Baty dial gauge with an accuracy of 0.002 mm and a range of 10mm. The bender elements, manufactured in-house, with instructions described in Sorensen (2006), were fitted into the top cap and base of the cell. A photo of the bender elements incorporated in the cell can be seen in Figure 4-3. The schematic drawing can be seen in Figure 4-4. The determination of the shear wave modulus, G_{VH} enabled by shear wave transmission along the vertical axis of the sample with a horizontal polarisation. The bender element generally protruded 2mm into the sample at either end, meaning that the vertical distance between the tips was 36mm which allowed for a greater range of the bender element test.

Figure 4-5. Bender element incorporated oedometer testing system setup

As can be seen in Figure 4-5 the test setup consists of a function generator (Agilent 33220A 20 MHz Function/Arbitrary Waveform Generator), a transmitting and a

receiving bender element set, intruding into the sample, at axially opposing ends and an Oscilloscope (Agilent InfinitiVision MSO3054A) with data logging capability.

4.2 Triaxial Testing System

4.2.1 100mm Triaxial testing equipment

A computer-controlled 100mm Bishop-Wesley triaxial testing equipment has been acquired from Imperial College (IC). IC design and build such systems in their workshops. The complete 100mm triaxial equipment can be seen in Figure 4-6 with a schematic drawing in Figure 4-7. The equipment is capable of testing 100mm diameter by 200mm height samples. It is equipped with local instrumentation, in cell temperature probe, Constant Rate Strain Pump for strain control and Imperial College design volume gauge.

Figure 4-6. The 100mm triaxial system

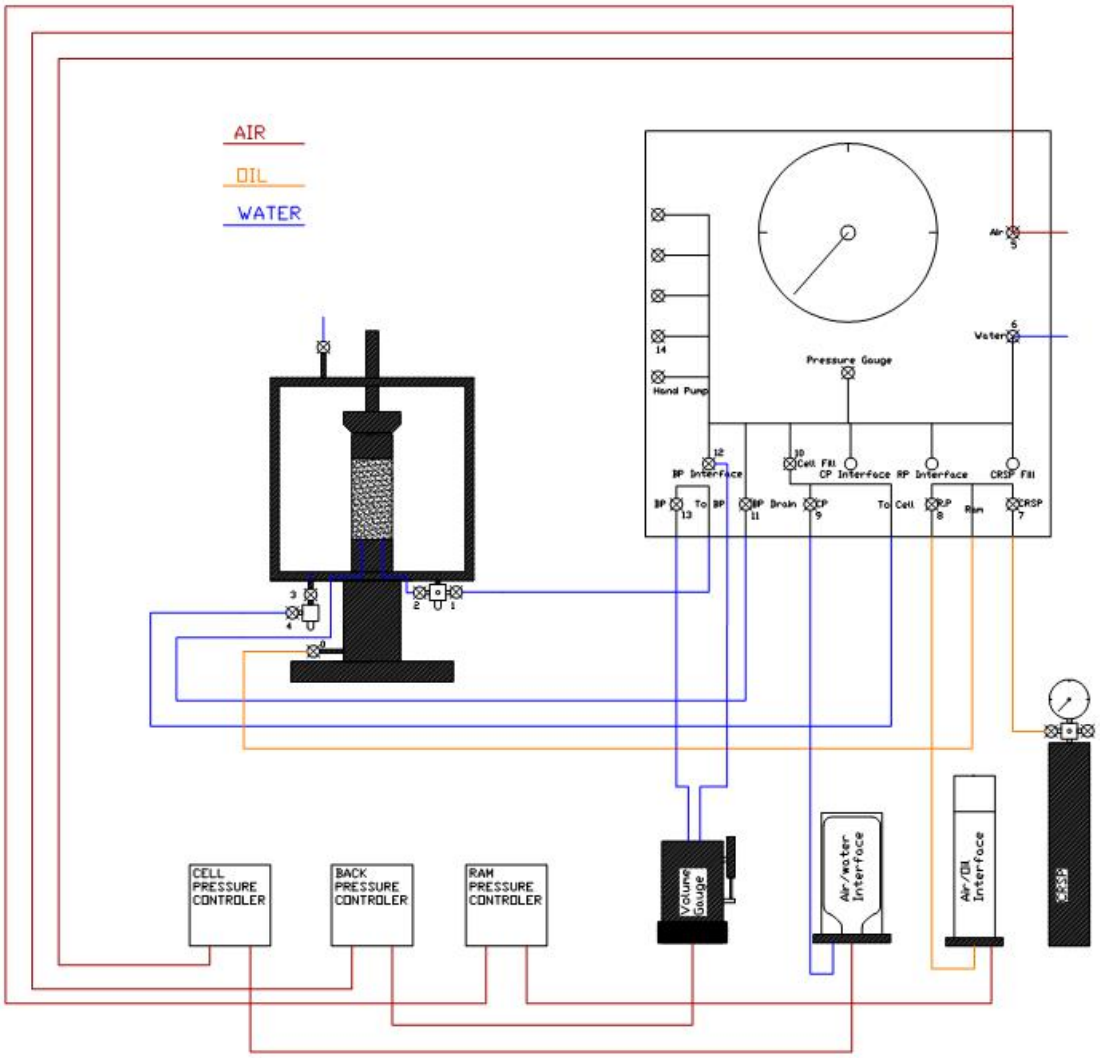

Figure 4-7. Schematic drawing of a 100mm triaxial system

An evaluation of the available literature in sample size effect on reinforced soils, allowed the author to acknowledged that 100mm diameter specimens will correspond better to the representative element volume (REV) which is more suitable to represent the overall fibre-reinforced behaviour of the Lambeth Group clay. Given the dimensions of fibre in the 38mm sample, due to the low mixing ratio (0.2% of the dry weight of soil), either no fibres or an insufficient amount of fibres were expected in the 38mm specimen, which will not allow the identification of the in-situ and laboratory-compacted reinforced Lambeth Group clay.

4.2.1.1 Test Cells and Top Cap

A 100mm triaxial cell is similar in design to the conventional hydraulic-operated stress path cell designed by Bishop & Wesley (1975). However, it is manufactured on a bigger scale to accommodate bigger samples. The concept of loading is the same as the 38mm triaxial system but with an improved top cap design. A special suction cap, that can be seen on Figure 4-8, is adopted for 100mm samples and is used in conjunction with a half-ball contact system that protrudes only 1mm from the top platen. As discussed by Gasparre (2005) this connection gives minimum disturbance to the sample due to the contact, between the sample top plate and the load, made through the half-ball which rotates, adjusting its direction to the load cell and absorbing the disturbance caused by the imposing alignment.

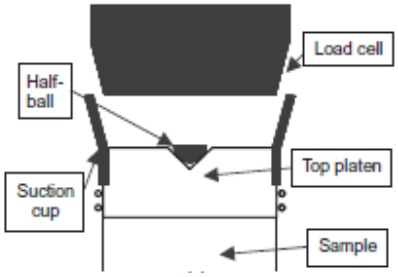

Figure 4-8. Special suction cup with a half-ball contact system

4.2.1.2 Loading System

A similar approach to the 38mm triaxial equipment is used, with some minor changes in pressure controllers, the CRSP system and the IC volume gauge. The pressure controllers used in this system are IC air pressure valve controllers. These are stepper-motor-driven precision air pressure regulators, supplied by IC, with a pressure range of 10 – 820 kPa. The pressures can be adjusted in increments of 0.07 kPa. They are driven through a PCI 836 card installed in a PCI slot in the computer.

In the 100mm triaxial system, a Constant Rate of Strain Pump (CRSP) is used to control the deviator stress. This is a stepper-motor-driven piston pump, supplied by IC. The pump has a capacity of 100 cc and the volume can be adjusted in increments of 0.0001 cc. The CRSP is driven by the same PCI card mentioned above with a computer control.

Another minor difference from the 38mm cell is the volume gauge where in the 100mm equipment the IC volume gauge used has a 100cc volume capacity, rather than the 50 cc capacity of the 38mm system.

4.2.1.3 Measurement Instrumentations

The back pressure and cell pressure systems are measured by a Wykeham Farrance (WF) pressure transducer, attached directly onto the base of the cell. Pore water flow is measured using the IC type volume gauge, mentioned above, with an LVDT displacement transducer attached (made by RDP). The gauge has a 100 cc capacity, which corresponds to a 30mm travel of the LVDT.

Figure 4-9. IC hydraulic control panel

The axial strain is measured externally using an LVDT displacement transducer placed under the base metal plate of a cell with a nominal stroke of 25mm. As the sample deforms, the axial displacement gauge measures the relative movement between the ram cylinder and the base metal plate of the chamber as the sample is fixed between the ram pedestal and the load cell.

A 5kN internal submersible load cell supplied by WF type STALC3 is used to measure the applied axial load. Characteristics of transducers and signal conditioning used in a 38mm triaxial system can be seen in Table 5.

Table 5. Characteristics of transducers and signal conditioning used in 38mm Triaxial cell.

Transducer	Type	Capacity	Resolution	Excitation (V)	Signal output range (V)
External axial Transducer	LS25	25 mm	0.002 mm	5 V DC	0 - 35 mV
Volume gauge Transducer	LS25	100 cc	0.002 cc	5 V DC	0 - 35 mV
Local axial LVDT 1	D5/200	+/-5 mm	0.0001 mm	5 V AC	+/- 5 V
Local axial LVDT 1	D5/200	+/-5 mm	0.0001 mm	5 V AC	+/- 5 V
Local radial LVDT	D5/200	+/-2.5mm	0.0001 mm	5 V AC	+/- 5 V
Internal load cell	STALC3	25kN	5 N	5 V DC	0 - 10 mV
Cell Pressure transducer	WF	10 Bar	0.1 kPa	5 V DC	0 - 50 mV
Pore pressure transducer	WF	10 Bar	0.1 kPa	5 V DC	0 - 50 mV
CRSP transducer	WF	10 Bar	0.1 kPa	5 V DC	0 - 50 mV

4.2.1.4 Local Instrumentation

Strain measurement through axial displacement transducers are prone to errors, which can be summarized as seating, bedding and alignment errors of the sample top cap and base porous stone (Head 1986). For overcoming the majority of the above-mentioned errors, local strain measurements were used over the middle 2/3 of the sample as described by Cuccovillo & Coop (1997) and can be seen in Figure 4-10.

The concept of Cuccovillo & Coop (1997) has been applied with slight changes to the LVDT armatures and the base seating plate. Axial LVDTs can be seen in Figure 4-10 where the armature rested on a lower mount. Additionally, it is attached with a large-headed screw that enabled small adjustments of the armature to be performed when the sample setting up is taking place (Figure 4-10).

Figure 4-10. Small strain local instrumentations

4.2.1.5 Mid-Height probe

The pore water pressure distribution in the samples was investigated by comparing the measurements at the base and mid-height of the sample. Figure 4-11. shows an example of the pore water pressure readings at the base (where it is also controlled) and mid-height of the sample. The pore water pressure was uniformly distributed, with both measurements being almost identical, until the formation of the shear plane. The shear plane formation was associated with a pore water pressure in the mid-height of the sample, which is in agreement with studies carried out by Sandroni (1977) and Gasparre (2005).

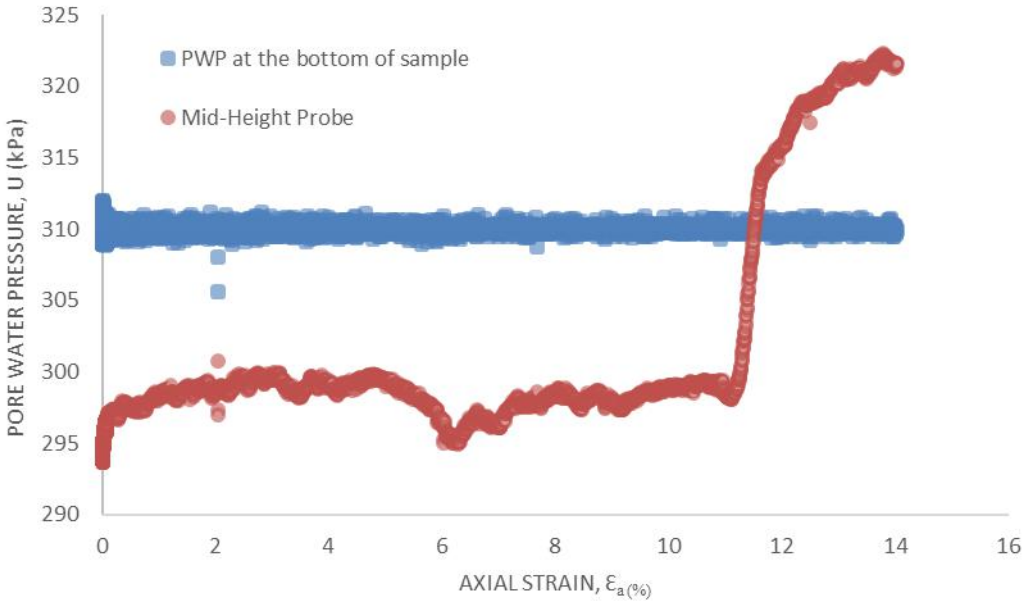

Figure 4-11. Pore water pressure development at the base and mid-height of a sample of DF100 sheared in compression

4.2.1.6 Signal Conditioning and Data Acquisition

The main difference between 100mm and 38mm triaxial systems, data acquisition, is the data logging systems. In this system, the MSL Datascan 7220 model by Measurement Systems Ltd is used to acquire data (Figure 4-12). This data logger provides 16 channels with the possible addition of extra channels if needed. The channels can be specified either as a 100 mV range, suitable for most strain-grouped devices, such as load cells, pressure transducers, displacement transducers, or alternatively as a 10v range.

Figure 4-12. Data acquisition system

The Triax software is used to control the equipment. It is a Windows-based software and developed by Durham University. The flexibility of the program allows it to be used with many other types of soil laboratory testing equipment. The Triax software is capable of controlling stresses, strains and displacement. Additionally, the software can monitor the pressures and allow the user to define the triaxial testing stages with automatic changes in the stress path. The visual interface of the Triax software can be seen on Figure 4-13. In the main window, shown on the figure, it is easy to see the monitor window, where the values measured by each sensor is displayed; the Control window, responsible for the control of the pressures in each stage of the test; the Scan window show the data being recorded and the many graphs that can be set up by the user.

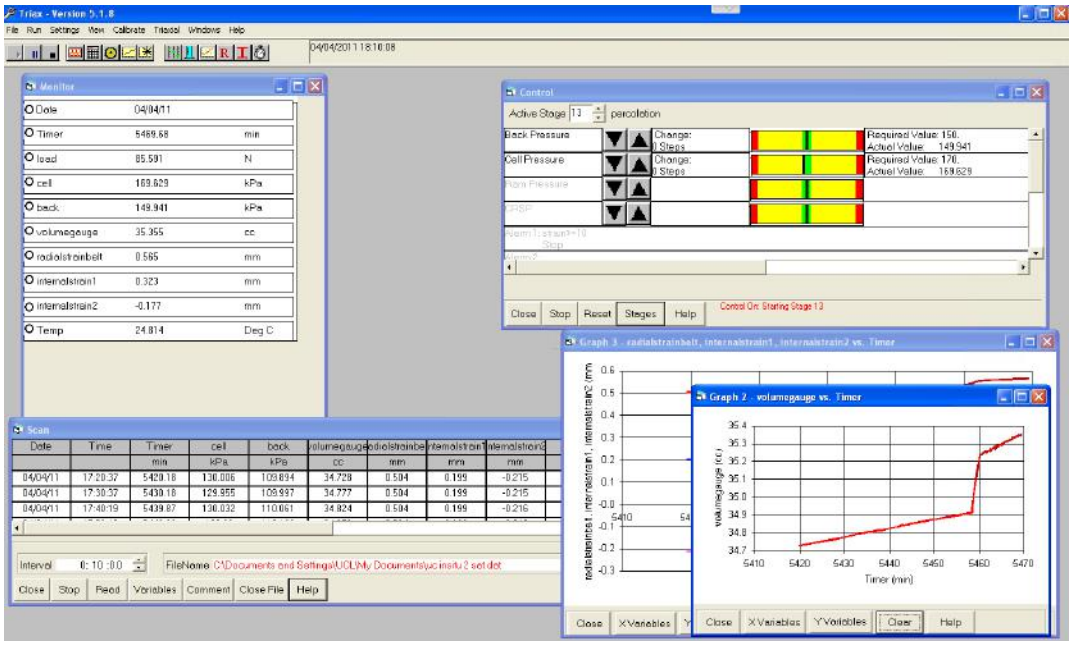

Figure 4-13. Visual Interface of the Triax software

4.2.1.7 Calibration of Transducers

The calibration of the transducers was carried out at the IC soil laboratory in the presence of the author.

For the calibration of pressure transducers (back, cell and ram pressure transducers), a dead-weight pump from Budenberg was used. In order to reduce any variance in pressure due to difference in elevation, pressure transducers were mounted at the same

level as the indicator (Bourdon gauge). The calibration curves for cell and back pressure transducers can be seen on Figure 4-14 and Figure 4-15.

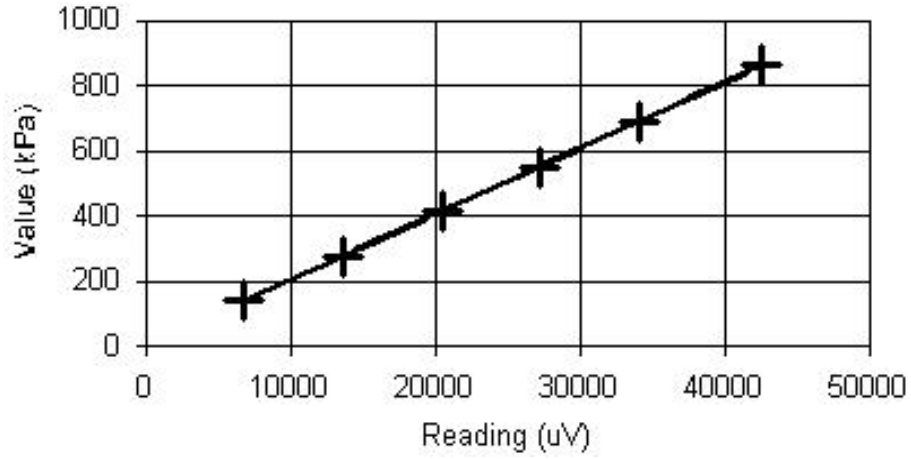

Figure 4-14. Cell pressure transducer calibration curve

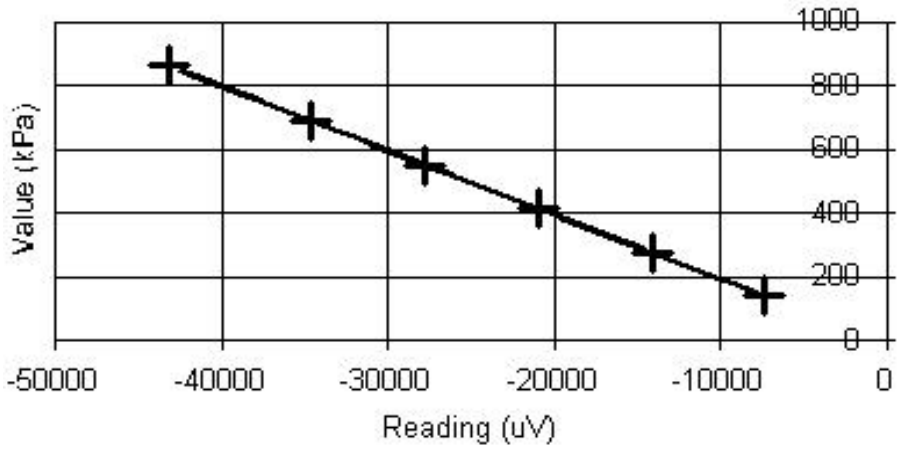

Figure 4-15. Back pressure calibration curve

The calibration of the axial displacement transducer was done by mounting the transducer to a purpose-made mount (Figure 4-16) against a micrometre with a resolution of 0.01mm. The local LVDTs were calibrated against a dial gauge with a resolution of 0.002mm. The same procedure was used to calibrate the local instrumentation gauges, including the radial LVDT adapted on the radial belt. The calibration curves can be seen on Figure 4-17, Figure 4-18, Figure 4-19 for Radial, Axial 1 and axial 2 LVDTs respectively.

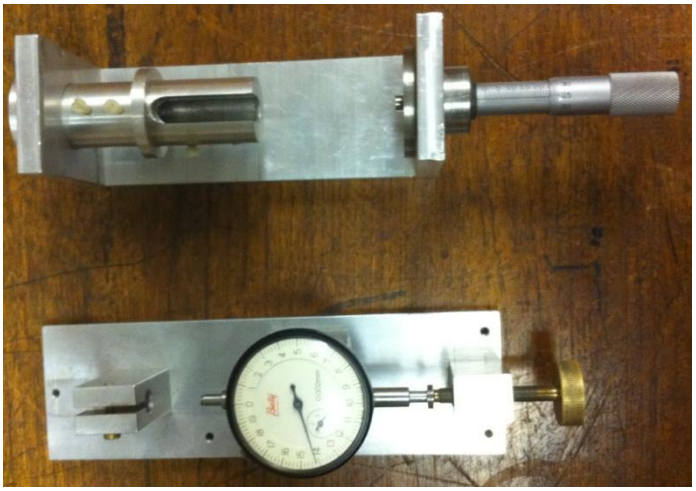

Figure 4-16.Purpose-made mounts for displacement transducer and Local LVDT calibration

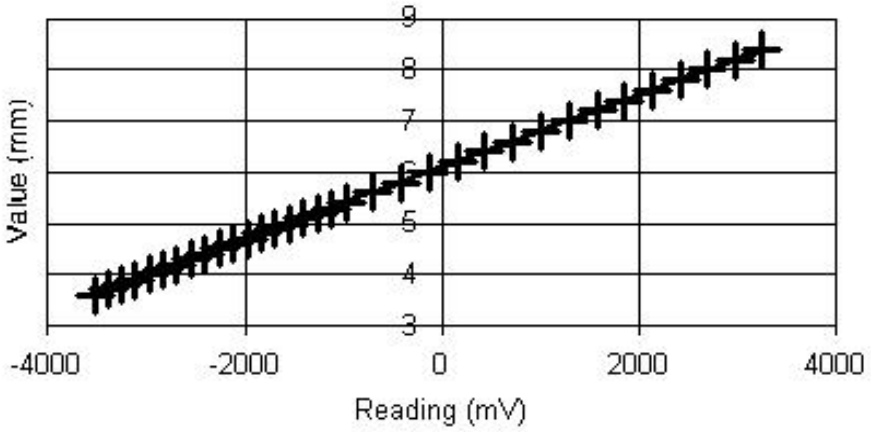

Figure 4-17. Radial LVDT calibration curve

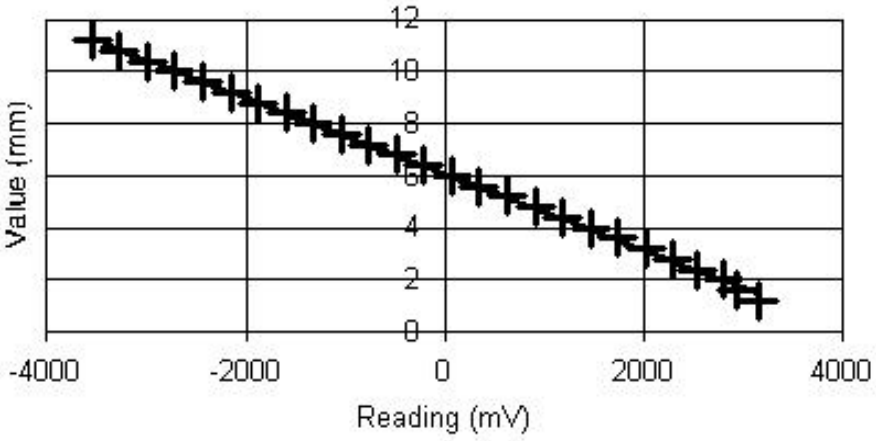

Figure 4-18. Axial 1 LVDT calibration curve

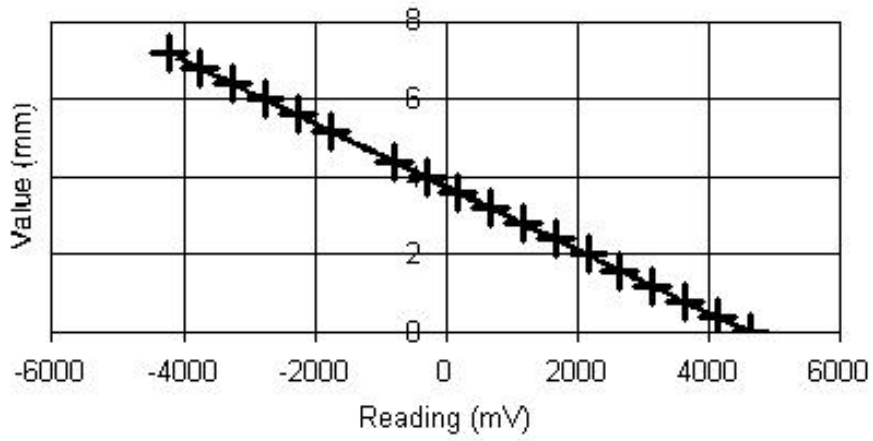

Figure 4-19. Axial 2 LVDT calibration curve

The volume gauge was calibrated by placing the volume gauge over a scale with an accuracy of 0.001 gr and pumping water in and out of the gauge with the help of a piston to push the water manually in and out of the volume gauge (hand-pump). By doing so, the volume gauge was calibrated against the measured weight of water where 1 cc is equal to 1 g (Figure 4-20).

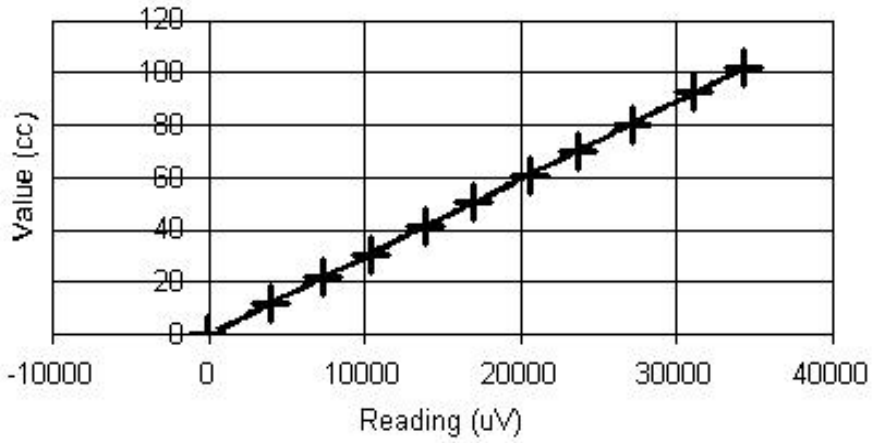

Figure 4-20. Volume gauge calibration curve

Finally, the load cell was calibrated for compressive stresses by using a specific build frame where a hydraulic jack is connected to a dead-weight Budenberg pump. By applying a known pressure the force exerted on the load cell is known and the calibration is possible (Figure 4-21).

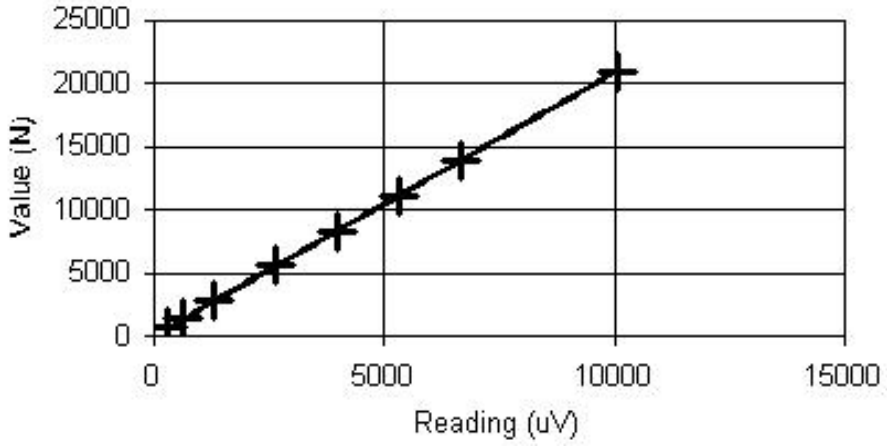

Figure 4-21. Load cell calibration curve

4.2.2 38mm Triaxial Testing System

A computer-controlled 38mm Bishop-Wesley triaxial testing equipment has been re-assembled with the help of the author by using available instrumentation at the UCL Soil Mechanics Laboratory. The current apparatus has been used for several research projects in the past, and, a refurbishment of the system was due. Therefore, with the use of available resources, the 38mm triaxial system was rebuilt to allow a fully computer-controlled stress path testing. A schematic diagram of the system can be seen in Figure 4-22. The system has been subjected to a few modifications that include the introduction of high-resolution miniature local LVDTs to improve the accuracy of the strain measurements (Figure 4-23).

The experience gained from testing the Lambeth Group clay on a 100mm Triaxial system has led the author to realise that, given the long test duration, it would be unlikely that the testing programme set at the beginning of the project could be achieved during the time allocated for the project. Therefore, a decision was made to refurbish the small equipment, capable of testing smaller samples, where saturation and consolidation durations would be shorter and consequently affect the shearing speed. However, it would not be possible to test the fibre-reinforced samples, due to the fibre lengths.

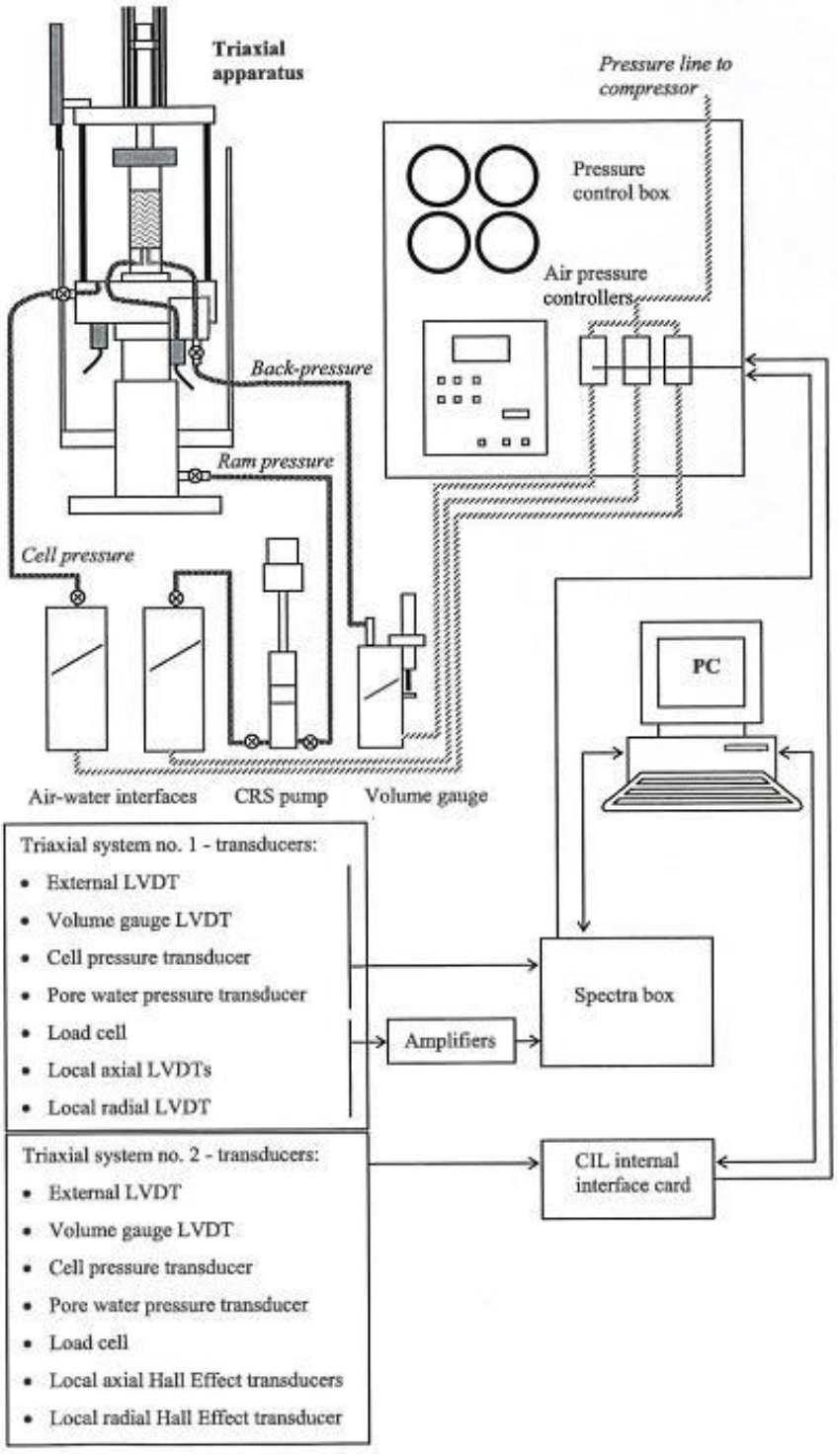

Figure 4-22. Schematic layout of a 38mm triaxial system (Sorensen 2006)

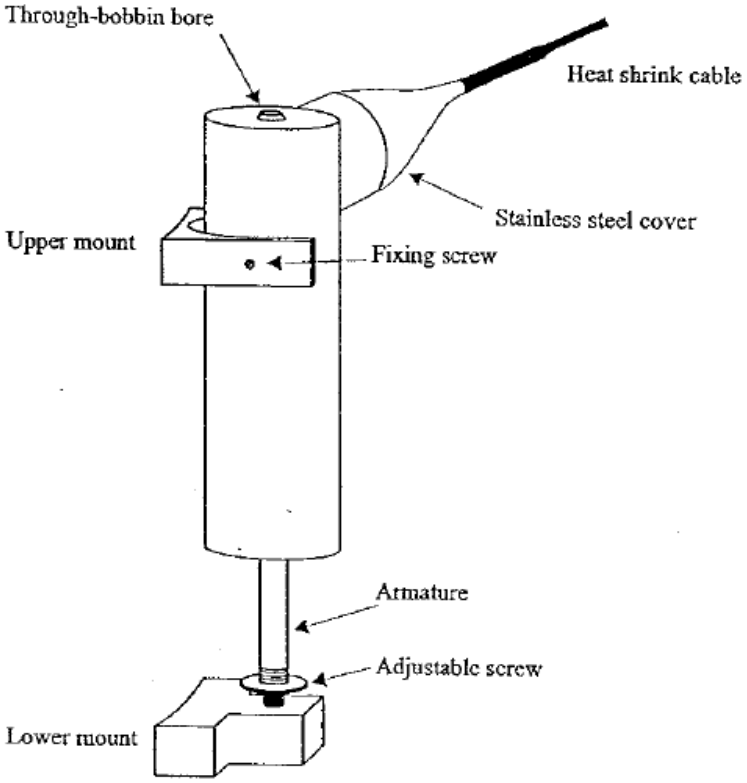

Figure 4-23. Axial LVDT with adjustable screw (Rolo 2003)

4.2.2.1 Test cells

The triaxial cell is similar in design to the conventional hydraulic-operated stress path cell designed by Bishop & Wesley (1975). Several modifications were made, such as introducing a drainage system through the top cap, to provide shorter drainage paths. A schematic drawing of the triaxial cell is shown in Figure 4-24. The triaxial cell consists of a Plexiglas outer cylinder and close-fitting metal top and bottom. The metal top and bottom are held tightly in place by tension bars. Through the centre of the metal bottom a piston moves up and down by generating differences in pressure between the cell and the lower pressure chamber; both isolated by rolling diaphragms manufactured by Bellofram. Linear bearings placed around the piston permit vertical movement and low friction whilst retaining the verticality of the piston. Controlling the stresses or strains in the lower chamber allows the transmission of stress and strain to the sample in the upper chamber.

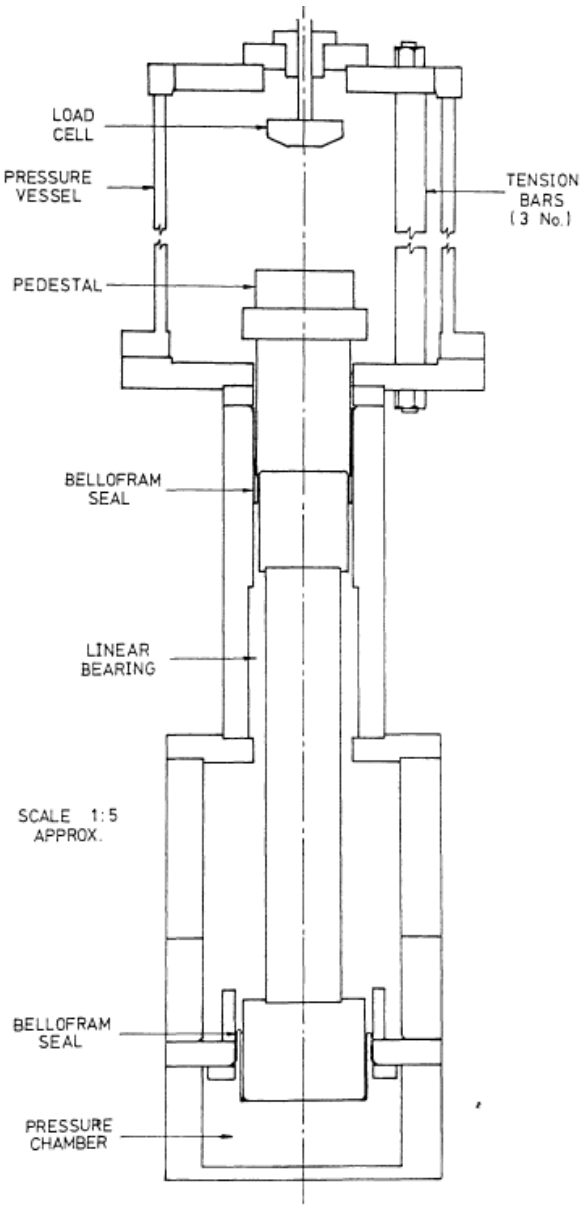

Figure 4-24. Schematic diagram of a standard 38mm stress path triaxial cell. (Clinton 1987)

At the top of the piston, inside the pressure vessel, a 38mm pedestals is attached where the sample sits. Attached to the top metal plate there is a Wykeham Farrance 5kN internal submergible load cell. Clinton (1987) stated that the load cell is fixed onto a metal rod that passes through two O-ring seals. The rod then screws internally into a thread ring which allows the internal load cell to be raised or lowered. The deviatoric force measurements are not affected by the frictional errors as the load cell is mounted inside the cell.

4.2.2.2 Loading System

The 38mm triaxial system is equipped with three pressure control units that regulate the back pressure, the ram pressure and the cell pressure, similar to the 100mm triaxial equipment described. The input air pressure comes from a vane air compressor that can produce maximum pressures between 900kPa to 1000 kPa. The pressures applied to the sample are managed by three stepper motors. When an increase or decrease in pressure is required, the computer system converts the required change in pressure to a number of pulses that are sent to the stepper motors., consequently changing the pressure in the required direction.

Regulated air pressures pass to the cell and ram via air/water interfaces. These consist of sealed cylinders where the water is pressurized by a flexible rubber separation membrane, in the shape of a bladder. The air pressure required is delivered to the inner side of the membrane and transferred to the water. Back pressure is provided by an Imperial College type volume gauge, also working as an air/water interface(Figure 4-25).

Figure 4-25. Imperial College volume gauge

4.2.2.3 Top Cap Connection

For testing of stiff compacted clay samples, which is the case in this study, connection between the load cell and top cap consisted of a half ball and cornered sealing on the top cap. This connection type allows free rotation and sliding between the loading ram and the top cap.

4.2.2.4 Measurement Instrumentations

The cell pressure and the back pressure systems are measured by a Wykeham Farrance (WF) manufactured pressure transducer, attached directly onto the base of the cell. Pore water flow is measured using an Imperial College type volume gauge with an LVDT displacement transducer attached (made by RDP). The gauge has a 50 cc capacity, which corresponds to 25mm travel of the LVDT.

The axial strain is measured via LVDT displacement transducer placed under the base metal plate of a cell with a nominal stroke of 25mm. As the sample deforms, the axial displacement gauge measures the relative deformation since the sample is firmly connected to the top and bottom of the cell.

The applied axial load is measured using a 5kN internal submersible load cell supplied by WF type STALC3. Characteristics of transducers and signal conditioning used in a 38mm triaxial system can be seen in Table 6.

Table 6. Characteristics of transducers and signal conditioning used in a 38mm triaxial cell. (Sorensen 2006)

Transducer	Type	Capacity	Resolution	Excitation (V)	Signal output range (V)
External axial LVDT	RDP LDC500A	25 (mm)	4 (μm) 0.005 (%) strain	9.9	-2.2 to 2.2a
Volume gauge LVDT	RDP LDC500A	25(mm) 50(cm^3)	4 (μm) 0.005 (%) strain	9.9	-2.2 to 2.2a
Local axial LVDT 1	RDP D5/200WRA	10(mm)	0.16(μm) 0.0002(%) strain	9.9	-3.3 to 4.5b
Local axial LVDT 1	RDP D5/200WRA	10(mm)	0.16(μm) 0.0002(%) strain	9.9	-3.2 to 4.4b
Local radial LVDT	RDP D5/200WRA	10(mm) 38(mm)	0.16(μm) 0.0002(%) strain	9.9	-3.4 to 4.2b
Internal load cell	WF 4958	5(kN)	0.1(kPa)	9.9	0 to 3.0b
Cell pressure transducer	WF17060	1000 (kPa)	0.1(kPa)	9.9	0 to 0.1
Pore pressure transducer	WF17060	1000 (kPa)	0.1(kPa)	9.9	0 to 0.1

4.2.2.5 Local Instrumentation

A change in the distance of travel of the armature inside the LVDT body produces a change in the output voltage where this voltage can be calibrated to obtain displacement in mm. The design of the lower mount allows the sample to barrel or develop a shear plane without disturbing the armature. These transducers have a linear calibration over a range of about 10mm displacement. In order to resolve very small strains at the start of the shearing, the LVDTs must be set to their electrical zero by adjusting the zero potentiometer in the transducer amplifier where this setting allows the data logger to work in its most sensitive range. Radial displacements are also measured with a similar approach by mounting a radial belt around the sample (Figure 4-26).

Figure 4-26. Setup of local instrumentation

4.2.2.6 Signal Conditioning and Data Acquisition

In the first two triaxial 38mm test a computer with an MS-DOS operation system connected to a 32+ input channel data logger (Spectra box model SB1-11) was used in the data acquisition. A triaxial control software written in Q-Basic™ code and

developed over several years by Prof. Matthew Coop was used for the calibration and monitoring of transducers, control of the stress path and recording of data.

For the rest of the 38mm test same data acquisition system and software was adapted as 100mm traxial system.

4.2.2.7 Calibration of Transducers

The same procedure used for the 100mm cell was followed for the calibration of the sensors but with small differences. For the calibration of the pressure transducers, a Budenberg dead-weight tester was used.

The axial displacement transducer was calibrated by mounting the transducer to a purpose-made mount against a micrometre with a resolution of 0.01mm where the local LVDTs were calibrated against a Baty dial gauge with a resolution of 0.002mm.

The volume gauge was calibrated with the use of a scale, following the procedure described previously.

Finally, the load cell was calibrated by placing dead weights on a hanger, attached to the load cell, similar to an oedometer equipment.

5. TEST PROCEDURES

The present chapter review the sampling of the fibre reinforced Lambeth Group Clay on site, the laboratory testing methods and the basic properties of the samples. The sampling procedures and methods are discussed in section 5.1. Additionally, basic properties such as index properties are discussed in section 5.5 in order to determine basic parameters for further use. Testing conditions and procedures for determining fibre alignment, shrinkage, compression, shear and stiffness behaviour of the tested soil are described in sections 5.6 to 5.9.

5.1 Sampling and Pre-processing

The author with help of the UCL Civil, Environmental and Geomatics Engineering Department staff recovered block samples during the Fall 2009. The blocks were obtained from the fibre-reinforced slope stabilization project, located on the M25, J23 (Figure 5-1). The site is located at approximately at Grid Reference 522735E, 200790N, adjacent to the slip road onto the northbound carriageway of the A1(M) motorway and close to service station at the junction with the M25 motorway. The location of the site is shown in Figure 5-1. The site consists of a cutting with a maximum height of approximately 5m and a maximum slope angle of approximately 15°. The slope is bound at the top by fields and at the bottom by the slip-road onto the northbound carriageway of the A1(M).

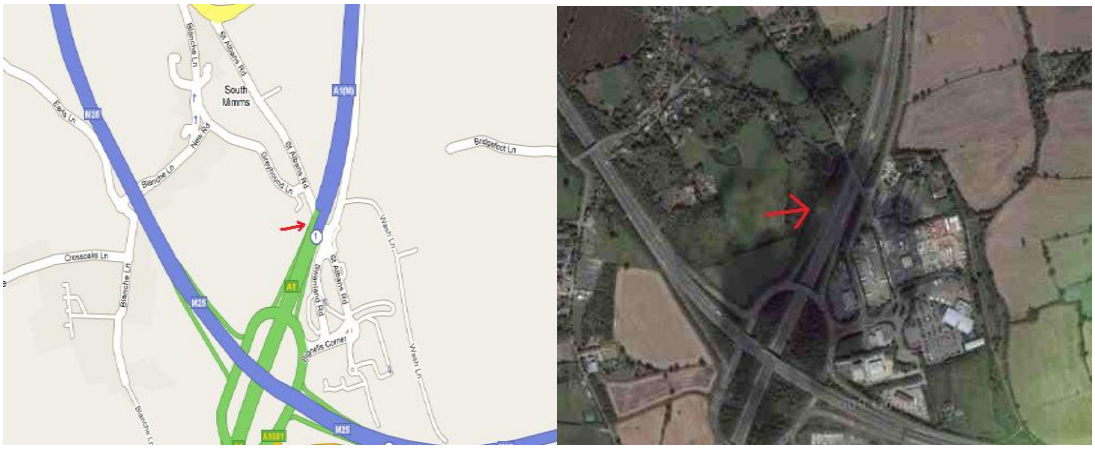

Figure 5-1. Location of Mouchel's trial site

The sampling process was carefully organized. Equipment's required were cling film, expansive foam, wooden boxes, safety kits etc. In addition, heavy duty equipment (electric hammer and an excavator) was required to create a trench to collect the block samples and it was provided by the industrial partner Mouchel.

Great care has been taken to comply with the UCL Health and Safety rules. On arrival at the site, a safety briefing was given to attendees about the hazards on site. Staff from the Imperial College Soil Mechanics Laboratory, who had experience in block sampling, accompanied the author during the process to obtain the samples.

5.2 Field Work

With the help of an excavator a trench was made on the compacted slope (Reinforced with fibres) which had been completed two weeks earlier. The trench was 600 mm deep and the excavator did not excavate closer than 300mm to the sample sides (Figure 5-2). Great attention was paid in order to limit the disturbance to samples and the final stage of the excavation were carried out with a pneumatic clay spade, a soil saw and a manual clay spades. Six 300 x 300 mm blocks were formed, wrapped with cling film and waxed to retain the moisture content. The samples were then placed into wooden boxes and transferred to the UCL Soil Laboratory where they stayed in a moisture-controlled environment. From the same location, 12 bags of clay that would be compacted in the slope were collected for laboratory use. The samples were placed in heavy duty bags and tied with cable ties to retain the in-situ moisture content.

Figure 5-2. Trench for block sampling

5.3 Important Observations

- While excavating the block samples, it was observed that the compacted clay layers were not properly connected with voids and large lumps of clay being seen. This was caused by a lack of proper control when compacting the layers and mixing the fibres in the soil with the rotovator.
- Stability treatment on site was carried out by compacting 100 mm thick fibre-reinforced clay layers each time until they reached the required height. A layer of large peds of clay at the natural moisture content was spread, with the desired percentage of fibres dispersed by hand. A rotavator was passed over the created layer to reduce the size of the clay peds to around 40mm, as well as mix the fibres into the clay. Afterwards a sheepsfoot roller passed over the layer compacting the soil to the required density. This process can be seen in Figure 5-4 and steps of the treatment can be seen in Figure 5-3. During the process of sampling, the author also observed separate layers of fibres between the two clay layers which indicates inadequate mixing.

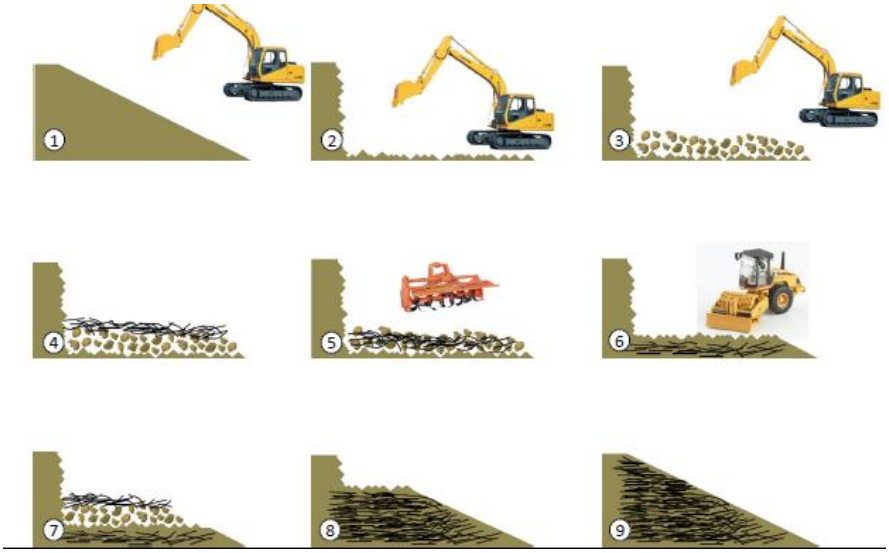

Figure 5-3. Steps of fibre reinforced slope treatment

- The slope where the block samples were retrieved had been treated two weeks prior to the sample collection. The author observed that the moisture content of the soil was too high and later, through the project manager, it was revealed that, during the treatment of the section, it had rained, causing an increase in the moisture content. In order to achieve the required strength, the fibre content was doubled. However, in the Literature review chapter it can be seen that exceeding the optimum fibre and moisture cause a reduction in the Unconfined Compressive Strength, increasing crack development and altering the compaction behaviour.

Figure 5-4. Mouchel's site treatment

- The author also observed that pebbles, with a variety of sizes, were present within the current reinforced slope. This is due to the construction of a drainage trench at the end back of the slope that contaminated the soil.

5.4 Sample Preparation

After the arrival of specimens at the UCL laboratory, samples were left at room temperature overnight. In the following day an additional paraffin layer was applied to the samples. Finally, expansive foam was applied to fill the gaps between the block sample and the box, keeping the soil under a small confinement. This process was done to preserve the in-situ moisture content until the samples were tested. Furthermore, the moisture content of each disturbed sample bag have been determined, to monitor the moisture change until testing the prepared specimens.

Figure 5-5. Waxed block sample

5.5 Characterization of Clay

Some of the engineering properties of soils are influenced by a number of factors such as geological history, organic material, particle size distribution and non-clay mineral composition. Nevertheless, for a wide range of soils, their mechanical properties are largely evaluated by the finest 20% of the constituent grains for the soil used, that is the fine silt and clay fraction. The preliminary tests performed were: specific gravity determination, atterberg limit tests and particle size distribution. These tests provide preliminary information for the soil which has been used later, in the analysis. Preliminary tests were also repeated for every other testing series, in order to check the consistency of the used material.

5.5.1 Atterberg Limit Test (Index Test)

The Atterberg limits are based on the moisture content of the soil. The plastic limit is the moisture content at which a soil passes from the plastic state to the solid state, and

becomes too dry to be in a plastic condition. A wide variety of soils' engineering properties are correlated to the liquid and plastic limits, and these are also used to classify the soil according to the Unified Soil Classification Systems. The main problem with the Atterberg limit tests is that they are heavily operator-dependent tests. Therefore, several repetitions by experienced operators can reduce the operator-induced errors. In this project, the Atterberg Limit test is carried out in accordance to BS 1377-2:1990. The summary of the properties of the clay sample used in this study is presented in Table 7.

Table 7.Geotechnical Properties of Lambeth Group Clay

Property	Values
Liquid Limit (wL)	72 (%)
Plastic Limit (wp)	33 (%)
Plasticity Index (Ip)	38 (%)

Depending on the results, the above-used clay is classified as inorganic clay of high plasticity (CH), according to USCS classification (ASTM 1993)

5.5.2 Particle Density Determination

Particle density refers to the ratio of the mass of solid matter of a given soil sample to the mass of an equal volume of water, V_w. The small pyknometer method was used in accordance with BS 1377-2:1990. This method is suitable for soils consisting of particles finer than 2 mm. The average value of particle density (ρs Avg.) was found to be 2.65 g/ml.

5.5.3 Particle Size Distribution

Figure 5-6 shows the soil classification curve used in this study. All soil classification tests were done in accordance with BS 1377-2:1990. Wet sieving was used to separate the soil into its size frictions. Any soil passing the finest mesh (0.063mm) was subjected to a sedimentation test to determine the distribution down to a particle size of 0.002mm.

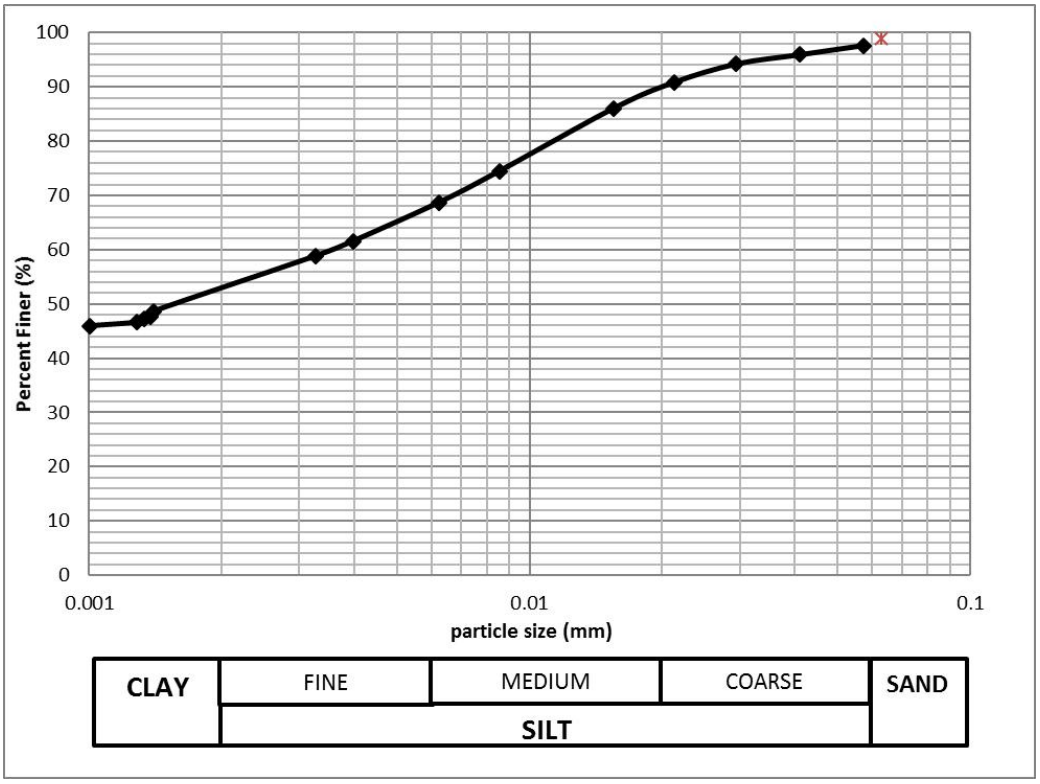

Figure 5-6. Grading curve

5.6 Fibre alignment studies sample preparation

The same procedure used to prepare the reinforced specimens for triaxial testing was followed for the preparation of specimens for fibre alignment studies. These were later desiccated and the alignment of the fibres measured. Detailed description of the procedure for preparation of samples are made in section 5.9.2.2.

5.7 Shrinkage Test Procedure

Samples were prepared in a CBR mould. The soil was obtained “as dug” from the site, brought to the laboratory and chopped in peds of roughly 15mm diameter. Samples were brought to the desired moisture content, around 2% below and above the optimum moisture content (Figure 5-8). The moisture contents used were 20, 22, 24 and 25%. Fibres were hand-mixed at 0%, 0.2% and 0.4% of the dry weight of the soil, and compacted using the light compaction method specified in BS 1377-4:1990.

Al-Rawas & McGown (1999) carried out an extensive review of the drying techniques, and concluded that there is no single technique that can be claimed to be the best for specimen drying. Therefore, all samples were subjected to air drying, at room temperature, for about 10 to 12 weeks. During this period, the weight was measured regularly and 6 measurements of the diameter and 4 measurements of the height of the sample were performed regularly. In order to improve accuracy, all measurements of height and diameter were performed at the same location on the sample. Moisture content, degree of saturation and volume change of the 12 samples were calculated afterwards, based on the new and the initial data obtained.

5.8 Oedometer Testing

5.8.1 Pre-checks, sample preparation and set-up

Before sample preparation was commenced, preparation of the testing equipment was carried out. This involved de-airing the upper and lower porous discs by means of boiling and vacuum application. Before the start of each test, a dummy sample with a known height was inserted into the oedometer cell to obtain a reference reading for the dial gauge. The actual sample height could then be obtained from the height of the dummy sample and the difference between the reference reading and the current reading from the dial gauge.

Oedometer tests were carried out on reconstituted, reinforced and unreinforced Lambeth Group clay. A method similar to the sample preparation for the triaxial tests was followed and is discussed in the following section. The main difference was that the soil was compacted into a 100x100mm compaction mould that contained two oedometer rings. In the preparation of the reinforced sample the author used fibre soil composite with 0.2 % fibre content and a moisture content 2 % wet of the optimum. Light compaction procedure, 1L mould with 2.5kg rammer, stated in BS 1377-4:1990 was used to produce identical samples. The samples were prepared by compacting it in 3 layers with 27 blows, maintain the same compaction energy. The height of each layer was calculated as 33mm where the height of the oedometer ring was 20mm. Therefore, after a trial run on a damaged ring, it was confirmed that the compactor-rammer would not damage the ring. The oedometer ring was placed at the bottom of the first layer and

the soil was carefully inserted without moving the ring from its central position. The same method was applied when it came to the 3rd layer compaction; another ring was placed at the bottom of the 3rd layer and compacted. Afterwards, the sample was extruded from the mould and with a straight-edge trimming blade, a hand-operated soil lathe and a wire saw were used to trim the sample smoothly to the outer edge of the ring. This process was found to be difficult for reinforced samples where fibres extend from the ring and needed careful trimming. The trimmed material was used for initial moisture content measurement.

5.8.1.1 Reconstituted Samples

A reconstituted clay is defined as one that has been thoroughly mixed at a water content equal to or greater than the liquid limit (w_L). At this stage the concept of intrinsic properties of a given clay is introduced. The term "intrinsic" is described by Burland (1990) and imply the properties of clays which have been reconstituted at a water content between w_L and 1.5 w_L, without being air dried or oven dried and then consolidated, preferably under one-dimensional condition. Therefore, in this study samples were remoulded to a water content varying between w_L and 1.5 w_L. Such variations were proposed intentionally to study the effects of the initial water content on the position and slope of the intrinsic Normal Compression Line.

After increasing the moisture content to the desired percentage and thoroughly hand mix the sample to a uniform slurry state, the sample was transferred to an oedometer ring where the side of the porous stones in contact with the soil was covered with a wet filter paper. Therefore the pore stone and filter paper were also acting as a base to facilitate the transfer of the slurry into the ring. In order to avoid trapped air inside the sample, the slurry was gently pressed against the ring.

5.8.2 Test Stages

The sample, prepared in the ring, was placed directly into the oedometer cell and the top cap was placed immediately at the top of the sample. After placing the oedometer cell in the frame, the loading arm was lowered until the sample was under a small pressure (<10kPa). Such pressure would ensure that the soil porous stone and load point came into contact and removed possible bedding errors. Afterwards distilled water was added to the cell up to the top edge of the loading plate. The sample was left under these

conditions for 24 hours. During the test, loads were doubled and the dial gauge was monitored until no change was observed for each loading stage. This period of reaching no volume change took around 24 hours between each loading and unloading stage. The loading stages used in this study were 2, 4, 8, 16, 32, 64, 32, 16, and 8 kg. The oedometer cell bath was checked frequently due to evaporation and the required distilled water was added. At the point of completion of the final stage, the water from the cell bath was carefully emptied with the help of a hand pump. This stage was necessary as once the soil is completely unloaded, the sample will start swelling and draw water, changing the final void ratio measurement. Once the water was removed, the samples were unloaded and removed from the oedometer cell together with its ring. Porous Stones were removed quickly. The retrieved sample was oven dried to obtain the final moisture content.

5.8.3 Data Acquisition, Data Monitoring and Data Post-processing

As mentioned above, the readings were recorded every 24 hours before the next loading or unloading stage. Baty dial gauges with an accuracy of 0.002 mm were used in this testing programme.

The recorded data was progressively transferred to an Excel spreadsheet for further analysis and for a more in-depth determination of the stress-strain behaviour.

5.8.4 Bender Element

Arrangement and specifications of testing equipment used in this study for shear wave modulus measurement have been given in Section 4.1.1 of this study. Same procedure of conventional 1-D compression testing has been adopted for the share wave modulus measurement and details of procedures have been given in Sections 5.8.1, 5.8.2 and 5.8.3.

5.9 Triaxial Testing

5.9.1 Pre-checks of testing equipment

To ensure that no free air would influence the measurements on the tested sample, the porous stones were de-aired by boiling and by applying a vacuum in a desiccator with the porous stones submerged. One day prior to the start of testing, the whole hydraulic system was flushed with water and pressurised at around 600 kPa in order for the trapped air to dissolve in the water and to check the system for any leakages. Afterwards all the electric devices were checked for noise on the readings. Axial displacement transducers were repositioned to allow enough free travel during loading. With saturation being the first stage of testing, the volume gauge was positioned close to a full position. Occasionally, at the beginning of the saturation stage, samples tend to slightly expand and push water into the volume gauge; this behaviour was generally observed when the samples were placed into the triaxial equipment, right after compaction of the sample.

If needed, the amplifiers for the local LVDTs were adjusted back to their reference state, which is the point at which the transducer signals were at their electrical zero without the armatures inside the transducer bodies. This was done to ensure that the correct linear ranges of the LVDTs were known before the start of the testing.

Finally, immediately before testing the back pressure, the cell pressure and axial displacement transducers were re-zeroed with the water level in the cell located the middle of the cell while the cell was being filled.

5.9.2 Sample Preparation

5.9.2.1 Reconstituted Samples

For the preparation of the triaxial reconstituted samples a 38 mm consolidometer was used to consolidate the slurry. The slurry preparation of the reconstituted samples was prepared in the same way as for the 1-D compression test samples as described in Section 5.8.1.1. Once the slurry was prepared, it was carefully transferred into the consolidometer with great attention to avoid any air trapping in the sample. The samples were left for a day to consolidate under its own weight. After this point, the top cap was

placed on the sample which was then loaded in stages to a maximum vertical effective stress, $\sigma_v^{`}$, of 88 kPa. Such pressure was chosen as the lowest possible pressure to obtain a specimen with enough consistence to be placed in the triaxial equipment. As soon as the sample was consolidated, it was taken out of the consolidometer and trimmed to the desired height of 78mm. Finally, the sample was directly transferred to the triaxial equipment and the mean effective stress for the consolidometer was calculated, using a K_0 of 0.5, and applied directly to specimen starting from the saturation stage.

5.9.2.2 Reinforced Samples

In order to simulate the in-situ compaction of heavily over-consolidated clays, the samples retrieved and stored in plastic bags (section 5.4) were chopped into small pieces of 10 to 15mm diameter and named as "ped" (Figure 5-7). There after the soil was stored in sealed barrels, as seen in Figure 5-7.

Compaction tests (Figure 5-8) were carried out to obtain the optimum moisture content (OMC) and the maximum density (MD). The results confirmed that there was little effect of fibres in the OMC and the MD of the soil, with the OMD being equal to 20.5% for the compacted samples and around 21.5% for the compacted soil with fibres. The maximum dry density of reinforced and non-reinforced compacted samples was found to be 1.70 and 1.68 g/cm^3 respectively (Figure 5-8).

Figure 5-7. Chopped clay peds in storage drum

In order to achieve the desired moisture content the soil in the barrel was either left to dry or moisture was added to achieve the desired moisture content. In order to permitted the water to penetrate the granules and achieve equilibrium, the distilled water was

sprayed at intervals onto the soil over a period of 24 hours, rotating the barrel in order to moist the peds' surfaces evenly. This has enabled the desired moisture content to be achieved. The clay peds were moistened to 1-2% wet of the optimum values (in order to be close to 0% saturation line), and once the required water content was achieved, the soils was sealed back into the barrel and stored in a controlled humidity room for several days.

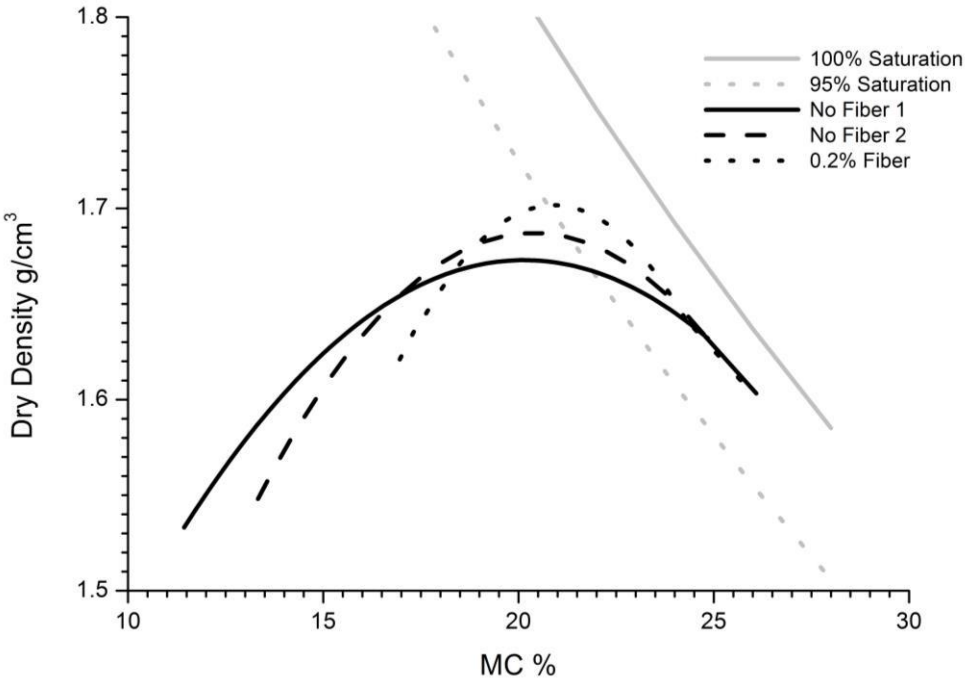

Figure 5-8. Compaction Curves of reinforced and non-reinforced samples

Every day, representative samples from three different positions in the barrel were collected and the moisture content was determined. As can be seen from the variation of the initial moisture contents in Table 12, the achievement of a same initial moisture content was difficult particulaly due to the presence of peds.

A model proposed by Brackley (1975) and improved by O`Connor (1994) considered that unsaturated clay soils exist as packets of soil particles, with each packet being completely saturated and the inter-pocket voids being filled with air (Figure 5-9). This meant that the soil mass was unsaturated whereas the individual soil packets were saturated. By assuming that the packets were saturated, Brackley (1975) developed the idea that the individual pockets retain the properties of the natural soil and the total

volume change of the soil mass would be due to the summation of the effects of swelling or compression of the packets and their shear behaviour.

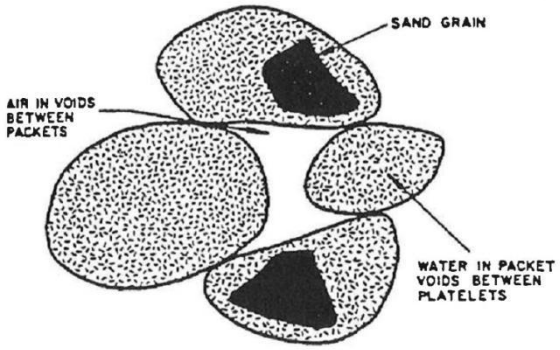

Figure 5-9. Model of unsaturated soil (Brackley 1975)

This is one of the assumptions of this work; as peds of heavily over-consolidated clay are compacted, the compaction energy applied is not enough to break/shear them and therefore inter-pocket voids, filled with air, will be present in the compacted soil. The air pockets were assumed to be connected, therefore facilitating saturation; however initial saturation tests on the compacted samples, indicate that on the wet side of the optimum, the saturation of the samples is faster, as would be expected.

The size of the peds was chosen to be 1/7 to 1/10 of the sample diameter, while the in-situ ped size was similar to the size of a “golf ball.

For preparation of the reinforced samples the previously calculated weight of clay peds and fibre (0.2% of the dry weight of soil) were hand mixed in bag. In order to avoid fibres lumping together. Considerable care and time was spent to get a homogeneous distribution of the fibres.

Studies of Ang & Loehr (2003) on specimen size effects have shown that test samples with diameters of 70mm or greater are likely to produce strengths that are reasonably representative of the “mass” properties of fibre-reinforced soils . Therefore, a 100 x 200mm compaction mould was manufactured. Because of the nonstandard dimensions of the mould. Compaction effort equivalent to the light compaction, described in the BS 1377-4:1990, was followed (Table 8). This procedure allowed to apply the same energy to all the laboratory prepared samples.

Table 8. Compaction of large specimens for triaxial test (BS1366-1:1990)

Specimen size diameter x length (mm)	Degree of compaction			
	2.5 kg rammer (See 3.3 of BS 1377-4:1990)		4.5 kg rammer (see 3.5 of BS 1377-4:1990)	
	No. of layers	Blows per layer	No. of layers	Blows per layer
100 x 200	5	25	8	27
105 x 210	5	29	8	31
150 x 300	8	54	13	54

Finally, the thoroughly mixed fibre and peds were transferred to the compaction mould and, as stated above, samples were compacted in 5 layers with 25 blows to each layer. Between the compaction of each layer, the surfaces of the compacted layers were scoured in an attempt to provide a reasonable bond between them.

Immediately after compaction, the sample was vacuumed into a plastic bag, in order to keep the moisture content constant until the triaxial equipment was prepared to initiate the test. This would normally vary between 1 to 2 hours. The remaining soil was sealed back into the barrel, where if any problem occurs during the test, another sample could be compacted and tested from the same material.

Figure 5-10. Reinforced sample compaction procedure

The two important reasons to follow such procedure are:;

a) To be able to retain some characteristics of the natural soil that would affect the mechanical response of the compacted soil;

b) to create samples that would be more representative of the in-situ behaviour of the compacted soil.

5.9.2.3 Unreinforced Samples

The unreinforced specimens were prepared using the same method. Where, in this case, fibres were not mixed in the soil. In order to achieve the overwhelming testing scheme proposed, 38mm specimens were used. Testing small samples have reduced the duration of the saturation and consolidation stages, consequently leading to shorter testing times . In this case, the 38x78mm specimens have been trimmed out of 100x200mm samples compacted samples.

In order to evaluate the effect of specimen size, as mentioned by David Suits et al. (2003), one unreinforced sample with 100x200mm have been tested and compared with a sample of 38x78mm at the same confined stress. Results of such analysis can be seen in section 9.3.

5.9.2.4 In-Situ Samples

In-situ samples have been trimmed from the block samples obtained with the help of the industrial partner's site and stored as described in Sections 5.1 and 5.2. The trimming process was laborious and lengthy due to the presence of fibres. Prior to trimming, the block samples were removed from wooden case and cut into quarters. The three quarters which were not going to be tested immediately were waxed and preserved for later use. The quarter which was going to be used was cut into a cylindrical shape with a diameter about 110mm and a height about 220 mm using the trimming blade. The cylinder than trimmed into the desired height (200mm) and diameter (100mm) with the help of a hand operated soil lathe, a wire saw and a trimming blade as can be seen in Figure 5-11. Throughout the process damp towels were placed around the lathe to keep the environment moist and keep the drying to a minimum.

Figure 5-11. Sample trimming tool

5.9.3 Sample set-up

Once the sample was out of the sealed bag, the specimen dimensions were measured and the weight recorded. The set-up of the sample was done as quickly as possible to avoid loss of moisture. The sample was placed on a metal block, which is similar to the pedestal of the triaxial equipment, since if it would come in direct contact with the pedestal of the equipment cell, it would probably absorb the water from the porous stone, allow air to be trapped in the back pressure system. The ample was kept on the metal block while the wetted side drains were attached to the sample, where both ends of the side drains allowed to connect to bottom and top porous stones. This was done in order to provide direct connection between the top and bottom porous stones to help with the saturation of the sample. The rubber membrane which was placed in a water bath for at least 24 hours was slipped over the sample with the help of a membrane stretcher suction device.

Before placing the previously de-aired porous stones, filter papers were attached to each end of the sample. Once the porous stones were placed, the top cap, previously waxed with silicone grease, was placed at the top of the sample and a rubber membrane was rolled onto the top cap. Two O-rings were placed and a complete sealing was achieved. Once this stage was completed, the sample was transferred to the triaxial equipment by sliding it onto the previously wetted bottom pedestal. The edges of the bottom pedestal

were smeared with silicon grease to improve the seal and the rubber membrane was rolled onto the pedestal. A specially designed split O-ring stretcher was used to place the two O-rings over the membrane on the pedestal.

Finally, the mount for the local strain gauges were glued onto the membrane using cyanoacrylate type glue. The radial strain belt was fixed at mid-height and the two axial strain gauges were positioned on diametrically opposite sides of the sample, with the upper and lower mounts placed approximately 70mm apart.

After finalising the sample set-up procedure, the cell chamber was closed and the cell was filled with water. A small cell and back pressures are applied, maintain an effective pressure of around 20kPa before the start of the saturation stage.

5.9.4 Saturation

At the beginning of the testing programme, it took two months and seven unsuccessful saturation attempts before successful saturation was achieved. The initial assumptions that: a) after the ped compaction the water would be able to circulate in between the peds and b) due to the reinforcement, the fibres would act like “drains”, and allow the saturation to occur at a faster rate were proved to be wrong. The longer saturation times were also verified during the oedometer tests and further discussions will be made in the analysis and discussion section of this report.

Once the sample setup was completed, the first pressures were applied: 50 kPa cell pressure and 30 kPa back pressure. Therefore, the sample was initially subjected to a 20 kPa effective stress. For the first 24 hours the sample was allowed to stabilize under the applied pressures. After this period, by maintaining an effective stress of 20kPa, all pressures started to increase by 1.5 – 2kPa/hr until the back pressure reached 300 kPa. Raising the pressures in such a slow manner was due to the size of the sample, and these values were chosen to allow drainage of the excess pore pressure out of the sample. On the other hand, 300 kPa was chosen because the previous trials show that pressures below 300 kPa gave low B parameter values, whilst by following this procedure B parameters around 0.98 were archived. This approach was followed for both 100mm and 38mm samples.

The degree of saturation was checked using Skempton's B-parameter (Skempton 1954 – Equation 14) which is a measure of the undrained pore water pressure response (Δu) to a change in the confining pressure ($\Delta\sigma_r$).

$$B = \frac{\Delta u}{\Delta \sigma r} \qquad 14$$

Therefore, once the 300kPa back pressure was reached, the samples were left overnight under a high back pressure and low effective stress, to allow further flow of water into the sample. Typically, after 24 hours, the volumetric flow into the sample was deemed insignificant and the B-value was checked, for an indicated of a satisfactory degree of saturation. During the remaining stages of the tests, the back pressure level was maintained at 300kPa to avoid the dissolved air from coming out of the solution.

The change in sample volume, during saturation, as measured by the local strain gauges, was observed to be very small. This confirms that the flow of water into the sample during saturation, was compressing/dissolving the air inside the sample. The local instrumentation data was used to correct the volume of the sample and, consequently, changing the specific volume of the sample.

5.9.5 Consolidation

After pore pressures had stabilized and the saturation of the sample was achieved, the isotropic compression stage was started. In this stage, to achieve the desired effective stresses, the rate of isotropic loading was chosen to be 2 kPa/hr. This rate was chosen to allow full drainage. During the testing process, the equilibrium of the pore pressure was checked by stopping isotropic compression at every 100 kPa to check the drainage conditions. This process was done by closing the drainage valve and checking the excess pore pressure. Similar to what Gaspare (2005) followed, at the end of the isotropic consolidation stage, the strains were allowed to stabilize long enough to achieve a rate of volumetric strain per hour 100 times smaller than the initial rate of axial strain during shearing. The voltages of the internal transducers were re-zeroed at the beginning and end of this stage.

Data acquired in the consolidation stage were used to obtain the initial rate of shearing (Table 9). This rate was obtained by drawing the volume change against the square root time graph.

Table 9. Rate of Shearing for completed Triaxial tests

Sample	Short Names	Shear Rate
		(%/hr)
CD_p'_38_Lab_NoFiber_50kPa	DN50	0.0390
CD_p'_38_Lab_NoFiber_50kPa_2	DN50_2	0.0349
CD_p'_38_Lab_NoFiber_100kPa	DN100	0.0158
CD_p'_38_Lab_NoFiber_300kPa	DN300	0.0053
CD_p'_100_Lab_Fiber_50kPa	DF50	0.0330
CD_p'_100_Lab_Fiber_100kPa	DF100	0.0120
CD_p'_100_Lab_Fiber_300kPa	DF300	0.0030
CU_38_Lab_NoFiber_50kPa	UNF50	0.2500
CU_38_Lab_NoFiber_100kPa	UNF100	0.0800
CU_38_Lab_NoFiber_150kPa	UNF150	0.0790
CU_38_Lab_NoFiber_300kPa	UNF300	0.0400
CU_38_Lab_NoFiber_500_300kPa	UNF500_300	0.0300
CU_38_Lab_NoFiber_500kPa	UNF500	0.0790
CU_38_p'_REC_150kPa	DREC150	0.1100
CU_38_REC_150kPa_2	REC150	0.1000
CU_38_REC_450_200kPa	REC450_200	0.0670
CU_38_REC_500 _125	REC500_125	0.0330
CU_38_REC_500	REC500	0.0400
CU_100_Insitu_Fiber_50kPa	INS50	0.2300
CU_100_Insitu_Fiber_100kPa	INS100	0.0190
CU_100_Insitu_Fiber_150kPa	INS150	0.0090
CU_100_Insitu_Fiber_500kPa	INS500	0.0180
CU_100_Lab_Fiber_100kPa	UF100	0.2000
CU_100_Lab_Fiber_150kPa	UF150	0.1530
CU_100_Lab_Fiber_300kPa	UF300	0.0500
CU_100_Lab_Fiber_500kPa	UF500	0.0053
CU_100_Lab_NoFiber_100kPa	UNF`100	*

5.9.6 Shearing

At the beginning of the shearing stage, the voltages of the internal transducers were re-zeroed. The data logging interval was set up to allow the calculation of stiffness at low strains. The shearing progress of the test was monitored and terminated once critical state was reached, i.e.; shear strains can occur with no change in the effective stress, volume or excess pore-water pressure.

5.9.7 Finalising the Test

The most important step, at this stage ,was to obtain the moisture content and weight of the sample immediately after testing. Therefore, as soon as the test was finalised, the following steps were carried out quickly and in succession. The first step was to stop the data logging and pressure controllers. If the test carried out was a drained test, the back pressure line was closed. By changing the valve configuration, the CRSP was eliminated from the system and the ram reservoir was connected to the air/oil interface. By reducing the ram pressure below the cell pressure, the bottom pedestal was pushed down and oil in the ram reservoir would flow to the air/oil interface. Once the ram cylinder was completely lowered, the cell pressure was reduced to zero. The cell pressure valve towards the cell was closed and the cell was consequently emptied via the bleed plug. At this point, the sample was removed with great care and attention, and once it was removed the sample was weighed without the top cap, porous stone and membrane. A sketch of the sample would be drawn to make a record of the failure zone. Finally, the sample was cut into two halves through the longitudinal axis. One half was used to take 5 representative samples for the moisture content measurements, including one from the slip failure zone. The other half was dried for a day and a picture was taken for recognition of features such as fissures, slip failure zone, fibre arrangement and soil structure.

5.9.8 Data Acquisition, Data Monitoring and Data Post-processing

The data obtained via “Triax” software was progressively transferred to an Excel spreadsheet for further analysis and for a more in-depth monitoring of the stress-strain behaviour. This was essential as the performed tests did not follow any standard testing procedures, and the in-depth monitoring of the stress strain behaviour was essential for the progressive planning and control of the tests.

6. CALCULATION AND CORRECTIONS

This chapter presents the calculations and corrections carried out for the adapted testing scheme. An extensive study was performed to improve as much as possible the data to calculate the void ratio\specific volume on the oedometer and specifically triaxial testing.

6.1 Oedometer Testing

6.1.1 Void Ratio

The initial dimensions of the sample were determined by measuring internal diameter and the height of the oedometer ring by comparing it with the reference height of a dummy sample. The determination of the initial moisture content was done by measuring the moisture content of the sample's trimmings. The slurry samples were assumed to be fully saturated in order to calculate the initial void ratio from initial dimensions and initial solid weight. Calculations via this method were found to correspond very well with the void ratio determined from the initial water content. Slightly more discrepancy was found when the initial void ratio was back-calculated from the final water content. Further description of void ratio calculations have been given together with specific volume determination of triaxial specimens in section 6.2.1.

6.1.2 Stress Measurement

In the oedometer test a flat cylindrical sample is compressed by applying a total vertical stress, σ_v at the top of the sample. The rigid confining ring prevents the sample from deforming in the lateral directions and compression is therefore only in the vertical direction. The total vertical stress acting at the top of the sample was derived from;

$$\sigma_v = \frac{(F_{dwh}.g).R}{A} \quad (15)$$

Where,

F_{dwh} = dead weight on the hanger

R = the lever arm ratio

A = cross sectional area

6.1.3 Shear Wave Modulus Measurement

One looking at the literature will find that four different methods have been suggested for the determination of travel time. Three of them are time domain methods; first arrival, travel time between characteristic points and cross-correlation, and additionally the phase-delay method in the frequency domain. In this study only first arrival method have been used.

Typically, the first arrival method is used in connection with a transmitted single sinusoid pulse. Using this method, the travel time of the transmitted shear wave is generally taken as the time between the start of the transmitted signal and the assumed first arrival of the shear wave at the receiving bender element. Abbiss (1981) took the first point of deflection (t_a) as the arrival time of the shear wave. Additionally Viggiani & Atkinson (1995) used the first point reversal (t_b) of the received signal because of the assumed influence of near-field effects. In this study the first point of inflection (t_c) which lies in between t_a and t_b, was used as proposed by Sorensen (2006). This method has been found to give more consistent travel times with the travel time estimated from other methods. The three interpretation methods are illustrated in Figure 6-1.

The velocity of the transmitted shear wave propagation through the soil is determined by using the techniques and interpretation methods described above. The elastic shear stiffness of the soil, G_{max} (or G_0) is then related to the velocity of the propagating shear wave, V_s, by;

$$G_{max} = G_0 = \rho V_s^2 = \rho \left(\frac{L}{T}\right)^2 \quad (16)$$

Where,

L = tip-to-tip travel distance

T = Travel time

ρ = Total density of the soil

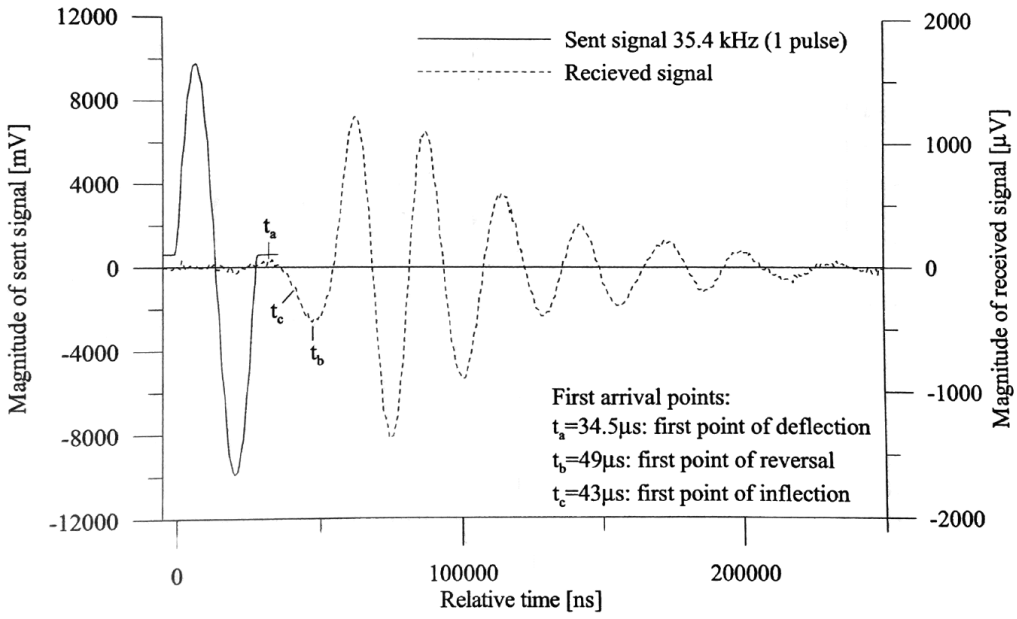

Figure 6-1. Estimating travel time of transmitted single pulse sinusoid wave through ample using first arrival method. (Sorensen 2006)

$$\rho = \rho_w \left(\frac{G_s + e}{1 + e}\right) \quad 17$$

ρ_w = density of water

6.2 Triaxial Test

In order to allow clear understanding of the results, all the basic formulation used in the analysis of this study have been presented in this section.

The deviatoric stress on the sample "q" was calculated based on the daviatoric force "F" and current sample area "A_{cr}", assuming the appropriate correction mentioned in section 6.2.4.

$$q = F/A_{cr} \quad (18)$$

The Axial Strain "ε_a" was calculated based on the change of axial length "Δl" over the initial sample length "l_0" for both internal and external axial displacements.

$$\varepsilon a = \frac{\Delta l}{l_0} \quad (19)$$

Some specific formulation used in this study have been presented within the text.

6.2.1 Specific Volume

The initial specific volume, v_i of the triaxial and oedometer test samples was calculated using four methods given in Equations 20 to 23. Similarly, in the triaxial test, the four methods given in Equations 20 to 23 used. Equation 23 calculates v_i using the final water content and the total volume change of the sample throughout the test. The laboratory prepared and in-situ samples were compacted 2% on the wet side of optimum moisture content and the initial saturation levels indicated a high saturation of the samples at the beginning of testing.

Equations 20 to 23 were based on the initial water content, w_i, the initial dry unit weight, γ_{di}, the initial bulk unit weight, γ_i and the final water content, w_f. Each method depends on various measurements, which include the initial water content, w_i, the initial wet mass, M_i, the initial height, h_i, the initial diameter, D_i, the final wet mass, M_f, the final dry mass, M_{sf} and the specific gravity, G_s.

Method 1:

$$v_i = w_i . G_s + 1 \quad (20)$$

Method 2:

$$v_i = \frac{G_s.\gamma_w}{\gamma_{di}} \quad (21)$$

Method 3:

$$v_i = \frac{G_s - 1}{\frac{\gamma_i}{\gamma_w} - 1} \quad (22)$$

Method 4:

$$v_i = \frac{w_f G_s + 1}{1 - \varepsilon_v} \quad (23)$$

By using all four methods mentioned above, the specific volume at any specific time can be calculated by knowing the volumetric strain of the sample, using the following formula;

$$v_{current} = v_i(1 - \varepsilon_v) \quad (24)$$

For each oedometer and triaxial test conducted, the values of v_i calculated from the four methods outlined above were compared and any inconsistent values were discarded. An average of the remaining values was taken and the resulting v_i was the value used for analysis. The variation of v_i, for the four methods was determined to be of ±0.01 to 0.02.

Additionally, in this study, the void ratio calculation took into account the specific gravity of the fibres, revealing that the void ratio variation is as low as 0.002, given the low fibre percentage.

6.2.2 Volumetric strain

UCL 100mm triaxial system, equipped with local instrumentation can accurately measure deformation on the sample during testing. For the samples fitted with local LVDT instrumentation, the volumetric strains were calculated from;

$$\varepsilon_v = \varepsilon_a + 2\varepsilon_r \quad (25)$$

Where ε_r and ε_a are the radial and axial strains from the local LVDTs. For this calculation, the sample was assumed to be of a cylindrical shape for the small strains range.

The second method of volumetric strain measurement is via Volume gauge. This has been achieved by recording the flow of water to and from the sample:

$$\varepsilon_v = -\frac{\Delta V}{V_0} \quad (26)$$

Where V_0 is the initial volume of the sample, calculated from each test stage and ΔV is the volume change measured by the volume gauge.

There are negative sides for both methods. The volumetric strain measurement with local instrumentations are limited to small strains where the effect of bulging is insignificant. However, at small strains the immediate volumetric response, calculated from the local strains, is believed to be more accurate than the measurements from the volume gauge.

The shear strains were calculated from:

$$\varepsilon_s = \frac{2}{3}(\varepsilon_a - \varepsilon_r) \quad (27)$$

6.2.3 Young's and Shear Modulus

The soil stiffness is generally expressed in terms of the shear modulus, G', calculated as follows:

$$G' = G_u = \frac{\Delta q}{3\Delta\varepsilon_s} \quad (28)$$

However, in cases where the radial strain measurements are deemed unreliable, the soil stiffness was expressed in terms of the effective Young's modulus E′ for drained conditions;

$$E' = \frac{\Delta\sigma'_a}{\Delta\varepsilon_a} \quad (29)$$

And undrained Young's modulus E_u from undrained conditions

$$E_u = \frac{\Delta\sigma_a}{\Delta\varepsilon_a} \quad (30)$$

6.2.4 Correction on Calculations

6.2.4.1 Area Correction

The current area, A, can be corrected by applying a right-cylinder correction. Failure modes of all samples can be seen in Figure 10-1. Where samples that had a barrelling shape, rather than single shear plane, have been corrected by applying the formula below for right-cylinder correction.

For drained tests:

$$A = A_0 \frac{1 - \varepsilon_v}{1 - \varepsilon_a} \quad (31)$$

For undrained tests:

$$A = \frac{A_0}{1 - \varepsilon_a} \quad (32)$$

Where,

A_0 = Initial cross-sectional area

ε_a = Axial and

ε_v = Volumetric strain

6.2.4.2 Drain Correction

For a 38mm diameter sample Head (1998) estimated that the correction of the deviator stress, due to side drains, to be approximately 0.5 kPa for every 0.1% of strain up to 2% and to remain constant at roughly 10 kPa. Where for 100mm diameter samples, it can be estimated to be 0.2 kPa for every 0.1% strain up to 2% and then 3.5 kPa for the remainder strain. Correction for the most usual specimen diameters are given in Table 2 of BS 1377-8:1990 and it applies to strains from 2% upwards. For strains below 2%, the correction should increase linearly from zero with the increase in strains.

6.2.4.3 Membrane Correction

The membrane correction to be applied to the measured deviator stress, with a barrelling type failure, is done with the membrane correction curve below (Figure 6-2);

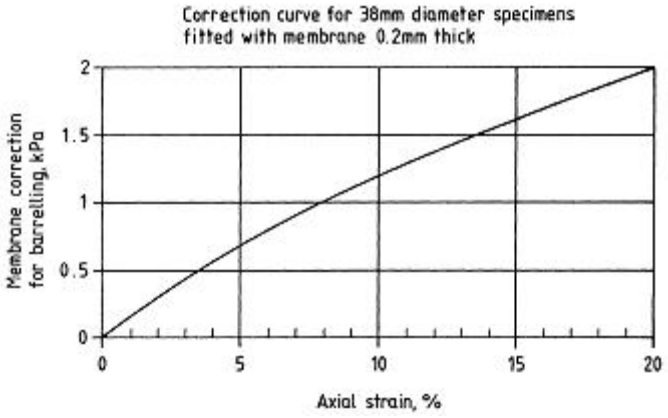

Figure 6-2 Membrane correction curve (BS 1377-8:1990)

The correction curve applies to a specimen of 38mm diameter fitted with a membrane 0.2mm tick. For specimens with different dimensions, the correction is multiplied by;

$$\frac{38}{D}.\frac{t}{0.2} \qquad 33$$

Where t is membrane thickness and D is sample diameter.

The corrected deviator stress can be calculated by taking into consideration the calculated membrane correction and drain correction with the following formula;

$$(\sigma_1 - \sigma_3) = (\sigma_1 - \sigma_3)_m - \sigma_{mb} - \sigma_{dr} \qquad 34$$

Where $(\sigma_1 - \sigma_3)_m$ is deviatoric stress before correction.

6.2.4.4 Barrelling and Slip Plane Correction

In order to calculate the cross-sectional area of the tested samples, the standard right cylinder assumption is typically adopted. In reality though, depending on the type and trusting conditions, samples tend to barrel or a shear plane formation is observed. The area correction, when a shear plane formation is observed, became more problematic. In a study, La-Rochelle et al. (1988) formulated the cross sectional area correction for samples failing or deforming by bulging (Figure 6-3), with no apparent shear plane. The following equation is the modified version of the formulas used in 6.2.4.1;

$$a_c = a_0 \frac{1 + \Delta V/V_0}{1 - \varepsilon a} \qquad 35$$

Where,

a_0 = *initial cross-sectional area at the beginning of the triaxial shear test (that is, after consolidation)*

$\Delta V/V_0$ =*unit change of volume during shear test*

ε_a = *axial strain*

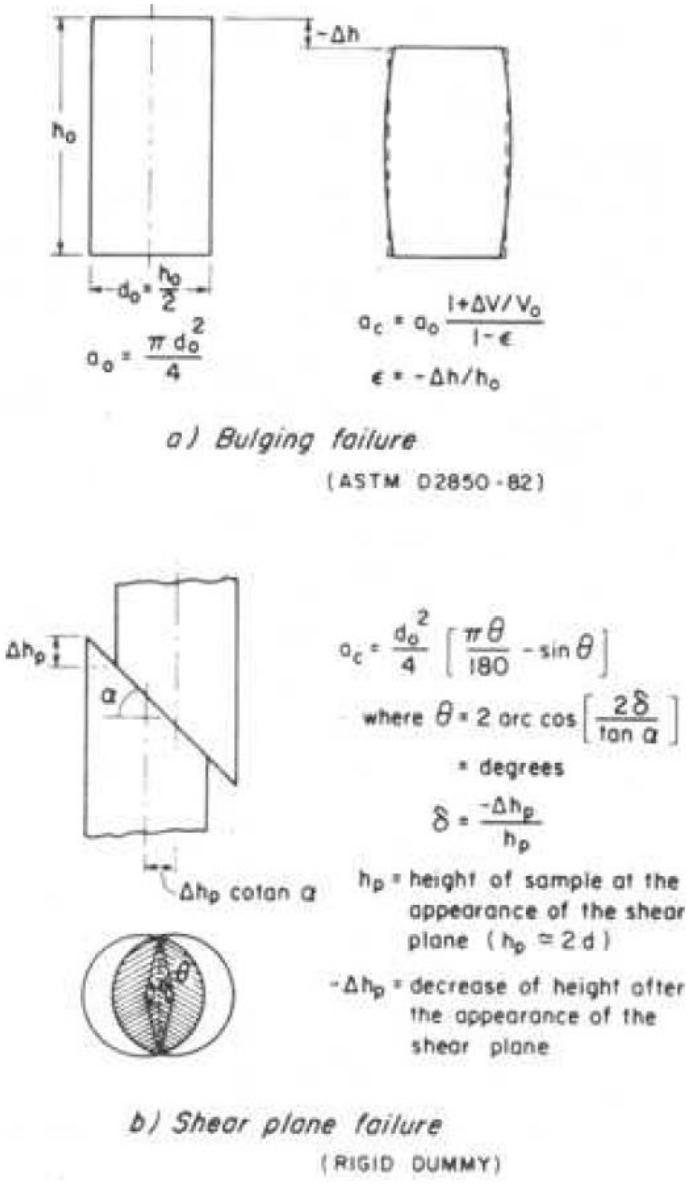

Figure 6-3. Illustration of correction for the cross-sectional areas: (a) bulging failure and (b) shear plane failure (La-Rochelle et al. 1988)

Additionally, La-Rochelle et al. (1988) corrected the shear plane failure (Figure 6-3a), by formulating the occurrence of a shear plane, in the case of a pre sheared rigid dummy sample, where a decrease in the cross-sectional area can be calculated by the expressions given in figure Figure 6-3b. the mentioned idealised condition, discussed above, meet the condition of very stiff clay and clay shales, but not softer clays. In such cases, bulging is also experienced around the edge of the shear plane. Therefore, the failure mechanism is the combination of shear plane formation and localized bulging. Where such scenario leads to both decrease of area due to the movement along the shear plane and an increase due to the localized bulging and such phenomena cannot be evaluated without an observation of the samples during or after the test.

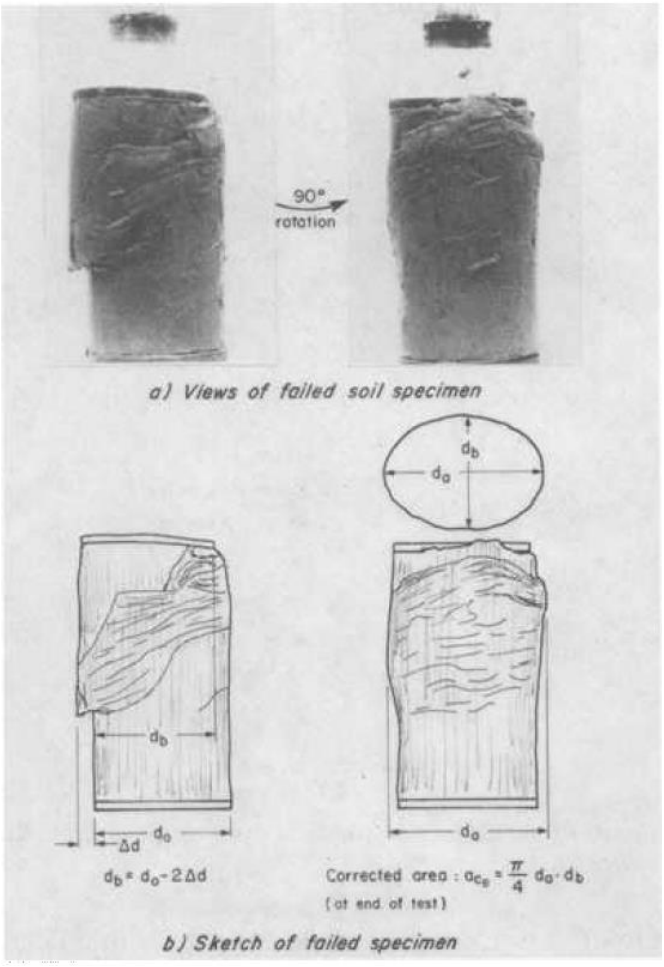

Figure 6-4. Correction of the cross-sectional area for a shear plane failure in a soil specimen. (La-Rochelle et al. 1988)

As can be seen on Figure 6-4 the authors suggested to calculate the corrected cross-sectional area (a_c), corresponding to the contact area on the shear plane between the two parts of the specimen at the end of the test;

$$a_c = \frac{\pi}{4} d_a . d_b \qquad 36$$

For the specimens failing with a combination of shear failure and bulging, the authors are suggesting to use Equation 35 to correct until the shear plane forms and for the reminder of the test, the reduction or increases of the cross-sectional area, as measured at the end of the test, according to the formulation given in Figure 6-4. The above mentioned correction should be applied proportionally with the strain from the formation of the shear plane to the end of the test as follows:

$$a_c = a_f + (a_{ce} - a_f)\left(\frac{\epsilon - \epsilon_f}{\epsilon_e - \epsilon_f}\right)$$ 37

a_f = *cross-sectional area at peak strength*

a_f = *cross-sectional area at end of test (Eq.36)*

ϵ_e = *axial strain at end of test*

ϵ_f = *axial strain at peak strength*

7. FIBRE ALIGNMENT STUDIES

7.1 Introduction

In order to verify the fibre alignment, samples with the same fibre and initial moisture content were dissected. The alignment of the fibres was observed by recording the X, Y and Z coordinates of one of the fibre ends. As the sample was dissected the horizontal and vertical angle of the fibre was determined. This procedure was followed for 100 randomly chosen fibres. A graphical representation of the procedure can be seen in Figure 7-1 while Figure 7-2 shows a series of photographs of the sample being dissected.

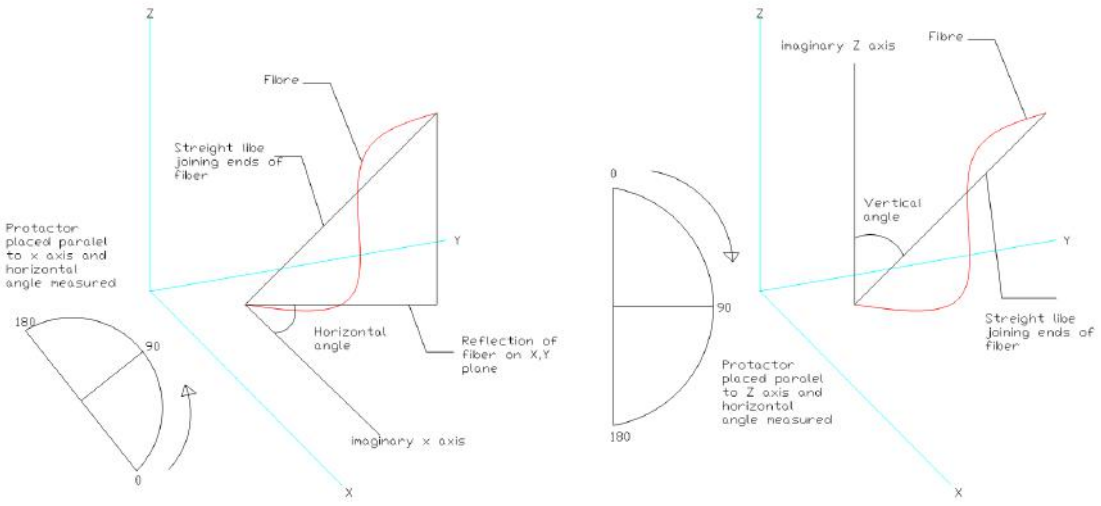

Figure 7-1. Method used in recording alignment of fibres in sample

Figure 7-2. Extracting fibres from the sample

The major challenge during this procedure was estimating the angles of the fibres which were circling peds, bent and overlapping others due to the mixing and compaction procedure.

7.2 Results

The methodology described previously was used to desiccate 10 samples reinforced with 0.2% of fibres. All samples were prepared with the same initial moisture content. The results showed that nearly 80% of the fibres are located within ±20º with the horizontal plane and 51% are aligned within ±10º. This is a consequence of the sample preparation procedure since the fibre length is longer than the thickness of a compacted layer in the sample (Figure 7-3). Additionaly, a preferential fibre orientation is anticipated due to the influence of fibres self-weight and the adapted compaction method.

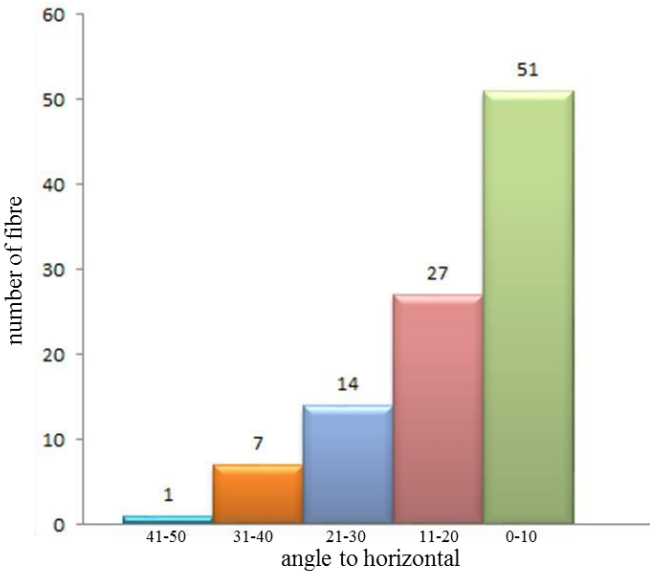

Figure 7-3. Alignment of fibres

The results are in agreement with Diambra et al. (2007); Özkul & Baykal (2006) and Özkul & Baykal (2007). These authors have also concluded that compacting soil-fibre mixtures during sample preparation leads to a preferential alignment of the fibres in a horizontal direction. Figure 7-4 shows a graphical representation of the fibre distribution on a dissected sample. It is worth to mention that on the horizontal plane they are well distributed.

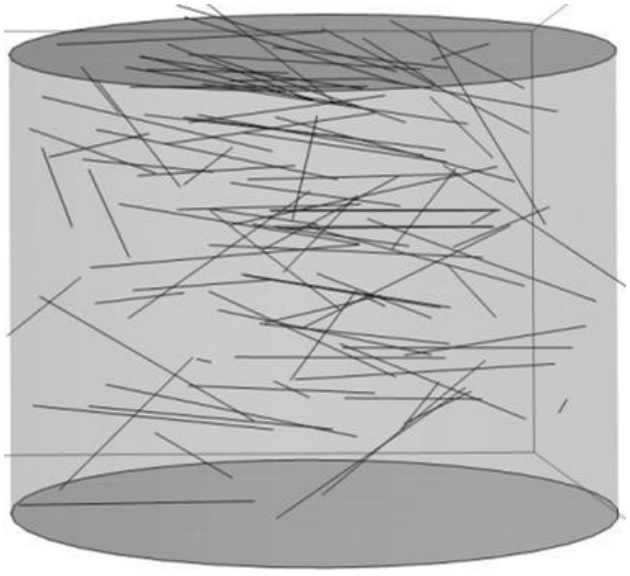

Figure 7-4. 3D orientation of the fibres on a dissected sample

8. SHRINKAGE STUDIES

8.1 Introduction

The stability of clay slopes and liners is intimately connected to desiccation cracking. To mitigate this problem, research has been performed on mixtures of soil with additives such as lime, cement and/or fibres. Chemical additives tend to generate stiff materials and may leach and create environmental problems; therefore, fibre reinforcement became an interesting alternative as it reduces the cracking formation and cracking propagation in soils subjected to wetting and drying cycles, as well as accommodating certain displacements. In this chapter, results of a pilot study on reinforced and unreinforced compacted samples of clay from the Lambeth Group, subjected to desiccation, are presented. The shrinkage study testing procedure has been reported in section 5.7 of this study.

8.2 Results

The results of the tests conducted on soils treated with a variety of fibre contents are presented in Table 10. The normalised mass against elapsed time is presented in Figure 8-1. The mass was normalised by dividing the weight of the soil specimen at each time W(t) by the initial weight of soil specimen W(0). The graph shows that the reduction in mass is mostly affected by the initial moisture content of the sample, before compaction. Therefore, higher moisture contents lead to higher mass loss.

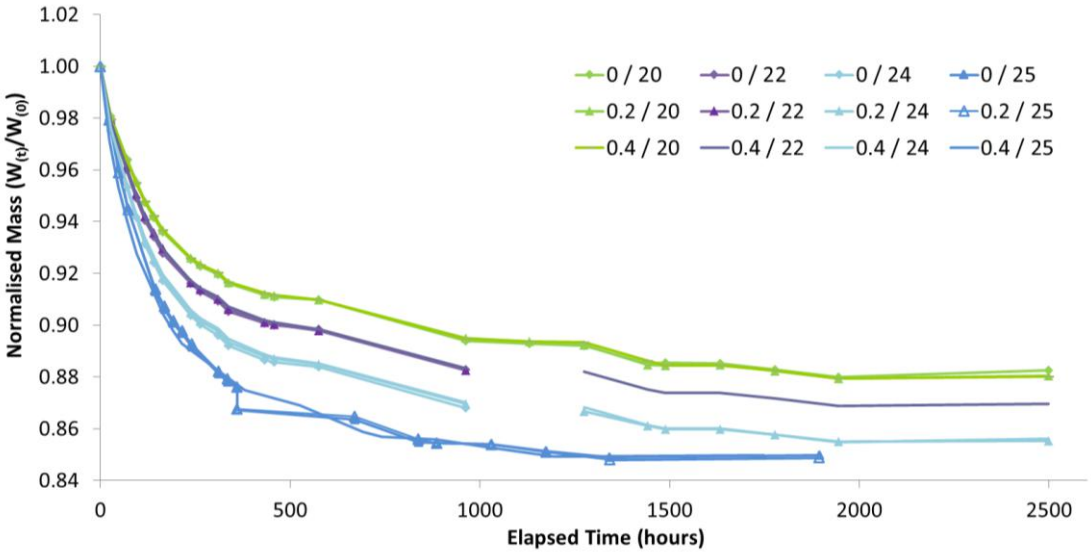

Figure 8-1. Change in normalised mass of reinforced and unreinforced samples due to free swell

Table 10. Results of free swell tests

Sample	0-20	0-22	0-24	0-25	0.2-20	0.2-22	0.2-24	0.2-25	0.4-20	0.4-22	0.4-24	0.4-25
Duration (hr)	1894	1894	1894	1894	1894	1894	1894	1894	1894	1894	1894	1894
MC (%)	20.00	22.00	24.00	25.00	20.00	22.00	24.00	25.00	20.00	22.00	24.00	25.00
FC (%)	0.00	0.00	0.00	0.00	0.20	0.20	0.20	0.20	0.40	0.40	0.40	0.40
Int. Height (mm)	127.73	127.31	127.02	128.06	128.53	127.52	127.66	128.29	128.56	127.59	127.48	127.83
Int. Diameter (mm)	151.89	151.89	152.15	152.35	151.98	152.04	152.47	152.00	152.12	152.12	152.02	152.33
Int. Volume (mm^2)	2314.22	2306.61	2309.48	2334.47	2331.43	2315.18	2330.65	2334.00	2336.47	2318.88	2313.84	2329.42
Final Height (mm)	124.84	123.12	121.66	121.56	126.65	123.55	122.44	122.45	126.42	123.98	122.98	122.24
Final Diameter (mm)	146.02	145.03	143.68	143.25	146.00	145.06	144.26	143.30	146.46	145.07	143.59	142.90
Final Volume (mm^2)	2050.53	1998.35	1961.70	1959.02	2058.37	2034.17	1982.49	1974.94	2103.77	2041.76	2003.86	2000.77
Hei. Shrinkage (%)	2.26	3.29	4.22	5.08	1.46	3.11	4.09	4.55	1.67	2.83	3.53	4.37
Dia. Shrinkage (%)	3.86	4.52	5.57	5.98	3.93	4.59	5.38	5.72	3.72	4.63	5.55	6.19
Vol. Shrinkage (%)	11.39	13.36	15.06	16.08	11.71	12.14	14.94	15.38	9.96	11.95	13.40	14.11

Figure 8-2 and Figure 8-3 present the percentage reduction in diameter and height, respectively, due to shrinkage, at the end of the drying period. It can be seen in Figure 8-2 that the reduction in diameter is proportional to the initial moisture content of the sample, while the fibre percentage does not seem to affect dramatically the shrinkage in diameter of the samples.

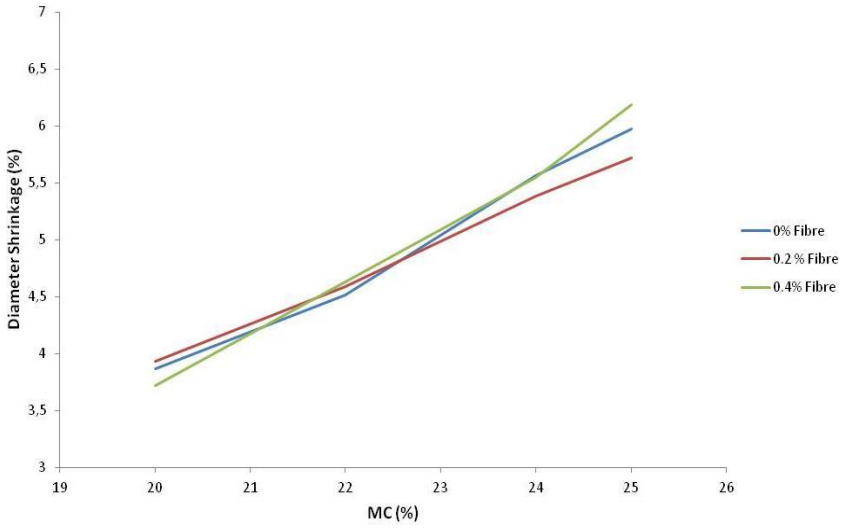

Figure 8-2. End of drying period diameter shrinkage of samples

In Figure 8-3, the response is adverse, where the reduction in height is proportional to the initial moisture content, with lower initial moisture contents showing less shrinkage than higher initial moisture contents, for every fibre content. However, the reduction in height of the samples is also affected by the fibre percentage. The samples without fibres have shown the highest reduction in height, while the reinforced samples, with 0.4% of fibres, have suffered the lowest height shrinkage. The samples with 0.2% of fibres assumed an intermediate place. The phenomenon of fibres not being effective in a horizontal direction, as would be expected, can be explained by analysing the fibre alignment during the compaction. As can be seen in Section 7, nearly 80% of fibres are aligned within ±20º in relation to the horizontal plane. This alignment is caused by the sample preparation procedure as the length of the fibres is longer than the compacted layers. Therefore, in the horizontal direction, the contribution of the fibres is negligible, while in the vertical direction, the soil particles directly act on the surface of fibres preventing shrinkage.

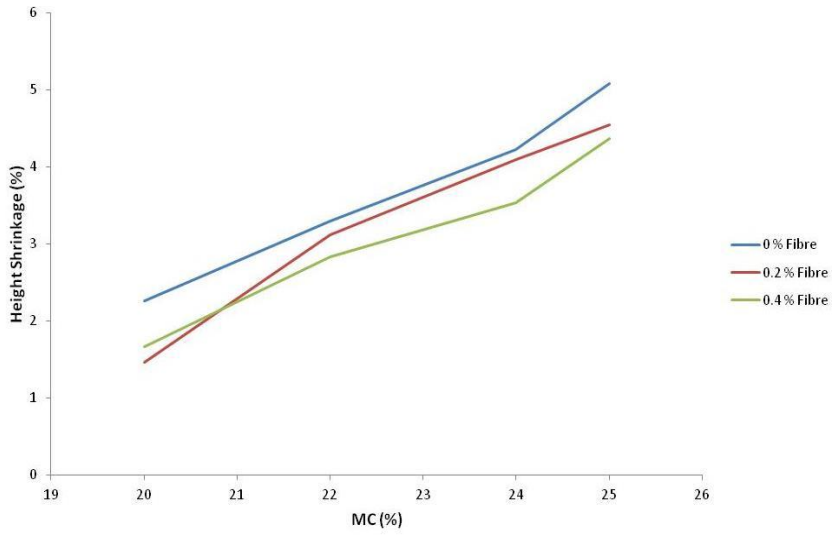

Figure 8-3. End of drying period height shrinkage of sample

Variations of the volume shrinkage as a function of fibre content and moisture content are shown in Figure 8-4. It can be seen that regardless of increasing moisture content, increasing fibre content resulted in a lower volumetric shrinkage. From the results, it is not clear whether a higher percentage of fibres could be used to reduce the shrinkage even further; however, higher percentages become difficult to mix in the soil mass.

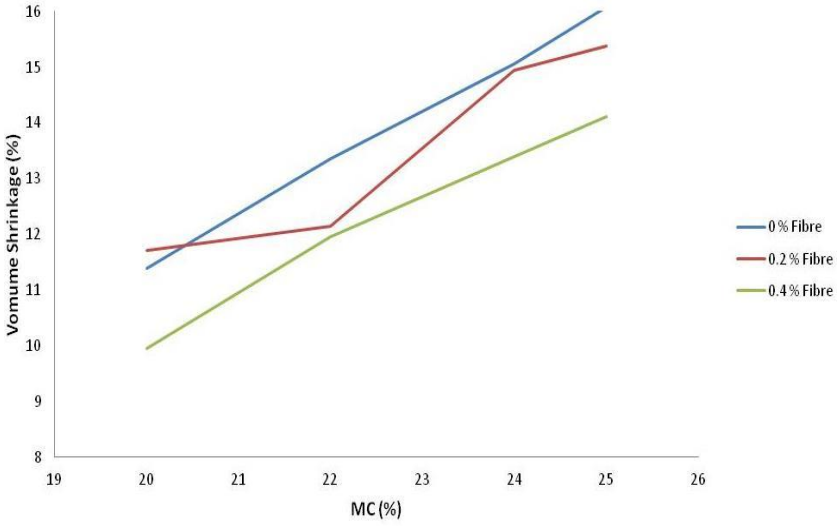

Figure 8-4. End of drying period volume of samples

Desiccation cracks occurring on the samples were monitored with the naked eye when measuring the sample dimensions. Figure 8-5 shows pictures of the samples monitored, according to the initial moisture content, fibre percentage and elapsed time. As can be seen in Figure 8-5, increases in initial moisture content do not improve the soil resistance to desiccation cracking. However, by introducing a fibre reinforcement, the

extent and depth of cracks were significantly reduced. It can be seen that in any moisture content of unreinforced samples, extensive, deep and wide cracks were formed. The reinforced samples, however, mainly experienced smaller volume reduction as mentioned above and no visible signs of crack formation on the surface of the sample. This clearly shows the effectiveness of fibre reinforcement in resisting and reducing desiccation cracking.

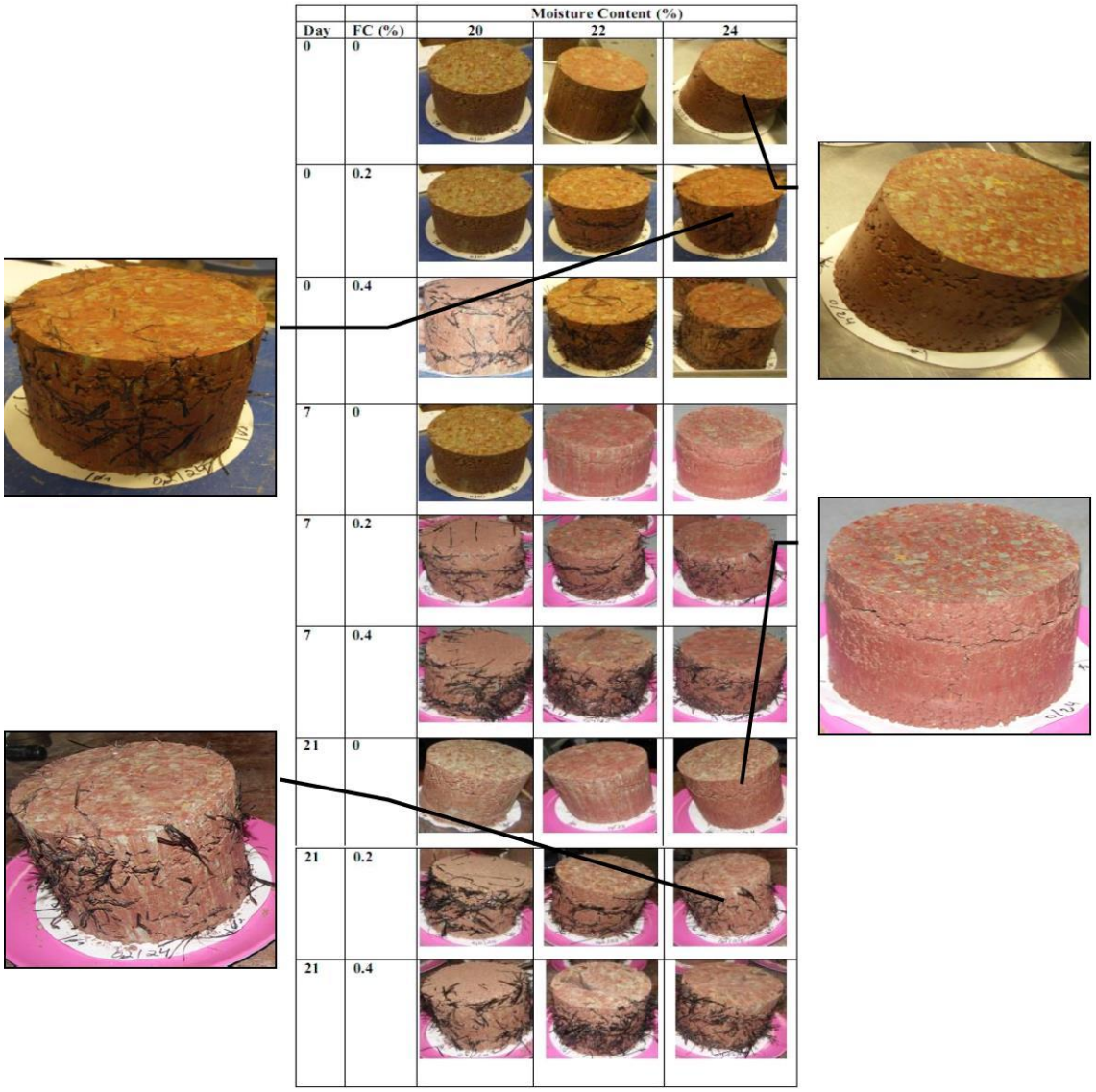

Figure 8-5. Desiccation cracking

9. COMPRESSION BEHAVIOUR

9.1 Introduction

The fibre reinforced soil; the compaction method, the fibre – specimen size ratio, fissuring and structure have all been assessed in one dimensional conditions. For this perspective, reconstituted samples have also been prepared and tested, in order to form a reference behaviour to compare and visualise the effects of reinforced and unreinforced materials in one-dimensional (Table 11) and isotropic compression.

Table 11. Specifications of 1-D Compression tests carried out for proposed study

Sample	MC	Diameter	Height
	(%)	(mm)	(mm)
Fibre 1	23.04	75.90	18.72
Fibre 2	24.03	74.60	19.95
Be_Fibre_OE_1	22.70	74.83	39.03
Be_Fibre_OE_2	24.69	74.82	39.03
Be_Fibre_OE_3	24.80	74.83	39.02
Be_Fibre_OE_4	24.80	74.82	39.04
NoFibre 1	21.88	76.10	18.60
NoFibre 2	23.67	74.60	19.92
NoFibre 3	23.32	74.60	19.93
NoFibre 4	23.32	74.50	19.94
Be_NoFibre_OE_1	28.30	74.83	39.04
Be_NoFibre_OE_2	24.81	74.82	39.03
Be_NoFibre_OE_3	28.14	74.84	39.04
A-REC	90.25	50.32	19.95
B-REC	92.75	50.40	20.07
D-REC	94.36	50.41	20.12

9.2 One-Dimensional Compression

The effect of fissuring on the compression behaviour of over consolidated clays is mentioned in the literature review section with Hight et al. (2004) reported that Lambeth group clays are heavily fissured. Nevertheless, it can be initially thought that due to the sample preparation method, where natural samples are chopped into 15 to 20 mm peds, the fissures were destroyed. However, due to the compaction technique and the presence of peds, the evaluation of the results revealed that new fissures have been introduced into the samples. Additionally, in the fibre orientation studies, at Section 7 and by Diambra et al. (2007), it was observed that these fissures are aligned horizontally, since fibres within the sample tend to be oriented along the horizontal plane. Given the single fissuring orientation of the tested clay, due to the compaction technique used, the tests were carried out with the fissuring direction roughly normal to the maximum principal stress.

Considering Figure 9-1 by Vitone & Cotecchia (2011), one can observe that reinforced and unreinforced one-dimensional specimens believed to be introduce fissures to specimens due to adapted preparation methods which represents ministructure characteristics. Compacting peds is believed to give ministructure fissuring characteristic to the material, since the compaction effort deforms and confines peds of several millimetre thickness, similar to plate like fragments called scales (Figure 9-1). Additionally, Vitone et al. (2005) proposed a chart that represents the soil fissuring identity (F-ID), where the tested reinforced and unreinforced specimens can be classified as I6 or highly fissured clay.

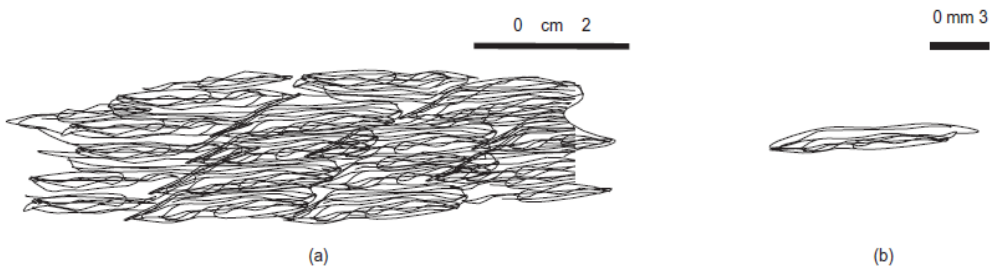

Figure 9-1. (a) Sketch of scaly meso fabric made up of scales: (b) scale-in-scale mini-fabric within a scale structure (Vitone & Cotecchia 2011)

Vitone & Cotecchia (2011) stated that fissuring intensity can be characterised either by the average volume of the clay elements between the fissures or by the average area of the discontinuity surface per unit volume, defined as the specific surface, S_s. Figure 9-2 represents the variation in S_s for a unit volume element with varying element shape. S_{s0} refers to a cubic shape. The ratio S_s/S_{s0}, defined as the fissuring shape index (FSI), decreases with increasing height (H) to length (L) ratio. Furthermore, authors stated that increase in FSI cause an increase in interaction between the soil elements and water.

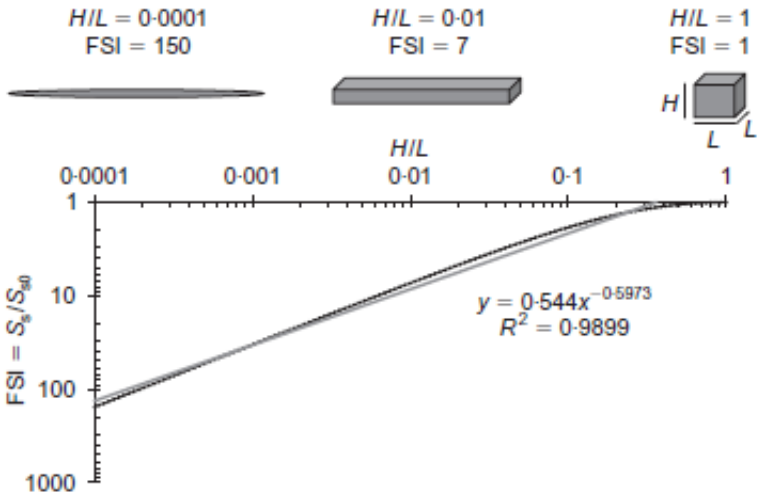

*Figure 9-2. Increase in specific surface (Ss) of 1m3 volume ped (Ss0=Ss for H=L=H0=1m) at increase of ratio H/L (*Vitone & Cotecchia 2011)

In this study, clays with plate shaped scales have high FSI index, around 100. The expected increase in interaction between soil elements and water with increasing FSI is believed to be further increasing with introduction of fibres. This behaviour have been shown in the pore pressure evaluation of the reinforced and unreinforced undrained shear tests, where reinforced specimens were responding with higher pore water pressure development, due to presence of fibres (section 10.6.1.3).

As can be seen on Figure 9-3, both reinforced and unreinforced samples are not following identical compression lines. Moreover, due to instrumental and procedural limitations, in order to test samples with 60mm long fibres, the 76mm oedometer ring was used. It can be observed, from Figure 9-3, that the odometer tests reached around 1MPa in compression, therefore this has only taken the soil through the initial, flatter, post yield part of the compression curve. Additionally, it is worth to note that evaluation

of Figure 9-3 have also revealed that even though the specimens were compressed to low vertical stresses, they are reaching down to a void ratio of 0.25 and the compression line of individual specimens seems not to converge to a unique normal compression line. Such response seems to indicate that these soil samples do not have a unique NCL, exhibiting a transitional soil behaviour.

Silva Dos Santos et al. (2010) also experienced similar offset in the reinforced specimens and explained that the offset in the compression lines could be due to the interlocking mechanism, created by the fibres, allowing the reinforced soil to exist with a larger range of void ratios.

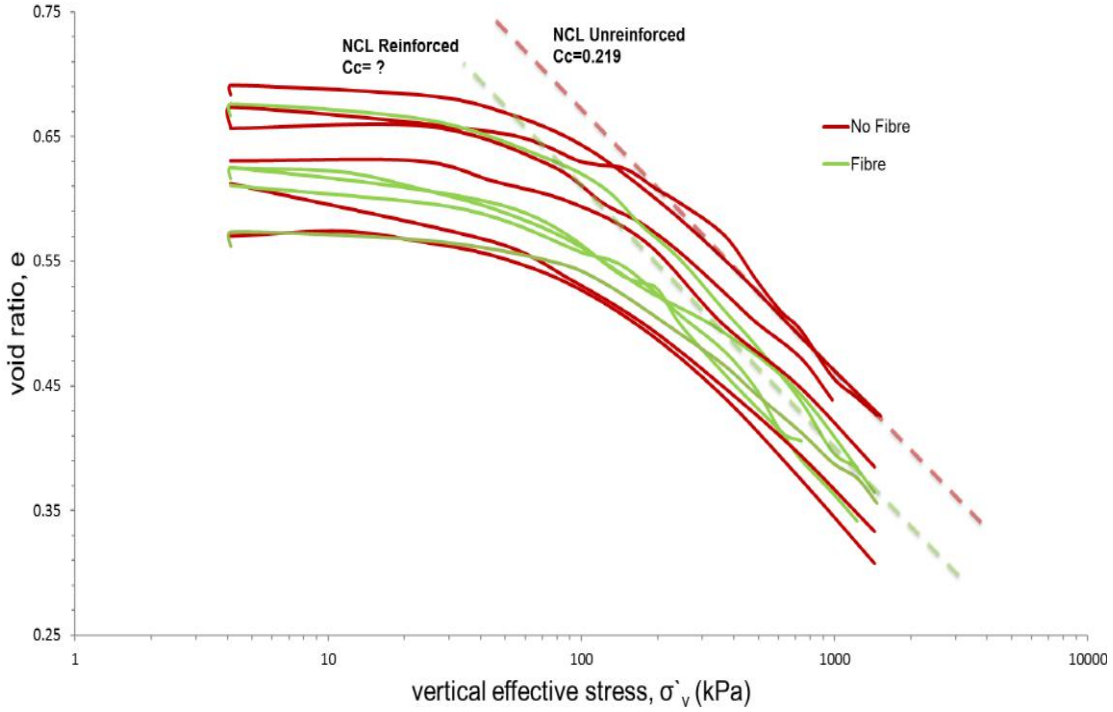

Figure 9-3. One-dimensional compression of fibre reinforced and un-reinforced samples

Ponzoni et al. (2014) introduced the parameter "m" in order to provides a convenient way of quantifying the degree of convergence and perhaps the transitional behaviour degree. Authors reported that for soils with converge to a unique NCL, m would be zero whilst for soils with perfectly parallel compression paths m = 1.

To quantify the degree of convergence Figure 9-4a illustrate how the initial specific volume may be plotted against that at 6000 kPa (V_{6000}), which is generally the maximum stress reached (1400 kPa for this study). For consistency the initial specific

volume was taken in each test at 20 kPa (V_{20}) vertical stress (4 kPa for this study). The permitted space for data in this graph is below the 1:1 line Figure 9-4b. It is worth pointing out that Ponzoni et al. (2014) used the specific volume on his calculations but the values shown here were calculated using void ratio.

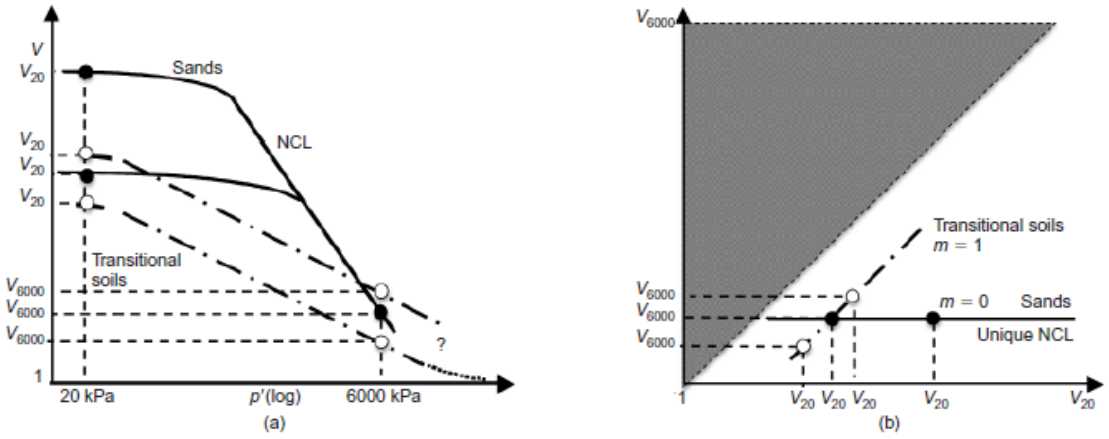

Figure 9-4. Quantification of the convergence of compression curves for intact specimens: (a) schematic compression curves; (b) calculation of m (Ponzoni et al. 2014)

As mentioned previously, it is not possible to estimate a distinct normal compression lines (NCL), for the fibre-reinforced and non-reinforced clay samples. Nevertheless, it can be seen that the unreinforced specimens are following a different compression line for each initial void ratio. Such behaviour is confirmed by Figure 9-5, where m= 0.96, confirming that the range of initial void ratios is similar to the range of final void ratios

The compression index, Cc, of the unreinforced specimens was determined as, Cc=0.219. However, the reinforced specimens seem to converge to a unique NCL (Figure 9-3) which make the determination of Cc difficult. Such behaviour is supported by an "m" value equal to 0.14, indicating that convergence but, at the same time, the non-uniqueness of the NCL, for the stresses reached (Figure 9-6). It could be argued that the current stress levels are not enough to reach a unique NCL, particularly in the case of the reinforced specimens, where an NCL could be reached at void ratios as low as 0.2, where the NCL would start becoming flatter. It is, however, evidential that the addition of reinforcement seems to reduce drastically the transitional behaviour effect.

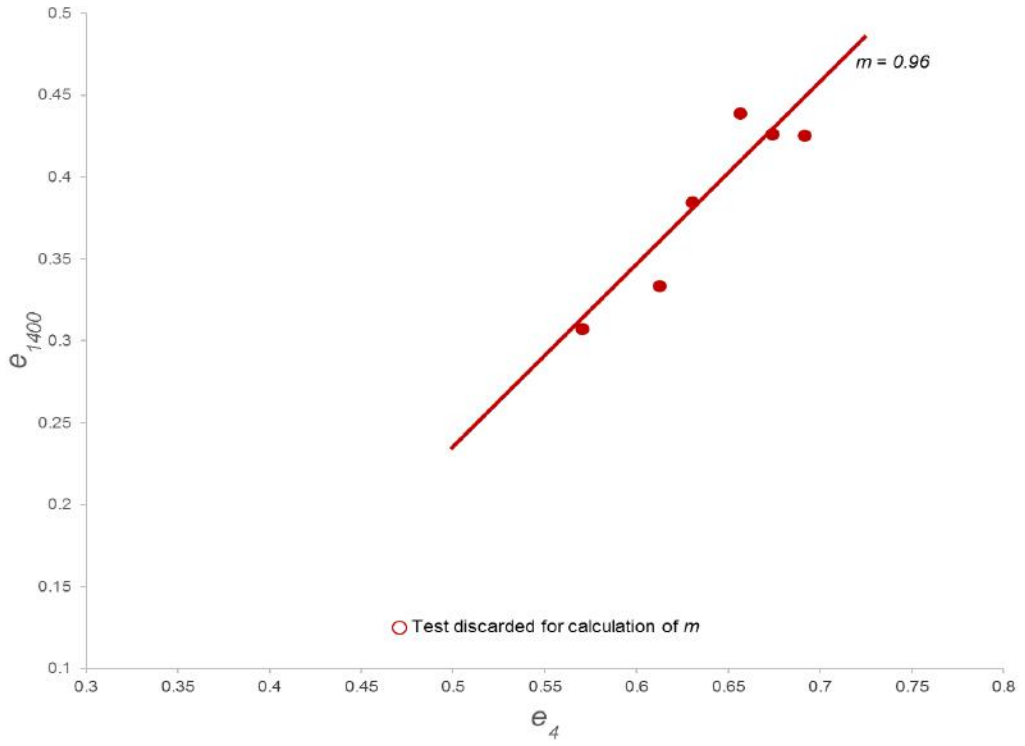

Figure 9-5. Calculation of m values for unreinforced specimens

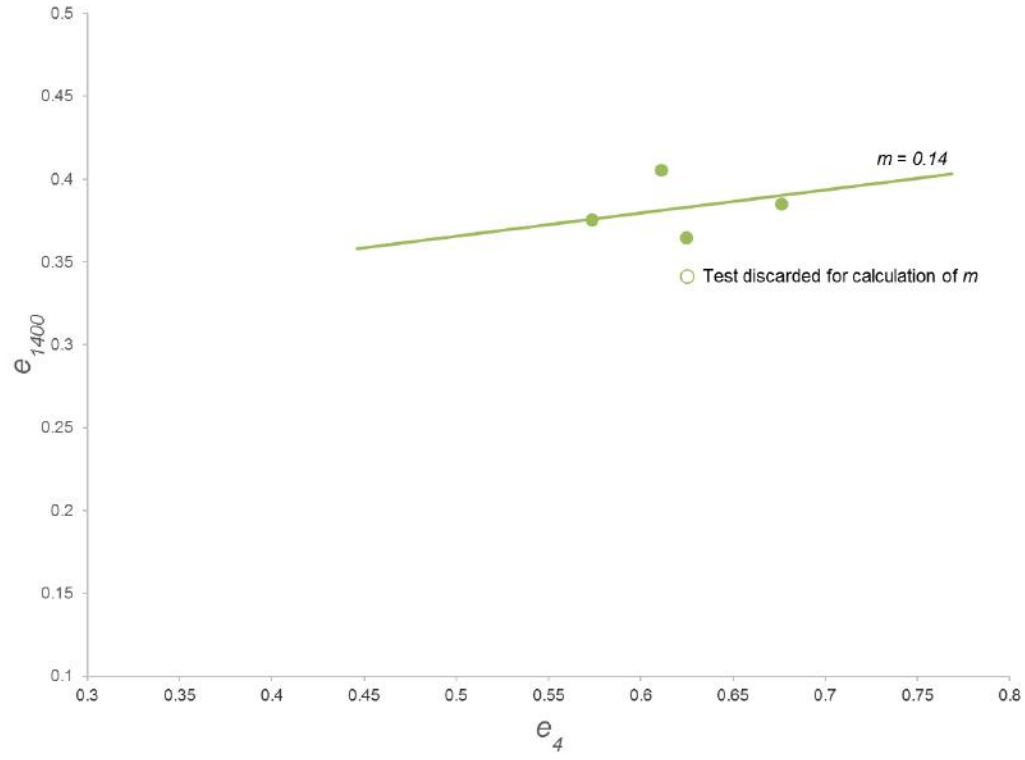

Figure 9-6. Calculation of m values for reinforced specimens

Intrinsic compression line of the reconstituted specimen can be seen on the Figure 9-7. Unlikely to reinforced and unreinforced specimens, it is possible to estimate distinct

normal compression lines (NCL), for the reconstituted specimens, where slope of compression line can be determined as, Cc=0.372. The one-dimensional compression curves of the samples lie on the left of the correspondent compression line of the reconstituted samples. Additionally, the reinforced and unreinforced samples yield before reaching the normal compression line of the reconstituted samples (i.e. the intrinsic compression line, ICL; Burland (1990), as already found for scaly clays by Fearon & Coop (2002)). Furthermore, according to Vitone and Cottecchia 2011, all I6 clays (intensely fissured on the the F-ID charts), will have the normal compression line below the ICL, irrespective of other fissuring features, such as fissuring orientation and element strength (intact soil undrained strength). Another feature common to the compression curve of all reinforced and unreinforced specimens is a very mild curvature with no abrupt yielding at any pressure (Figure 9-3).

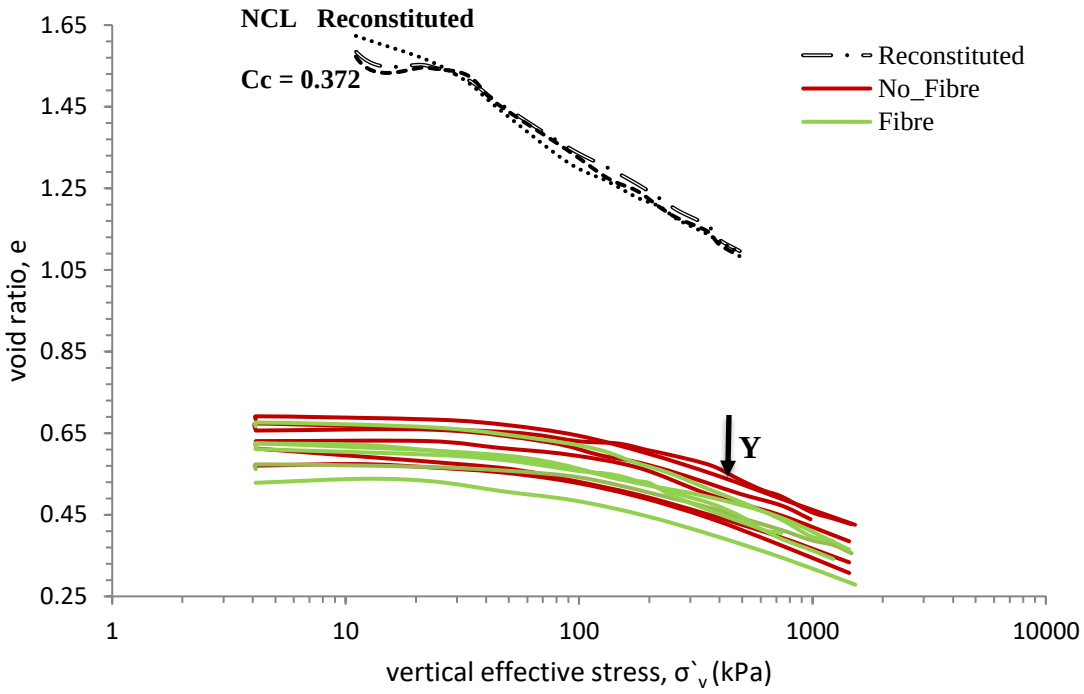

Figure 9-7. Reinforced and un reinforced specimens corresponding to Reconstituted compression line

One can see on Figure 9-8 the normalizing parameter I_v used to compare reinforced and unreinforced samples with the corresponding ICL. On the same graph it can be observed that the compression lines obtained via oedometer test, compared to the compression lines obtained via the theoretical equations derived by Burland (1990). Where both theoretically obtained and measured results coincide with small variations.

At present point, it has not been possible to calculate exact stress sensitivity ratio proposed by Cotecchia & Chandler (2000) where the parameter $S_\sigma=\sigma`_y/\sigma^*_e$ (where σ^*_e is the equivalent pressure on the ICL), due to the high difference in the initial void ratio between the reconstituted and the compacted samples. Where compaction had led to denser specimens and made such a comparison impossible in low vertical stresses that tests have been carried out. Nevertheless, with a qualitative analysis, it can be observed that Figure 9-8 indicates values of $S_\sigma < 1$ for reinforced and un-reinforced specimens. Therefore, the combination of compaction induced fissuring with the clay microstructure is found to weaken the clay by comparison with the reconstituted soil in one-dimensional space, irrespective of the addition of fibres. Additionally, effect of orientation due to compaction method on one-dimensional consolidation can be seen regardless of reinforcement where specimens are yielding before reaching ICL. Furthermore addition of fibres seem to erase the fissuring effect due to connection of fissures via fibres.

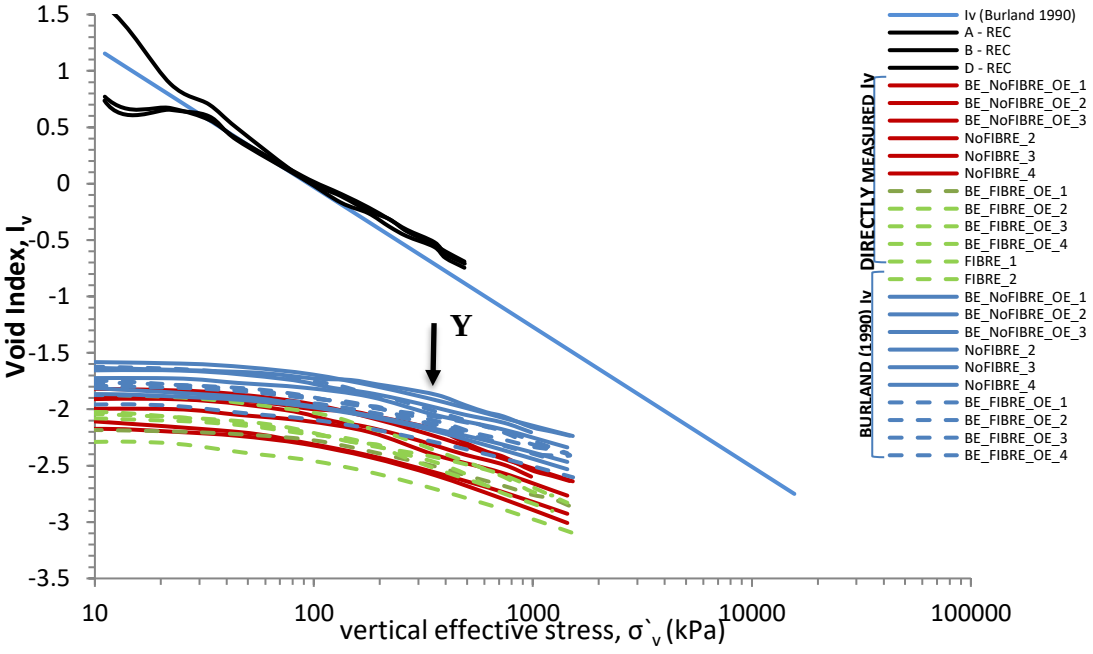

Figure 9-8. Normalised one-dimensional compression curves of fibre reinforced and un-reinforced samples

9.3 Isotropic Compression

Figure 9-9 shows the results of the isotropic compression of reinforced and unreinforced specimens, before shearing, in the triaxial equipment.

Similar to the one-dimensional behaviour, it is not possible to estimate a distinct isotropic normal compression line (iso-NCL) for the reinforced and unreinforced specimens. Therefore, a transitional behaviour of the reinforced and unreinforced specimens are monitored in isotropic compression. Nevertheless, the slope of each individual specimens seem to be parallel. Therefore, by using equation 4, where N= specific volume at a p'=1kPa (the intercept on a logarithmic scale) and λ= gradient of the isotropic NCL, the only calculated parameter that characterise these two NCLs are: λ=0.0923 for the unreinforced specimen and λ=0.0613 for the reinforced specimen.

It was also monitored that reinforced and in-situ specimens, even with a slow enough compression rate of 2 kPa/hr, continued to compress even after reaching the targeted confining stress.The addition of fibres to the ped-compacted material enabled it to compress to higher stresses, similar to a structured soil. It is worth pointing out that within the range of stresses used in the tests, this structure seems to be stable.

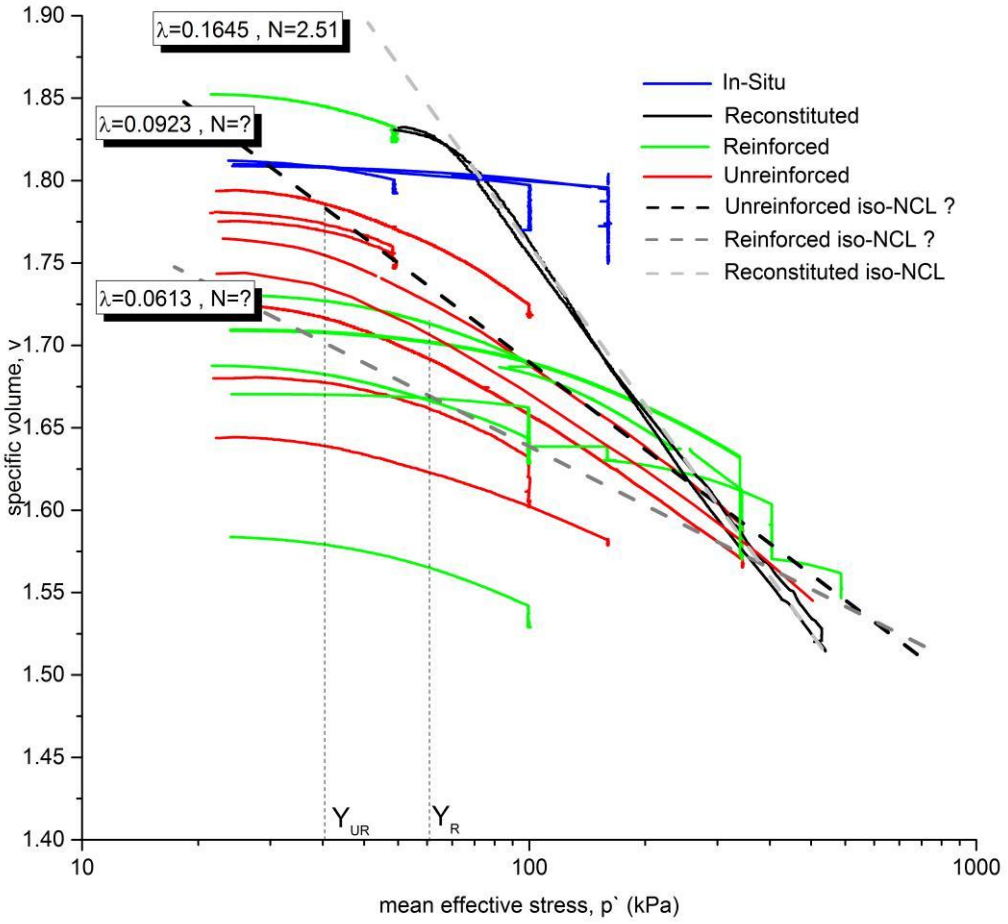

Figure 9-9. Isotropic compression path of reconstituted, reinforced, un-reinforced and in-situ specimens

Figure 9-9 shows the specific volume (v) and mean effective stress (p`) stress path following the isotropic compression of reinforced, un-reinforced and in-situ specimens. The figure also shows the stress path followed by reconstituted clay specimens, representing the ICL. As can be observed reconstituted specimens have followed a unique compression line and the parameters that characterise this ICLs are: N=2.51 and λ=0.1645. By using equation 6, the relationship between the isotropic and one dimensional compression reveals that, if the constant K_0 is assured, the λ calculated by using the Compression Index (Cc) for unreinforced and reconstituted, specimens is, 0.0950 and 0.1615, respectively. These values are in agreement with the parameters obtained via isotropic compression of the same materials.

Unreinforced samples show an apparent yield point and, similar to the one dimensional compression, yielding on the left of the ICL. When yield occurs outside of the ICL, it is defined as strong bonding and weak when it occurs inside, as illustrated in Figure 9-10.

In the case of strong bonding, Cuccovillo & Coop (1999), after studying cemented soils, summarised the behaviour as elastic up to a yield that occurs stresses higher than would be required to initiate particle breakage in an un-cemented soil, so that the cement is carrying some of the confining stress and preventing breakage. Where, in the case of fibre reinforcement, since bond breakage will not occur, it might be the mobilisation of the fibres, which contributes in a similar way to soils with a "strong bond".

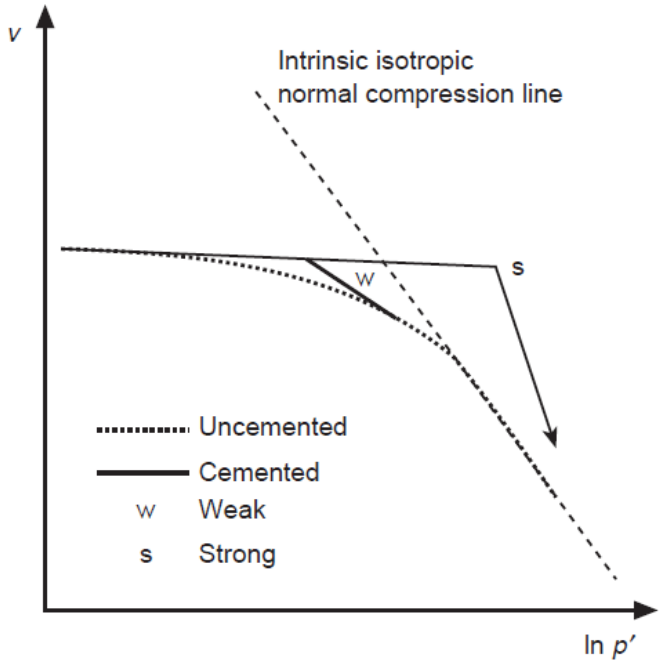

Figure 9-10. Schematic comparison of the isotropic compression of weakly and strongly cemented carbonate sand (Cuccovillo & Coop 1999)

Hight et al. (2007) plotted data of intact and natural samples on Figure 2-34 and concluded that the yield of the natural London Clay is poorly defined. Similarly, as can be seen on Figure 9-9 fibre reinforced specimens show an extensive yielding zone, with yielding occuring (Y_R=70 kPa) on the right hand side of the unreinforced samples (Y_{UR}=40 kPa), at a closer position to the INCL*. Additionally, the isotropic compression line gradient, λ, of both specimens was found to be smaller than the gradient of the Intrinsic normal compression line. As presented in section 2.4.2, this response shows a change in behaviour via the introduction of fissures by the the fibres and ped compaction. Similar to the behaviour of scales on intensive fissured clays reported by Vitone & Cotecchia (2011).

Consoli et al. (2005) proposed a mechanism explaining the effect of fibre reinforcement in the isotropic compression of reinforced sandy soils (Figure 9-11). In this mechanism, discrete randomly distributed fibres act as a spatial three dimensional network that will interlock soil grains. The authors believe that this will help the grains to form a coherent matrix and restrict the radial displacement and restrain the volumetric changes inside the sample, therefore shifting the NCL to the right. Tang et al (2007) concluded that, because of the interfacial force, the fibres in the matrix have difficulty to slide and they are able to bear tensile stress. In light of the above mechanism, when the compression of a reinforced soil starts to occur, the flexible polypropylene fibres in the soil are stretched and tensioned, resisting the further compression of the samples. In the case of Consoli et al. (2005) stretch is between sand particles where, in this study, stretch might be in between the clay peds.

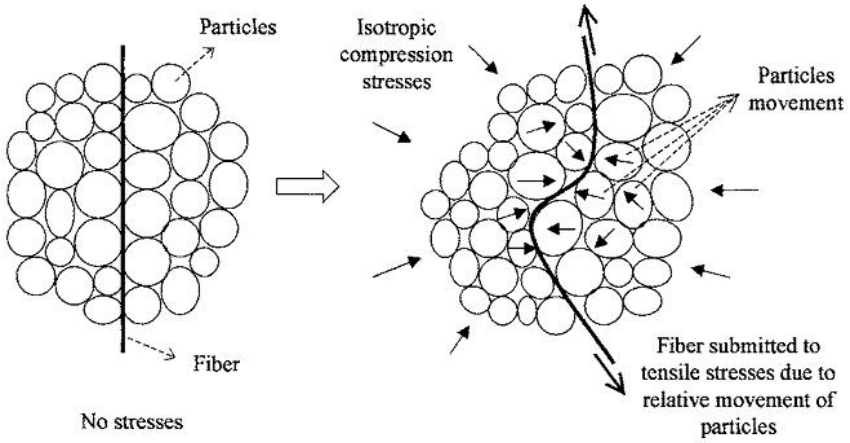

Figure 9-11. Illustration of proposed mechanism of fibre breakage under isotropic loading. (Consoli et al. (2005)

As can be seen on Figure 9-9 in-situ specimens appear to carry a stress history higher than the laboratory reinforced specimens. These specimens yielded at much higher effective stresses and, on the right hand side of the ICL. This is due to the compaction effort used on site, as it is believed that it was much higher than the effort used in laboratory conditions. Furthermore, peds used in the in-situ compaction were between 50 to 300 mm which are likely to retain the natural properties of the soil. Burland (1990) confirms a similar behaviour for the sedimentation compression line of the intact London clay.

10. LARGE STRAIN BEHAVIOUR

10.1 Introduction

In the current chapter, stress-strain, pore water pressure change, failure mode, effective stress paths, stress ratio and pore pressure increments with strain of the tested samples have been studied in the light of the Critical State framework. A list of all the tests analysed, together with the confining pressure at shearing is in Table 12.

The tests are named in a way that the author believes will make it easier to understand the test procedure, sample size, preparation method and confinement level chosen for a particular sample. The first portion of the name refers to stress path the specimen followed. Subsequent numbers are the size of the specimens, followed by an indication of reinforcement and finally the consolidation stress path. The letters on the table indicate:

CD = Consolidated Drained
CU = Consolidated Undrained
P` = Constant p' stress path test
Lab = Prepared in laboratory
Insitu = Block samples collected from site
REC = Reconstituted
Fibre = Reinforced
No Fibre = Unreinforced

For example, CD_p'_100_Lab_Fiber_300kPa is a triaxial test on a sample prepared in the laboratory, reinforced with fibres, that was consolidated to 300kPa effective stress and sheared following a drained stress path.

In addition to long names, short names are also introduced to make the referencing within the text easier. Therefor for short names, the first letter indicates drainage condition which is followed by the effective stress test performed. In the case of reconstituted testing, the first letter changes to REC, where for in-situ samples it is changed to INS. The letters indicate:

DNF = Drained No Fibre
DF = Drained Fibre
DREC = Drained Reconstituted
UNF = Undrained No Fibre
UF = Undrained Fibre
REC = Undrained Reconstituted
INS = Insitu

Table 12. Summary of all triaxial tests

Sample	Short Names	Compaction	Height	Diameter	Weight	Moisture Content	Confinment
			(mm)	(mm)	g	(%)	(kPa)
CD_p'_38_Lab_NoFiber_50kPa	DNF50	27x3	78.77	37.62	174.63	23.30	50.00
CD_p'_38_Lab_NoFiber_50kPa_2	DNF50_2	27x3	77.64	39.21	183.57	26.00	50.00
CD_p'_38_Lab_NoFiber_100kPa	DNF100	27x3	78.57	38.21	175.36	28.10	100.00
CD_p'_38_Lab_NoFiber_300kPa	DNF300	27x3	77.59	37.80	177.54	27.95	300.00
CD_p'_100_Lab_Fiber_50kPa	DF50	27x3	199.51	105.68	3410.00	30.71	50.00
CD_p'_100_Lab_Fiber_100kPa	DF100	27x3	200.04	104.80	3455.00	25.10	100.00
CD_p'_100_Lab_Fiber_300kPa	DF300	27x3	199.75	104.96	3361.00	26.84	300.00
CU_38_Lab_NoFiber_50kPa	UNF50	27x3	77.92	38.87	176.44	27.49	50.00
CU_38_Lab_NoFiber_100kPa	UNF100	27x3	78.00	39.00	183.08	24.26	100.00
CU_38_Lab_NoFiber_150kPa	UNF150	27x3	78.05	38.97	188.43	23.00	150.00
CU_38_Lab_NoFiber_300kPa	UNF300	27x3	79.46	38.20	185.36	25.30	300.00
CU_38_Lab_NoFiber_500_300kPa	UNF500_300	27x3	76.96	37.59	172.15	27.36	500_300
CU_38_Lab_NoFiber_500kPa	UNF500	27x3	79.25	38.99	181.92	24.28	500.00
CD_38_p'_REC_150kPa	DREC150	REC	71.92	38.00	144.66	40.96	150.00
CU_38_REC_150kPa_2	REC150	REC	73.00	38.00	153.00	46.67	150.00
CU_38_REC_450_200kPa	REC450_200	REC	78.75	38.00	155.00	36.92	450_200
CU_38_REC_500 _125	REC500_125	REC	74.00	38.00	154.00	35.92	500_125
CU_38_REC_500	REC500	REC	73.00	38.00	149.68	37.77	500.00
CU_100_Insitu_Fiber_50kPa	INS50	Block	203.20	102.00	3178.00	25.28	50.00
CU_100_Insitu_Fiber_100kPa	INS100	Block	205.00	112.00	3221.00	28.74	100.00
CU_100_Insitu_Fiber_150kPa	INS150	Block	198.80	99.17	2926.50	28.60	150.00
CU_100_Insitu_Fiber_500kPa	INS500	Block	205.00	119.10	3080.00	30.88	500.00
CU_100_Lab_Fiber_100kPa	UF100	27x3	200.00	101.12	3455.00	26.47	100.00
CU_100_Lab_Fiber_150kPa	UF150	27x3	200.00	101.00	3474.50	21.67	150.00
CU_100_Lab_Fiber_300kPa	UF300	27x3	200.00	105.00	3400.00	25.85	300.00
CU_100_Lab_Fiber_500kPa	UF500	27x3	199.00	105.22	3500.00	24.40	500.00
CU_100_Lab_NoFiber_100kPa	UNF`100	27x3	200.11	101.03	3207.00	29.61	100.00

Three different normalisation techniques were adopted to determine the state boundary surfaces for each group of specimens. Discussions and comparisons of the results (i.e. reconstituted, reinforced, unreinforced and in-situ tests) have been made in order to

identify changes in behaviour due to the introduction of fibres following the compaction methodology and how these compare to the in-situ samples. Additionally, observed behaviour changes are highlighted and discussed in relation to the structure of the natural soil.

Figure 10-1 shows the representative drawing of the failure modes of each specimen tested. These were drawn based on measurements taken at the end of each test. Samples DREC150, UNF100 and DN50_2 were not included in Figure 10-1 as these were used to crosscheck the repeatability and size effect. Sample DN50_2, however, was observed to have instrumental errors and was discarded.

It is clear that the reinforced specimens show a barrelling failure in both drained and undrained conditions, whilst the other tests have failed with either barrelling or barrelling and the formation of a shear plane. This figure will be referenced and discussed further in the following sections.

Confinement	Reconstituted	Undrained Unreinforced	MC (%)	Undrained Reinforced	MC (%)	In-situ	MC (%)	Drained Unreinforced	MC (%)	Drained Reinforced	MC (%)
50			31.05 31.85 **33.12** 27.82 29.70				**33.60** 31.89 **32.10** 31.26 30.79		25.71 25.81 25.93 **30.30** 23.52		28.26 27.30 28.29 27.49 28.67
100			26.14 23.59 27.25 24.74 27.80		27.89 29.28 28.23 29.23 27.86		28.71 29.11 **30.62** 29.05 29.11				22.58 22.58 21.28 23.31 24.29
150			21.57 21.75 20.73 **22.13** **22.25**		23.83 23.30 24.43 23.40 24.85						
300			25.61 24.59 **27.80** 24.67 **28.49**		23.43 23.76 24.73 24.05 24.53						23.79 23.50 23.49 23.67 23.07
500_125											
500_300		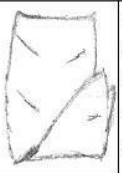	21.32 20.00 21.05 21.88 **25.60**								
450_200											
500							28.86 29.93 29.00 **31.22** 29.89				

Figure 10-1. Shear plane characteristics for triaxial test of all specimens

10.2 Reconstituted Clay Behaviour

The reconstituted behaviour of a soil can be used to measure the effect of structure when being compared with the natural properties, where else in current study, effect of peds and reinforcement. The tests carried out on reconstituted samples are presented in Table 12, that presents the initial dimensions, moisture content and the effective confinement stress at the beginning of the testing stages.

Figure 10-2 to Figure 10-6 present the stress-strain curves, pore water pressure change stress path, stress ratio and pore pressure increments with the strain rate of the reconstituted clay from Lambeth group, used throughout this study. The method used for the preparation of samples was described in section 5.4 of the current study. The prepared reconstituted samples were sheared undrained, at different isotropic stress levels, to determine the failure envelope based on triaxial tests. The visual observations (Figure 10-1), during the shearing stage, revealed that all the samples bulged during shearing. The appropriate corrections in calculations is described in Section 6.2.4. The general behaviour of the samples, in the stress-strain space (Figure 10-2) is contractive with a strain hardening at medium to high strains, with the exception of REC500; this sample showed a mild strain softening at high strain level. At large strains, all samples reached a constant stress level, as expected.

Figure 10-3 shows the change in pore pressure generated within the reconstituted samples. Similar to the stress strain relationship, pore water pressure increase is dependent on the effective stress level applied to the samples. In general, the excess pore pressure reached a plateau before the deviatoric stresses for the samples tested in the reconstituted state with sample REC500 reaching a very high level of pore-pressure, when compared with the others.

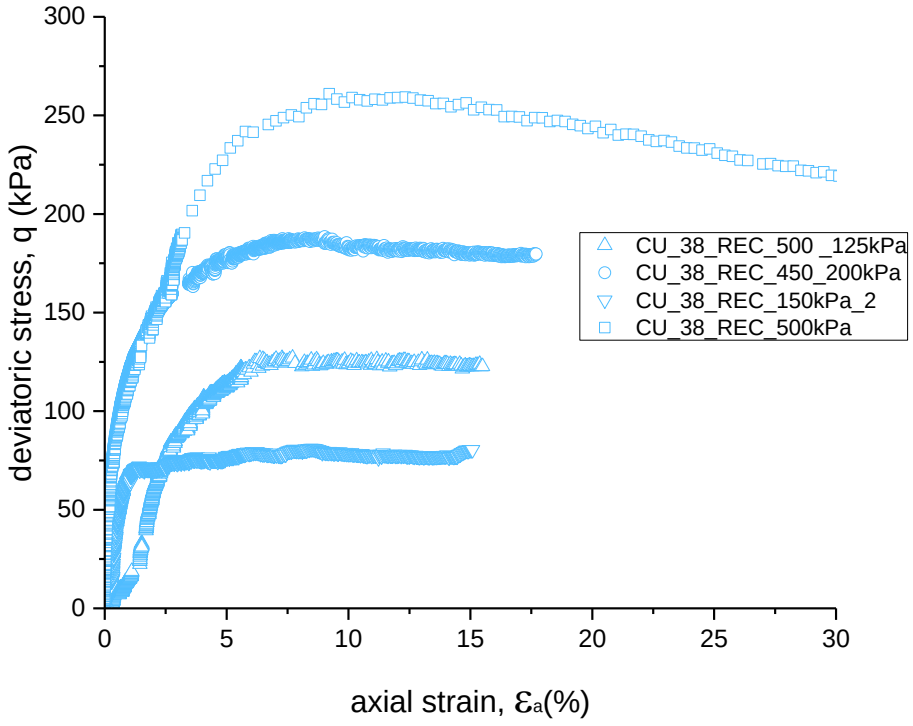

Figure 10-2. Stress-strain relationship of undrained reconstituted samples

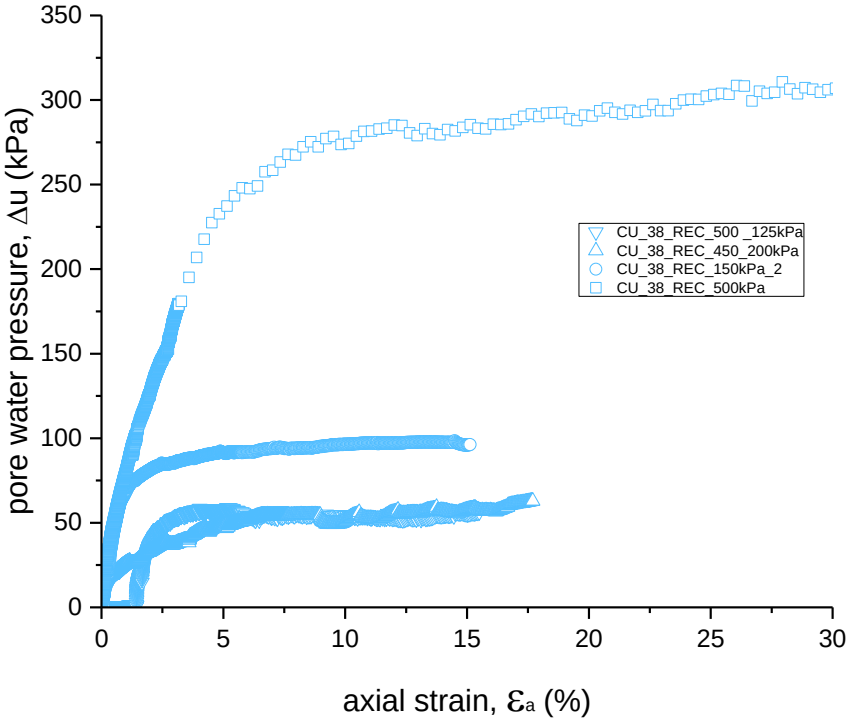

Figure 10-3. Pore pressure change in undrained reconstituted samples

As can be seen in Figure 10-4, samples REC500, REC450_200 and DREC150 were reached to critical state line. Where remaining tests show tendency to reach the chosen critical state line. The critical state stress ratio parameter (M) of the reconstituted Lambeth group clay, the slope of the CSL, was found to be 0.85, being coincident with the study of Gasparre (2005) on reconstituted London Clay.

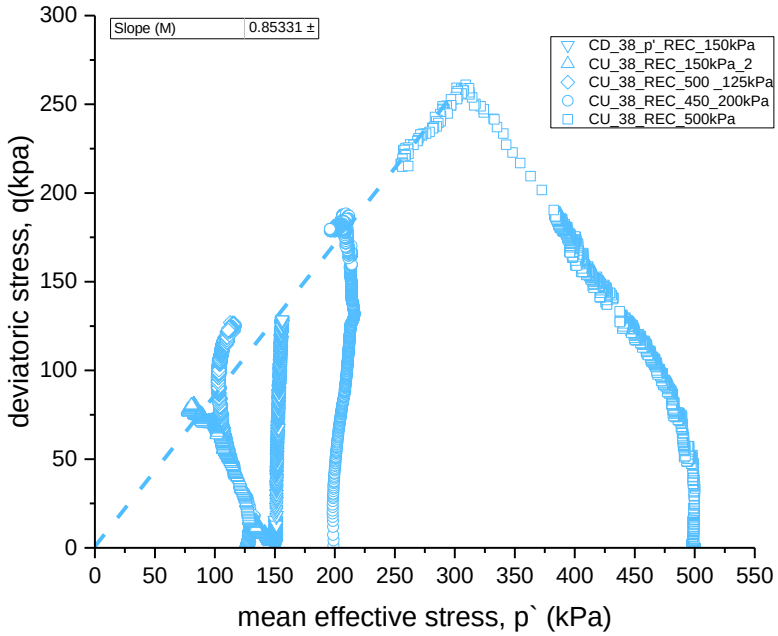

Figure 10-4. Stress paths for the undrained reconstituted samples

The stress ratio plot in Figure 10-5, confirms that there is a tendency for the REC500 and REC 450_200 samples to converge towards a unique critical state stress ratio, M, which was determined from effective stress path plot. Where, on the other end, samples REC150 and REC500_125 do not seem to have reached the critical state. Such occurrence might be due to the differences in initial specific volume of the specimens, causing the samples end of test state position to be away from the CSL. Nevertheless, in the light of current plots it cannot be concluded that all specimen were observed to reach unique critical state ratio (M).

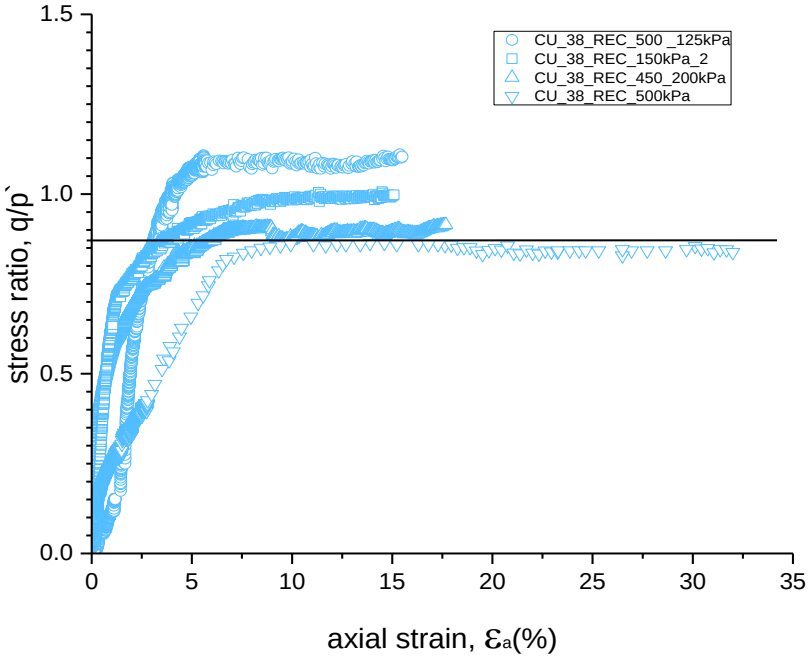

Figure 10-5. Stress ratios for undrained reconstituted samples

The change in pore pressure increments with strains for the undrained reconstituted samples is plotted in Figure 10-6. Similar to the observations made on Figure 10-5, the curves of sample REC500 and REC 450_200 seem to converge, at large strains, towards a unique stress ratio as observed previously.

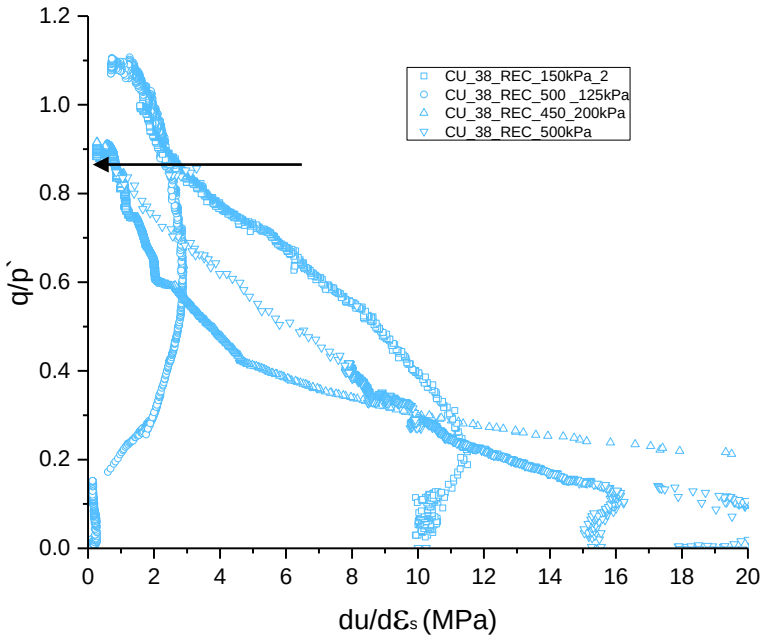

Figure 10-6. Pore pressure increments for undrained reconstituted samples

As can be seen in Figure 10-6 samples REC500_125 and REC150 are away from the critical state stress ratio determined through other specimens therefore they reached to higher stress ratio where further reduction of pore pressure was necessary to approach the critical state stress ratio determined for the other samples.

In the light of above evaluation, the evaluation of the critical state of the samples, which were tested in the reconstituted state, are more pronounced in stress path space when compared to stress ratio and pore pressure increment spaces.

10.3 Unreinforced Clay Behaviour

Figure 10-7 to Figure 10-11 present the stress-strain curves, change in pore water pressure, effective stress paths, stress ratio and pore pressure increments with strain rate for the unreinforced Lambeth group clay used in this study. The sample preparation method used for these samples is described in section 5.4 of this report.

Figure 10-7 shows the deviatoric stress against the axial strain of the undrained triaxial tests performed. As can be seen, all samples show a strain-hardening behaviour at medium to high strain level, followed by constant stress behaviour. The unreinforced samples sheared at a confining pressure above and including 150kPa, failed with the formation of a distinct shear plane that became visible from around 5% strain onwards. Samples with distinct shear plane have undergone an appropriate area correction as described in Section 6.2.4.

Figure 10-8 shows the pore water pressure generated within the unreinforced samples. Similar to the stress-strain relationship, the pore water pressure is proportional to the level of confining pressure. The normally consolidated and overconsolidated samples tested at 300kPa of confining pressure reached a constant excess pore pressure at approximately 5% strain. Samples UNF50 and UNF100 reach a plateau with a slight drop in the pore water pressure afterwards. Additionally, it can be observed that in sample UNF500, the pore water pressures starts to decrease slowly. This may be caused by the extensive strain localisation, causing the water to drain towards the shear zone. Sample UNF150 showed a barrelling failure mechanism and, as can be observed in Figure 10-8, an extensive drop of pore pressure was monitored. This was followed by a reduction of pore water pressure at the point of reaching critical state.

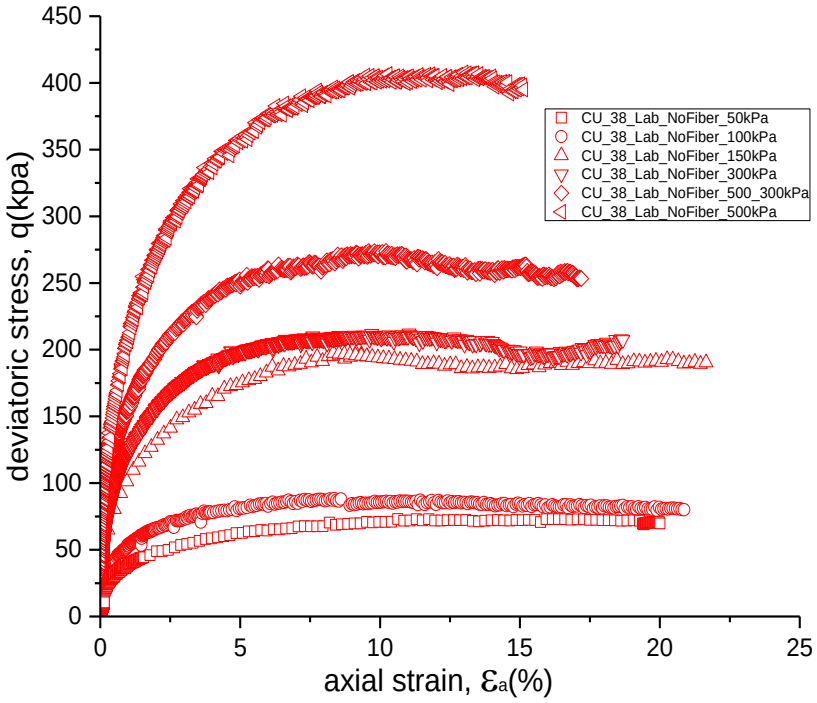

Figure 10-7. Stress-strain relationship of undrained unreinforced samples

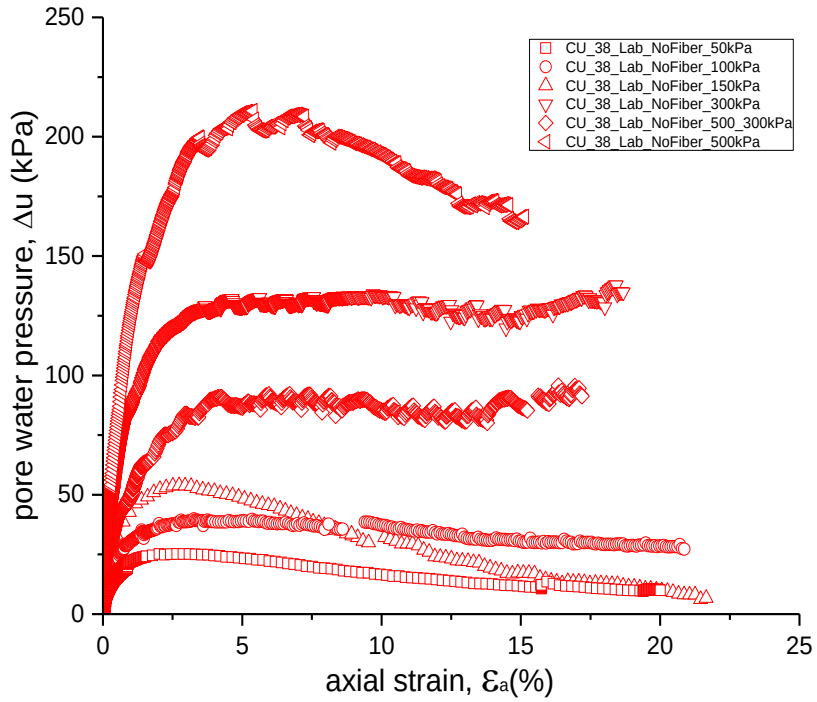

Figure 10-8. Pore pressure change in undrained unreinforced samples

As can be seen in Figure 10-9, all samples other than UNF50, were reached to critical state line. Where sample UNF50 show tendency to reach the chosen critical state line.

Therefore, it can be confirmed that the critical state stress ratio parameter (M) of the unreinforced specimens, the slope of the CSL, was found to be 0.89.

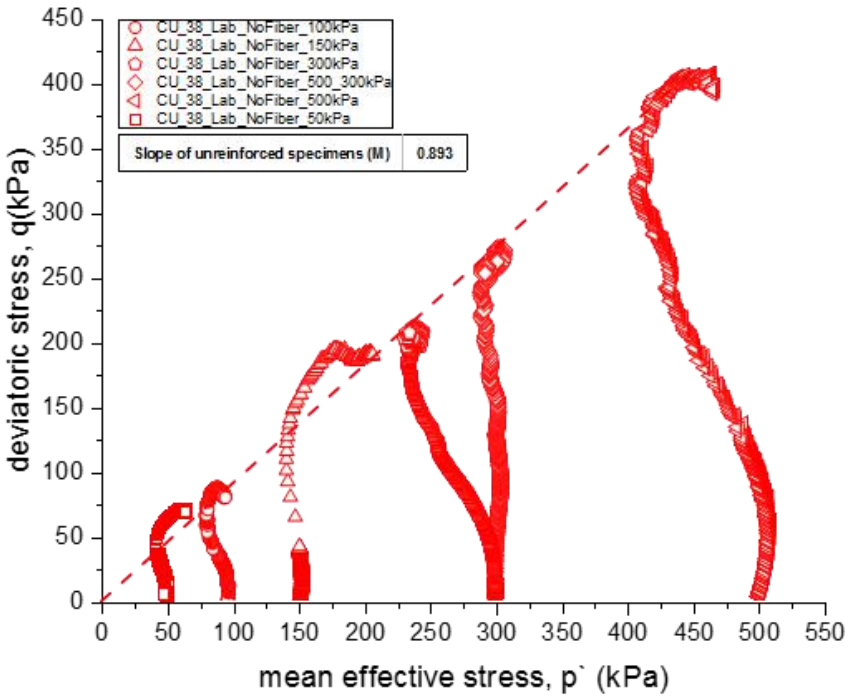

Figure 10-9. Stress paths for the undrained unreinforced samples

The stress ratio curves for the unreinforced samples are shown in Figure 10-10. The samples have the tendency to converge towards a distinct critical state stress ratio, M value, which is approximately 0.89. Looking at Figure 10-10 one can observe that the specimen UNF50 needs further strain increment in order to be able to reach to a critical stress ratio other specimens are experiencing. Nevertheless, due to the triaxial equipment limitations, it might not be possible to reach such high strains. It is believed that the cause of the such behaviour is the distance between the initial state and the critical state, particularly since the compaction effort locks stresses in the sample, similar to overconsolidation.

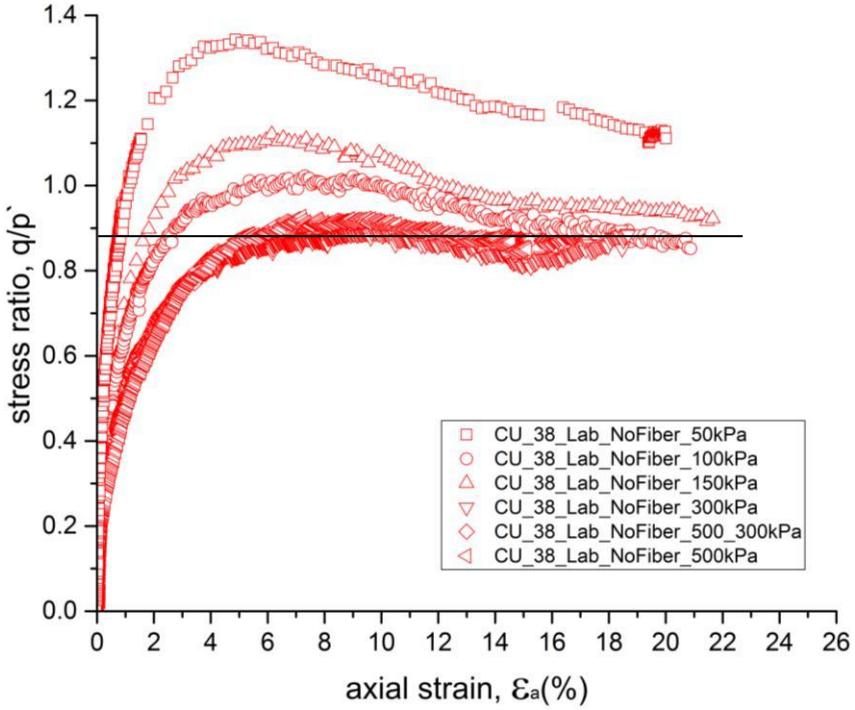

Figure 10-10. Stress ratios for undrained unreinforced samples

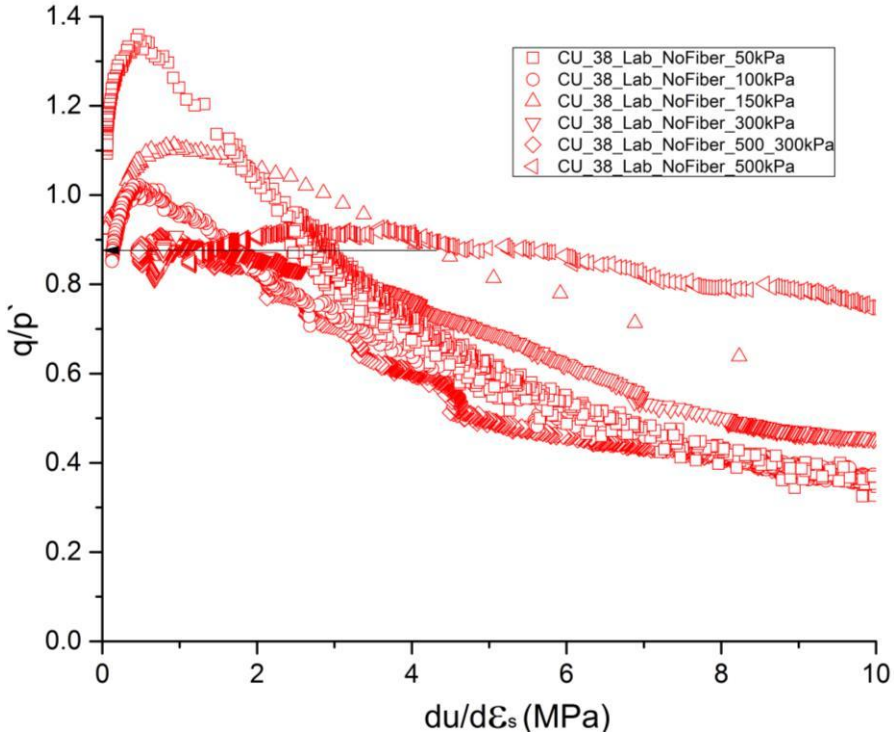

Figure 10-11. Pore pressure increments for undrained unreinforced samples

Figure 10-11 revealed a picture similar to what was observed on the stress ratio plot. The data for all samples, with the exception of samples UNF50 and UNF150, seems to converge to a value of stress ratio at critical state estimated to be around 0.89, similar to

the value determined via stress path and stress ratio plots on same specimens. Samples UNF50 and UNF150 are, in the pore pressure increment versus strain rate space, approaching to the critical state stress ratio determined by the data from the other samples.

In addition to the undrained tests, 3 unreinforced samples were tested in drained conditions, following a constant p' stress path. The results are shown in Figure 10-12 to Figure 10-15. Once again, the sample preparation method used is described in section 5.4 of this report.

Figure 10-12 shows the stress-strain relationship of the samples. All three conducted test failed by strain localization, together with barrelling, therefore the data obtained was corrected according to Section 6.2.4.4. Once again, Samples DNF50 and DNF100 show strain hardening behaviour at medium to high strain levels, followed by a stabilisation of the deviatoric stress, whereas sample DNF300 shows strain softening behaviour with a gentle peak stress.

Figure 10-13 displays the volumetric strain variation of the drained unreinforced specimens. Samples DNF100 and DNF300 show the highest contraction amount of the 3 samples tested, spreading through a large axial strain. Additionally, sample DNF50 shows the highest dilation rate, spanning over a much smaller strain. For this sample, this is manifested by a greater change in volumetric strain which spans over a shorter strain range. For the samples DNF100 and DNF300, the net volumetric strain is negative, similar in magnitude and reaching a steady state condition at the end of the tests. Sample DNF50, however, has a negative net volumetric strain, showing a continued dilative trend until the end of the test, indicating that steady state conditions have not been reached.

It is worth mentioning that during the test of sample DNF300, the compressor providing pressure for the triaxial cell failed two times during the test, and the pressure loss effects of such failure can be seen on the volumetric strains axial strains of 5% and 11% strain.

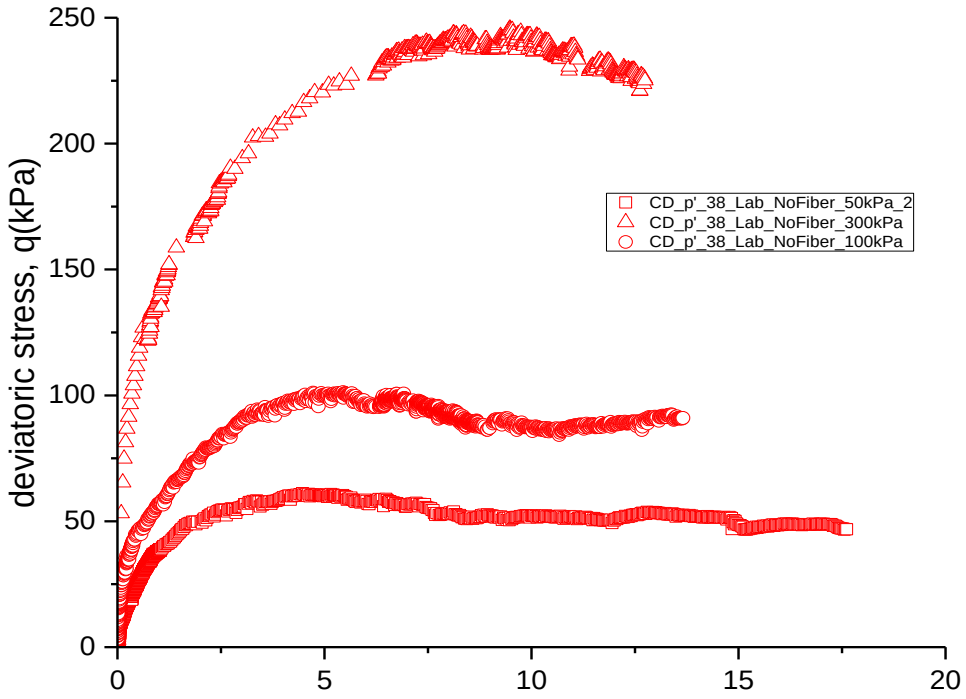

Figure 10-12. Stress-strain relationship of drained (constant p`) unreinforced samples

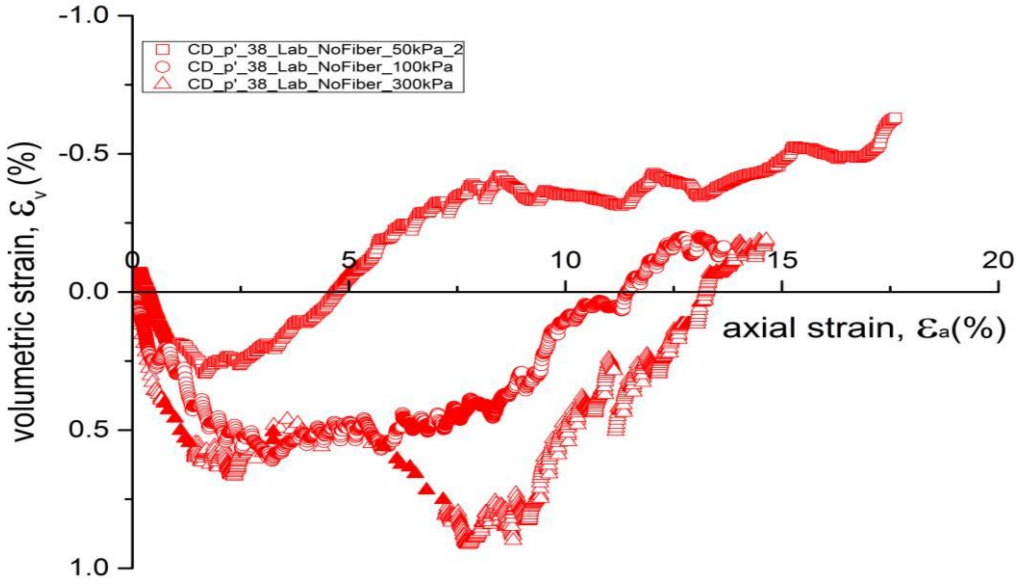

Figure 10-13. Change in volumetric strain of drained (constant p`) unreinforced samples

Figure 10-14 enabled the assessment of drained and undrained unreinforced samples in the stress space q:p'. As can be seen all samples, other than the UNF50, reached to critical state and tests discontinued closer points to the chosen critical state line. The slope of the drained unreinforced specimens critical state line was found to be 0.89 (M) which is confirming the evaluation done on undrained specimens.

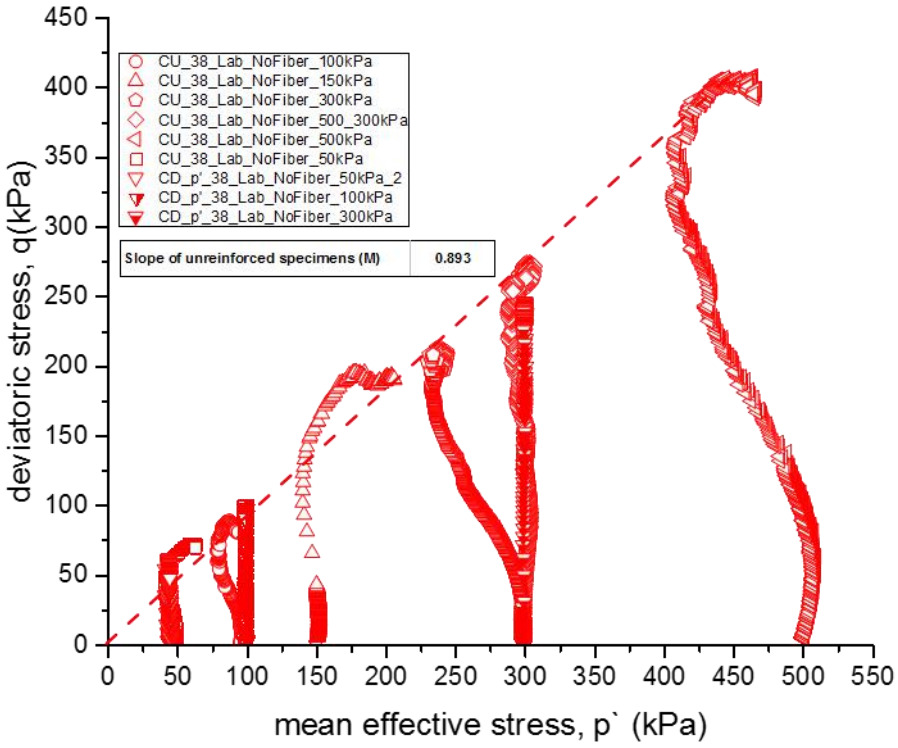

Figure 10-14. Stress paths for the drained and undrained unreinforced samples

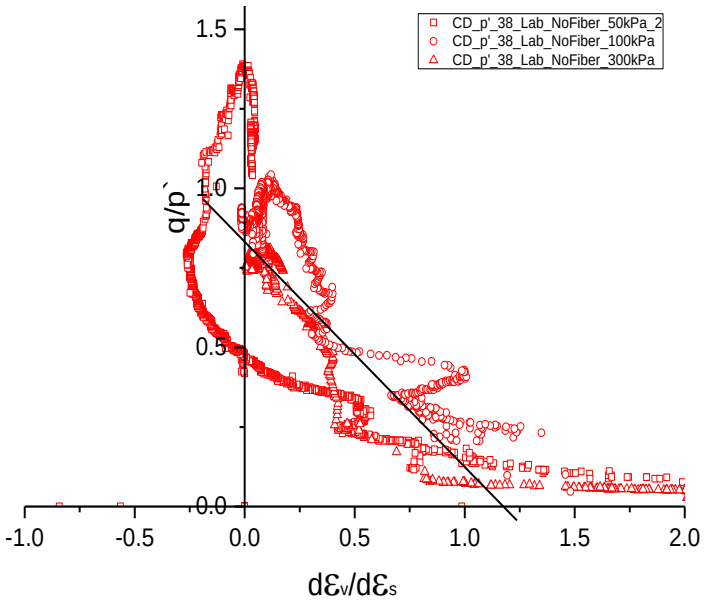

Figure 10-15. Stress: dilatancy relationship for drained (constant p`) unreinforced samples

The confining pressure seems to influence the dilatancy behaviour (Figure 10-15): at lower confining stress levels (DNF50), the compression does not stop at reaching a rate of volumetric change $d\varepsilon_v/d\varepsilon_s = 0$, but is followed by a dilative behaviour where steady state is not reached. Adversely samples DNF100 and DNF300 compress to the critical

state, with a rate of compression that reduces with the increase in stress ratio. Both samples mentioned reach critical state at a stress ration of 0.89. Similar to the value obtained from the undrained test on similar specimens.

10.4 Reinforced Clay Behaviour

The stress-strain curve, pore water pressure change, effective stress path, stress ratio and pore pressure increments with strains of the reinforced clay tested in undrained condition are presented on Figure 10-16 to Figure 10-20. The sample preparation method followed is presented in section 5.9.2.2. Visual observations of the shearing stage revealed that all the samples bulged (barrelling) during shearing and this was taking into account when performing the area correction, described in Section 6.2.4.

At low strains, small shear planes become visible through the membrane, at the centre of the reinforced specimens. As the shear progresses, the shear planes spread along the sample with sample barrelling taking place. Even at 20% strain, there is no obvious single shear plane visible.

As can be seen on Figure 10-16, all samples show a strain hardening behaviour between medium to high strain level where UF100, UF300 and UF500 reach a constant stress level while sample UF150 continued to follow an extended strain hardening path where mentioned sample reached to constant stress level at much higher strain levels comparing to other specimens.

Figure 10-17 shows the pore water pressure build up in the fibre reinforced samples. It can be seen that samples UF500 and UF300 are experiencing fast pore pressure development up to 5% strains, followed by a constant pore pressure up to a high strain level. Samples UF100 and UF150 reached their maximum excess pore pressures faster than the previous two samples, after which they experienced a continuous reduction of pore water pressure even at high strains.

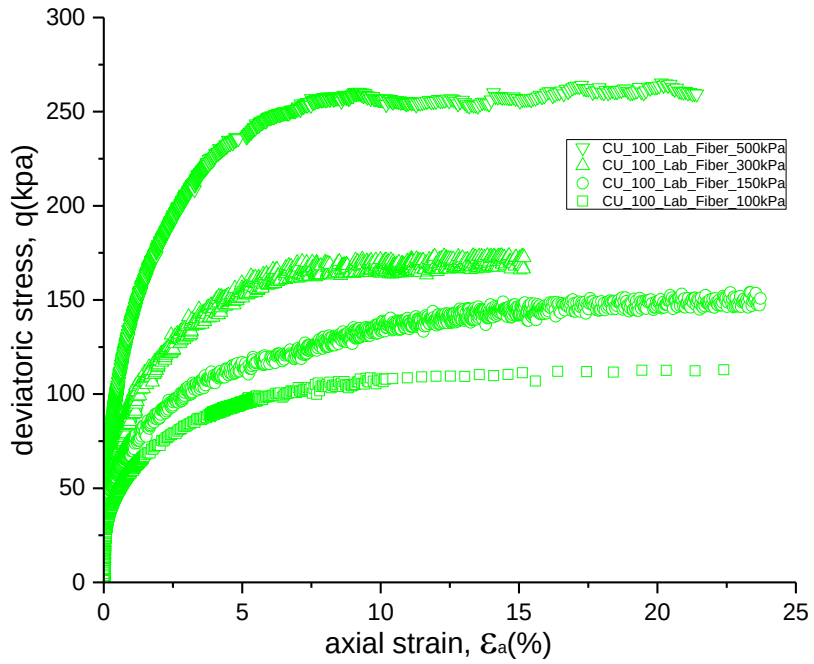

Figure 10-16. Stress-strain relationship of undrained reinforced samples

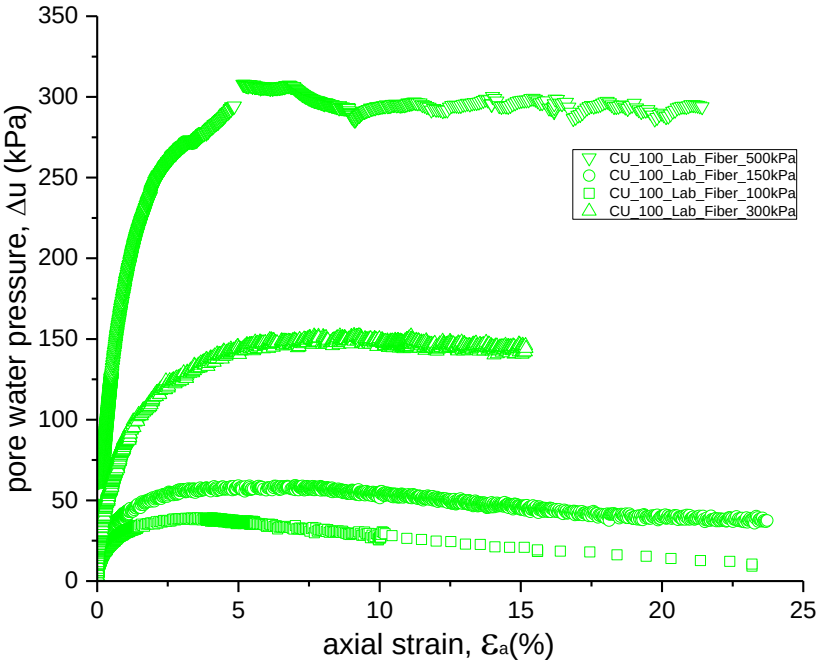

Figure 10-17. Pore pressure change in undrained reinforced samples

As can be seen in Figure 10-18, in agreement with the previous evaluation, samples UF300 and UF500 were reached to critical state line. Where sample UNF100 and UNF150 show tendency to reach the chosen critical state line. Therefore, it can be confirmed that the slope of the CSL was found to be 0.87.

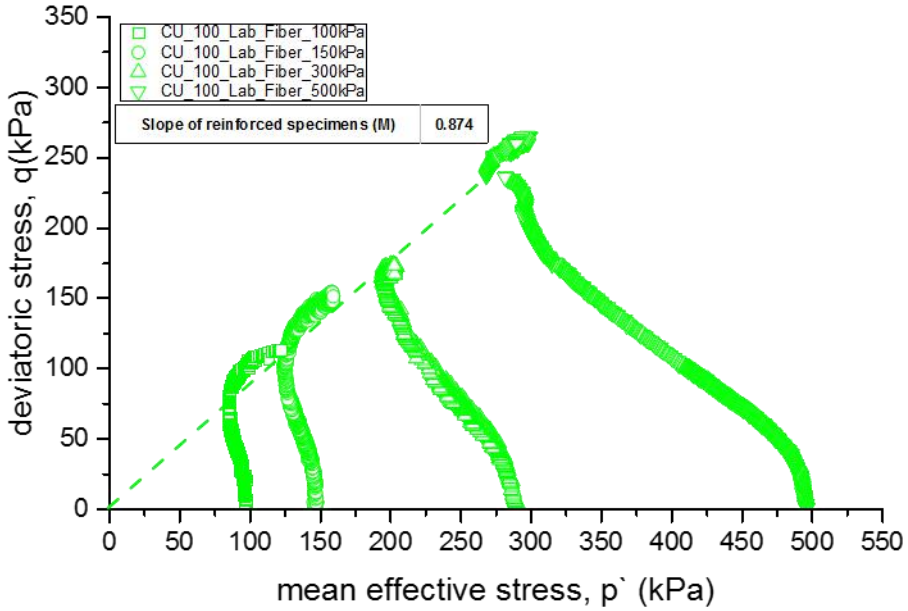

Figure 10-18. Stress paths for the undrained reinforced samples

The stress ratio for the undrained reinforced samples is plotted in Figure 10-19. As can be seen samples UF500 and UF300 seem to converge, at large strains, towards a unique stress ratio, which, can be estimated about 0.87. Unlikely, as mentioned in the stress-strain and pore water pressure discussions, samples UF100 and UF150 are not reaching critical state due to a continued reduction in pore water pressure and stresses, even at high strain levels, this is also reflected in the stress ratio graph. Nevertheless, samples UF100 and UF150 show a trend that, with further strain increase, seem to reach the same stress ratio determined for samples UF500 and UF300.

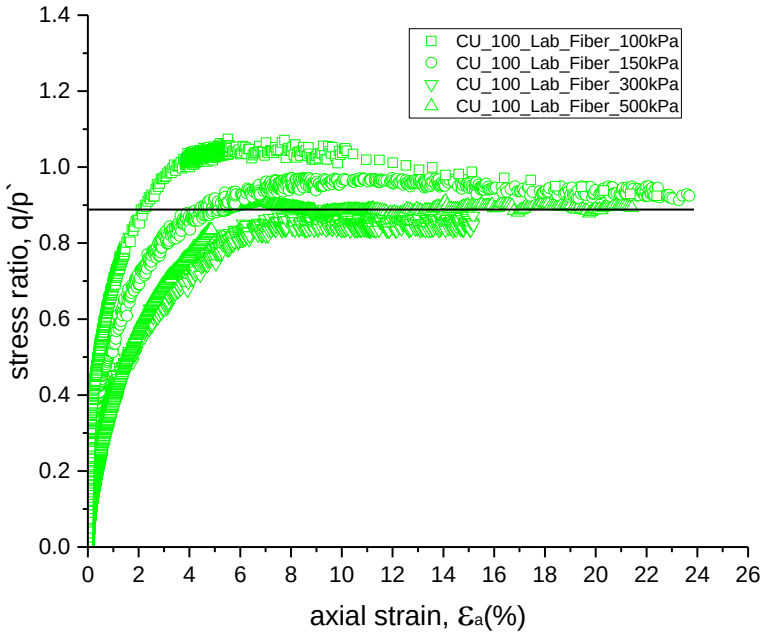

Figure 10-19. Stress ratios for undrained reinforced samples

The stress ratio versus change in pore pressure with the strain increment for the reinforced samples is shown on Figure 10-20. Samples UF300 and UF500 converge to a constant stress ratio which is approximately 0.87. In a fashion similar to the stress ratio graph on Figure 10-19, samples UF100 and UF150 seem to be developing further reduction in stress ratio towards a critical state ratio.

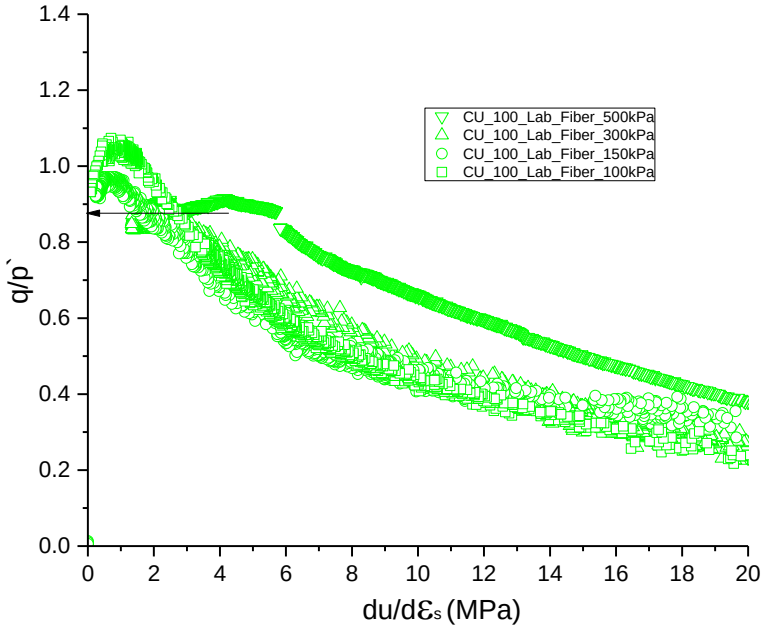

Figure 10-20. Pore pressure increments for undrained reinforced samples

In addition to the undrained tests, 3 drained tests have been conducted, following a constant p' stress path. Figure 10-21 to Figure 10-24 evaluates the stress-strain, volumetric strain, effective stress path and the dilatancy behaviour of the samples tested. It is worth mentioning that there were experimental problems with the tests on samples DF50 and DF300. At 5% strain, approximately, the load cell used in the test of sample DF300 failed, therefore an extraordinary set of readings were logged. Additionally, during the testing of sample DF50, the cell pressure line was closed between the pressure transducer and the cell, therefore there was no control on the cell pressure to maintain a constant p' stress path until 1% strain, where the error was noticed. Therefore, once the problem was noticed, the sample was allowed to equilibrate and the test progressed. This procedural error has affected the initial behaviour of the sample DF50 as it is not possible to know the confining stress applied in the sample during the initial part of the test.

The Stress-strain relationship graphs in Figure 10-21 show that all three samples follow a strain hardening path between medium to high strains, where afterwards a constant stress is seen. Visual observations of samples during and after the testing revealed that the samples failed with a barrelling shape. Closer examination of samples show that shear planes are occurring around the sample on a mini scale (20-30 mm), starting once a maximum stress level is reached.

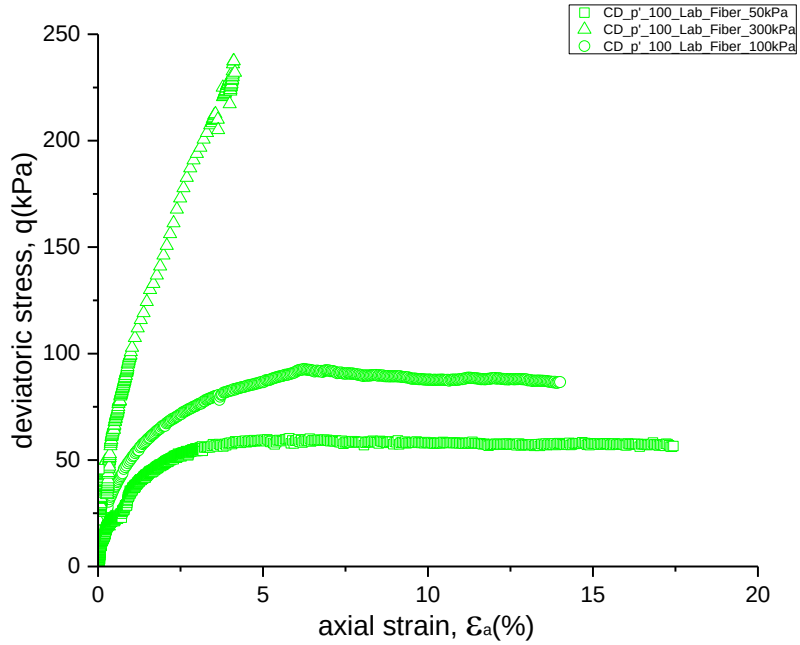

Figure 10-21. Stress-strain relationship of drained (constant p`) reinforced samples

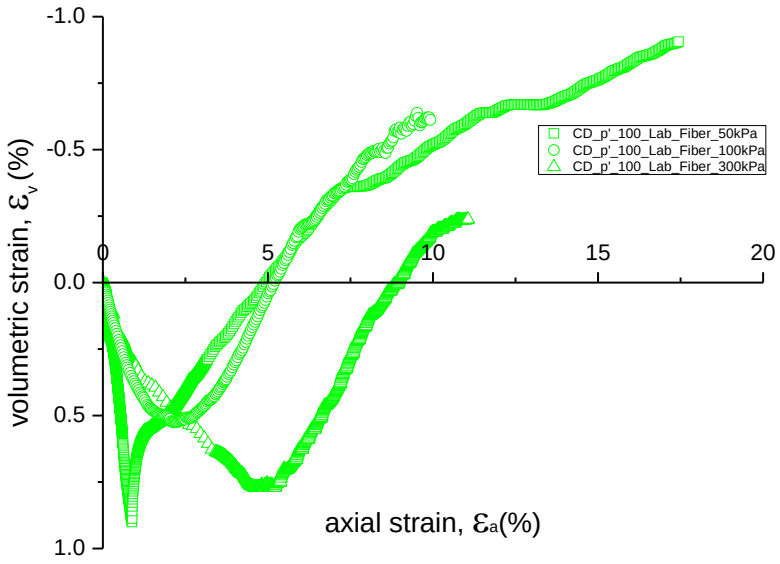

Figure 10-22. Change in volumetric strain of drained (constant p`) reinforced samples

Due to the experimental problems encountered, an evaluation of the volumetric response and stress: dilatancy relationship of the reinforced drain samples should be treated with caution. All three samples show a similar initial contraction, which is spread over a great range of strain. Due to the nature of the triaxial equipment used, it is possible to see the initial contractive behaviour of sample DF50; with the confining pressure control valve closed, the confining pressure increased and the sample was subjected to an increment of confining stress not measured, showed by the large initial contraction when compared to the other samples. Additionally, samples DF100 and DF50 show a faster dilation rate then the DF300 sample. This is established by a greater change in volumetric strain which spans over a shorter range of strains. For all samples, the net volumetric strain is negative and has different magnitudes Such difference might be due to effective confining stress of the samples. Samples DF100 and DF300 reached a steady state condition at the end of the tests. Correspondingly sample DF50 net volumetric strain is negative, however show continuing dilative trends at the end of the test, indicating that steady state conditions have not yet been reached.

Figure 10-23 present the results of drained and undrained reinforced samples in the stress space q:p'. As can be seen all samples, other than the DF50, UNF100 and UNF150, reached to critical state line, and mentioned tests discontinued closer points to the chosen critical state line. The critical state line of the drained reinforced specimens can be drown together with undrained specimens. That leads to a same critical state stress ratio of 0.87 (M)

The experimental problems encountered seem to influence the dilatency behaviour (Figure 10-24), despite of expectations from volumetric behaviour of samples, all three samples compressed and reached a rate of volumetric change $d\varepsilon_v/d\varepsilon_s = 0$, and followed by a dilative behaviour where steady state is reached in order to achieve critical state. Sample DF100 compresses to the critical state, with a rate of compression that decreases with the increasing in stress ratio, reaching a critical state ratio of approximately 0.87 (M). This is a value similar to the value obtained from the undrained tests on reinforced specimens. However, due to the experimental problem with sample DF300, specimen has followed the same path as DF100 up to a point where load cell failed and continue to shear to higher stress ratio. Nevertheless, the trend

followed by the DF300 is promising to approximate that both samples DF100 and DF300 were reaching to same critical state ratio(M=0.87).

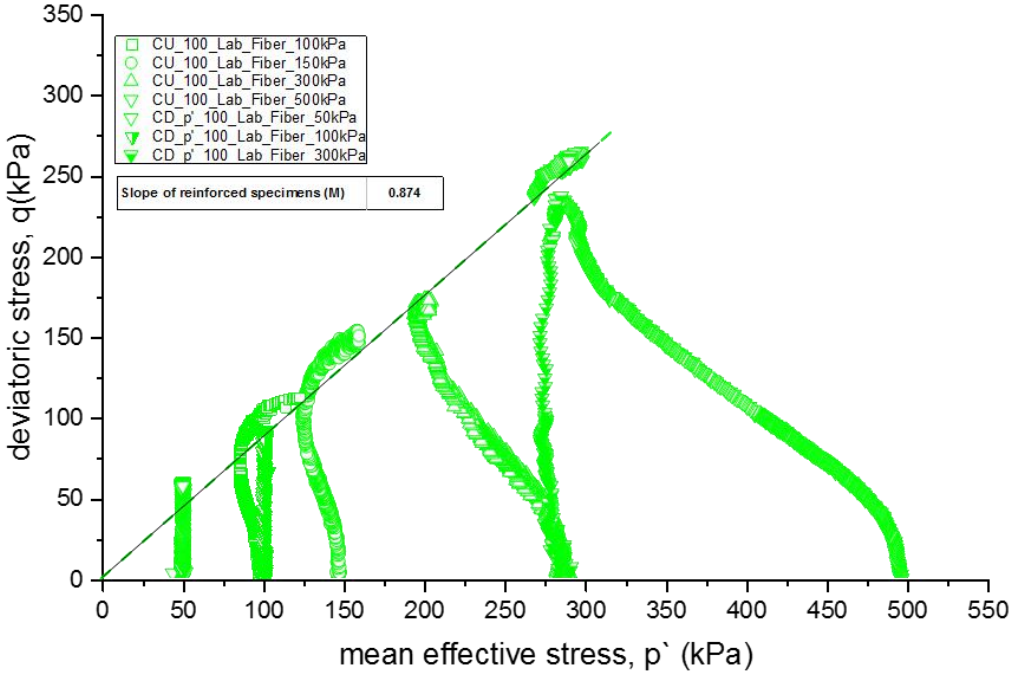

Figure 10-23. Stress paths for the draind and undrained reinforced samples

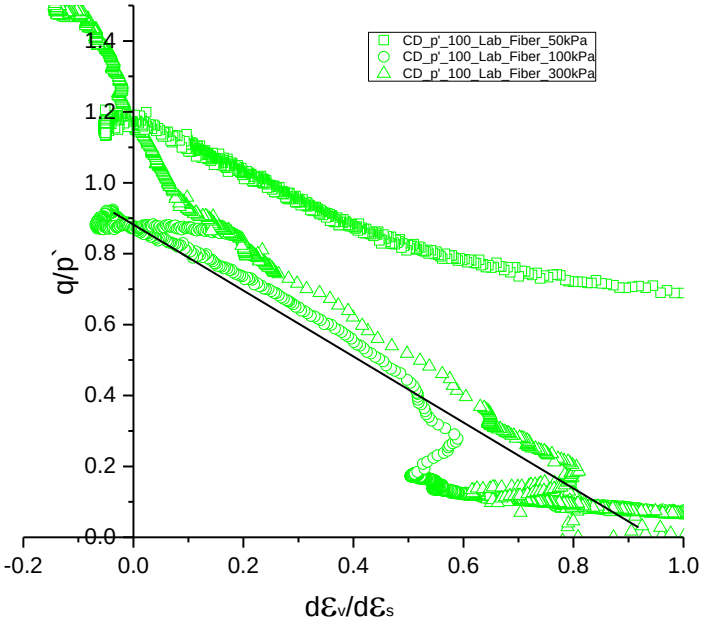

Figure 10-24. Stress: dilatancy relationship for drained (constant p`) reinforced samples

10.5 Insitu Clay Behaviour

Figure 10-26 to Figure 10-30 present the stress-strain, pore water pressure development, effective stress path, pore water pressure increment against the strain increment and the stress ratio curves obtained from the triaxial test results.

A visual observation of the samples (Figure 10-1) revealed that samples INS50 and INS100 failed with barrelling and a slight occurrence of a shear plane. In this section the behaviour of the in-situ compacted samples is discussed. The triaxial samples were prepared using the sample preparation procedure described in Section 5.2 and 5.9.2.4. Samples INS150 and INS500 failed with barrelling and a distinct shear plane. According to the observations, the appropriate corrections to the data obtained was performed according to Section 6.2.4.

Looking at Figure 10-26 one can see that, depending on the stress strain behaviour obtained from reinforced and unreinforced specimens sheared at 500 kPa confinement the stress strain behaviour of sample INS500 is lower than expected. The cause for such behaviour seems to be revealed once the sample was removed from the cell and further visual analyses of the shear plane was done. As can be seen on Figure 10-25, there were two large stones, passing through the shear zone of the sample. One of them is crossing the shear plane whilst the other is immediately above it. Another important feature to note are the shine areas seen at the top and middle of the sample, indicating that the particles are aligned along the shear direction in these areas. It is also easy to note that presence of stones contributes in occurrence of the shear plane through those point of weaknesses in soil strata. Furthermore, no presence of fibres was observed through the shearing zone, indicating that the site fibre mixing system is not as generating mixtures that could be characterised as homogeneous; these are discussed in section 5.4 of this report.

Figure 10-25. Picture of INS 500 sample at the end of testing

Inspection of Figure 10-26 show that all of the in-situ samples show a steep strain hardening behaviour, from small to medium strains, followed by a constant stress up to high strains.

According to the pore pressure development curves, displayed in Figure 10-27, samples INS500 and INS100 reached a maximum value of change in pore-pressure and maintained this value constant until the end of the test. Samples INS50 and INS150 experienced a negligible amount of reduction, after reaching a maximum pore water pressure value, where it could be considered as constant.

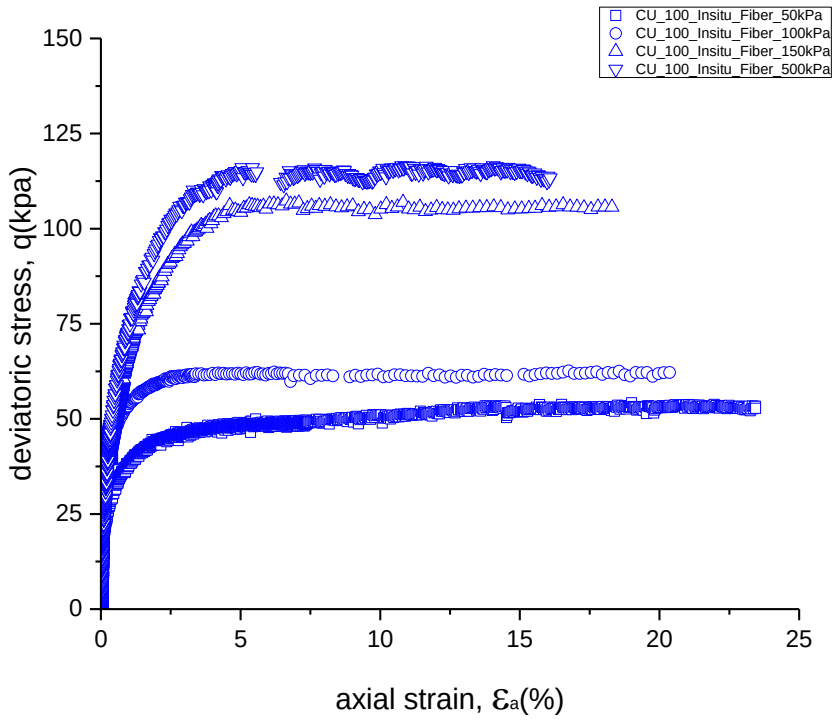

Figure 10-26. Stress-strain relationship of undrained In-Situ samples

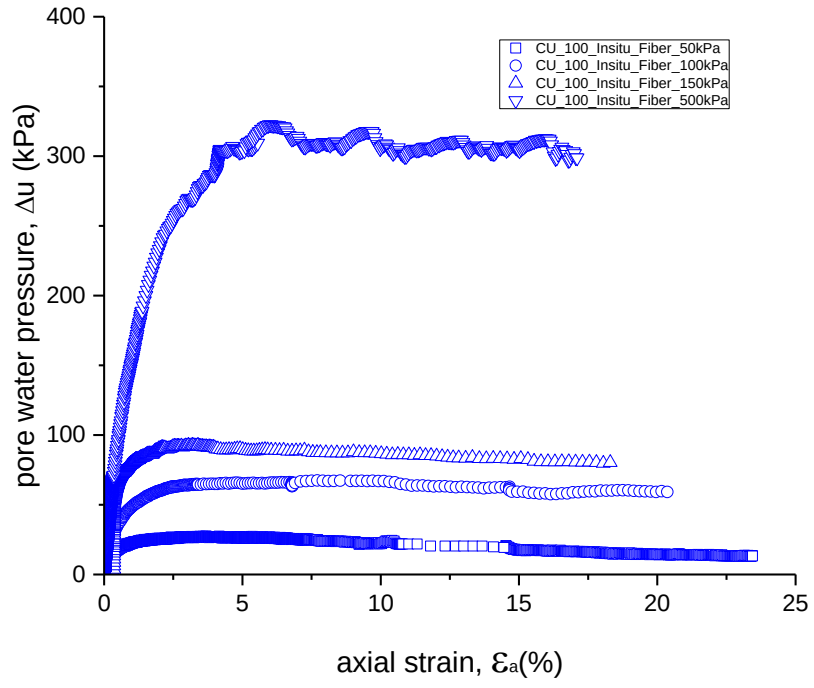

Figure 10-27. Pore pressure change in undrained In-Situ samples

Evaluation of the in-situ samples can be made from stress path space of specimens in Figure 10-28. As mentioned before, due to strain localisation of INS500 sample, pore water pressures concentrated in the shearing zone. Therefore, it can be seen that there is a reduction in the effective stress of the INS500 sample.

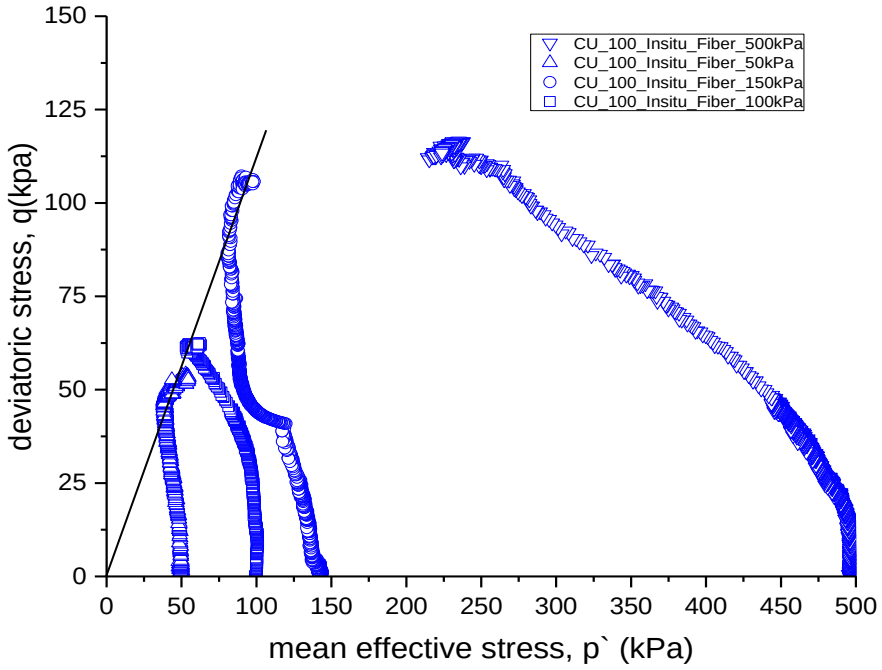

Figure 10-28. Stress paths for the undrained In-Situ samples

Considering the stress ratio and the change in pore water pressure with the strain increments of the in-situ samples on Figure 10-29 and Figure 10-30; all samples other than INS500 converged to a constant stress ratio which is approximately 0.98. Further analysis of the same samples, done through the evaluation of the stress ratio relationship, as seen in Figure 10-30, show that all samples, other than sample INS500, converge to a critical stress value of 0.98, (M).

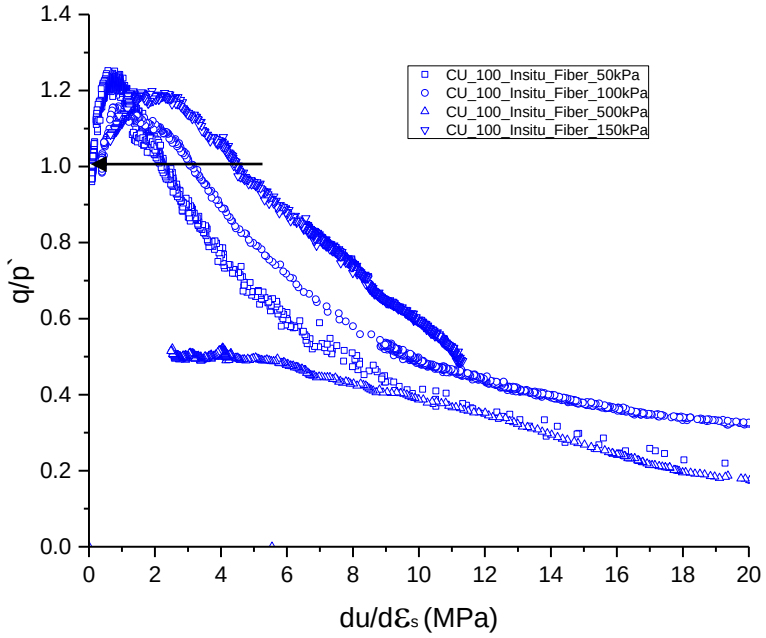

Figure 10-29. Pore pressure increments for undrained In-Situ samples

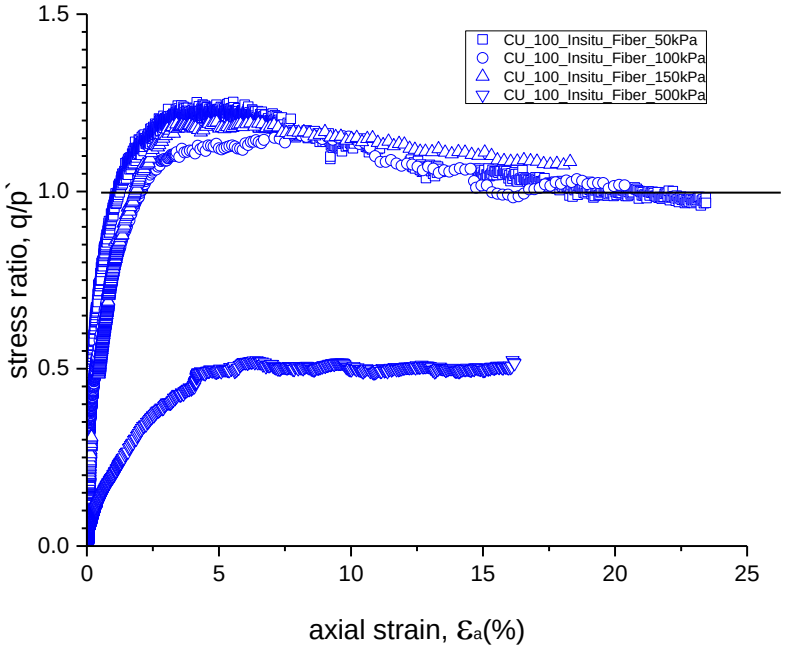

Figure 10-30. Stress ratios for undrained In-Situ samples

10.6 Discussion and Comparison

In this chapter a comparison between the results shown on the previous part will be performed in order to highlight differences and similarities between the different types of samples.

10.6.1 Reinforced vs Unreinforced

10.6.1.1 Stress-Strain Behaviour with PWP and failure plane

Figure 10-31 shows the stress-strain curves of the reinforced and unreinforced specimens sheared under undrained conditions.

The analysis of the triaxial testing results has provided an insight into how the inclusion of fibres change the failure mechanism of the samples. As discussed in Section 10.4 and 10.5, all reinforced samples showed a strain-hardening behaviour throughout the medium to high strain levels, while the unreinforced samples, tested at confining stresses of 150 kPa, present a moderate reduction in deviatoric stress at strains higher than 14%.

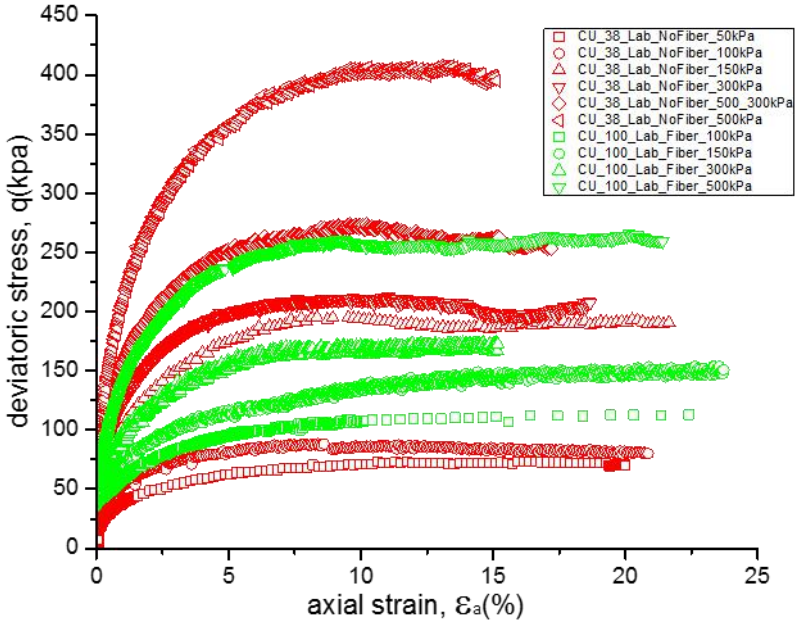

Figure 10-31. Stress-strain response of Lambeth Group clay and fibre-reinforced clay samples.

The similar behaviour was observed by Özkul & Baykal (2007) and the difference in behaviour was attributed to the effect of fibres in the potential shearing zone; these stretch across the shearing area and restrict the development of a slip plane by transferring some of the shear stress and strains to zones further away. A limitation to the contribution of the fibres in the deviatoric stress has also been seen in Figure 10-31. This behaviour is similar to what was observed by Maher and Gray (1990) and Li and Zornberg (2005); for lower confining stress (100kPa in this series of tests), the reinforced sample reached a higher deviatoric stress then the unreinforced sample tested at the same confining stresses. In contrast, above this value of confining stress (150, 300 and 500kPa), the unreinforced samples reached a higher deviatoric stress than the maximum stress achieved by the reinforced samples.

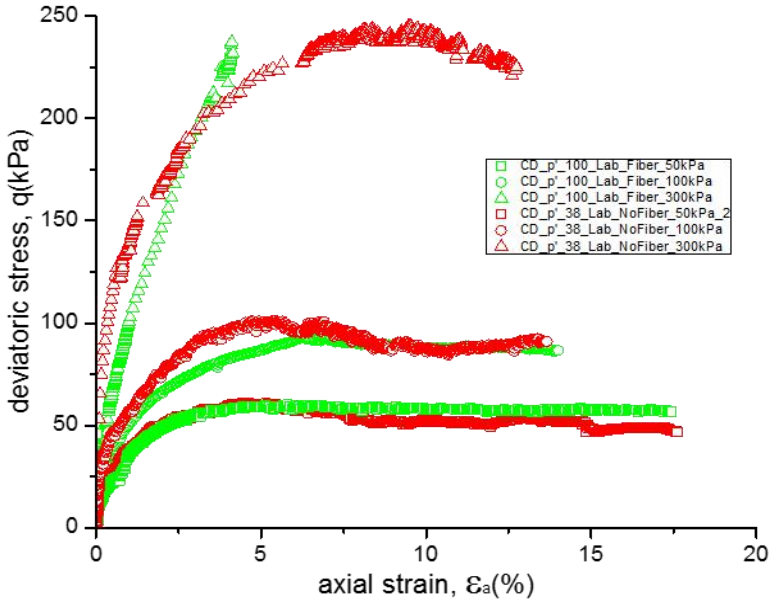

Figure 10-32. Stress-strain response of Lambeth Group clay and fibre-reinforced clay samples in drained condition

The evaluation of the stress-strain response of reinforced and unreinforced specimens, under drained conditions, can be seen at Figure 10-32. The results indicate that the strength mobilisation of the reinforced specimens is lower than the unreinforced specimens. The unreinforced specimens reach a slight peak and experience noticeable reduction. Where reinforced specimens are showing strain hardening, followed by a constant stress at high strain levels. The effect of confinement, on the contribution of the fibres in deviatoric stress have been monitored similarly to the undrained conditions. It seems that up to 100kPa confinement reinforced specimens are mobilising and contributing the deviatoric stress.

The author believes that the reason for observing a critical confining pressure may be related to the volumetric behaviour of the samples; at lower stresses the samples tend to have a high dilative behaviour that would allow the mobilisation of tensile stresses on a larger number of fibres. With the increase in confining stress this tendency is reduced. Furthermore, at low confinement, the reinforced and unreinforced specimens have not shown a tendency to have a localised shear failure, therefore, stretched or broken fibres or even a fibre sliding mechanism were not observed, when the samples were examined at the end of the test. In high confinement tests, the specimens formed shear bands where the fibres started to slide on the large surface of the shear band. This is believed to be due to slickensided surfaces introduced by the fibres, reducing the observed strength of the reinforced samples, when compared to the unreinforced ones.

10.6.1.2 Failure Mode

The analysis of the test specimens at the end of the shearing stage enabled the visualisation of the failure modes taking place during shearing. A sketch of the sheared specimen was done at the end of every test, in order to represent, as best as possible, the failure mode of each sample (Figure 10-1). The results obtained via such visual observation in this study, are similar to the results obtained by Freilich et al. (2010), Li et al. (2008) and Özkul & Baykal (2007). At low strains, small shear planes or cracks become visible through the membrane, at the centre of the reinforced specimens. As the shear progresses, the shear planes spread along the sample and sample barrelling takes place. Even at 20% strain, there is no obvious single shear plane visible. The unreinforced samples, however, show the formation of a distinct shear plane from around 5% strain onwards. Fibre reinforcement on soils causes stresses on the soil mass to be redistributed, transferring stresses along a much wider area, restricting the development of a shear zone and changing the failure mode of the samples.

The failure mode observations in this study are comparable to the study of Freilich et al. (2010) on fibre reinforced clay. The authors reported that the axial deformation of the unreinforced specimens resulted in the development of a shear zone, while the reinforced specimens were observed to barrel. Furthermore, authors stated that such behaviour indicates an increase in the ductility (the deformation required to reach failure) of the fibre reinforced soil. Özkul & Baykal (2007) correlated the failure mode of the specimens to the initial moisture content, the plastic limit and the loading

condition during testing. However, Özkul & Baykal (2007) failure mode proposition, regarding the different failure modes on the wet or on the dry side of the Plastic limit, does not agree with the results in this study. These authors proposed that the specimens prepared on the dry side of the plastic limit are expected to respond with strain localisation. Where a network of microcracks and a wider shear zone was observed. Even though, in this study, all specimens were prepared on the dry side of the plastic limit, it was observed that the specimens were not bound to the plastic limit and failed in barrelling, disagreeing with Özkul & Baykal's (2007) study on clay reinforced with rubber fibres.

10.6.1.3 Pore pressure and Volumetric strain response

The pore water pressure generated within the reinforced soil samples, during shearing, were consistently higher than the unreinforced samples (Figure 10-33). The higher pore water pressures generated are related to the effect of fibres on the sample deformation. Li (2005) attributed this increase in pore pressures on the fibres distributing stresses within the soil mass and therefore increasing the contractive deformations within the fibre-soil matrix. This also provides evidence that the deformation characteristics of a soil might influence how well fibres affect the composite behaviour.

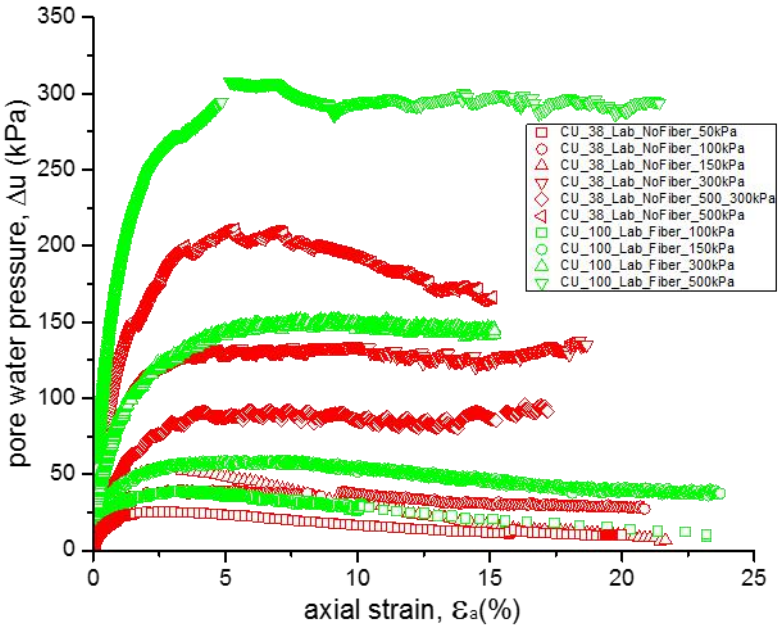

Figure 10-33. Pore-pressure response of Lambeth Group clay and fibre-reinforced clay samples in undrained condition.

Additionally, the failure mechanisms are in agreement with pore water pressure distribution on each sample. In unreinforced samples, at strains around which the shear plane is formed, the pore water pressures start to drop slightly as the water drains towards the shear zone (Figure 10-34a) and this excess water causes a reduction in shear stress (Sandroni, 1977). For the fibre-reinforced samples, a shear plane is not formed due to the tensile strength provided by the fibres (Figure 10-34b). Such observation is in agreement with the moisture content measurements taken from five different height locations within the specimens, at the end of the shearing stage (Figure 10-1).

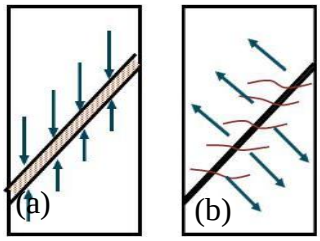

Figure 10-34. Pore pressure distribution illustration: (a) unreinforced specimen; (b) reinforced specimen.

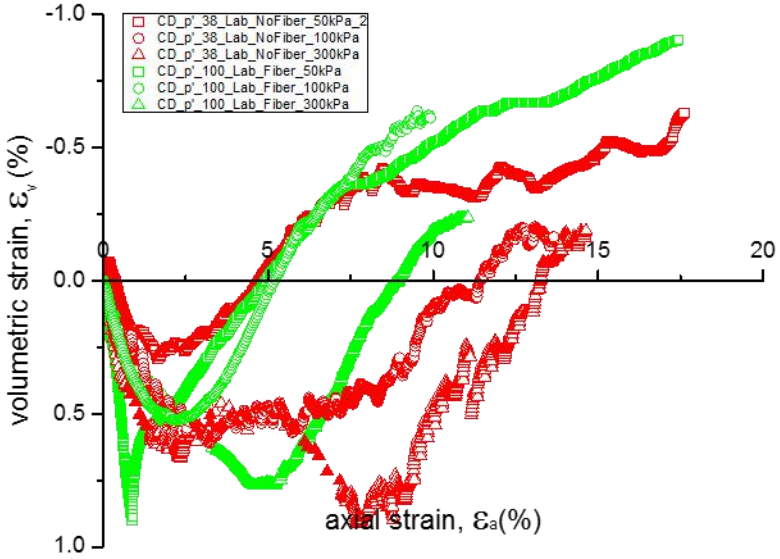

Figure 10-35. Change in volumetric strain of drained (constant p`) reinforced samples

As can be seen in Figure 10-35 the volumetric changes experienced due to the shearing process differs slightly for the reinforced and unreinforced samples. Nevertheless, the final volumetric strains are similar. Unreinforced specimens show that the maximum rate of dilation is achieved at larger strains than the reinforced ones with the exception of DF50. Additionally, the rate of dilation of reinforced samples seems to be faster than unreinforced samples. The net volumetric strain is negative at the end of the test for all samples. Additionally, at the end of the tests, the reinforced samples are showing greater dilation for similar effective stresses, however, this could change when samples reached a steady state condition.

10.6.1.4 Stress Path

The increase in the pore pressure of reinforced specimens are more pronounced in specimens tested at high confinements. This behaviour of reinforced specimens decreases the effective stress within the soil mass, yet results in a lower shearing strength such behaviour is more pronounce with increase of confining pressure. This phenomenon can be seen on stress path plots of reinforced and unreinforced specimens on Figure 10-36. for verity of confinements.

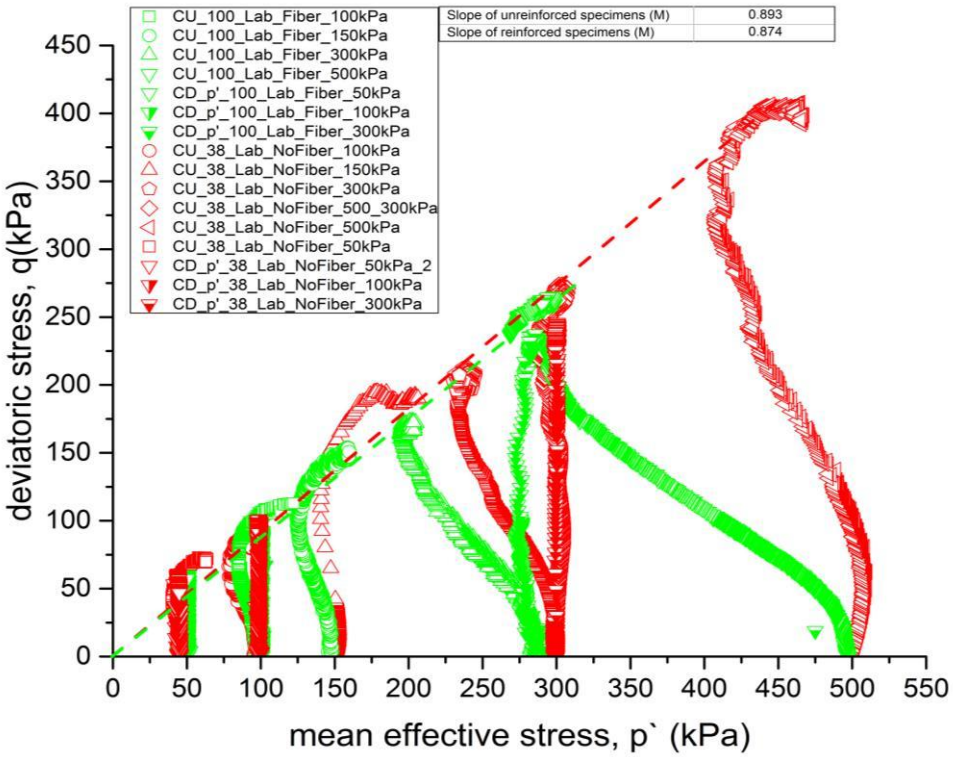

Figure 10-36. Stress paths for fibre-reinforced and un-reinforced Lambeth group clay samples from drained and undrained triaxial testing

Additionally, as presented in Section 10.4 and 10.5 the stress ratio (M) for reinforced sample (0.87) found to be slightly lower then unreinforced samples (0.89). Such observation is also confirmed in the gradients of the critical state line reached by reinforced and unreinforced specimens in Figure 10-36, due to the reduction of pore water pressure in reinforced samples.

10.6.2 Reconstituted vs Unreinforced

The stress-strain relationship of the unreinforced specimens have been compared to reconstituted soil in Figure 10-37. Although the reconstituted samples were overconsolidated and tested at different confining stresses, there is a good agreement the effect of confinement and strength. i.e., higher confining stress equals to higher shear strength.

It can be seen clearly that the unreinforced samples have sustained higher deviatory stresses in all confining pressures. Although some of the reconstituted samples where overconsolidated to a ratio of 4, this difference in strength was expected, since the unreinforced samples are composed of compacted peds. These are likely to have retained the structure of the original soil (heavily overconsolidated), therefore capable to reach higher shear strengths.

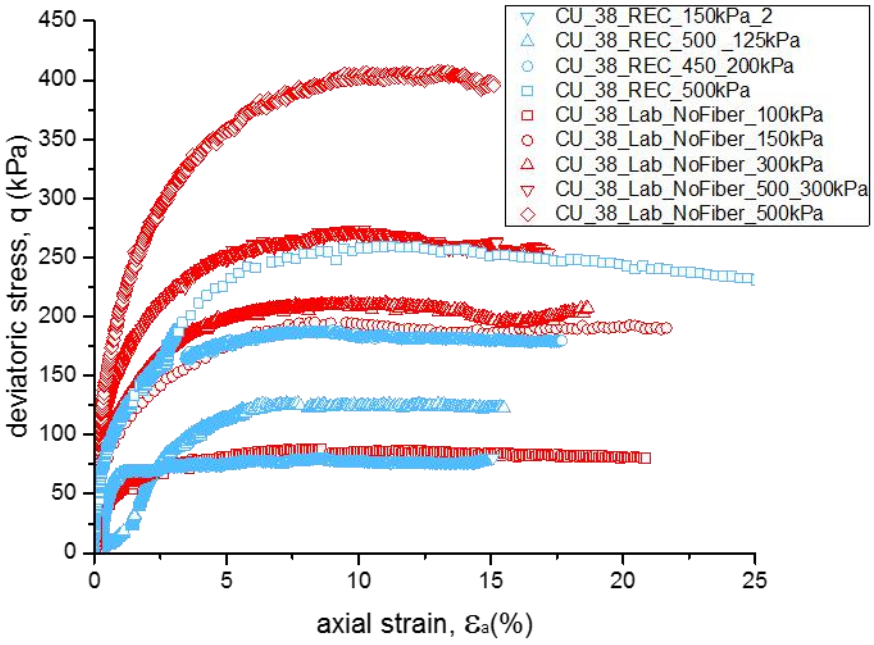

Figure 10-37. Stress-strain response of unreinforced and reconstituted clay samples

In the case of excess pore water pressure development, as can be seen in Figure 10-38, samples at the same confining pressure, such as samples tested at 150 and 500 kPa, on both reconstituted and unreinforced soils, are experiencing identical increases of excess pore pressure up to 2% strain and then evidential difference. From 2% strain onwards, the reconstituted samples are showing moderate to constant increase in pore pressure while unreinforced samples are experiencing reduction in pore water pressure.

In order to explain the pore pressure response of the specimens, the failure mechanism of the samples, after shearing stage are analysed in detail. The barrelling failure mode of the reconstituted specimens leaded to a constant pore water pressure distribution throughout the sample and this response has been reflected in the graphs with a constant change in pore pressure from medium to high strain levels. In the unreinforced specimens, especially for confinements higher than 100kpa, it leads to a shear plane formation which, as mentioned in Section 10.6.1.2, cause the excess water to drain towards the shear plane, causing a reduction in the global pore pressure of the sample, once the formation of the shear plane occurs.

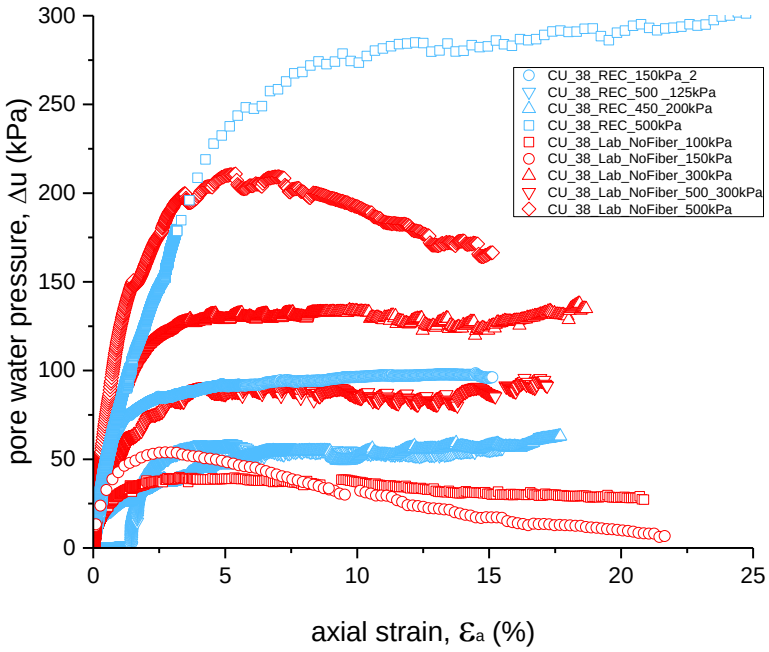

Figure 10-38. Pore-pressure response of in-situ compacted fibre-reinforced and reconstituted clay samples

Furthermore, in the stress space previously mentioned, a reduction on the deviatoric stress due to the build-up of pore pressure was seen for the samples tested at high confinements. The critical state stress ratio (M) for unreinforced samples (0.89) was found to be higher than the one determined from the reconstituted specimens results (0.85). This critical state stress ratio of reconstituted samples found to be similar value of 0.85 found by Gasparre (2005) for reconstituted London clay.

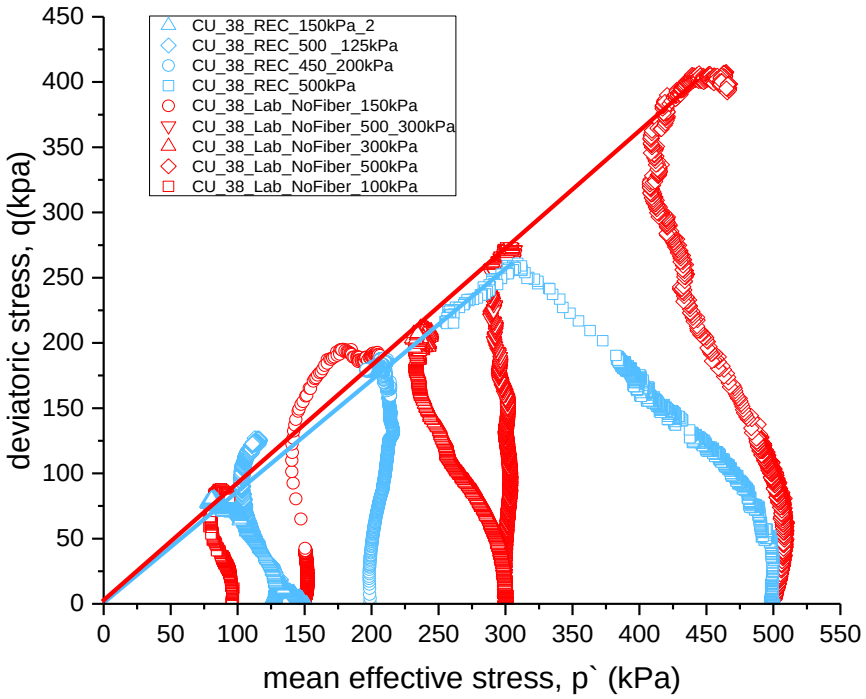

Figure 10-39. Stress paths of in-situ compacted fibre-reinforced and reconstituted clay samples

10.6.3 In-situ vs Reinforced

As mentions in the section 1.3 of this study, the in-situ samples were tested in order to evaluate whether the laboratory preparation method would offer a better alternative to the conventional methods in describing this reinforced soil behaviour.

Figure 10-40 shows the stress-strain curves of the in-situ and laboratory compacted fibre-reinforced clay samples. Let alone the differences of confinement stresses between the two specimen groups, it is clear that the laboratory compacted specimens are consistently reaching higher deviatoric stresses. However, both sets of test are showing a constant strength after medium strain levels.

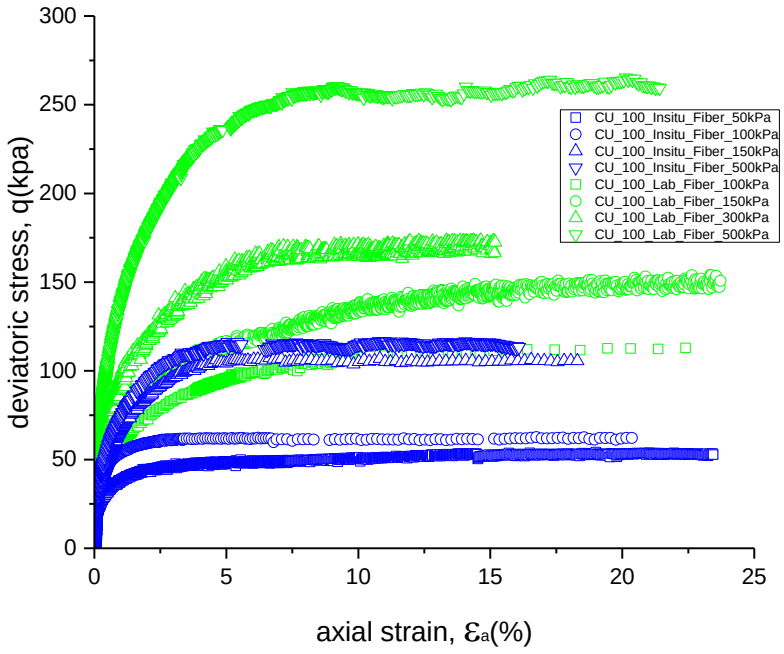

Figure 10-40. Stress-strain response of in-situ and laboratory compacted fibre-reinforced clay samples

The excess pore pressure developed during the triaxial tests of these two specimens groups are shown in Figure 10-41. The figure shows that the in-situ compacted specimens are responding with higher development of excess pore water pressure, where, in low confinement, the difference is more pronounced.

Due to the unexpected formation of a shear plane in samples INS150 and INS500, a reduction on pore water pressure was expected. However, for all in-situ samples, regardless of failure mechanism, the pore pressure increased to a constant value and was kept at this constant level until the end of the test, indicating that the fibre distribution in the two samples mentioned above was not uniform as fibres were not seen crossing the shear plane (Figure 10-25).

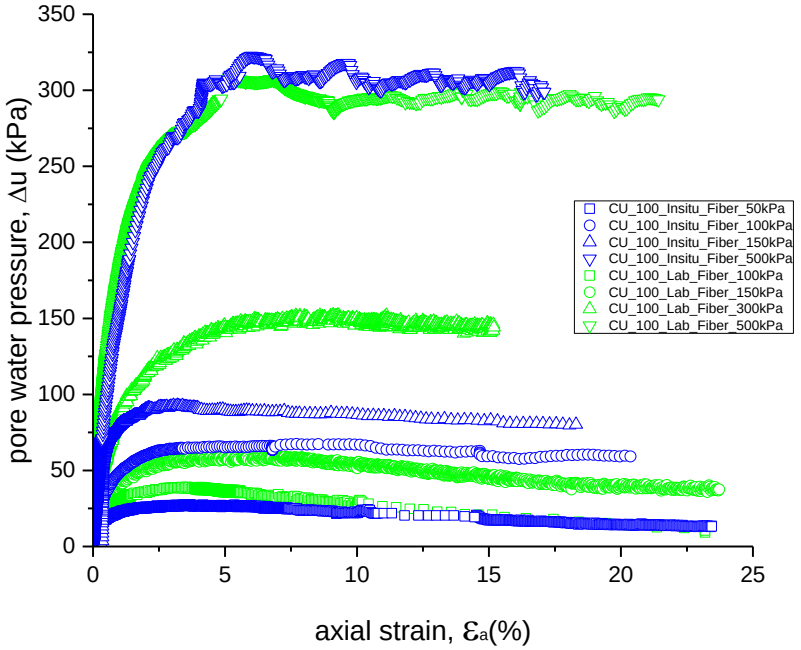

Figure 10-41. Pore-pressure response of in-situ and laboratory compacted fibre-reinforced clay samples

In addition, the stress path graphs, in Figure 10-42, show that the difference in stress ratio between the samples, where the stress ratio (M) for the reinforced samples (0.87) was found to be lower than the in-situ samples (0.98). Nevertheless, as discussed in Section 10.5, the reason for such increase might be due to the low confinement tests on in-situ specimens.

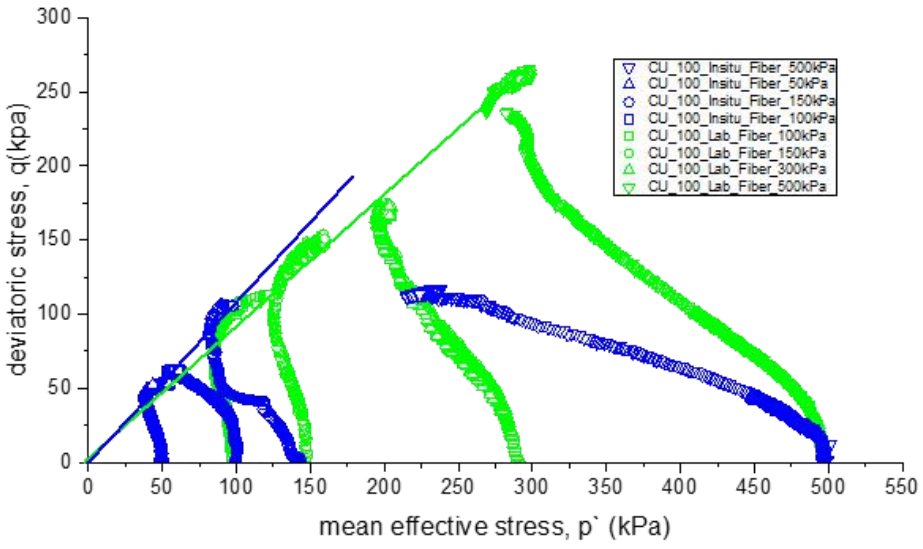

Figure 10-42. Stress paths of in-situ and laboratory compacted fibre-reinforced clay samples

It seems that the sample preparation followed in the laboratory is creating specimens with different fabrics, not allowing a proper comparison with the site compacted samples. There might be various reasons for such differences, as mentioned in the section 5.3. One was the high moisture content of the soil during site compaction, particularly as rain was falling. Consequently, it can be seen in Table 12, that the in-situ specimens have higher initial moisture content at the beginning of the triaxial testing. As expected, such increase have lead the in-situ specimens to a lower dry density, which in return, have made the specimens reach lower deviatoric stresses when sheared at the same p', when compared to the lab compacted specimens.

It is worth point out that the peds created on site are much larger than the peds used in the laboratory. Therefore, it is believed that the laboratory samples would have a much denser fissuring pattern than the site compacted samples. Additionally, another variable that may also contribute to the differences are related to the compaction moisture content, given that the site moisture content is up to 5% higher than the one used in the lab compacted tests, therefore the number of passes of the compaction equipment was increased.

10.7 Normalization

In this part of the report, the triaxial test results are normalised using the methodology described in the Critical State Soil Mechanics theory and reviewed in Section 2.3.8 of the Literature Review chapter. Figure 10-43 defines the pressure variables and their location on the space v versus lnp'. These are named as follows:

- $p`_{cs}$ – equivalent pressure on the critical state line, where the critical state line was defined by the end points of the triaxial tests of a particular group of samples (reconstituted, reinforced, unreinforced and in-situ).

- p_e* - equivalent pressure on the intrinsic normal compression line of the reconstituted samples, where the intrinsic compression line was determined as seen in Figure 10-43.

- $p`_{cs(in)}$ - Normalisation with regards to the individual critical state line of each specimen. This line was determined by locating end of state position of the sample under shearing in v:lnp` space. Subsequent to locating critical state point, the critical state line determined that may be estimated to be parallel to the individual normal compression line of the specimen. Finally, equivalent mean effective pressure, $p`_{cs(in)}$, was obtained at the current state of the specimen.

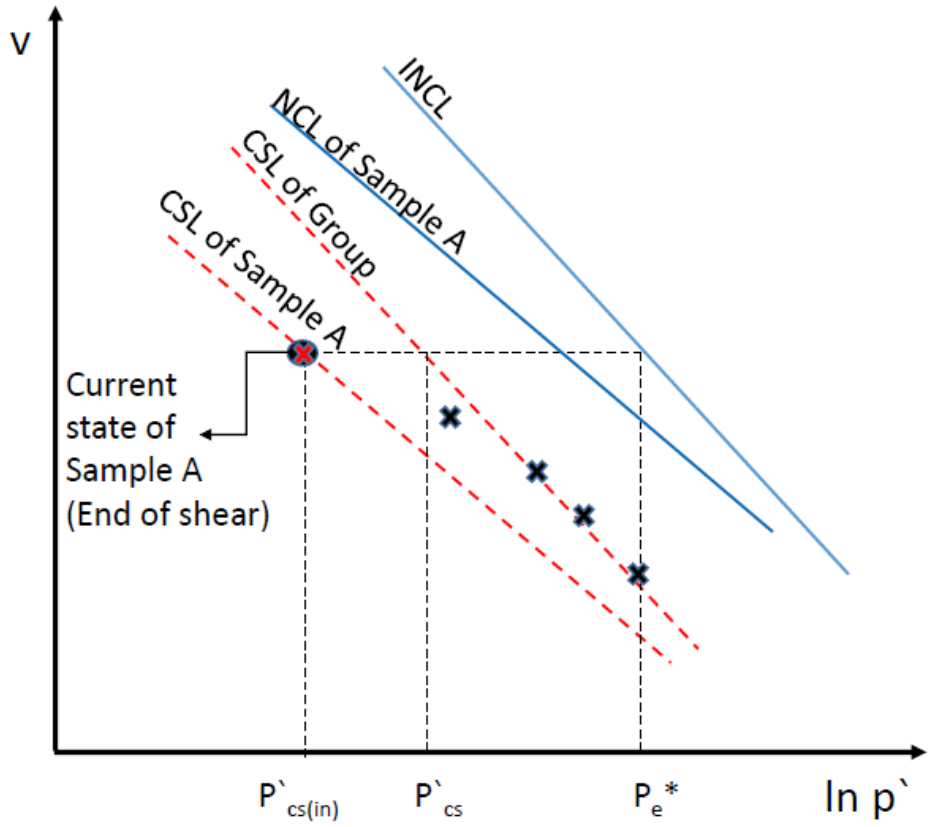

Figure 10-43. Definition of the normalising parameters

10.7.1 Normalisation regarding the Group Critical State Line

Figure 10-44. End-of-test states for the reconstituted samples shows the state of the samples at the end of the shearing, in the v:lnp` space. The points were obtained from the end of the triaxial tests or when the samples are seen to reach a steady state or a critical state. The arrows indicate the direction the tests that did not reach a critical state were following, when they were terminated. The least complete tests were those with the lowest confining stresses (REC150 and REC500_125) which were still experiencing further increase in stress and reduction in pore water pressure. As seen in Section 10.2 samples REC500 and REC 450_200 reached critical state by showing a constant shear strength and a constant excess pore-pressure. In addition, a single drained test has been performed with a reconstituted sample (DREC150); as there is only one drained test, the stress-strain and volumetric strain plots are shown in Figure A-0-5 and Figure A-0-6, on the appendix chapter. These tests appear to define a CSL line, parallel to the NCL previously determined, with parameters λ=0.1645 and Γ=2.4983.

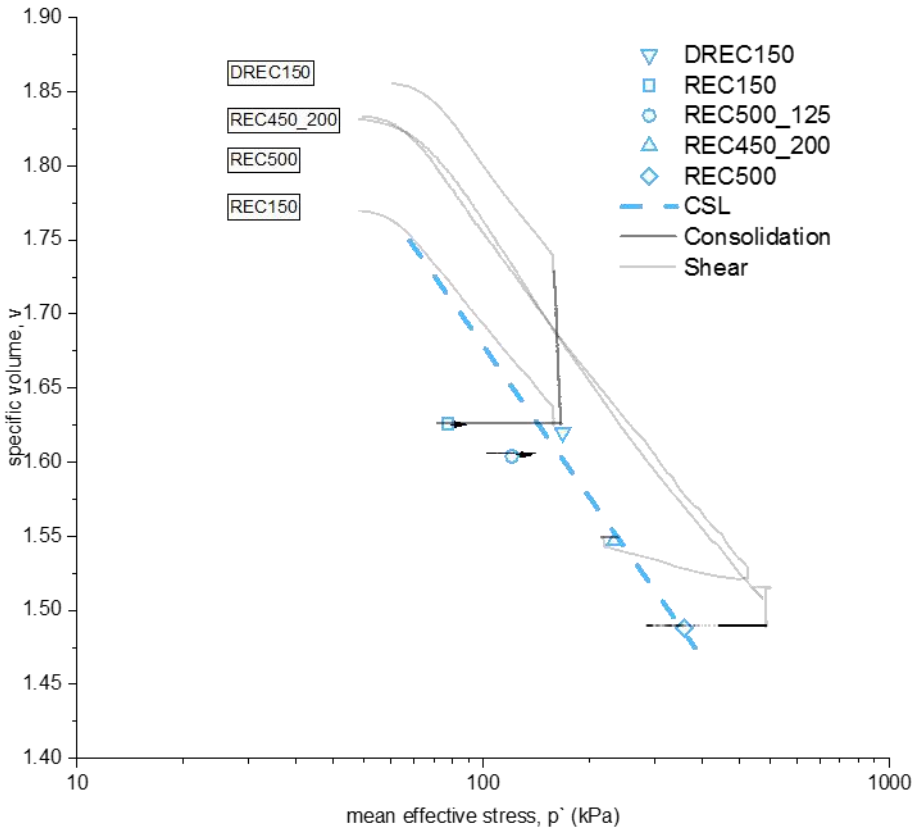

Figure 10-44. End-of-test states for the reconstituted samples

The stress paths were than normalised by the equivalent pressure on the critical state line, p'_{cs}, (Equation 38) and shown in Figure 10-45.

$$p`_{cs} = exp\frac{\Gamma - v}{\lambda} \qquad 38$$

As can be seen, all specimens initially follow an almost vertical path, towards the critical state line, with the exception of the tests that are starting near the NCL, where a more curved pattern is seen. The critical state line is reached by three of the tests with one of them following towards a lower value, whilst other specimens ended without actually reaching the critical state. The critical state stress ratio parameter (M) was found to be 0.85.

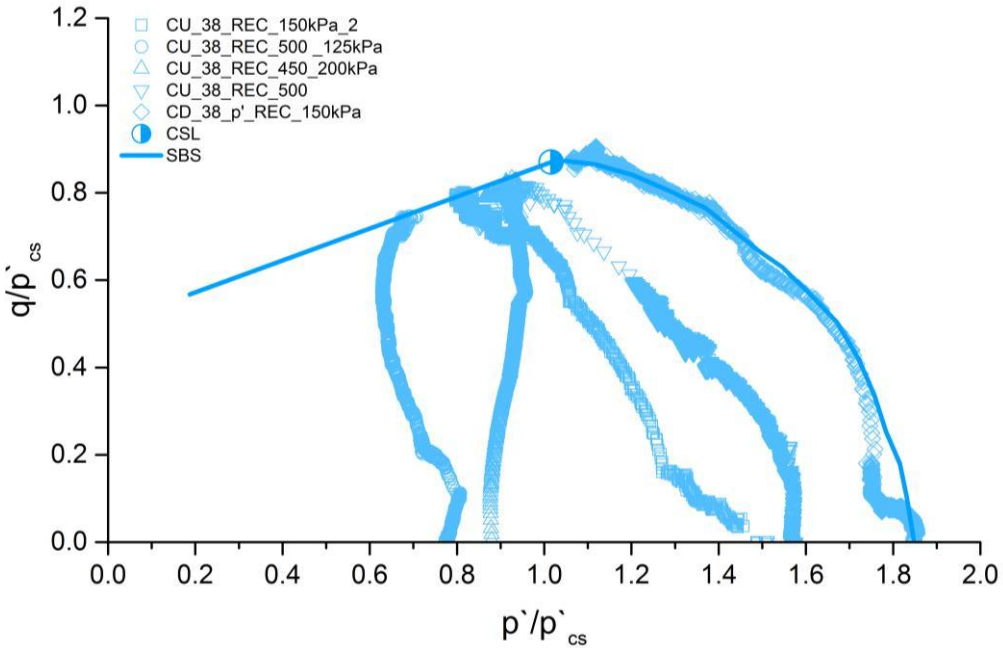

Figure 10-45. Critical State Normalised stress paths of reconstituted samples

Figure 10-46 shows the critical state in the v:lnp` space for the drained and undrained unreinforced specimens. As concluded in section 10.3, the unreinforced clay behaviour section, specimens other than UNF50 and DNF50 are reaching critical state. However, in addition to those samples, sample UNF100, DNF100, DNF300 were found not reaching the CSL_1, determined in the v:lnp` space. Furthermore, the drained specimens DNF50, DNF100 and DNF300 are on the wet side of the CSL_1 and dilating away from the CSL_1, towards a different critical state line. Additionally, the undrained specimen UNF50 is also following a path away from the CSL_1. It should be recalled that the one dimensional compression behaviour of the unreinforced specimens show that there are multiple parallel NCLs, dependent on the initial void ratio of the specimens. Ponzoni et al. (2014) reported that transitional soils, at defined specific volume ranges, can follow individual NCLs. Therefore, a second Critcal State line (CSL_2) has been introduced, similar to Ferreira & Bica (2006). This new CSL has the same slope of CSL_1 and the NCLs. The slope of the iso-NCLs have been determined in section 10.3 and was found to be similar if calculated via the compressibility index, Cc. The parameters defining the CSL_1 and CSL_2 for the unreinforced soil are $\lambda = 0.0923$, $\Gamma_1 = 2.071$ and $\Gamma_2 = 2.157$.

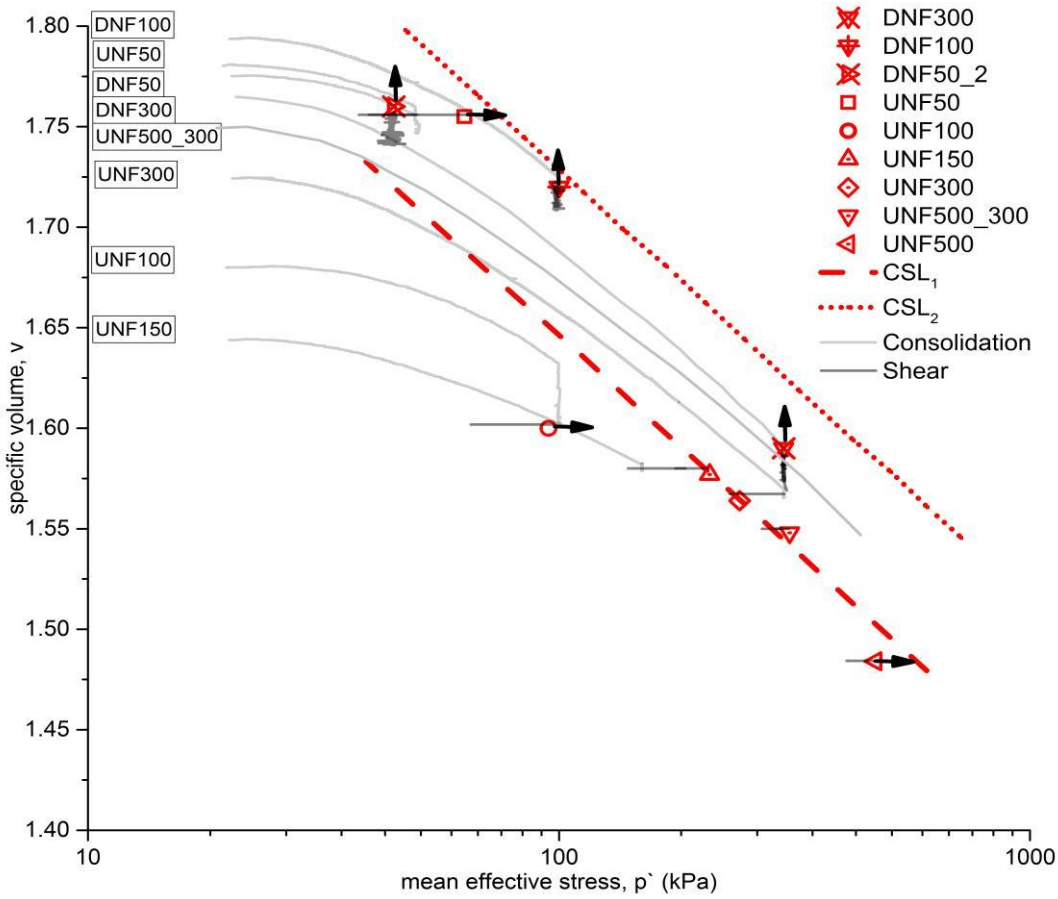

Figure 10-46. End-of-test states for the drained and undrained unreinforced samples

Furthermore, looking at Figure 10-46, one can notice that, if the evaluation done on Section 10.3 revealed that the samples reach a steady state, it could be accepted that all samples other than UNF50 and DNF50 reached critical state, and both CSLs seem to be curved, in a fashion similar to the NCLs at low stresses. Such behaviour is commonly observed in granular soils and unlikely to occur in clay soils. Therefore, further low stress testing at different initial void ratios is required to cement this observation.

As can be seen in Figure 10-46, the drained samples are dilating away from the CSL1, therefore normalising the data with the CSL_1 alone would be unsuccessful as these test would move away from the critical state line on the normalised space Hence the data was normalised using both CSLs (Figure 10-47).

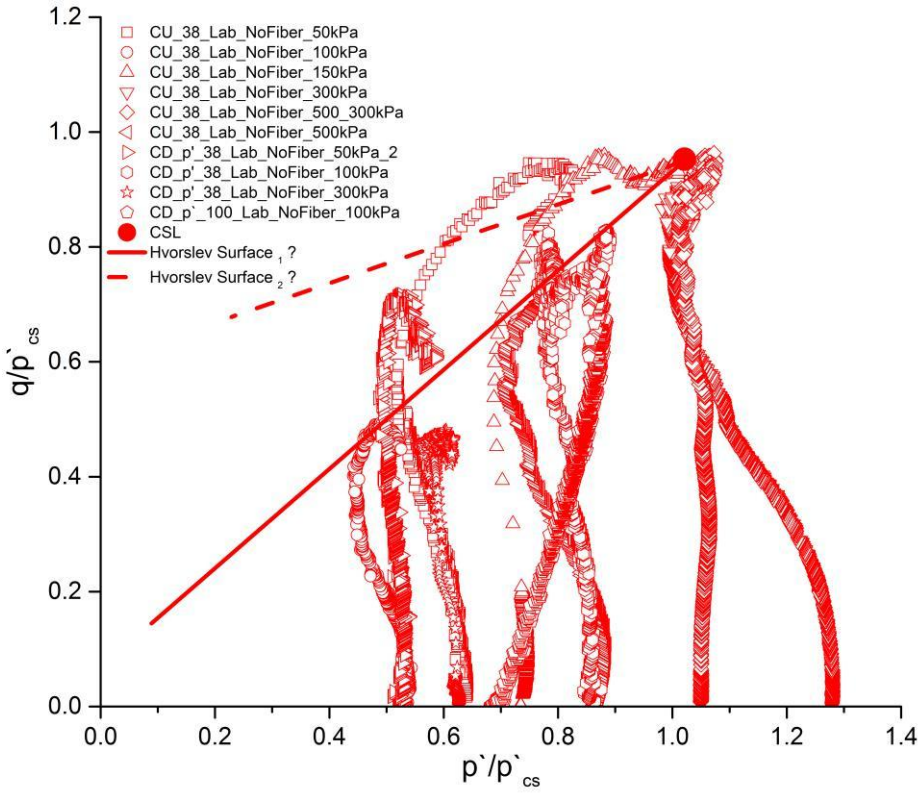

Figure 10-47. Critical State Normalised stress paths of drained and undrained unreinforced samples

The specimens that are on the critical state line on v-lnp` space have reached the critical state point on the normalised space. In addition to that, the end of test results of the samples that were on dry side of both critical state line, at the start of the shearing stage, reached a boundary surface and then show a tendency to follow the same path towards the critical state point. It is difficult, on the normalised space (Figure 10-47), to identify a single Hvorslev surface for the unreinforced specimens as it could have any slope in between the two lines shown on the graph. The critical state stress ratio parameter (M) was found to be equal to 0.89, being coincident with the evaluation done in section 10.3.

Figure 10-48 show the end of test points for the compacted samples with fibres. As can be seen, specimens DF100, UF300 and UF 500 have reached a critical state line that is parallel to the compression line obtained in isotropic compression stage and confirmed via one-dimensional compression of reinforced specimens. As conclude through the one-dimensional and isotropic compression testing, specimens tend to converge to unique NCL at high stresses. The parameters defining the critical state line for the reinforced soil are λ= 0.0613 and Γ=1.8926. Sample UF150 finished near the CSL whilst samples DF50 and UF100 have finished far from the CSL determined.

Nevertheless, unlikely to unreinforced specimens, reinforced specimens which are not on the CSL are showing tendency to reach a single critical state line. Unfortunately, the load cell failed when testing sample DF300 and erroneous measurements were taken, therefore DF300 specimen was not used from this point onwards. Plots of that test is presented in the appendix Figure A-0-7.

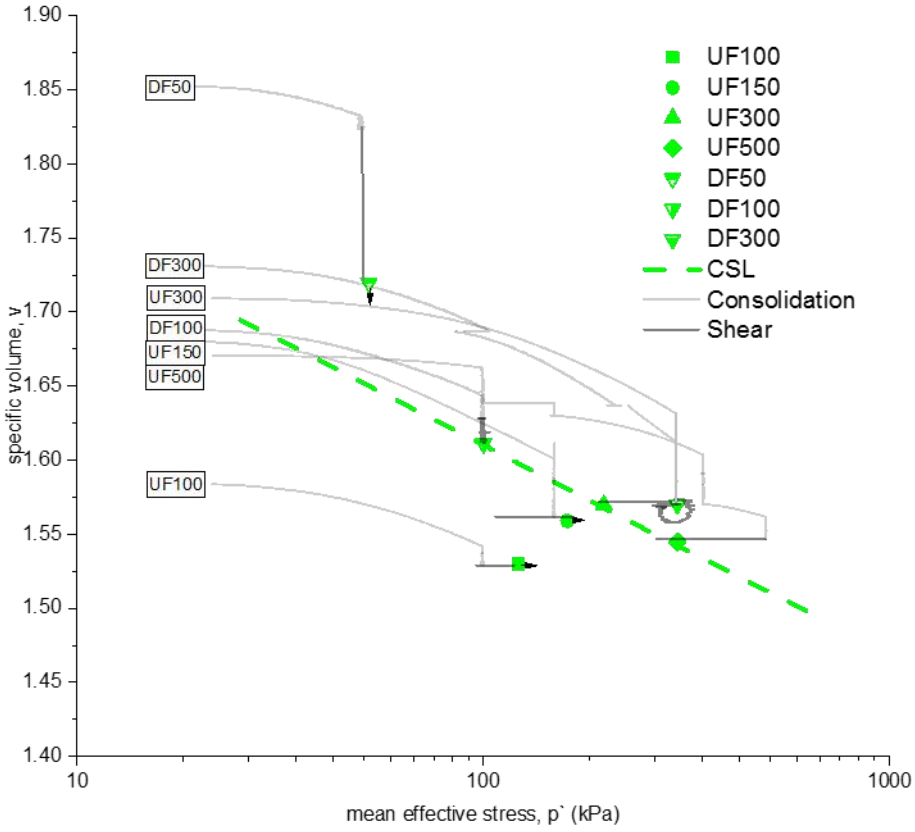

Figure 10-48. End-of-test states for the drained and undrained reinforced samples

Figure 10-49 shows the normalised stress path for the reinforced drained and undrained specimens. The data have been normalised with respect to group critical state line. Samples UF100 and UF150 initially followed an almost vertical path, reaching the state boundary surface and showing a tendency to follow it towards the critical state line. Samples DF100, UF300 and UF500 directly followed a path towards the critical state. Critical state line has been found to have a value of M of approximately 0.87, confirming the previous evaluation.

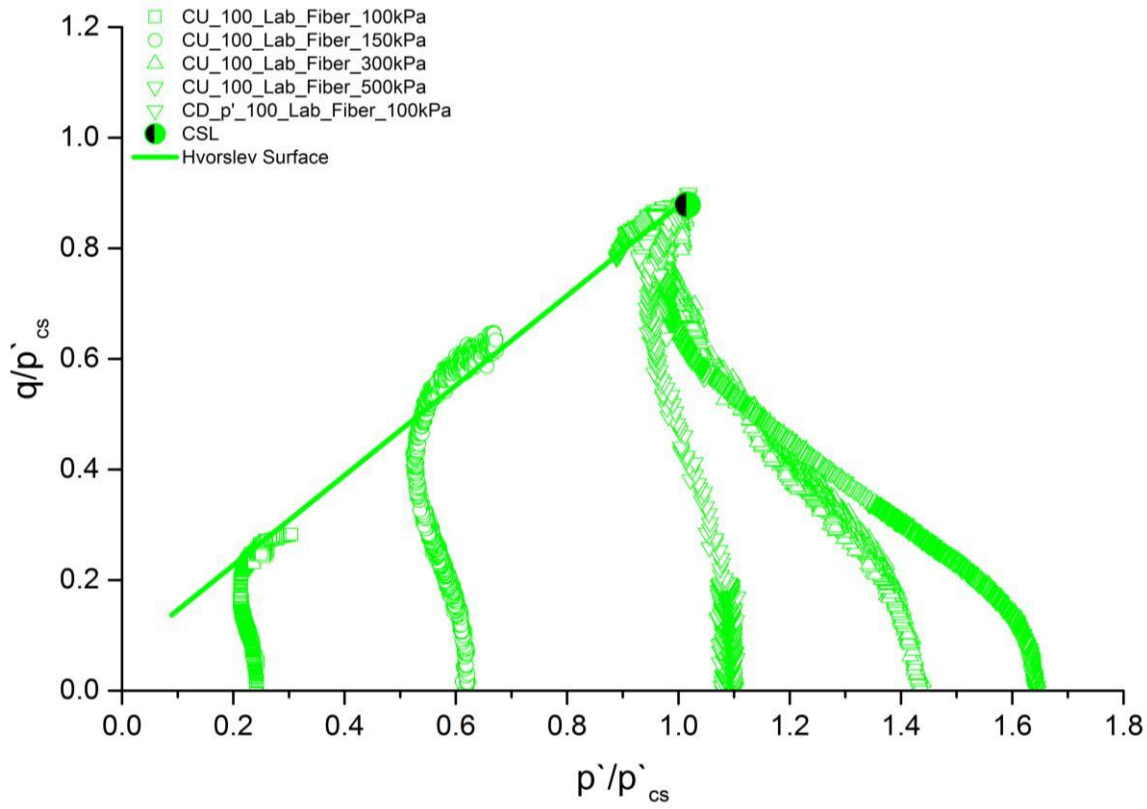

Figure 10-49. Critical State Normalised stress paths of drained and undrained reinforced samples

The end of test state of the in situ samples is shown on Figure 10-50, together with the consolidation curves for some of the high confining stress tests. Samples INS50, INS100 and INS 150 have reached critical state. Sample INS500 was expected to reach the critical state due to its high confinement, however, as mentioned before, due to a pebble causing the sample to shear through a weaker zone and the high initial specific volume, the sample has stopped far from the critical state line, but presents constant deviatoric stress and pore water pressure.

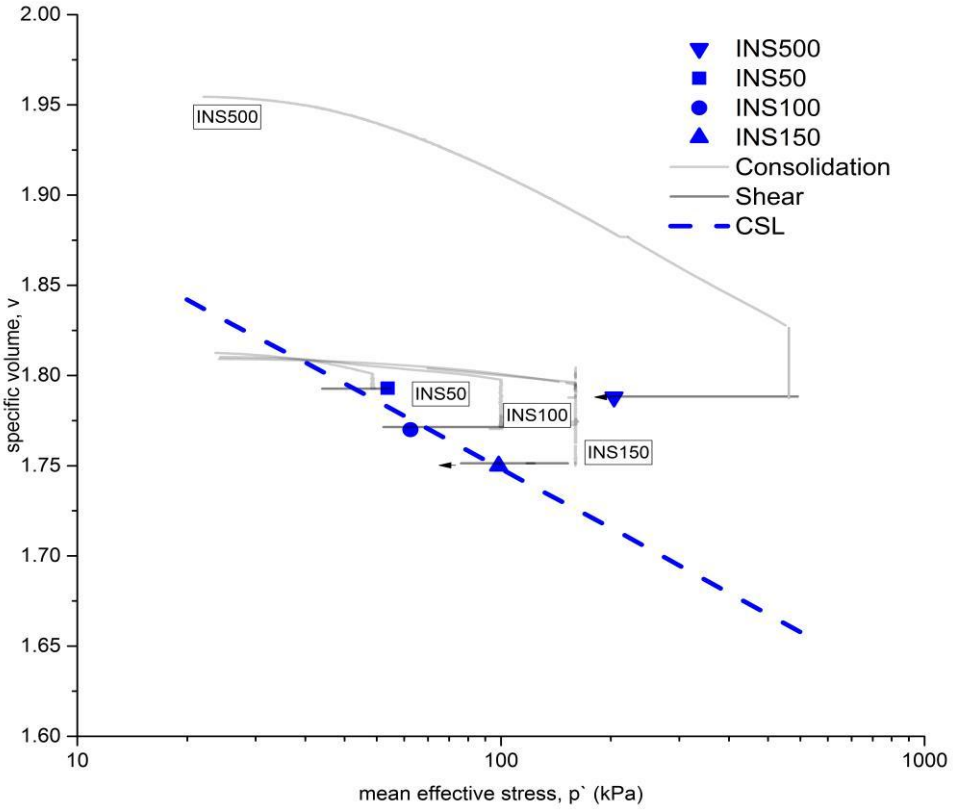

Figure 10-50. End-of-test states for the undrained in-situ samples

End points of isotropic normal compression lines of INS50, INS100 and INS150 have been used as a guidance to determine the CSL of the site compacted specimens, where even a slow enough compression rate (2 kPa/hr) was not achieved, therefore after reaching the targeted confining stress, the sample continued to compress. The parameters defining the critical state line for the in-situ soil are λ= 0.0612 and Γ=2.034

Figure 10-51 show the normalised stress paths of the in-situ specimens. The data have been normalised with respect to the critical state line determined in Figure 10-50. Samples INS50, INS100 and INS150 initially followed an almost vertical path, reaching the state boundary and following it towards the critical state. As for the normalisation of sample INS500, the point was found to have a large offset between the effective stress at the end of the shearing and the effective stress at the critical state line. The initial specific volume of the sample was much higher than the other specimens and it seems that this sample reached a relationship between void ratio and isotropic stress that is above the compression lines achieved by the other tests. Such behaviour might be the indication that transitional behaviour occurs for the in-situ compacted material. However, due to problems encountered on specimen INS500, (mentioned in section

10.5), INS500 was not taken into consideration when the data was normalised. If the CSL, determined by samples INS50, INS100 and INS150, is accepted as the correct Critical state line, the previous value of M determined to be approximately 0.98 is in agreement with the results obtained in this section. The Hvorslev surface plotted in Figure 10-51 should be treated as representative, since the available stress paths does not allow the full determination of this surface.

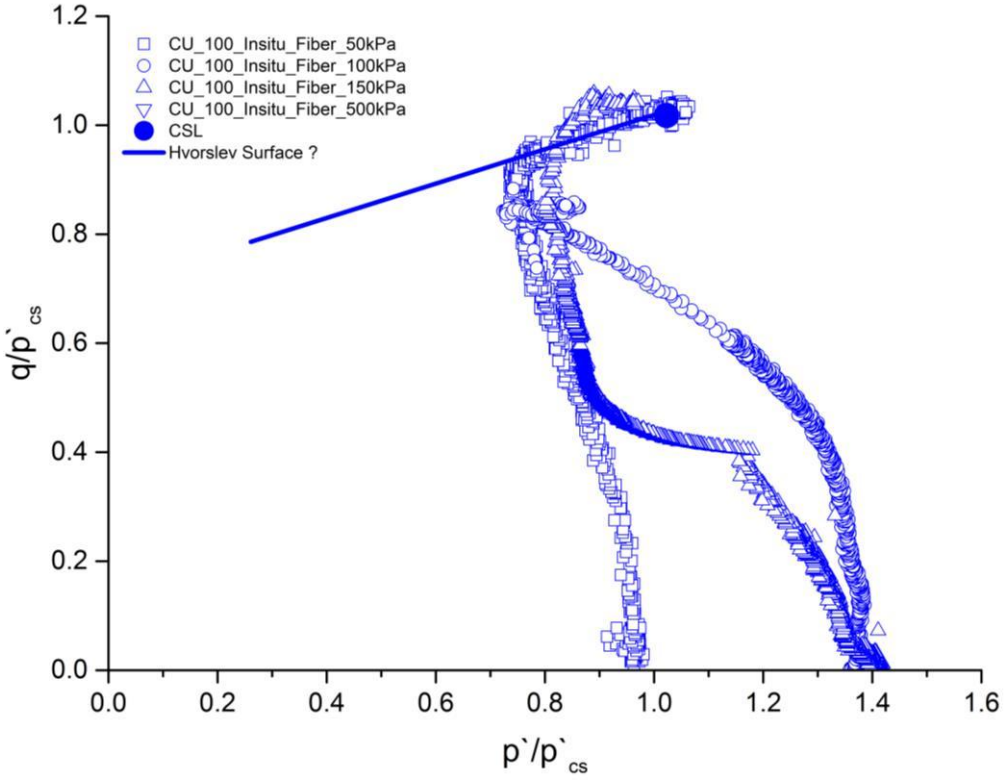

Figure 10-51. Critical State Normalised stress paths of undrained in-situ samples

Figure 10-52 present the normal compression lines, together with the critical state lines determined throughout this section and the intrinsic and intact normal compression lines of reconstituted London clay, determined by Gasparre (2005). It can be observed that the ICL of the reconstituted soil, tested in this study, is parallel to the ICL determined by Gasparre (2005) for London clay; since they belong to adjacent geological groups and have similar characteristics, this may not be a coincidence. The parameters of the normal compression and the critical state lines for all the groups, plotted on Figure 10-52, are shown in the Table 13.

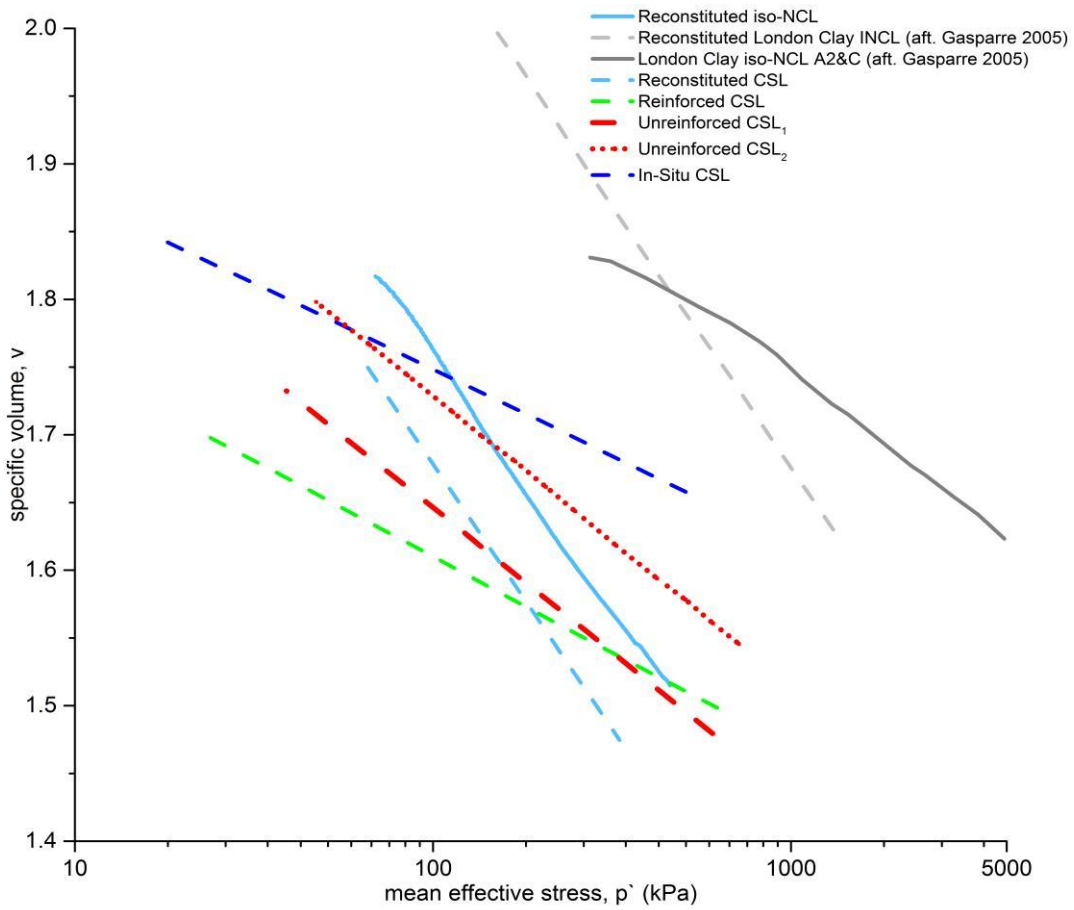

Figure 10-52. Determined CSLs and NCLs of ALL samples

Table 13. CSL and NCL parameters for the lines on Figure 10-52

Soil	N	Γ	λ	M
Reconstituted CSL	-		0.1645	0.8500
Reconstituted NCL	2.5100	-	0.1645	-
Unreinforced CSL_1	-	2.0710	0.0923	0.8900
Unreinforced CSL_2	-	2.1570	0.0923	0.8900
Reinforced CSL	-	1.8930	0.0613	0.8700
In-situ CSL	-	2.0340	0.0612	0.9800
Reconstituted London Clay INCL*	2.8300	-	0.1680	0.8500
London Clay iso-NCL A2&C*	-	-	0.0920	-

*(after. Gasparre 2005)

Additionally, Figure 10-52 also shows that the NCL of intact samples of London clay (Gasparre, 2005) have a slope similar to the unreinforced specimens tested in this study. Such behaviour might be due to the changes in the fabric of the soil, initial void ratio, preparation method or stress level at which specimens are tested.

Figure 10-53 presents the normalised stress paths of all samples. Each sample was normalised by the equivalent pressure on the critical state line determined for each group. The reconstituted samples were all in the wet side of the critical state line, therefore having the tendency to "contract" towards the CSL. As for the reinforced, unreinforced and in-situ samples, higher testing stresses are necessary to construct the full state boundary surfaces. Therefore, for those samples, only Hvorslev Surface was determined. As can be seen from the plot, samples that are reaching critical state, followed a path to the critical state point and differences in the M value were confirmed by the normalisation.

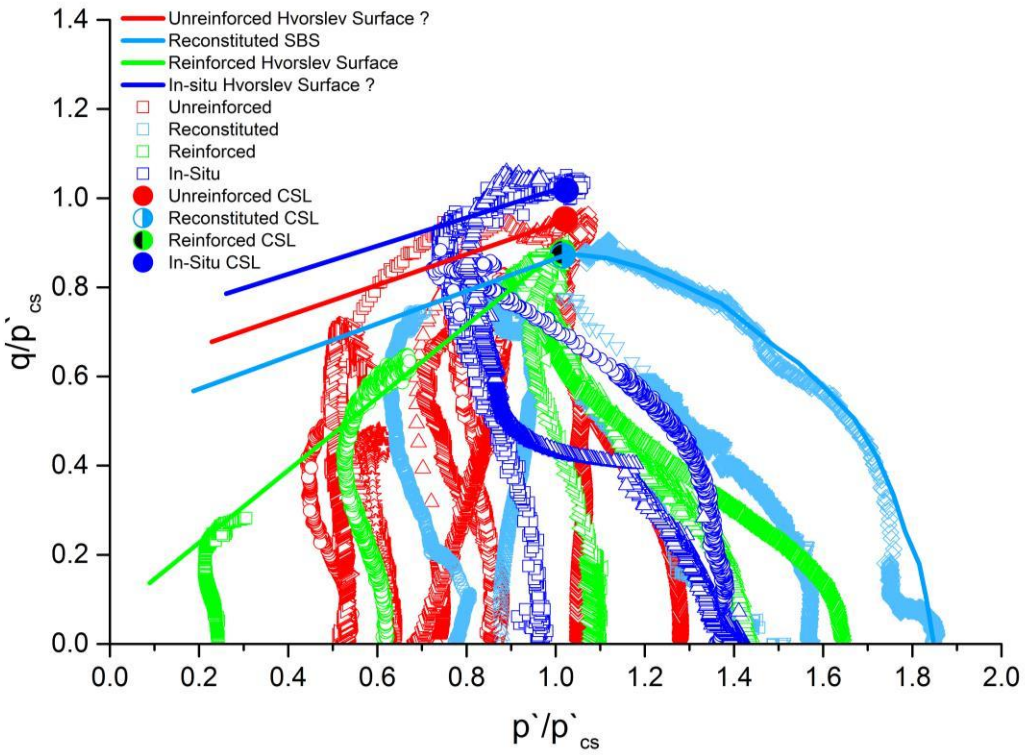

Figure 10-53. Normalised state paths for ALL samples via group parameters

The results of reinforced, unreinforced and in-situ specimens seem to show that the CSL is not unique but proportional to the initial void ratio range of the samples tested as discussed previously by Ponzoni et al. (2014), therefore each group of sample would have its own critical state line depending on the range of initial specific volumes. The same observation was made on the analysis of the one-dimensional compression behaviour of unreinforced specimens as even at 1 MPA none of the different void ratio samples, have converge to a unique NCL. Hence there is a strong evidence that the soil used in this study is a transitional material.

Depending on the location of the critical state line and the end of state plots of the unreinforced drained samples, it was expected that the samples would compress to reach the critical state line, whereas the drained samples (DNF50, DNF100 and DNF300) dilated. Therefore, this is further indication of presence of second critical state line as named samples was tested at higher initial specific volume.

Normalisation of the reconstituted and unreinforced specimens revealed that there is an effect of structure in the unreinforced specimens through the retained characteristics of the "parent" soil and adapted preparation method. This is clearly seen given by the location of the CSL and the apparent state boundaries. Difficulties were encountered in determining the location of the Hvorslev surface for the unreinforced and in-situ soils, however, when all the normalised stress paths are plotted together, it seems reasonable to plot the Hvorslev surfaces of the unreinforced and the in-situ specimens parallel to the Hvorslev surface of the reconstituted soil. Particularly since the in-situ specimens, after shearing, only had a few fibres crossing the shear surface and, in some occasions, none; indicating that the in-situ soil may be behaving as an unreinforced soil for this size of samples.

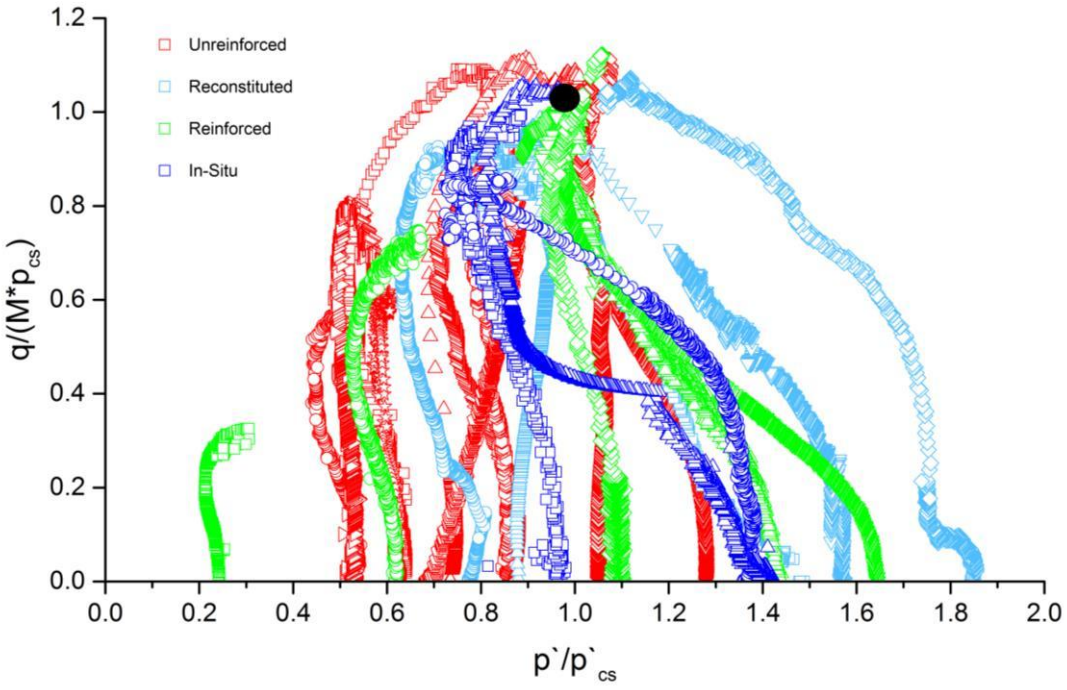

Figure 10-54. Further M Normalised state paths for ALL samples

One can argue that the M values of the samples were close to each other, therefore it is not clear whether or not there is an influence of the addition of fibres or the ped compaction (preparation).Moreover, determination of the CSL via preliminary evaluations in section 10.2 to 10.5 might be misleading, therefore normalisation in regarding to intrinsic normal compression line, p_{e^*}, and individual critical state line, $p`_{cs(in),}$ have been performed in Section 10.7.2 and 10.7.3 respectively, in order to draw solid conclusions.

10.7.2 Normalisation regarding the Intrinsic Compression Line (ICL)

According to the test results, the reconstituted soil has a unique normal compression line, therefore all tests were normalised according to this line. The parameters defining the intrinsic compression line for the reconstituted soil are λ= 0.1645 and N=2.51. Therefore, from Figure 10-55 to Figure 10-59 the stress paths of the reconstituted, reinforced, unreinforced and in-situ samples, normalised with regards to the ICL, are presented.

The tests on reconstituted samples, normalised the ICL are shown on Figure 10-55. The normalised results show that it is possible to determine a unique boundary surface, represented by the dashed line. It is also possible to see that the CSL is located at the apex of the SBS*. Since only undrained tests were used to determine this boundary, the normally consolidated tests performed define a Local Boundary Surface (LBS), according to undrained test wet side of the surface represents a local boundary surface as defined by (Zdravković & Jardine 2001). Nevertheless, if the plasticity of the specimen was considered, the true SBS* should not be expected to plot far above the LBS. Therefore, LBS identified here will be treated as Roscoe-Rendulic Surface of the group.

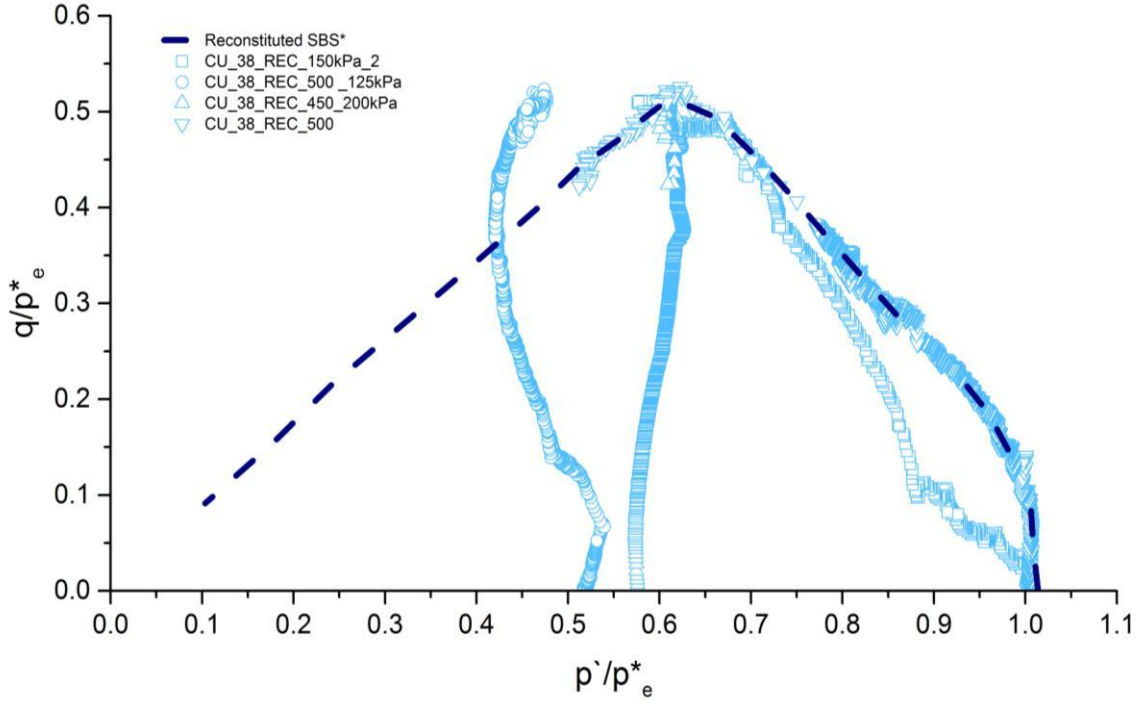

Figure 10-55. Normalised stress path with State Boundary Surface of undrained reconstituted samples

The normalised stress path for the unreinforced specimens is presented with intrinsic boundary surface in Figure 10-56. Only the dry side of the boundary surface of the unreinforced specimens could be drawn. As discussed in Section 10.7.1, the samples were not compressed to large enough stresses in order to reach the NCL and define the Roscoe/Rendulic surface. Starting from the low pressures, the boundary surface of the unreinforced specimen's extend well above the intrinsic boundary surface, SBS*, showing clear sign of the effect of the existing structure created by the compaction of the peds.

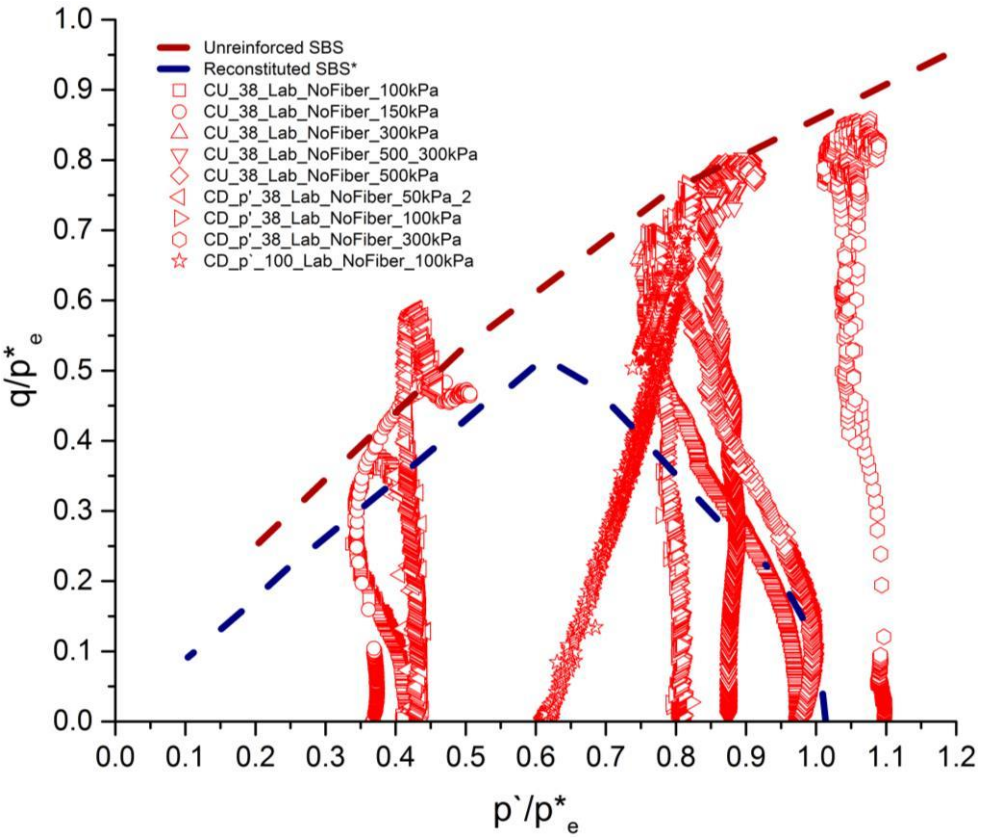

Figure 10-56. Normalised stress path with State Boundary Surface of drained and undrained unreinforced samples

Figure 10-57 presents the ICL normalised stress paths of the fibre reinforced samples, together with the reconstituted boundary surface and the unreinforced boundary surface previously determined. As mentioned before, during the test of samples DF50 and DF300, the load cell failed and, these tests were omitted from the figure.

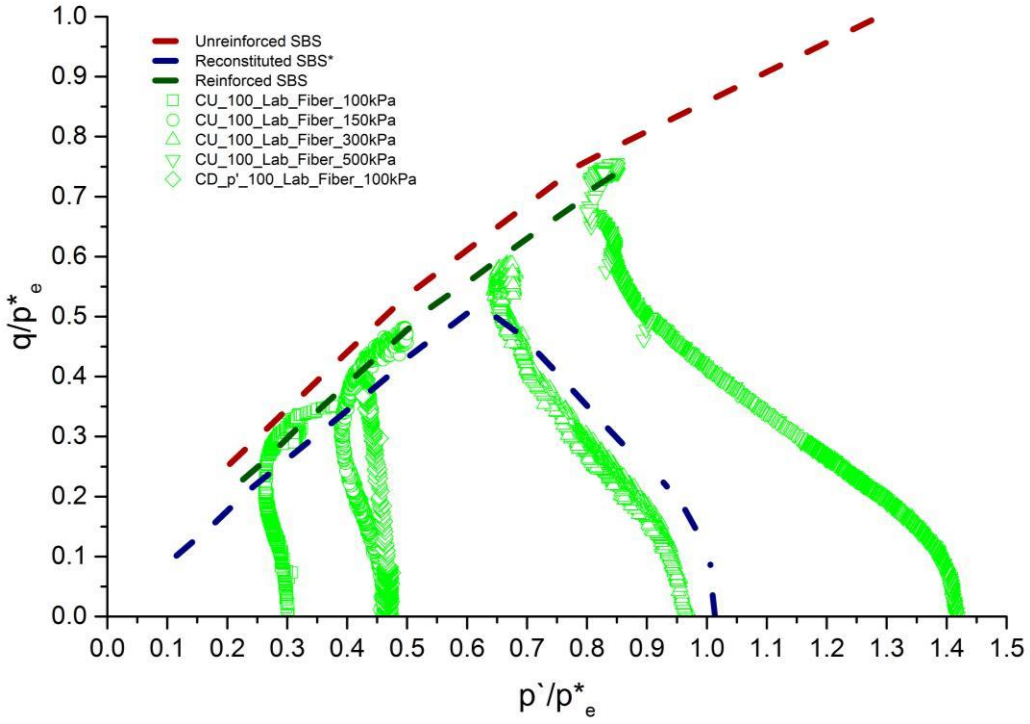

Figure 10-57. Normalised stress path with State Boundary Surface of drained and undrained reinforced samples

It can be seen that the addition of fibres to the ped compacted specimens produced a state boundary surface slightly smaller than the the boundary surface of the unreinforced samples. Similarly, due to the lower confining stresses used, no samples appear to have reached a condition similar normally consolidated state, therefore only the dry side of the critical state has been defined.

The stress strain and the change pore-pressure response of sample INS500 seem to indicate that a steady state was reached. However, as mentioned in Section 10.7.1, due to the initial specific volume, at the end of consolidation, the sample seemed to reach a much higher compression curve. Similarly, at the end of the shearing, the results show that the steady state achieved does not coincide with the other tests, indicating that it is reaching a different critical state line. Therefore, the sample INS500 was not plotted on Figure 10-58, where the normalisation of the in-situ samples with regards to the intrinsic normal compression line is presented. Starting from low pressures, the in-situ boundary surface determined extends well above all the other boundary surfaces, showing a clear sign of the improvement achieved on site.

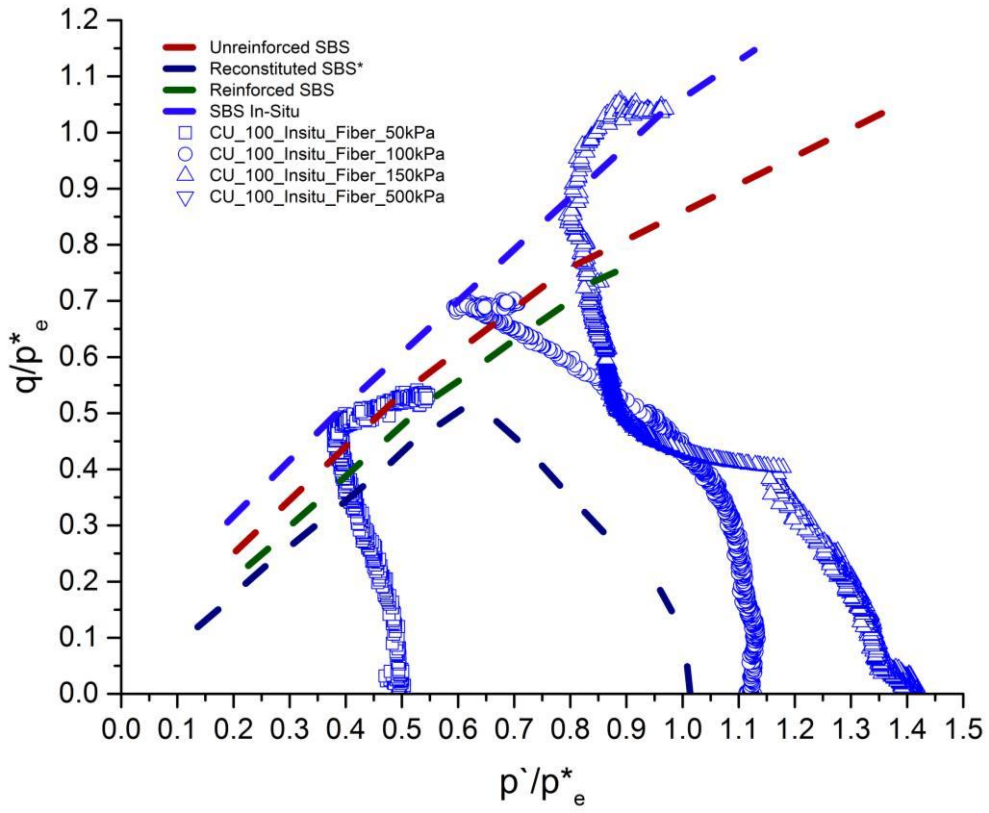

Figure 10-58. Normalised stress path with State Boundary Surface of undrained in-situ samples

The increases on the boundary surfaces are due to different factors and can not be attributed only to the fibres but also to the compaction effort and the presence of the structure in the peds. It might as well evidential that the samples are carrying some structure of their intact soil. Additionally it is interesting to see that the intact London clay boundary surface, presented by Gasparre (2005), in Figure 10-59 falls exactly in the same position of the unreinforced specimens boundary surface. Although this may be a coincidence, it could also be that the peds are still retaining part of their structure even after compaction, creating a fabric that is similar to the one found in London Clay. Particularly since both soil groups have, in some cases, similar geological history.

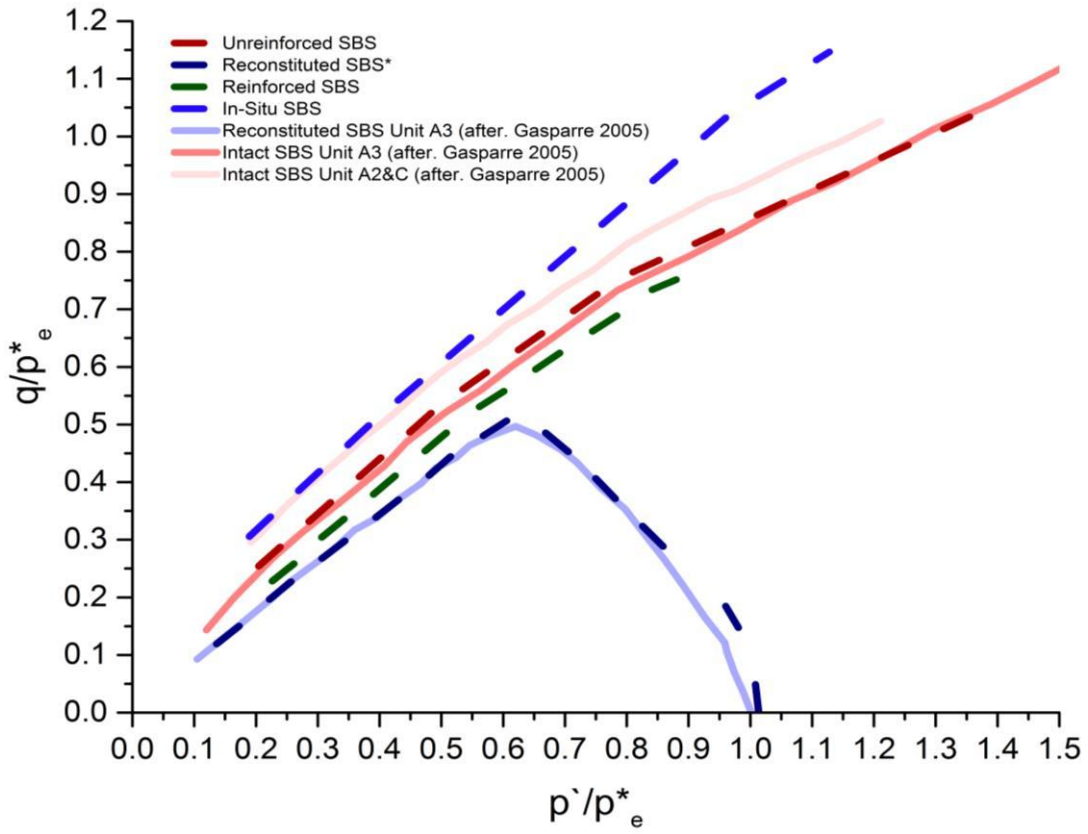

Figure 10-59. State Boundary Surface of ALL samples against Gasparre (2005) *reconstituted, Intact Unit A3, B2&C*

It was initially assumed, in this study, that the use of fibres would enlarge the boundary surface, particularly since the fibres provide extra strength in shearing, however this was not the case. In their studies, Fearon & Coop (2002) on highly fissured clays and Vitone & Cotecchia (2011) on scaly clays found that, due to the heavily sheared and slickensided nature of the scale surfaces, the peak strengths of the natural soil are lower than the critical state of the reconstituded soil. Whereas if the fissured material has matt surfaced fissures, the reduction is less pronounced and the peak strength generally remains above the critical state. Therefore, it might be the case that the ped compaction provides a matt surfaced fissuring in the soil, contributing to an increase in the boundary surface, whilst the introduction of fibres provide slickensided surfaces, reducing the critical state strength and causing a reduction in the boundary surface.

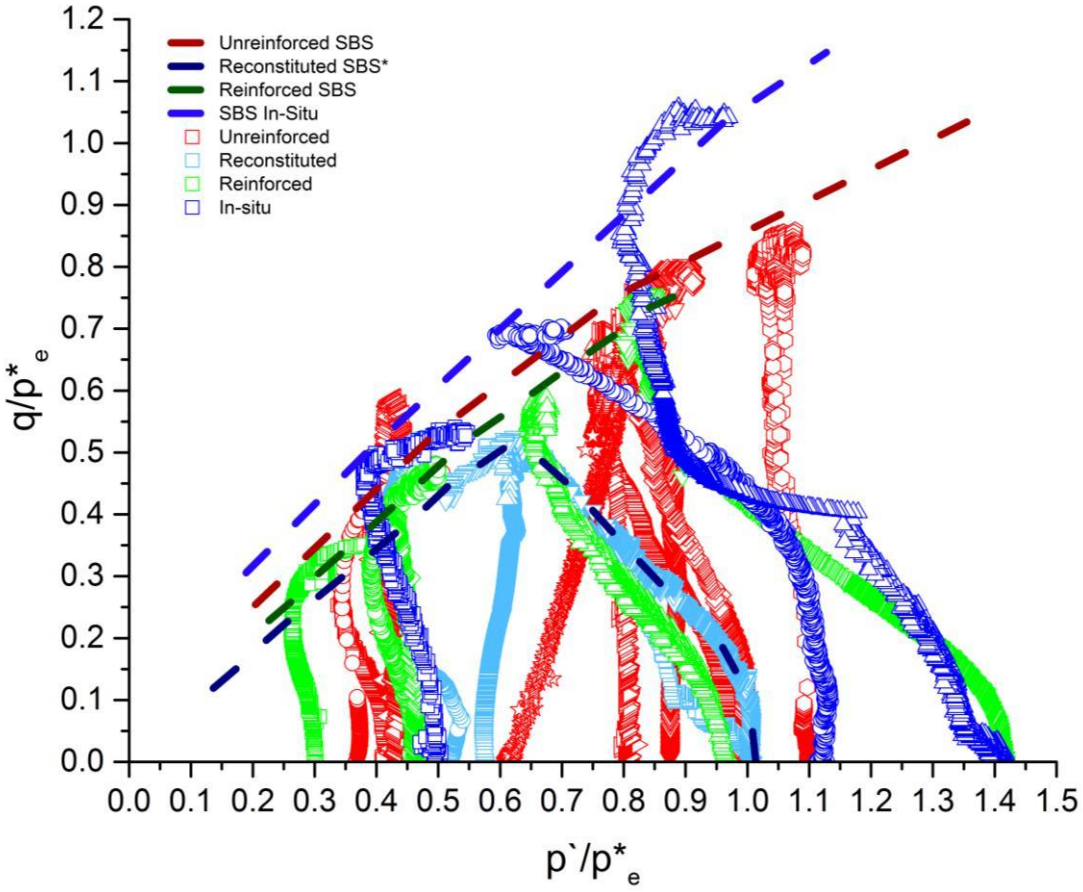

Figure 10-60. State Boundary Surface of ALL specimens normalised with intrinsic NCL.

Hight et al. (2007) agreed with such phenomena, concluding that there are two boundaries of effective stress parameters. The strength of the upper bound is defined by the peak failure envelope of the intact clay, without presence of fissures, whilst a lower bound is given by the parameters defining the shear strength of a fissure. Additionally, authors reported that the effective stress parameters that apply to a particular volume of clay will lie between these two bounds and will be determined by the spacing, extent and orientation of the fissures, by the direction of shearing, and by the kinematic constants – that is, whether potential shear surfaces can seek out the lower-strength fissures. Therefore, it might be the case that, in reinforced samples, the compaction of only peds might be introducing a fissure pattern and the addition of fibres can be extending the length of the present fissure surfaces and altering the direction of the fissures created by the compaction of peds plus fibres. Furthermore, a close examination of the samples after shearing (Figure 10-61) show slickensided surfaces caused by the sliding of the fibres during the shearing.

Figure 10-61. Examination of samples after shearing stage

An evaluation of the boundary surfaces in Figure 10-59 has revealed that even though the initial density of the samples is different and there may be a tendency to follow a set of parallel NCLs, the normalisation of the specimens with the ICL seems to show better results with the definition of the state boundary surface of these soils on the dry side of the critical state. It can be concluded that when transitional behaviour is observed in dense clay specimens, normalising with regards to the intrinsic normal compression line can offer the best alternative for evaluating the effects of structure.

10.7.3 Normalisation regarding the Individual Critical State Line

In this section each individual test has been normalised by its own individual critical state line. As an example of the normalisation procedure, Figure 10-62 shows the critical state, in the v:lnp` space, of sample REC150 compared with the isotropic compression and critical state lines. For each specimen, the stress-strain, pore water pressure development, stress ratio and pore pressure increment were evaluated in order to observe whether or not the specimen was reaching critical state. The outcome of such evaluation allowed the location of the end of state point of the sample in the v:lnp` space. Subsequent to locating the critical state point, the critical state line was determined by assuming it to be parallel to the compression line of individual specimens, and given by

$$v = \Gamma - \lambda lnp` \qquad 39$$

Where $\Gamma = 2.26$ and $\lambda = 0.144$ as obtained in Figure 10-62. Furthermore, the evaluation of the stress ratio and pore pressure increment relationship, enabled the determination of the critical state ratio, M for each specimen. The value of M for specimen REC150 was found to be 0.99.

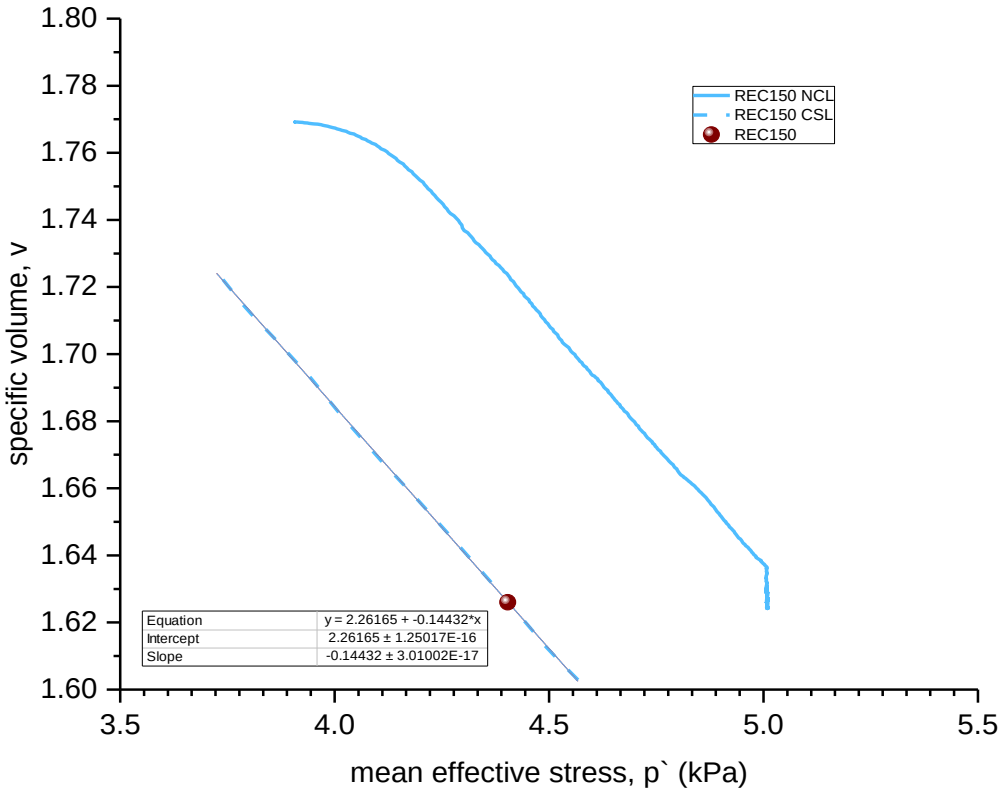

Figure 10-62. Representation of obtaining critical state parameters for individual normalisation

The same procedure was followed for all specimens where the evaluation of the results from Sec 10.2– 10.5 lead to a critical state point. Table 14 shows the values of Γ, λ and M parameters of each soil used in the normalisation. It is worth mentioning that the slopes of the individual critical state lines are increasing in value with the confining stress, reaching relatively stable values at the highest stresses tested. The same can be said for Γ. This indicates a convergence to a unique set of parameters with the confining stresses tested.

Table 14. Critical state parameters of individual specimens

Samples	Critical State Parameters		
	Γ	λ	M
CU_38_Lab_NoFiber_50kPa	1.950	0.048	1.110
CU_38_Lab_NoFiber_100kPa	1.856	0.057	0.870
CU_38_Lab_NoFiber_150kPa	1.855	0.052	0.920
CU_38_Lab_NoFiber_300kPa	2.021	0.083	0.870
CU_38_Lab_NoFiber_500_300kPa	1.994	0.078	0.870
CU_38_Lab_NoFiber_500kPa	1.882	0.075	0.870
CU_38_REC_150kPa_2	2.260	0.144	0.990
CU_38_REC_450_200kPa	2.317	0.144	0.920
CU_38_REC_500 _125	2.128	0.110	1.100
CU_38_REC_500	2.300	0.142	0.830
CU_100_Insitu_Fiber_50kPa	1.900	0.024	0.970
CU_100_Insitu_Fiber_100kPa	1.900	0.034	0.970
CU_100_Insitu_Fiber_150kPa	1.900	0.034	1.080
CU_100_Insitu_Fiber_500kPa	2.070	0.055	0.520
CU_100_Lab_Fiber_100kPa	1.720	0.048	0.920
CU_100_Lab_Fiber_150kPa	1.865	0.060	0.920
CU_100_Lab_Fiber_300kPa	1.892	0.061	0.850
CU_100_Lab_Fiber_500kPa	1.884	0.059	0.890

Figure 10-63. present the normalised stress paths of all specimens observed to reach critical state with regards to its individual critical state parameters. As observed from other adopted normalisation methods as well, it has been possible only for the reconstituted specimens to determine a full state boundary surface. As for the fibre reinforced, unreinforced and in-situ samples, tests with higher confining stresses were necessary. Therefore, for those samples the Hvorslev Surface was determined. Even though each specimen was normalised with regards to different critical state parameters, it can be seen that each individual group of soil (reinforced, unreinforced, reconstituted and in-situ) are reaching the M value determined for each group.

In agreement with the previous two normalisation methods, the reconstituted specimens are constructing the smallest boundary surface, followed by the reinforced, unreinforced and, with the largest boundary surface, the In-situ specimens.

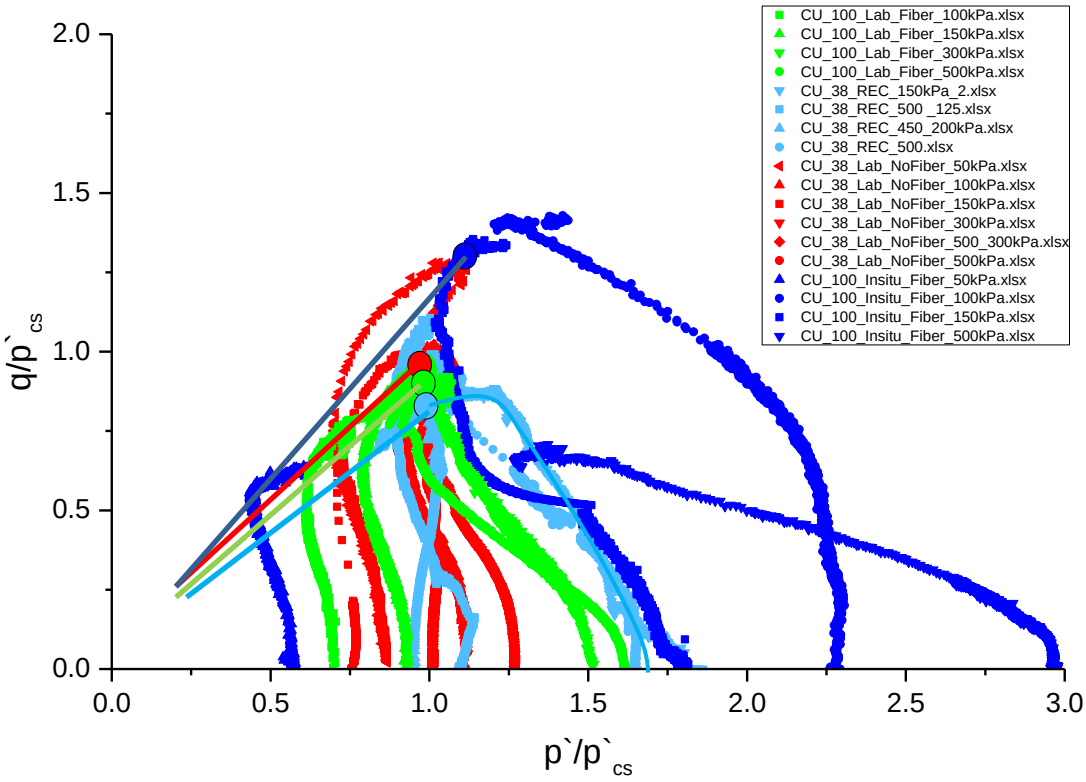

Figure 10-63. Normalised state paths for ALL samples via individual NCL and CSL of specimens

On Figure 10-64, all the specimens were further normalised by their individual M values. Once again, it can be seen that in-situ specimens are constructing a coherent and complete boundary, despite some of the problems found during testing.

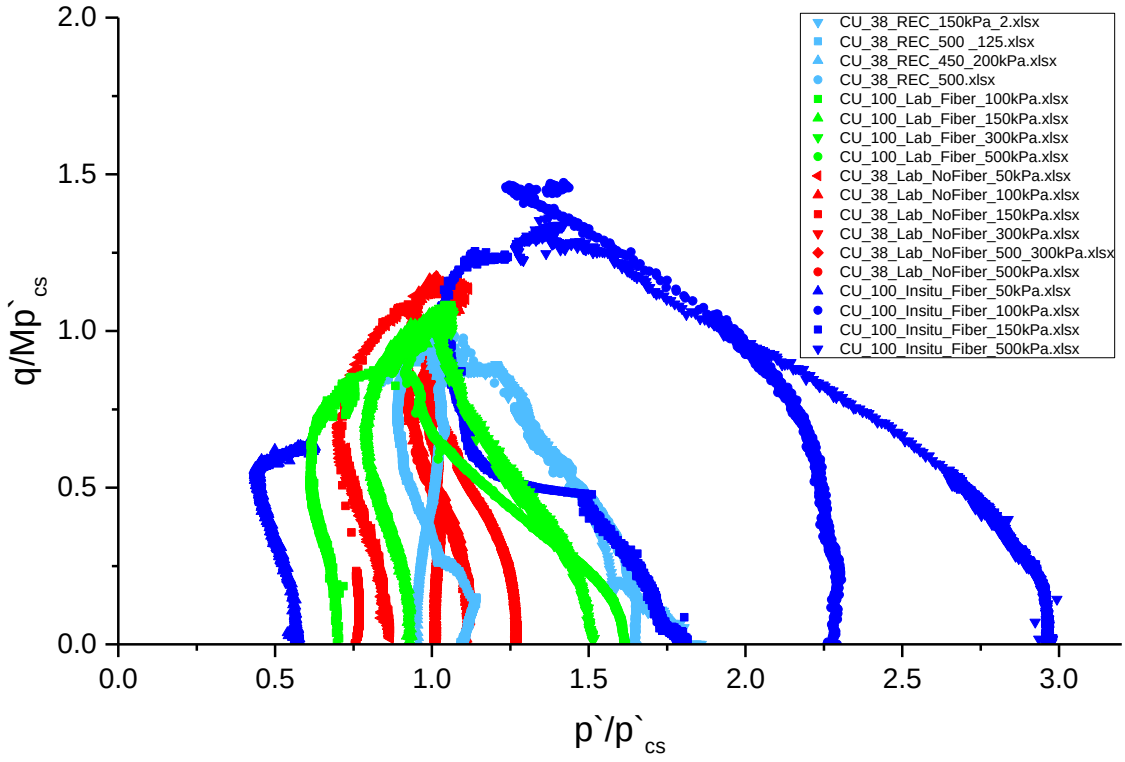

Figure 10-64. Further M Normalised state paths for ALL samples via individual NCL and CSL of specimens

11. SMALL STRAIN BEHAVIOUR

11.1 Introduction

In this chapter, the small strain behaviour of the reconstituted, reinforced, unreinforced and in-situ Lambeth group clay samples are examined using Bender Elements on a modified oedometer cell and using the internal strain measurements available on the triaxial equipment. 6.2.3.

11.2 Shear Stiffness in One – Dimensional compression

Figure 11-1 demonstrates the influence of the fibre inclusion on the elastic shear modulus, plotted against the effective vertical stress for the reinforced and unreinforced samples. It can be observed that there is a linear relationship between the vertical stress and the elastic shear modulus for both soils reinforced and unreinforced. The results also show that the inclusion of fibres reduce the elastic shear modulus of the reinforced soil for every vertical stress.

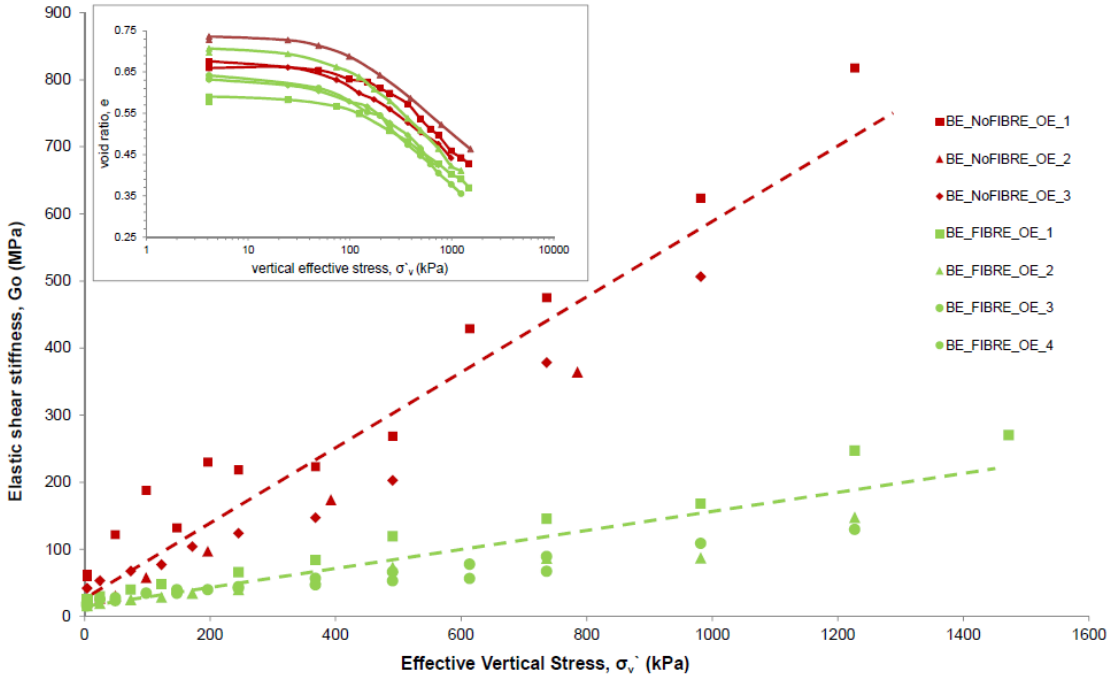

Figure 11-1.Relationship between G_0 and σ_v` in One-Dimensional compression test of reinforced and unreinforced specimens

Figure 11-2 shows the influence of fibre inclusion on the elastic shear modulus plotted against the void ratio on a logarithmic scale. It is clear that the elastic stiffness increase with the reduction in void ratio for both types of samples. It also shows that, for any particular void ratio, the stiffness of the reinforced samples is lower than the stiffness of the unreinforced ones. In other words, it appears that, to achieve a similar elastic modulus, the fibre reinforced samples are compressing more than the unreinforced ones.

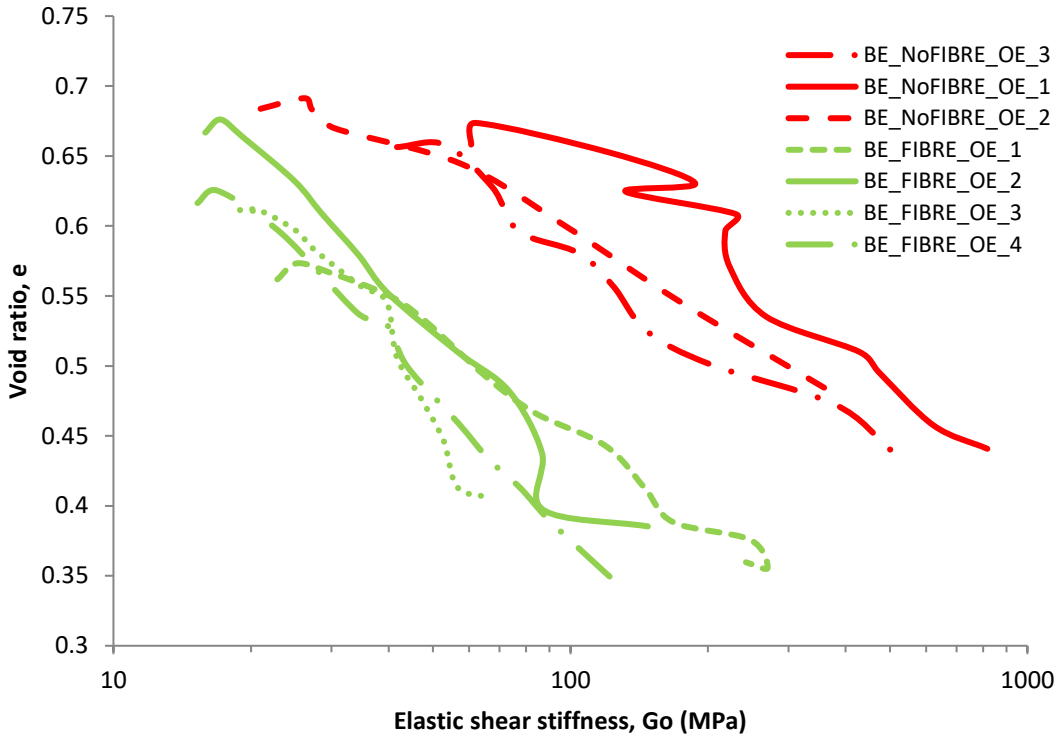

Figure 11-2. Relationship between e and G_0 in One-Dimensional compression test of reinforced and unreinforced specimens

This phenomenon can be also due to drainage path that fibres create in samples as Jardine (1992) reported that drainage is affecting the elastic shear stiffness.

Figure 11-3 presents all the available one dimensional bender element test data with a logarithmic scale on both axis. This figure shows that the values are not converging to a unique line, showing a pattern of behaviour different than the one presented by Lohani et al. (2001) in Figure 11-4, where samples located on the NCL define a boundary for the values of the elastic shear modulus. These results, therefore, indicate that the samples have not reached a unique normal compression line. Given the transitional nature of this material, each compression test would define a different boundary, as can be seen in Figure 11-3, where each curve appears to be parallel to each other.

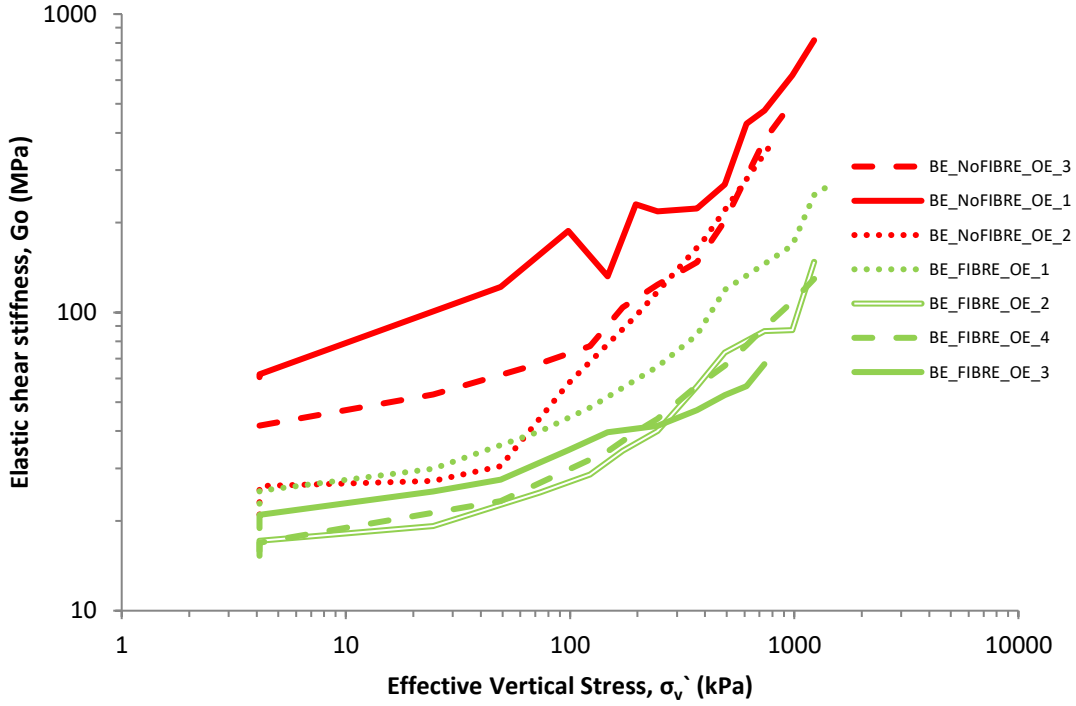

Figure 11-3. log Relationship between G_0 and σ_v` in One-Dimensional compression test of reinforced and unreinforced specimens

Moreover, specimens converge to a unique line at higher confining pressure (unique line mentioned by Jovičić & Coop (1998) which might be due to low stress level used in testing. An example of the effect of delayed convergence due to different densities for reinforced and unreinforced samples can be seen in Figure 11-3, where unreinforced specimens needs much higher level of vertical stress to converge to the final NCL. Even though the addition of fibres has little effect on the stiffness of the soil, the behaviour is solely attributed to the different initial densities of the two samples.

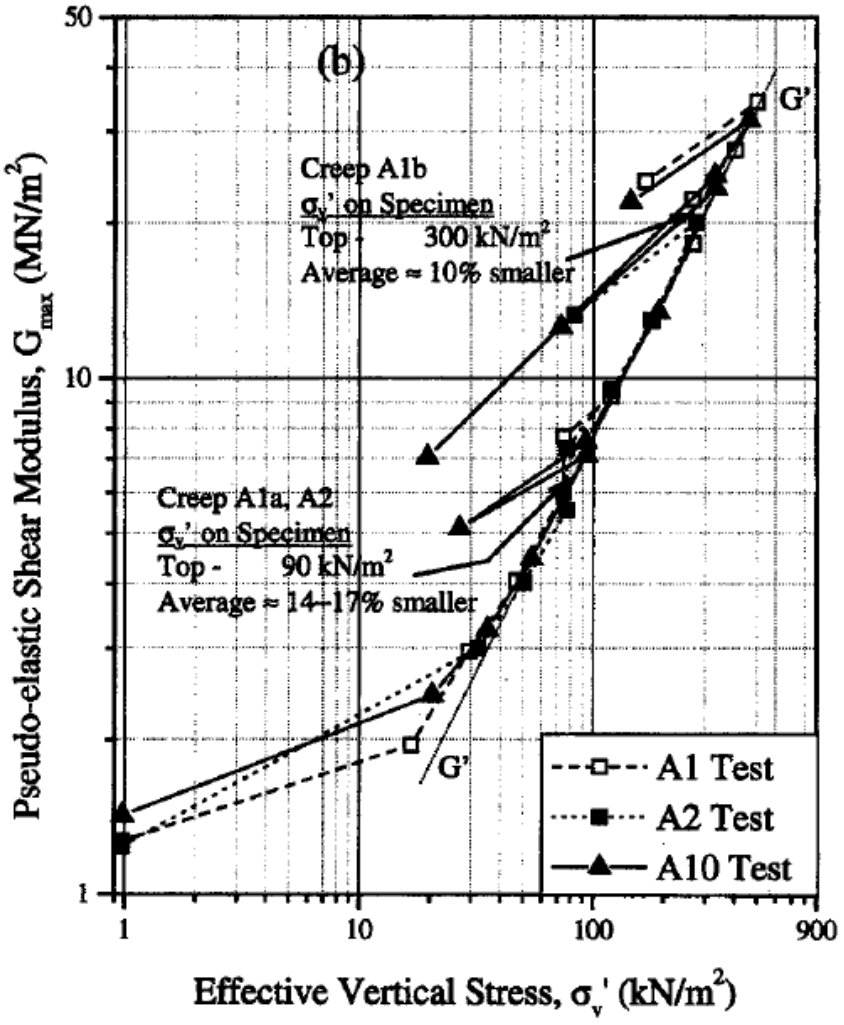

Figure 11-4. log Gmax vs sig v` (Lohani et al. 2001)

11.3 Monotonic Shear Moduli

The initial stiffness was calculated by using deviator stress with shear strain of the consolidated undrained triaxial tests. Internal LVDTs attached to sample have been used as described by Jardine et al. (1984) for undrained secant shear stiffness calculations.

Figure 11-5 shows the undrained shear modulus, G_u, calculated for the reconstituted specimens. It was expected to see confinement effect on the tested specimens. However, samples REC150 and REC500 seems to show similar stiffness degradation curves. The reason for this might be due to variations in local strain measurements as mentioned in Section 4.2.1. Additionally, it was expected that both overconsolidated samples, REC450_200 and REC500_125, would follow a similar degradation curve and a stiffer

response then sample REC150. Where sample REC450_200 had responded in an expected way, however, sample REC500_125 showed a lower stiffness response than all other samples. Additionally, this contrast in behaviour is likely to be due to the different initial density of the specimens. It has not been possible to locate the Y_1 surface, since more precise strain measurement were required in such material.

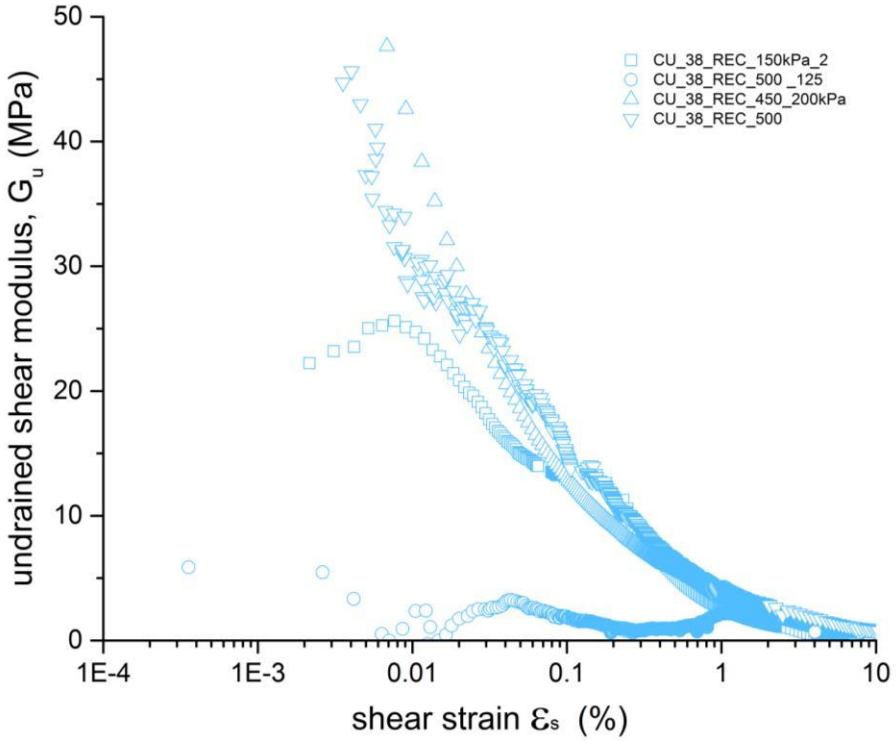

Figure 11-5. Shear modulus degradation curves for undrained reconstituted samples.

As can be seen in Figure 11-6 there is a good correlation between confining pressure and stiffness for the unreinforced specimens. This is particularly clear for strains higher than 0.02%, where the stiffness is proportional to the confining stress. The sample tested at 500kPa of confining stress (UNF500) shows lower values of stiffness for strains below 0,02%; this is due to the local instrumentation as the LVDTs were returning measurements that indicated that the sample was not deforming in an homogeneous way.

Similar behaviour has been observed on the stiffness degradation curves of the drained tests performed on the unreinforced samples, as seen in Figure 11-7, i.e. the initial stiffness is proportional to the confining stress. It is important to mention that, two samples were tested at 100kPa of confining pressure, one with 38mm and another with

100mm in diameter. The sample with 100mm diameter displays the largest stiffness at small strains, although the difference is not very large. The results are similar to Gasparre et al. (2007b), where the degradation curves of different sample size specimens were found to be similar.

Figure 11-8 present the stiffness degradation curves for the reinforced samples in undrained conditions. It can be seen that, for lower strains, samples UF150 and UF300 have similar stiffness values above the values determined for sample UF500. Sample UF100, however, presented a much lower initial stiffness than the rest. At large strains, the response changes and all samples present stiffness values that are proportional to the confining stresses, i.e. higher confining stresses higher stiffness values for similar strains. Similarly to the reconstituted specimens, it has not been possible to locate Y_1 surface since lower strain measurement was required.

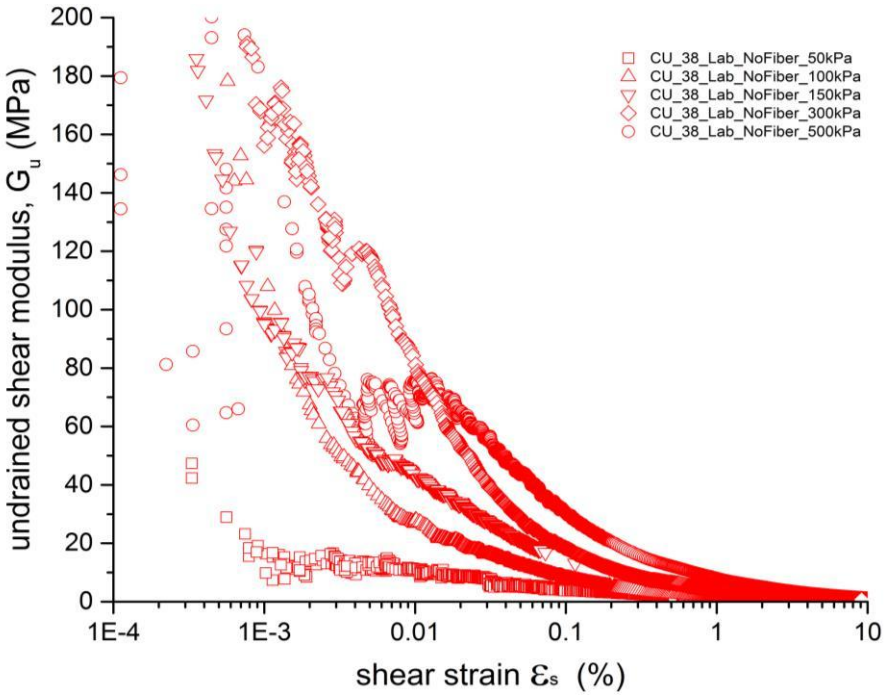

Figure 11-6. Shear modulus degradation curves for undrained unreinforced samples.

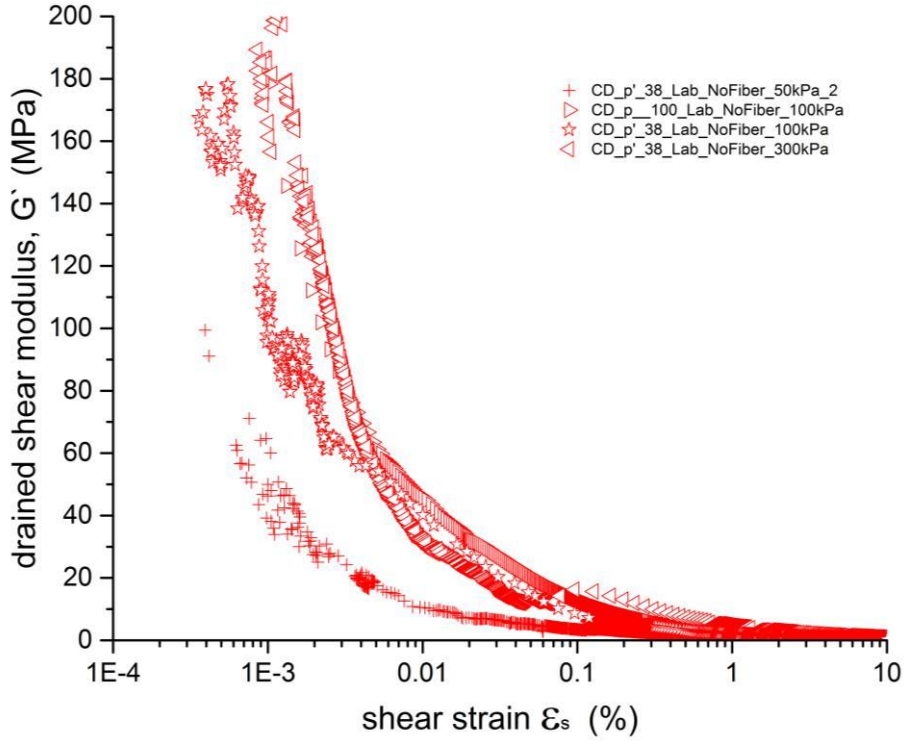

Figure 11-7. Shear modulus degradation curves for drained unreinforced samples.

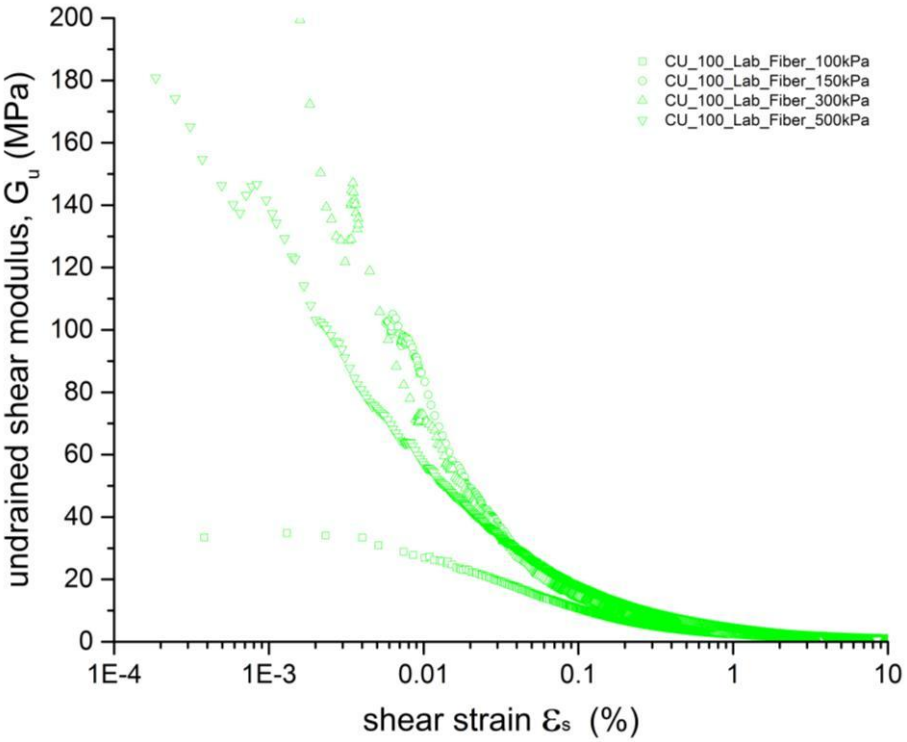

Figure 11-8. Shear modulus degradation curves for undrained reinforced samples.

Unlike the undrained tests on fibre reinforced samples, the effect of confining pressure was monitored in drained tests(Figure 11-9). In addition, a flat region, which indicates the linear elastic behaviour at low strain levels, can be defined in these samples. Such response allowed the determination of the elastic region. Y_1 surface of the fibre reinforced samples can be defined because of the slickenside surface as mentioned to act like forming shear surfaces similar to re-shearing. As stated in literature the re-shearing of previously shear surface caused reduction in stiffness. However due to the textured surface of the unreinforced specimens the increase from the reference material have been monitored.

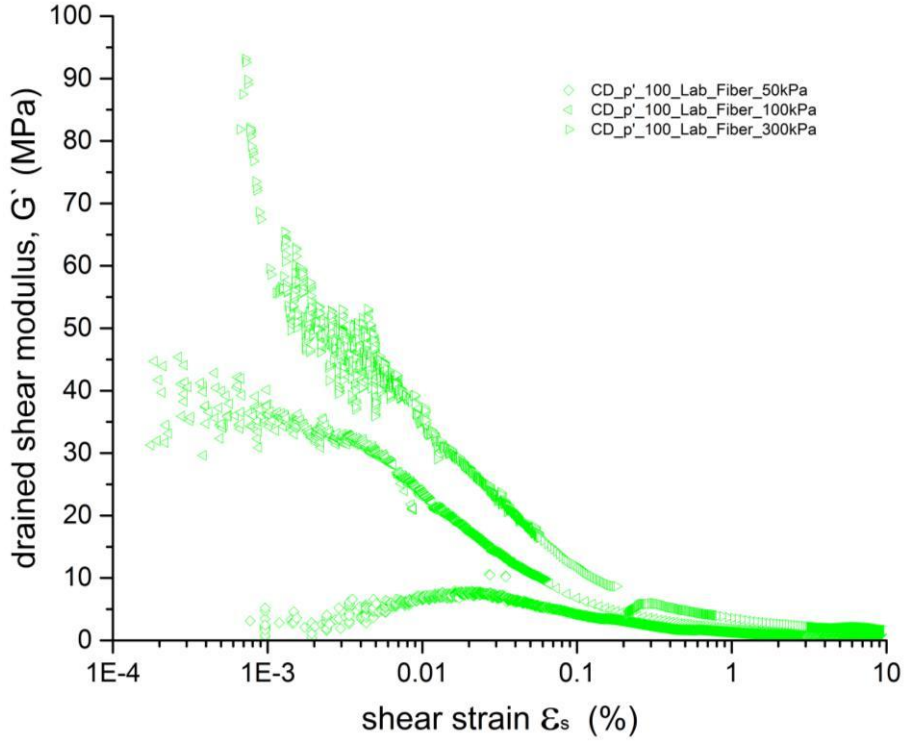

Figure 11-9. Shear modulus degradation curves for drained unreinforced samples.

The stiffness curves for the in-situ samples are presented in Figure 11-10. Low confining specimens, INS50, INS150 and INS500 have very similar initial stiffness, clustering with a large scatter, making it difficult to spot the differences in behaviour. Sample INS100 plotted high above the other samples and has not shown a linear elastic response at small strain levels. It is also worth mentioning again that this particular samples had a variety of problems due to site preparation method applied.

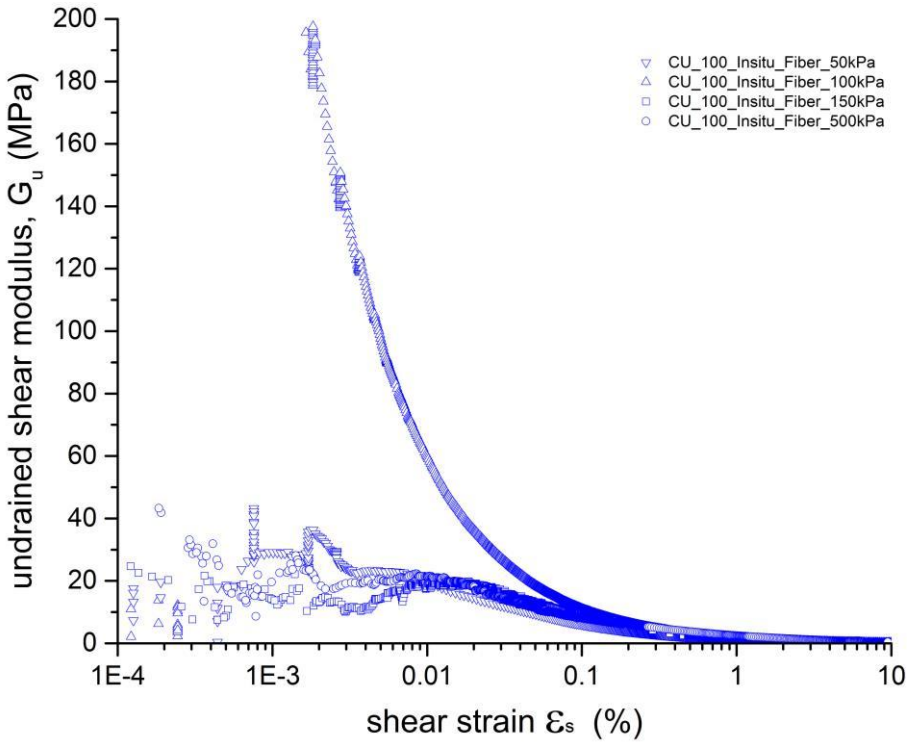

Figure 11-10. Shear modulus degradation curves for undrained in-situ samples.

11.4 Discussion and Comparison

Contrary to the findings of Maher and Woods (1990) and Heineck et al (2005), mentioned in literature section, it can be seen on Figure 11-11 that the fibre reinforced samples show a stiffer behaviour when compared with the unreinforced samples. This behaviour indicates that the tensile strength of the fibres starts being mobilized at small strains, most likely even during consolidation.

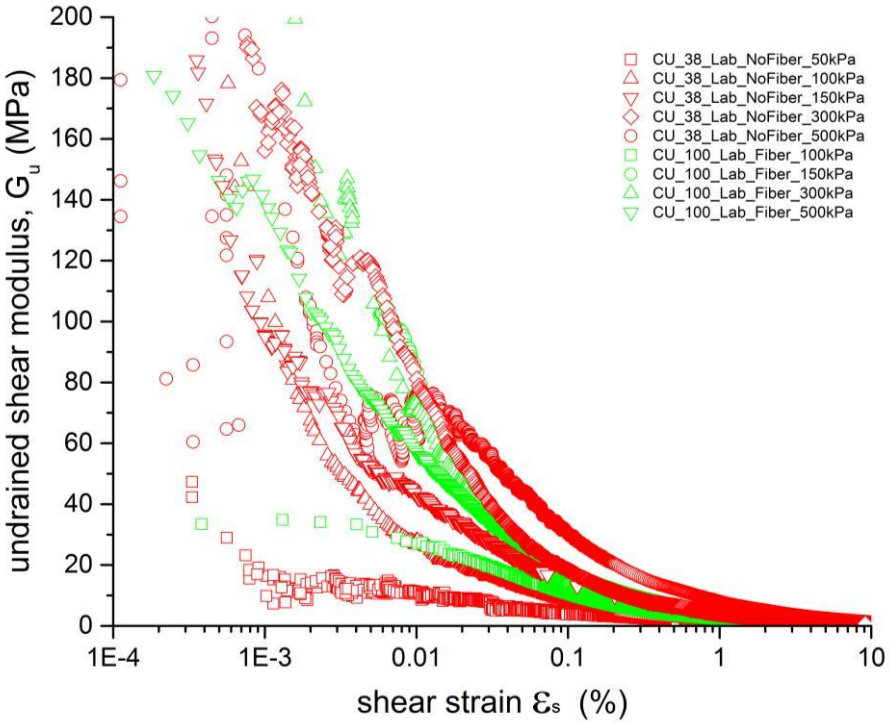

Figure 11-11. Comparison of undrained secant shear degradation curves of fibre reinforced and un-reinforced specimens

Furthermore, the facts presented in Consoli et al. (2002) about the influence of the confinement in initial stiffness have been also monitored in unreinforced samples, where increase in confinement leads to an increase in the initial shear stiffness of the sample. Adversely, in reinforced samples, the effect of confinement is not pronounced.

In order to investigate the variation of stiffness with the effective confining pressure, the shear modulus of the drained and undrained tests of the reinforced, unreinforced and in-situ samples have been plotted against the mean effective stress at two specific strain levels: 0.01% and 0.1% (Figure 11-12). In order to be able to incorporate experiments with both high and low confining pressures in the same plot, a logarithmic scale was

used for both axes. This does not distort in any way the shape of the potential trend formed but merely allow all results to be plotted and compared in a single graph.

Figure 11-12 shows the equivalent monotonic shear modulus at shear strain of 0.1%. graph represent only the undrained plots of all specimens. The stiffness's in within a narrow band that is almost linear. Figure 11-12 shows that the reinforced samples, at low confining pressures, are showing a higher initial stiffness whilst for the higher confining pressures the unreinforced samples show the highest stiffness values. This phenomenon is in agreement with the stress strain behaviour of the reinforced and unreinforced specimens, presented in section 10.6.1.1. Additionally, this is showing that the fibres are starting to be mobilised at small strain levels.

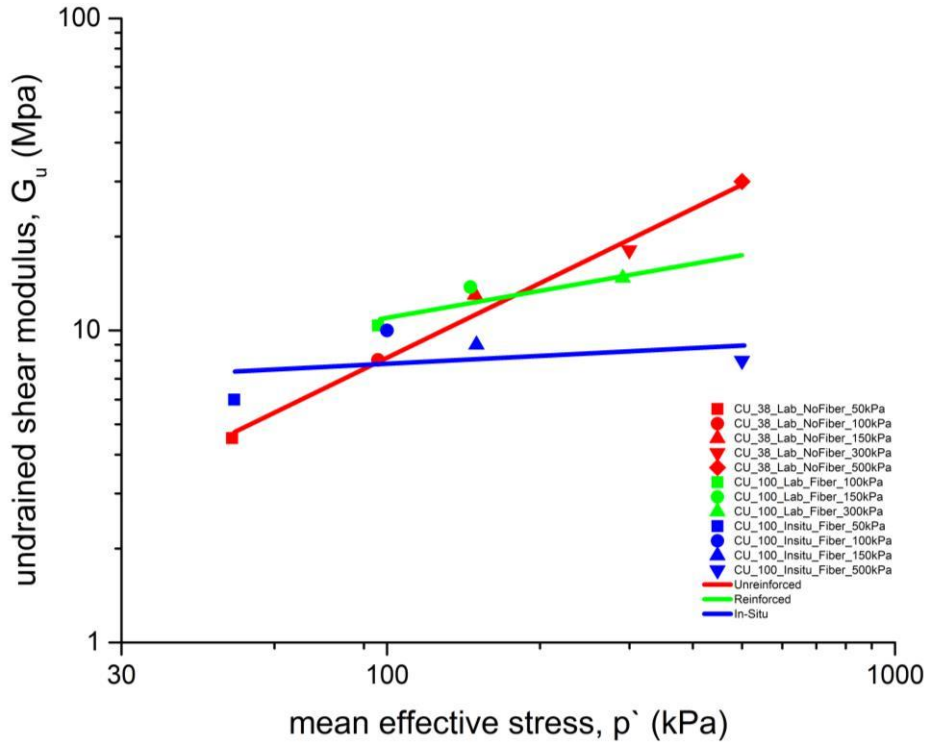

Figure 11-12. Undrained shear modulus @ 0.1% ε_s – undrained reinforced, unreinforced and in-situ sample comparison – undrained shear modulus trends

Furthermore, the in-situ specimens are showing a linear relationship, parallel to the reinforced specimens, at lower initial stiffness. Where, if compared to the unreinforced trend, only at lowest confinement the in-situ samples are showing higher shear modulus.

Figure 11-13 shows the shear moduli at 0.1% strain level, for the drained tests on reinforced and unreinforced specimens. The data reveals that the shear modulus of the reinforced specimens is higher than the unreinforced for all effective stress levels. Additionally, both specimen trend lines have similar slopes with a slight offset. As seen in the results from the undrained specimens, the larger differences in stiffness are at lower confinements, decreasing as the confinement stress increases.

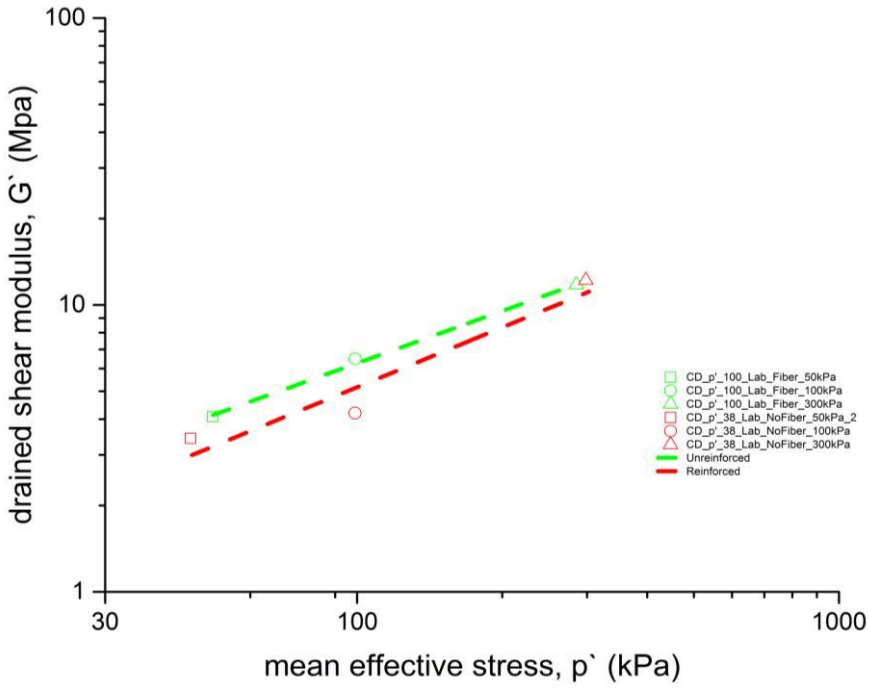

Figure 11-13. Drained shear modulus @ 0.1% ε_s – drained reinforced and unreinforced sample comparison - drained shear modulus trends

Figure 11-14 presents the results of all undrained and drained tests for a strain of 0.1%. It is clear that the drained tests have lower stiffness than the undrained tests. Additionally, when comparing the slopes of the trend lines, it seems that the trend lines of the drained tests and the undrained unreinforced are parallel for this particular strain. The results are revealing that the effect of fibres is more effective in undrained conditions, at low confinement and at 0.1% strain. It can be seen that the fibre reinforced soil has a critical confinement pressure where, above, the stiffness of the reinforced soil is lower than the unreinforced. For pressures below this critical value, the reinforced soil shows higher stiffness values. This critical confinement is between 170 to 200 kPa for the undrained condition. The drained tests seem to show that

something similar may happen at a stress of around 300kPa, however tests at higher stresses are necessary to confirm this.

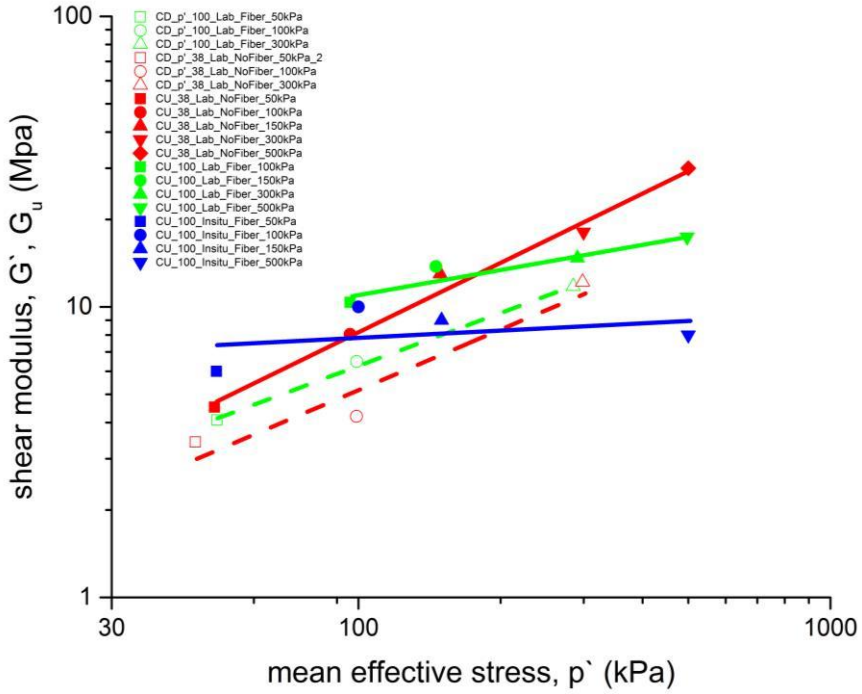

Figure 11-14. Drained and undrained shear moduli @ 0.1% ε_s– ALL sample comparison – drained and undrained shear modulus trends

Figure 11-15 shows the equivalent monotonic shear modulus at a shear strain of 0.01%. The graph presents only the undrained plots of all specimens. The stiffness's are within a wider band than the values determined for 0.1% strain. At lower strains, the values seem to be reaching a plateau with the increase in confinement. There may be some scatter at such small strain levels, related to the local LVDTs.

It is easier to see a linear relationship between the confining pressure and the shear modulus for the unreinforced specimens than for the other groups of specimens. The results show that, at small strains, the reinforcement seems to provide a constant stiffness value for stresses larger than 150kPa; the response of the in-situ specimens is also similar, however with a larger scatter. This is also visible at 0.1% (Figure 11-14). Where this behaviour is not usual as increase in confinement expected to increase the monotonic shear modulus therefore such respond of specimens can be attributed to the initial density of the sample.

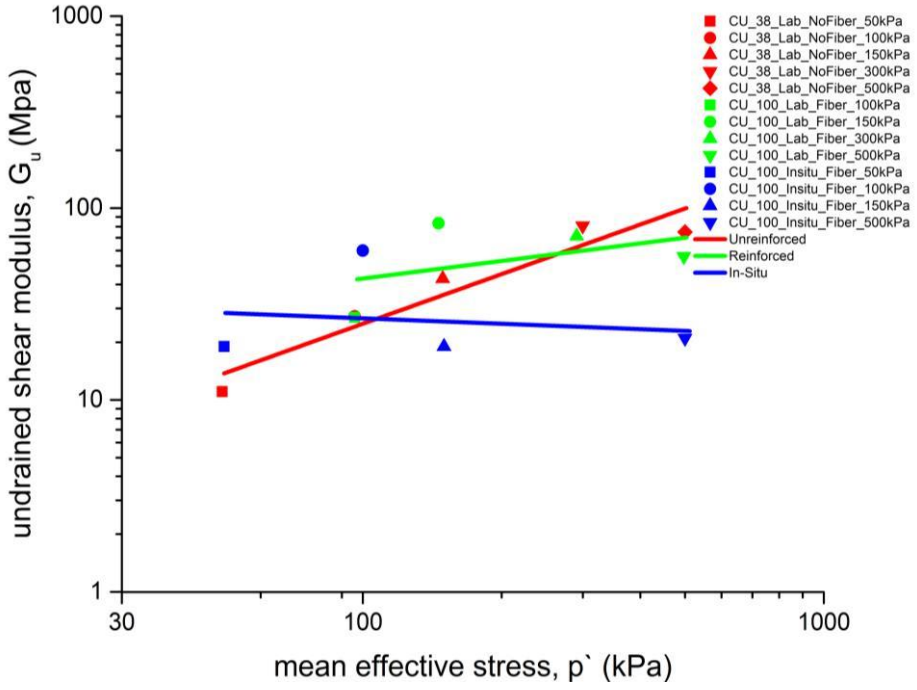

Figure 11-15. Undrained shear modulus @ 0.01% ε_s – undrained reinforced, unreinforced and in-situ sample comparison – undrained shear modulus trends

Evaluating the drained condition on reinforced and unreinforced specimens (Figure 11-16) shows that at low confinement levels the unreinforced samples show higher shear modulus then the reinforced ones and as the confinement of samples increase the behaviour of the groups converge to a similar level of shear modulus.

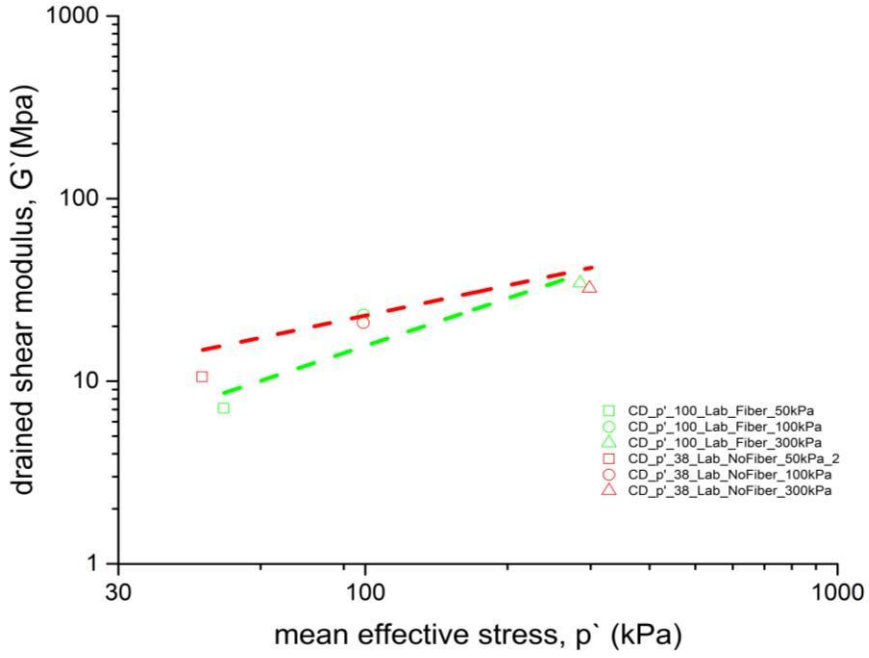

Figure 11-16. Drained shear modulus @ 0.01% ε_s – drained reinforced and unreinforced sample comparison - shear modulus trends

Finally, the evaluation of all reinforced and unreinforced samples on a single space with drained and undrained condition shows that, similarly to the 0.1% strain evaluation, the drained specimens plot below the undrained specimens. These also seem to reach a constant shear modulus at high confining pressures. This was also observed at 0.01% strain level.

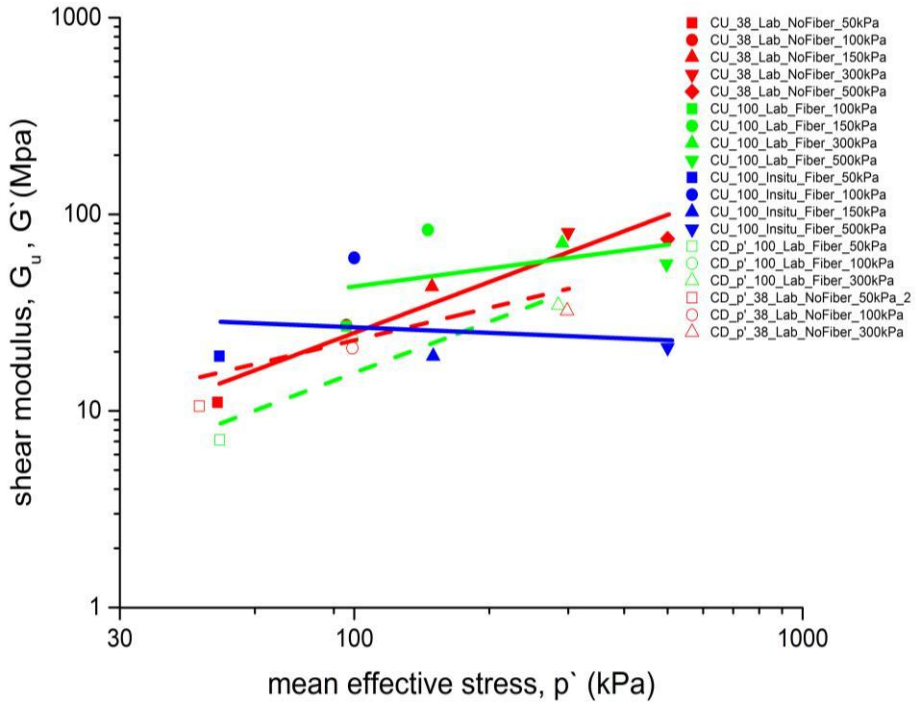

Figure 11-17. Drained and undrained shear modulus @ 0.01% ε_s – ALL sample comparison - shear modulus trends

12. CONCLUSIONS

12.1 FIBRE ALIGNMENT STUDIES

The study performed on the fibre alignment have revealed that nearly 80% of fibres are aligned within ±20º with the horizontal plane. This is a consequence of the sample preparation procedure, since the fibre length is longer than the thickness of a compacted layer in the sample.

Hight et al. (2004) reported that the Lambeth group clays are heavily fissured. Although it can be initially thought that, due to the sample preparation method developed, where natural samples are chopped into 15 to 20 mm peds, fissures were destroyed. However, due to compaction technique and the presence of peds and fibres a new fissuring pattern seem to be introduced into the samples. This is clearly shown in the fibre orientation study as it was observed that these fissures are aligned horizontally, where the fibres within the sample are located and tend to be oriented with the horizontal plane.

Hight et al. (2007) and Vitone & Cotecchia (2011) reported that fissuring intensity, extend, orientation, fissure spacing and the fissuring surfaces are important parameters, influencing the effective stress parameters of the soil. Such parameters were found to remain constant due to the adapted preparation method. The introduction of fibres caused changes on some of the fissuring properties listed above, believed to have lead to a change in the mechanical response of the soil as concluded in the following sections. Unreinforced specimens are believed to have a mat fissuring surface and discontinuous fissures due to the compaction of peds. Whereas reinforced specimens have slickensides and polished fissures given the presence of fibres in the fissures. Additionally, due to length of fibres peds are connected to each other resulting in longer fissure length.

Therefore, these are likely to be the cause of a decay in the mechanical properties of the reinforced clay.

12.2 SHRINKAGE STUDIES

The experimental data from this part of the research work shows that:

- Regardless of the different fibre content, the reduction in mass is mostly influenced by the initial compaction moisture content of the samples.

- The contribution of the fibres is more pronounced in the height of the samples as reinforced samples had a lower reduction in height due to desiccation. This behaviour is attributed to the fibre alignment due to the compaction process.

- Increasing fibre content leads to a reduction in the volumetric due to improvement in the soil tensile strength.

- Finally the visual observations clearly show that fibre reinforcement is effective in resisting and reducing desiccation cracking.

12.3 COMPRESSION BEHAVIOUR

One dimensional compression response of the specimens revealed that it is not possible to estimate a distinct normal compression line (NCL) for the fibre-reinforced and non-reinforced clay samples. It can be seen that the unreinforced specimens are following different but parallel compression lines for each initial void ratio. However, the reinforced specimens seem to converge to a unique NCL, making the determination of Cc difficult. Such response of the soil seems to be due to the transitional behaviour of the compacted peds. It could be argued that the current stress levels are not enough to reach a unique NCL, particularly in the case of the reinforced specimens, where a NCL could not be reached for void ratios as low as 0.2, however it is believed that, at this density, the NCL would start becoming flatter and the concept of a unique NCL would lose its meaning. It is, however, clear that the addition of reinforcement seems to reduce drastically the transitional behaviour effect for the samples tested.

Irrespective of the addition of fibres, the combination of compaction induced fissuring with the clay microstructure is found to weaken the clay in comparison with the reconstituted soil in the one-dimensional space. Additionally, the weakening effect on one-dimensional consolidation can be seen regardless of the reinforcement where specimens are yielding before reaching the ICL.

A comparison of the isotropic compression line between the 38mm and 100mm samples revealed that the Compression line of both specimens seams to yield the same compression line, indicating no sample size effect.

In isotropic compression, reinforced samples are yielding at higher stresses than the unreinforced specimens. Nevertheless, the yielding is occurring on the left side of the intrinsic compression line, showing a weaker behaviour. Furthermore, by comparing the location of the reinforced and unreinforced yielding points' it can be concluded that, in isotropic compression, fibres seem to allow the soil to reach a higher p' for a given specific volume. This response shows a change in behaviour when compared to the 1-D compression. Similar behaviour, regarding the intensive fissuring scales, have been observed by Vitone & Cotecchia (2011).

12.4 LARGE STRAIN BEHAVIOUR

The analysis of the data from Chapter 10 allow the formulation of the following conclusions:

At low confining stresses, the reinforced samples showed higher shear strength than the unreinforced samples; for stresses higher than 150kPa, the presence of fibres tends to degrade the shear strength and the shear strength of the unreinforced samples is higher than the reinforced ones.

Drained tests on reinforced specimens show slightly higher contraction, followed by a dilative behaviour when compared to the unreinforced samples, consequently, a tendency to generate higher excess pore water pressures when undrained.

The evaluation of the failure mechanisms of the specimens shows that the addition of reinforcement changes the failure mode of the specimens by transferring stresses to

other areas of the sample and restricting the formation of a shear plane. The end of test inspection of the specimens revealed that the fibres are not stretching or braking but sliding, causing small shear surfaces within the soil sample.

The moisture content data collected at the end of the shearing revealed that samples failing by barrelling (reinforced) have a uniform distribution of moisture content throughout the sample. Whilst samples that have failed with the occurrence of a shear plane, have higher moisture contents where the shear surface is located (in certain cases the differences of 3% were observed) reducing towards the ends of the sample.

During shearing, it has been observed, in all three normalisation methods, that the reinforced specimens are constructing a Hvorslev surface that is lower than the unreinforced one, this is clearly seen by the location of the CSL points. As described above, changes in fissure dimension and fissure surfaces might led to such behaviour.

When the samples are normalised by the critical state line determined for the group of specimens, the boundary surface formed by the reinforced samples lies below the boundary surface of the reconstituted soil. However, the boundary surface of the unreinforced samples lies above the reconstituted one. This is characteristic of intensely fissured clays according to Vitone & Cotecchia (2011).

The increase in the boundary surface for the unreinforced samples is attributed to the contact between peds, forming a matt surface, whilst the lower boundary surface of the reinforced samples is attributed to the fibres existing in between the peds, creating polished surfaces, therefore mobilising lower friction forces and reducing the size of the boundary surface of the material. These results are similar to Fearon & Coop (2002) and Vitone & Cotecchia (2011) where the nature of the fissures dominates the soil behaviour and consequently the location of the state boundary surface.

The Hvorslev surfaces of the unreinforced, in-situ and reinforced samples were defined as parallel lines, particularly since the in-situ specimens, after shearing, only had a few fibres crossing the shear surface and, in some occasions, none; indicating that the in-situ soil should be behaving similarly to the unreinforced soil.

Normalisation with regards to the group critical state line was found to be the least successful, due to the normalisation of the unreinforced specimens. This was caused by the difficulty in determining a unique CSL for the unreinforced specimens, particularly since some of the results indicate that more than one CSL exist.

The results of the reinforced, unreinforced and in-situ specimens seem to show that the CSL is not unique but proportional to the initial void ratio of the samples tested as shown previously by Ferreira and Bica (2006) and Ponzoni et al. (2014). Similar observation was made for the 1-D compression with regards to the NCL. Hence there is a strong evidence that the sample preparation method, generates a transitional material.

Even though the initial specific volumes of the samples are different and there may be a tendency to follow a set of parallel NCLs, the normalisation of all specimens with the ICL was the most successful. It showed that it is possible to determine a state boundary surface for the reconstituted soil and state boundaries, related to the stress levels tested, for the other materials. The definition of the full state boundary surface of these soil will require tests done at higher stresses.

12.5 SMALL STRAIN BEHAVIOUR

The addition of fibres eliminated the effects of confinement on the initial stiffness of soil. Furthermore, it can be concluded that the presence of fibres, at high confinements, tends to degrade the strength and stiffness of the clay.

In 1-D compression, the results show that the inclusion of fibres reduce the elastic shear modulus of the reinforced samples. It is also observed that the effect of fibre inclusion on the elastic shear modulus appears to be most significant in high stress levels.

Similar to the strength, the data shows that the fibre reinforcement has a critical confinement pressure, between 170 to 200 kPa, above this pressure the fibres reduce the initial stiffness of the soil, whilst below the shear modulus is higher than the unreinforced soil. The critical confining pressure was seen to be different for the drained case and more drained tests are required to properly define this pressure. This pressure was also found to change with regards to the shear strain, where at 0.01% strain level, the critical confining pressure was found be higher than the 0.1% strain, found to be

around 250kPa. Evaluating the drained condition on reinforced and unreinforced specimens, show that, at low confinement levels, the unreinforced samples show higher shear modulus then the reinforced ones and, as the confinement stress increases, the behaviour of groups converge to a similar level of shear modulus.

13. FUTURE WORK

It was observed that the unreinforced (ped compacted) and reconstituted specimens of the tested soil are determining similar boundary surfaces, similar to the natural London clay tested by Gasparre (2005). Where such finding indicates that the peds are retaining the structure of the natural specimen. Nevertheless, in order to properly explain such hypothesis undisturbed specimens of the same unit of Lambeth group clay should be tested to determine the intact behaviour of this particular soil group.

As concluded, the incorporation of fibres in the soil degrades the mechanical properties of the ped compacted specimen, via the introduction of polish surfaces between the peds. Further study should be commenced with regards to different fibre content, in order to verify if this would reduce the boundary surface even further. Furthermore, a scanning electron microscopy analysis should be performed on compacted specimens with and without fibres, before and after shearing. This will allow the understanding of the fissuring mechanism with the two different surface properties, matt and polished.

Based on the theory, the normal compression line should be a unique line that lies parallel to the critical state line. In the case of reinforced and unreinforced specimens, unique NCL was not found even at lower void ratios which is the characteristic of transitional soils. Further research should be carried out with other overconsolidated clays using the same preparation method and different compaction efforts. This would clarify if all overconsolidated clays, when compacted, present a transitional behaviour or not.

Additionally, as have been monitored, the Roscoe surfaces of the reinforced and unreinforced specimens could not be determined. This might be a result of the apparent high “overconsolidation ratio” of the materials or the low stress levels used in the tests. Therefore, specimens prepared in the same way should be tested at higher confining pressures, to determine the complete state boundary surfaces.

REFERENCES

Abbiss, C.P., 1981. Discussion: A comparison of the stiffness of the chalk at Mundford from a seismic survey and a large scale tank test. *Géotechnique*, 31(4), pp.561–563.

Abdi, M.R., Parsapajouh, A. & Arjomand, M.A., 2008. Effects of Random Fiber Inclusion on Consolidation , Hydraulic Conductivity , Swelling , Shrinkage Limit and Desiccation Cracking of Clays. *International Journal of Civil Engineering*, 6(4), pp.284–292.

Ahmed, I., 1993. Laboratory Study on Properties of Rubber-Soilsm. *Joint Highway Research Project, Indiana Department of Transportation and Purdue University, West Lafayette, Indiana*.

Al-Akhras, N.M. et al., 2008. Influence of fibers on swelling properties of clayey soil. *Geosynthetics International*, 15(4), pp.304–309.

Albright, W.H. et al., 2004. Field water balance of landfill final covers. *Journal of environmental quality*, 33(6), pp.2317–2332.

Al-Rawas, A.A. & McGown, A., 1999. Micro structure of Omani expansive soils. *Canadian Geotechnical Journal*, 2(36), pp.272–290.

Al-Tabbaa, A. & Aravinthan, T., 1998. Natural clay-shredded tire mixtures as landfill barrier materials. *Waste Management*, 18(1), pp.9–16.

Ang, E. & Loehr, J., 2003. Specimen Size Effects for Fiber-Reinforced Silty Clay in Unconfined Compression. *Geotechnical Testing Journal*, 26(2), p.10410.

ASTM, 1993. Standard classification of soils for engineering purposes. *ASTM D 2487-93*, Philadelph.

Atkinson, J.H. & Bransby, P.L., 1978. *The mechanics of soils, an introduction to critical state soil mechanics*, London: McGraw-Hill Book Co.

Baudet, B., 2009. *Lecture Notes; Advance Soil Mechanics Lecture Notes*, University

College London, London.

Bishop, A.W. & Little, A.L., 1967. The influence of the size and orientation of the sample on the apparent strength of the London Clay at Maldon, Essex. In *Proceedings of Conference in Shear Strength Parameters of Natural Soils and Rocks*. Oslo, pp. 89–96.

Bishop, A.W. & Wesley, L.D., 1975. A hydraulic triaxial apparatus for controlled stress path testing. *Géotechnique*, 25(4), pp.657–610.

Boots M, E., 1986. *The Effects of Slaking on the Engineering Behavior of clay Shales*. Thesis. University of Colorado.

Brackley, I.J.A., 1975. *The interrelationship of the factors affacting heave of an expansive, unsaturated clay soil*. University of Natal.

British Standards Institution, 1990a. BS 1377-2:1990 Methods of test for soils for civil engineering purposes Part 2: Classification tests. *Methods for civil engineering purposes*, (1).

British Standards Institution, 1990b. BS 1377-4:1990 Methods of test for soils for civil engineering purposes Part 4: Compaction-related tests. *Methods for civil engineering purposes*, (1).

British Standards Institution, 1990c. BS 1377-8:1990 Methods of test for soils for civil engineering purposes Part 8: Shear strength tests (effective stress). *Methods for civil engineering purposes*, (1).

Burland, J.B. et al., 1996. A laboratory study of the strength of four stiff clays. *Géotechnique*, 47(2), pp.390–390.

Burland, J.B., 1990. On the compressibility and shear strength of natural clays. *Géotechnique*, 40(3), pp.329–378.

Cai, Y. et al., 2006. Effect of polypropylene fibre and lime admixture on engineering properties of clayey soil. *Engineering Geology*, 87(3–4), pp.230–240.

Carl, F., 1999. Engineering and Design - Guidelines on Ground Improvement for Structures and Facilities. In *Department of the Army US Army Corps*. Washington, pp. 47–67.

Cedergren, H.R., 1977. *Seepage, drainage, and flow nets*, New York: John Wiley.

Cetin, H., Fener, M. & Gunaydin, O., 2006. Geotechnical properties of tire-cohesive clayey soil mixtures as a fill material. *Engineering Geology*, 88(1–2), pp.110–120.

Chen, C.W. & Loehr, J.E., 2008. Undrained and Drained Triaxial Tests of Fiber-Reinforced Sand. , pp.114–120.

Chiu, A.C.F., Zhao, X. & Yuan, J.P., 2010. State Boundary Surfaces for an Aged Compacted Clay. *Journal of Geotechnical and Geoenvironmental Engineering*, 136(9), pp.1251–1262.

Clinton, D.B., 1987. *The determination of soil parameters from stress path tests*. City University of London.

Consoli, N.C. et al., 2002. Engineering Behavior of a Sand Reinforced with Plastic Waste. *Journal of Geotechnical and Geoenvironmental Engineering*, 128(6), pp.462–472.

Consoli, N.C., Casagrande, M.D. & Coop, M.R., 2005. Effect of Fiber Reinforcement on the Isotropic Compression Behavior of a Sand. *Journal of Geotechnical and Geoenvironmental Engineering*, 131(11), pp.1434–1436.

Consoli, N.C., Prietto, P.D.M. & Ulbrich, L.A., 1998. Influence of Fiber and Cement Addition on Behavior of Sandy Soil. *Journal of Geotechnical and Geoenvironmental Engineering*, 124(12), pp.1211–1214.

Coop, M., 2015. Limitations of a Critical State Framework Applied to the Behaviour of Natural and Transitional Soils. In *Deformation Characteristics of Geomaterials - 6th International Symposium*. Buenos Aires, Argentina, pp. 115–155.

Coop, M.R., 2005. On the mechanics of reconstituted and natural sands. In H. Di

Benedetto, ed. *Deformation Characteristics of Geomaterials*. London: A.A. BALKEMA PUBLISHERS, pp. 29–58.

Coop, M.R., 1999. The influence of particle breakage and state on the behaviour of sands. In *International workshop on soil crushability, IWSC '99*. Japan.

Costa-Filho, L.M., 1984. A note on the influence of fissures on the deformation characteristics of London clay. *Géotechnique*, 34(2), pp.268–272.

Cotecchia, F. et al., 2006. The mechanical behaviour of intensely fissured high plasticity clays from Daunia. In *Proc. 2nd Int. Workshop on Characterisation and Engineering Properties of Natural Soils*. Singapore, pp. 1975–2003.

Cotecchia, F. & Chandler, R.J., 2000. A general framework for the mechanical behaviour of clays. *Géotechnique*, 50(4), pp.431–447.

Cripps, J.C. & Taylor, R.K., 1987. Engineering characteristics of British over-consolidated clays and mudrocks, II. Mesozoic deposits. *Engineering Geology*, 23(3–4), pp.213–253.

Cuccovillo, T. & Coop, M.R., 1999. On the mechanics of structured sands. *Géotechnique*, 49(6), pp.741–760.

Cuccovillo, T. & Coop, M.R., 1997. Yielding and pre-failure deformation of structured sands. *Géotechnique*, 47(3), pp.491–508.

Desrues, J. et al., 1996. Void ratio evolution inside shear bands in triaxial sand specimens studied by computed tomography. *Géotechnique*, 46(3), pp.529–546.

Diambra, A. et al., 2007. Determination of fibre orientation distribution in reinforced sands. *Géotechnique*, 57(7), pp.623–628.

Dobry, R. & Ng, T., 1992. Discrete modelling of stress-strain behaviour of granular media at small and large strains. *Engineering Computations*, 9, pp.129–143.

Duncan, J.M., Wright, S.G. & Brandon, T.L., 2014. *Soil strength and slope stability*,

New Jersey: John Wiley & Sons Inc.

Dzulynski, S., 1977. Origin, geological history and environmental factors leading to the development of structurally complex formations. In *Proceedings of the international symposium on the geotechnics of structurally complex formations*. Capri, pp. 157–169.

Ellison, R.A. et al., 1994. A revision of the lithostratigraphical classification of the early Palaeogene strata of the London Basin and East Anglia. *Proceedings of the Geologists' Association*, 105(3), pp.187–197.

Ellison, R.A. & Lake, R.D., 1986. *Geology of the country around Braintree, memoir for 1:50000 geological sheet 223*, London: H.M.S.O.

Esna-ashari, M. & Asadi, M., 2008. A Study on shear strength and deformation of sandy soil reinforced with tire cord wastes. In *Proceedings of the 4th Asian Regional Conference on Geosynthetics*. pp. 355–359.

Fearon, R.E. & Coop, M.R., 2002. The influence of landsliding on the behaviour of a structurally complex clay. *Quarterly Journal of Engineering Geology and Hydrogeology*, 35(1), pp.25–32.

Ferreira, P.M. V & Bica, A.V.D., 2006. Problems in identifying the effects of structure and critical state in a soil with a transitional behaviour. *Gèotechnique*, 56(7), pp.445–454.

Freilich, B., Li, C. & Zornberg, G., 2010. Effective shear strength of fiber-reinforced clays. *9th International Conference on Geosynthetics*, (Icd), pp.1997–2000.

Gasparre, A., 2005. *Advanced Laboratory Characterisation of London Clay*. Imperial College London.

Gasparre, A. et al., 2007. The influence of structure on the behaviour of London Clay. *Géotechnique*, 57(1), pp.19–31.

Gasparre, A. et al., 2014. The laboratory measurement and interpretation of the small-

strain stiffness of stiff clays. *Géotechnique*, 64(12), pp.942–953.

Gasparre, A. et al., 2007b. The stiffness of natural London Clay. *Géotechnique*, 57(1), pp.33–47.

Gens, A., 1982. *Stress-strain and strength characteristics of a low plasticity clay*. University of London.

Grammatikopoulou, A., Zdravkovic, L. & Potts, D.M., 2008. The influence of previous stress history and stress path direction on the surface settlement trough induced by tunnelling. *Géotechnique*, 58(4), pp.269–281.

Harianto, T. et al., 2008. Effects of fiber additives on the desiccation crack behavior of the compacted Akaboku soil as a material for landfill cover barrier. *Water, Air, and Soil Pollution*, 194(1–4), pp.141–149.

Head, K.H., 1998. *Manual of soil laboratory testing. vol. 3*, Chichester: Wiley.

Heineck, K.S., Coop, M.R. & Consoli, N.C., 2005. Effect of Microreinforcement of Soils from Very Small to Large Shear Strains. *Journal of Geotechnical and Geoenvironmental Engineering*, 131(8), pp.1024–1033.

Hight, D.W. et al., 2007. Characteristics of the London Clay from the Terminal 5 site at Heathrow Airport. *Géotechnique*, 57(1), pp.3–18.

Hight, D.W., 1998. Soil characterisation: the importance of structure and anisotropy. In *38th Rankine Lecture, 18 March 1998, British Geotechnical Society*. London: Geotechnique, in preparation.

Hight, D.W., Ellison, R.A. & Page, D.P., 2004. *Engineering in the Lambeth Group*, London: Ciria.

Hill, R., 1963. Elastic properties of reinforced solids: Some theoretical principles. *Journal of the Mechanics and Physics of Solids*, 11(5), pp.357–372.

Holtz, R.D. & Kovacs, W.D., 1981. *An introduction to geotechnical engineering*,

Englewood Cliffs, N.J.: Prentice-Hall.

Hosseini Kamal, R. et al., 2014. The post-yield behaviour of four Eocene-to-Jurassic UK stiff clays. *Géotechnique*, 64(8), pp.620–634.

Ikizler, S.B. et al., 2009. Effect of fibers on swelling characteristics of bentonite. In *2nd International Conference on New Developments in Soil Mechanics and Geotechnical Engineering*. pp. 328–335.

Ishihara, K., Tatsuoka, F. & Yasuda, S., 1975. Undrained deformation and liquefaction of sand under cyclic stresses. *Soils and Foundations*, 15(1), pp.29–44.

Jardine, R.J. et al., 2004. Developments in understanding soil behaviour. In *Advances in geotechnical engineering, Proceedings of the Skempton Conference*. London: Thomas Telford, pp. 103–206.

Jardine, R.J., 1995. One Perspective On The Pre-Failure Deformation Characteristics Of Some Geomaterials. In *Proceedings of the international symposium on pre-failure deformation characteristics of geomaterials*. Hokkaido, Japan, pp. 885–886.

Jardine, R.J. et al., 2001. Some fundamental aspects of the pre-failure behaviour of granular soils. , pp.1077–1111.

Jardine, R.J., 1992. Some Observations on the Kinematic Nature of Soil Stiffness. *Soils and Foundations*, 32(2), pp.111–124.

Jardine, R.J., Symes, M.J. & Burland, J.B., 1984. The measurement of soil stiffness triaxial apparatus. *Géotechnique*, 34(3), pp.323–340.

Jones, C.J.F.P., 1996. *Earth reinforcement and soil structures*, London: Thomas Telford.

Jovičić, V. & Coop, M.R., 1998. The Measurement of Stiffness Anisotropy in Clays with Bender Element Tests in the Triaxial Apparatus. *Geotechnical Testing Journal*, 21(1), pp.3–10.

Kerisel, J., 1975. Old structures in relation to soil conditions. *Géotechnique*, 25(3), pp.433–483.

Khong, C., 2004. *Numerical Modeling of Soil Deformation*. Thesis. The University of Nottingham.

Kumar, A., Walia, B.S. & Mohan, J., 2006. Compressive strength of fiber reinforced highly compressible clay. *Construction and Building Materials*, 20(10), pp.1063–1068.

Kumar, S. & Everett, T., 2003. Strength Characteristics of Silty Clay Reinforced with Randomly Oriented Nylon Fibers. *EJGE Paper*, 10.

Kuwano, R. & Jardine, R.J., 2007. A triaxial investigation of kinematic yielding in sand. *Géotechnique*, 57(7), pp.563–579.

La-Rochelle, P. et al., 1988. Observational Approach to Membrane and Area Corrections in Triaxial Tests. In *Advanced triaxial testing of soil and rock*. ASTM STP 977, pp. 715–731.

Leroueil, S. & Vaughan, P.R., 1990. The general and congruent effects of structure weak rocks. *Géotechnique*, 40(3), pp.467–488.

Li, C., 2005. *Mechanical Response of Fiber-Reinforced Soil*. University of Texas at Austin.

Li, C. & Zornberg, J., 2005. Interface shear strength in fiber-reinforced soil\r. *Proceedings of 16th International Conference on Soil Mechanics and Geotechnical Engineering*, (US-70), pp.1373–1376.

Li, C. & Zornberg, J.G., 2003. Validation of Discrete Framework for Fiber Reinforcement. In *Proceedings of the 2003 North American Conference on Geosynthetics*. Winnipeg, Canada, pp. 285–293.

Li, G., Chen, Y. & Tang, X., 2008. *Geosynthetics in Civil and Environmental Geosynthetics in Civil and Environmental Engineering*,

Lo, K.Y., 1970. The Operational Strength of Fissures Clays. *Géotechnique*, 20(1), pp.57–74.

Loehr, J.E., Paul, A. & Bowders, J.J., 2000. Reduction of Soil Swell Potential with Fiber Reinforcement. In *GeoEng2000*. Melbourne, Australia.

Lohani, T. et al., 2001. Gmax of fine-grained soils at wide void ratio range, focusing on time-dependent behavior. *Soils and foundations*, 41(5), pp.87–102.

Maher, M.H. & Gray, D.H., 1990. Static Response of Sands Reinforced with Randomly Distributed Fibers. *Journal of Geotechnical Engineering*, 116(11).

Maher, M.H. & Ho, Y.C., 1994. Mechanical Properties of Kaolinite/Fiber Soil Composite. *Journal of Geotechnical Engineering*, 120(8).

Marsland, A., 1971. The shear strength of stiff fissured clays. In *Proceedings of the Roscoe Memorial Symposium*. Cambridge, pp. 59–68.

Michalowski, R.L. & Čermák, J., 2003. Triaxial Compression of Sand Reinforced with Fibers. *Journal of Geotechnical and Geoenvironmental Engineering*, 129(2), pp.125–136.

Miller, C.J. & Rifai, S., 2004. Fiber Reinforcement for Waste Containment Soil Liners. *Journal of Environmental Engineering*, 130(8), pp.891–895.

Mirzababaei, M. et al., 2009. *Undrained Behaviour of Clay Reinforced with Surplus Carpet Fibres*, Bolton.

Mitchell, J.K., 1993. *Fundamentals of Soil Behavior*, New York: Wiley.

Munfakh, G.A., 1997. Ground improvement engineering - the state of the US practice : part 1. Methods. *Ground Improvement*, 1, pp.193–214.

Nishimura, S., 2005. *Laboratory Study on Anisotropy of Natural London Clay*. Imperial College London.

O`Connor, 1994. *Swelling Behaviour of Unsaturated Fine Grained Soils*. City

University of London.

Omidi, G.H., Thomas, J.C. & Brown, K.W., 1996. Effect of desiccation cracking on the hydraulic conductivity of a compacted clay liner. *Water, Air, and Soil Pollution*, 89(1), pp.91–103.

Özkul, Z.H. & Baykal, G., 2007. Shear Behavior of Compacted Rubber Fiber-Clay Composite in Drained and Undrained Loading. *Journal of Geotechnical and Geoenvironmental Engineering*, 133(7), pp.767–781.

Özkul, Z.H. & Baykal, G., 2006. Shear strength of clay with rubber fiber inclusions. *Geosynthetics International*, 13(5), pp.173–180.

Pantelidou, H. & Impson, B.S., 2007. Geotechnical variation of London Clay across central London. *Géotechnique*, 57(1), pp.101–112.

Ponzoni, E. et al., 2014. Identification and quantification of transitional modes of behaviour in sediments of Venice lagoon. *Géotechnique*, 64(9), pp.694–708.

Prabakar, J. & Sridhar, R.., 2002. Effect of random inclusion of sisal fibre on strength behaviour of soil. *Construction and Building Materials*, 16(2), pp.123–131.

Punthutaecha, K. et al., 2007. Volume Change Behaviors of Expansive Soils Stabilized with Recycled Ashes and Fibers. *Journal of Materials in Civil Engineering*, 19(7), pp.616–617.

Rolo, R., 2003. *The anisotropic stress-strain-strength behaviour of brittle sediments*. Imperial College of Science, Technology and Medicine, London.

Roscoe, K.H., Schofield, A.N. & Wroth, C.P., 1958. On The Yielding of Soils. *Géotechnique*, 8(1), pp.22–53.

Sandroni, S., 1977. *The Strength of London Clay in total and effective stress terms*. Thesis. University of London.

Schofield, A.N. & Wroth, C.P., 1968. Critical State Soil Mechanics. *Soil Use and Management*, 25(3), p.310.

Shulley, S., Leshchinsky, D. & Ling, H.I., 1997. *Effects of Short Polymeric Fibers on Crack Development in Clays - REMR-GT-25*, Vicksburg, MS.

Silva Dos Santos, A.P., Consoli, N.C. & Baudet, B.A., 2010. The mechanics of fibre-reinforced sand. *Géotechnique*, 60(10), pp.791–799.

Skempton, A.W., 1954. The Pore-Pressure Coefficients A and B. *Géotechnique*, 4(4), pp.143–147.

Skempton, A.W. & Petley, D.J., 1967. The strength along structural discontinuities in stiff clays. In *Proceedings of the Geotechnical conference*. Oslo, pp. 29–45.

Sorensen, K.K., 2006. *Influence of Viscosity and Ageing on the Behaviour of Clays*. University College London.

Spink, T.W., 1991. Periglacial discontinuities in Eocene clays near Denham, Buckinghamshire. *Geological Society, London, Engineering Geology Special Publications*, 7(1), pp.389–396.

Steinberg, M., 1998. *Geomembranes and the control of expansive soils in construction*, New York: McGraw-Hill.

Tang, C. et al., 2007. Strength and mechanical behavior of short polypropylene fiber reinforced and cement stabilized clayey soil. *Geotextiles and Geomembranes*, 25(3), pp.194–202.

Terzaghi, K., 1944. Ends and means in Soils Mechanics. *Engineering Journal(Canada)*, 27, p.608.

Terzaghi, K., 1936. Stability of slopes in natural clays. In *Proceedings of 1st Conference in Soil Mechanics*. Harvard, pp. 161–185.

Thorne, C.P., 1984. Strength assessment and stability analyses for fissured clays.

Géotechnique, 34(3), pp.305–322.

Vardanega, P.J. et al., 2013. Stiffness of Clays and Silts : Normalizing Shear Modulus and Shear Strain. *Journal of Geotechnical and Geoenvironmental Engineering*, 9(September), pp.1575–1589.

Ventouras, K., 2005. *Engineering behaviour of thanet sand*. Imperial College of Science, Technology & Medicine.

Viggiani, G. & Atkinson, J.H., 1995. Stiffness of fine-grained soil at very small strains. *Géotechnique*, 45(2), pp.249–265.

Vipulanandan, C. & Leung, M., 1991. Seepage Control in Contaminated and Permeable Houston Clay: A Laboratory Study. *Hazardous Waste and Hazardous Materials*, 8(1), pp.17–32.

Viswanadham, B.V.S., Phanikumar, B.R. & Mukherjee, R. V., 2009. Swelling behaviour of a geofiber-reinforced expansive soil. *Geotextiles and Geomembranes*, 27(1), pp.73–76.

Vitone, C. et al., 2005. Preliminary results of a comparative study of the compression behaviour of clays of different fissuring. In *Proceedings of the international conference on problematic soils*. Cyprus, pp. 1173–1181.

Vitone, C. & Cotecchia, F., 2010. On the geotechnical characterisation of a stiff medium fissured clay from italy. In *21st ALERT Workshop*. Aussois.

Vitone, C. & Cotecchia, F., 2011. The influence of intense fissuring on the mechanical behaviour of clays. *Géotechnique*, 61(12), pp.1003–1018.

Wang, Y. et al., 2003. Recycling of Carpet and Textile Fibers. In L. A. A, ed. *Plastic and The Environment: A Handbook*. New York: John Wiley & Sons, pp. 697–725.

Weibull, W., 1939. A statistical theory of the strength of materials. In *Royal Swedish Institute for Engineering Research*. Stockholm, pp. 1–45.

Yetimoglu, T., Inanir, M. & Esatinanir, O., 2005. A study on bearing capacity of randomly distributed fiber-reinforced sand fills overlying soft clay. *Geotextiles and Geomembranes*, 23(2), pp.174–183.

Yilmaz, E., Belem, T. & Benzaazoua, M., 2015. Specimen size effect on strength behavior of cemented paste back fi lls subjected to different placement conditions. *Engineering Geology*, 185, pp.52–62.

Yong, R.N. & Warkentin, B.P., 1975. *Soil Properties and Behaviour*, Amsterdam: Elsevier Scientific Publishing Company.

Zdravković, L. & Jardine, R.J., 2001. The effect on anisotropy of rotating the principal stress axes during consolidation. *Géotechnique*, 51(1), pp.69–83.

Ziegler, S. et al., 1998. Effect of short Polymeric Fibers on Crack Development in Clay. *Soils and Foundations*, 38(1).

APPENDIX

BS1377 : Part 2 : Clause 9 : 1990

Determination of Particle Size Distribution

Window Sample:	WS1001	Description: Mottled grey, brown and purple very slightly sandy SILT / CLAY
Sample Number:	-	
Depth (m):	2.20	

BS1377 : Part 2 : Clause 9.2 : 1990 Wet Sieving Method
BS1377 : Part 2 : Clause 9.4 : 1990 Sedimentation by the Pipette Method

SIEVE	
Sieve	% pass
200 mm	100
125 mm	100
90 mm	100
75 mm	100
63 mm	100
50 mm	100
37.5 mm	100
28 mm	100
20 mm	100
14 mm	100
10 mm	100
6.3 mm	100
5 mm	100
3.35 mm	100
2 mm	100
1.18 mm	100
600 µm	100
425 µm	100
300 µm	100
212 µm	100
150 µm	100
63 µm	96

PIPETTE	
Particle size	% pass
20.0 µm	92
6.0 µm	77
2.0 µm	56
Preparation: No Pre-treatment used	

Temp (°C)	20

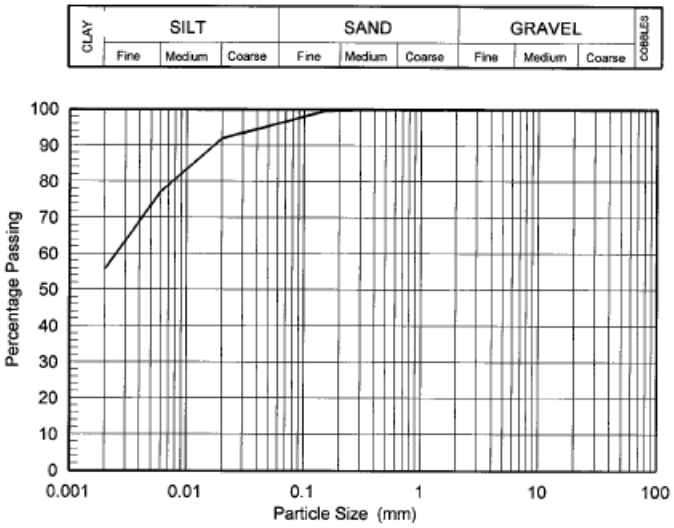

Particle Proportions		
Cobbles	0.0	%
Gravel	0.0	%
Sand	3.7	%
Silt	40.5	%
Clay	55.7	%

Figure A-0-1. Particle size distribution curve of material obtained near side trench where specimens for this study obtained (obtained from industrial partner).

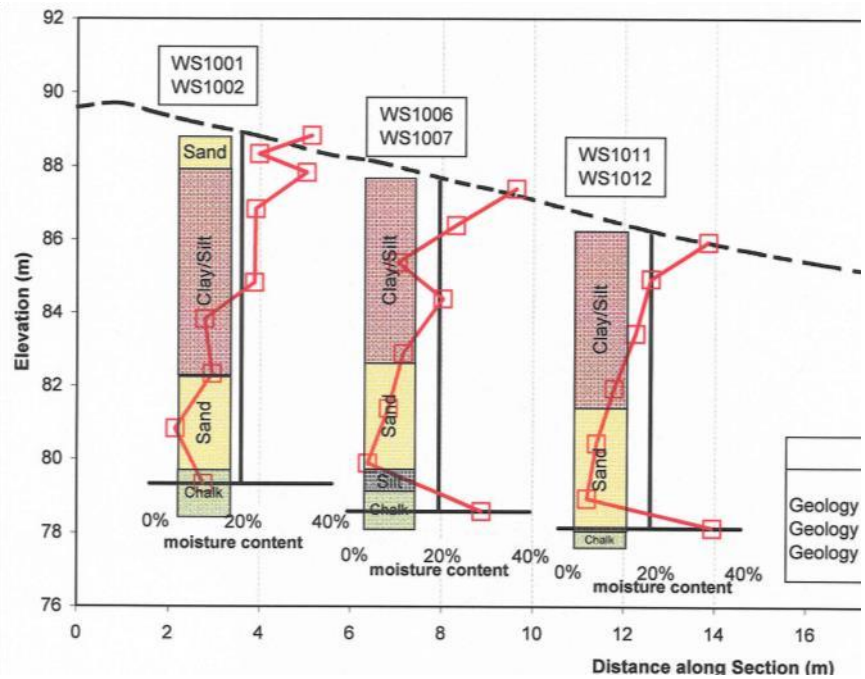

Figure A-0-2. Cross-Section of site indicating soil moisture content profiles and Geology (obtained from industrial partner)

BS1377 : Part 4 : 1990

Moisture Content / Dry Density Relationship

Borehole No:	3009	Description: Firm light brown grey red mottled sandy silty CLAY with occasional fine to medium gravel and pockets of unevenly dispersed fibres
Sample No:	-	
Depth:	0.00 - 1.20	

BS1377 : Part 4 : Clause 3.3.4.1 : 1990 2.5 kg Compaction Test

Sample Preparation: Material was air dried. Single sample
Particles greater than 20mm were removed

Particle Density: 2.74 (assumed)

Material Retained
on 20 mm test sieve: 2 %
on 37.5 mm test sieve: 0 %

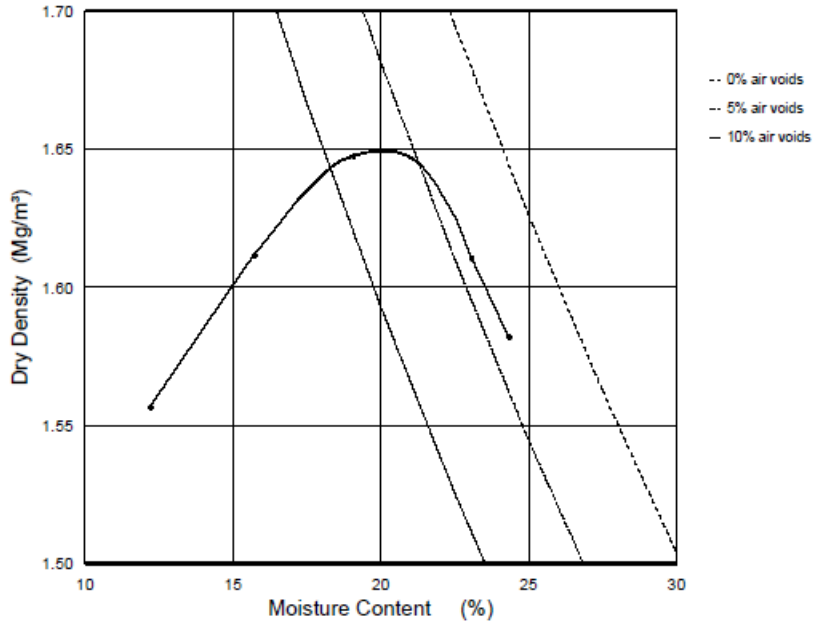

Maximum Dry Density	**1.65 Mg/m³**
Optimum Moisture Content	**20 %**
Natural Moisture Content	**25 %**

Figure A-0-3. Compaction curve of material obtained near side trench where specimens for this study obtained (obtained from industrial partner)

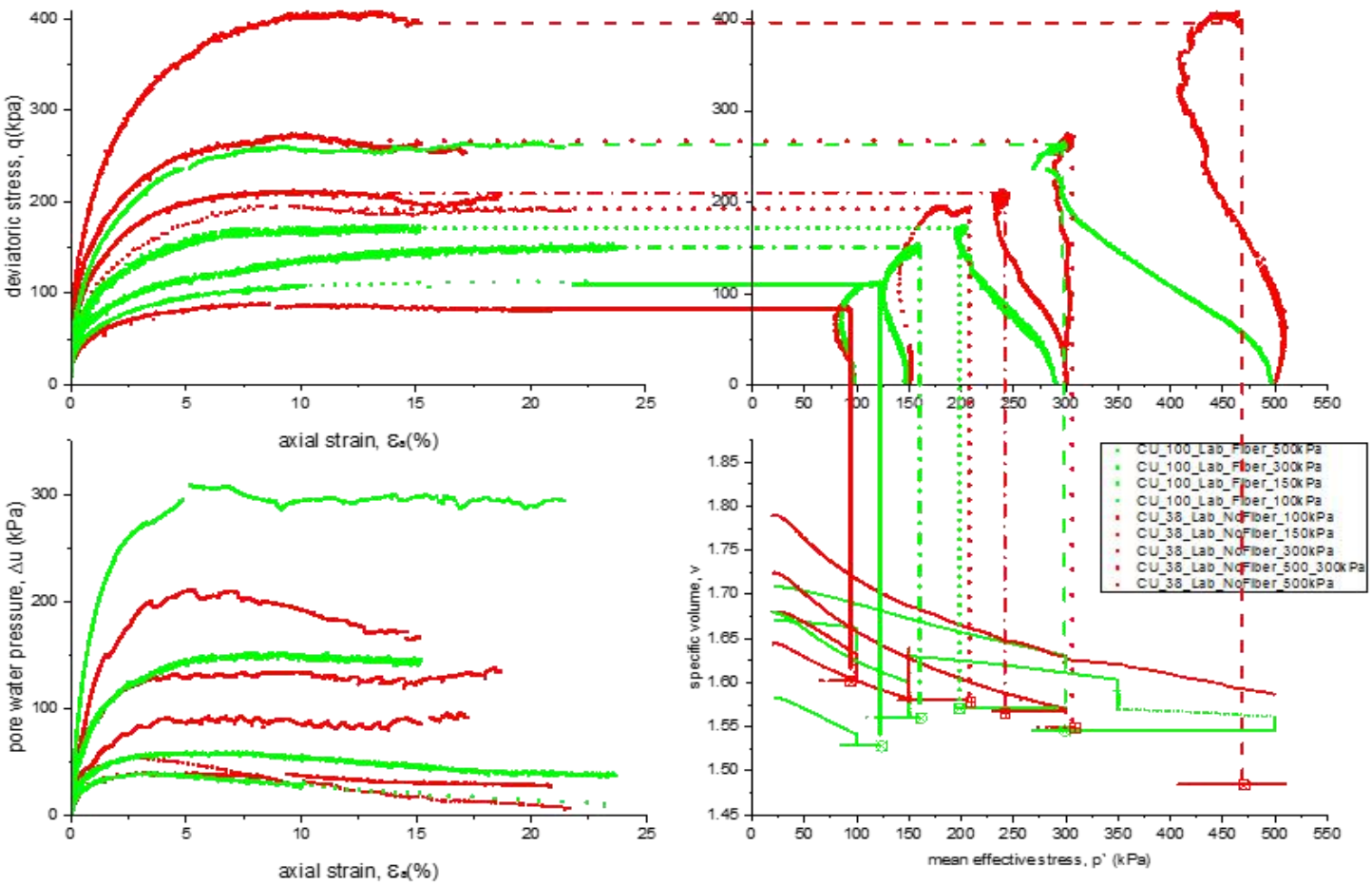

Figure A-0-4. Schematic diagram of evaluating critical state of reinforced and unreinforced specimens

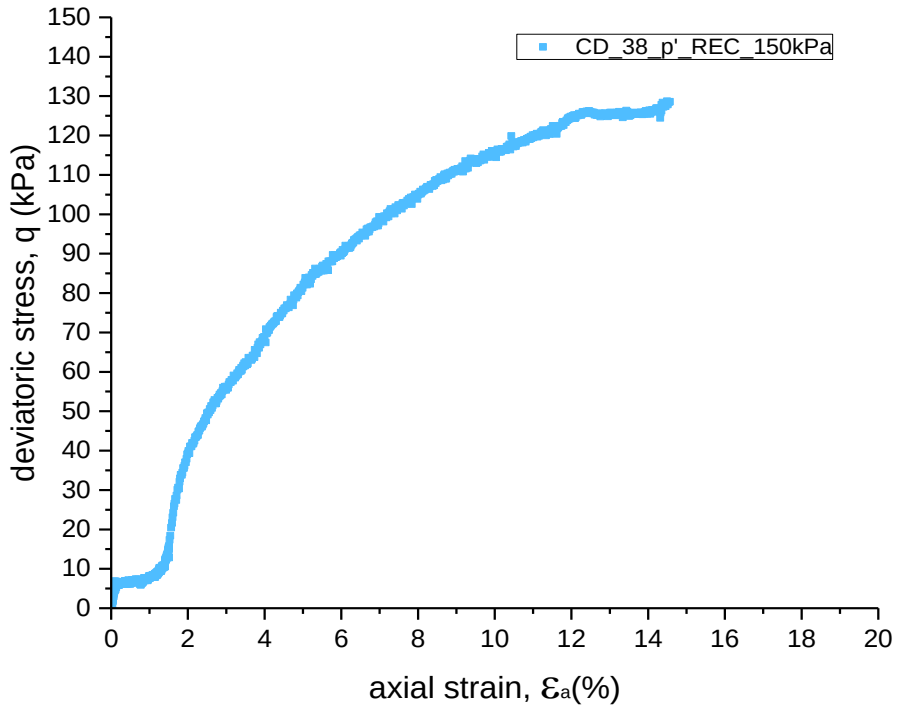

Figure A-0-5. Stress-strain response of drained reconstituted sample (DREC150)

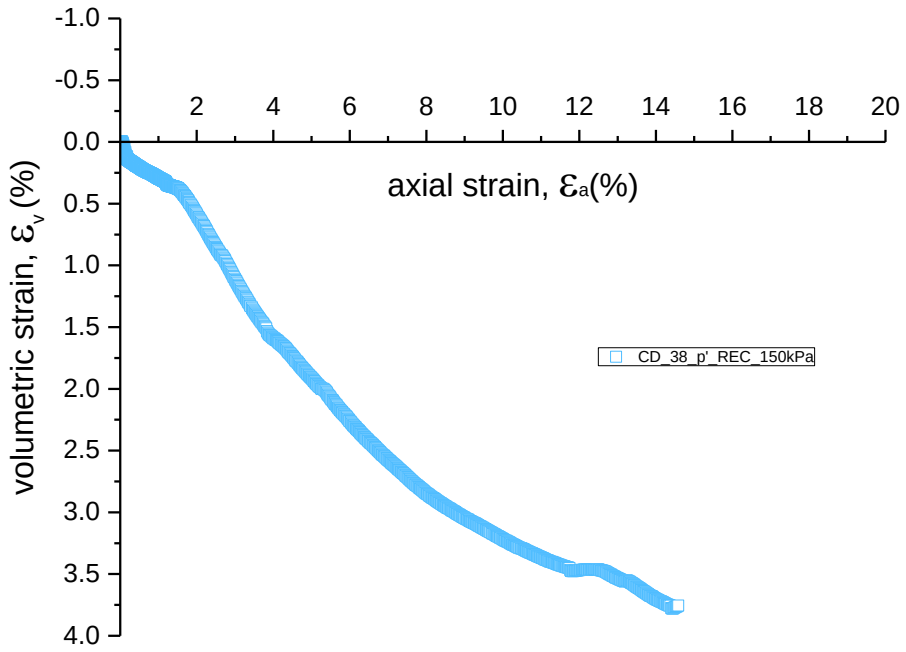

Figure A-0-6 Change in volumetric strain of drained reconstituted sample (DREC150)

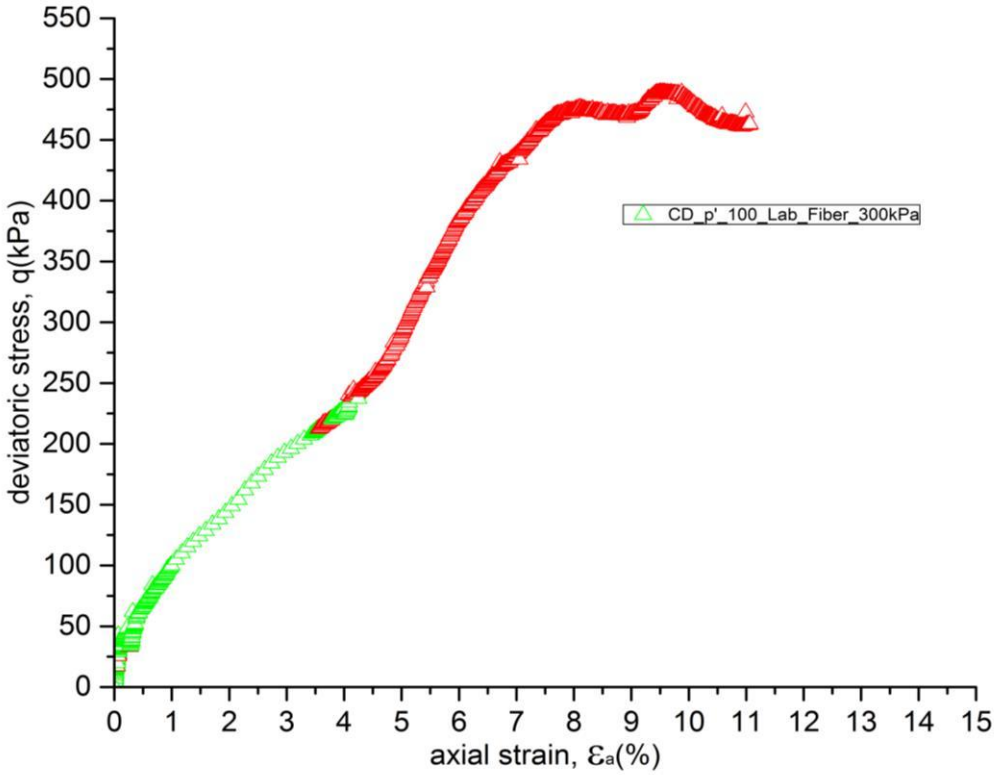

Figure A-0-7. DF300 specimens which was not taken into consideration due to load cells failure